The Oxford Vehicle Model: A tool for modeling and simulating the powertrains of electric and hybrid electric vehicles

Reed Doucette

Hertford College

Department of Engineering Science

University of Oxford

Supervisor: Dr. MD McCulloch

Dissertation submitted for the degree of Doctor of Philosophy

Declaration

The work presented in this dissertation was carried out between October 2008 and November 2011 under the supervision of Dr. Malcolm McCulloch.

This dissertation has not been submitted (in part or in whole) to any other university for a degree, diploma, or other qualification. All of the work contained herein, except for commonly understood and accepted ideas or where reference is made to the work of others, is entirely the work of the author, including nothing which has resulted from work done in collaboration.

Acknowledgement

I owe a deep debt of gratitude to my supervisor, Dr. Malcolm McCulloch, whose support and vision have been crucial to the success of this project.

I want to express my thanks to the Rhodes Trust, Warden, and staff at Rhodes House. Their assistance and encouragement made this work possible and made my experience at Oxford something truly special.

I want to thank my family, whose love transcends any attempt I can make to describe it. I hope this work shows in some small way my heartfelt appreciation for all they have given me.

Abstract

This dissertation addresses the challenges of scoping and sizing components and modeling the tank to wheel energy flows in new and rapidly evolving classes of automotive vehicles. It introduces a system of computer models, known as the Oxford Vehicle Model (OVEM), which provide for the novel simulation of the powertrains of electric (EV) and hybrid electric vehicles (HEV). OVEM has a three-level structure that makes a unique contribution to the field of vehicle analysis by enabling a user to proceed from performing scoping and sizing exercises through to accurately simulating the energy flows in powertrains of EVs and HEVs utilizing existing and emerging technologies based on real world data.

Level 1 uses simplified models to support initial component scoping and sizing exercises in an analysis environment where uncertainty regarding component specifications is high. Level 2 builds on Level 1 by obtaining more refined component scoping and sizing estimates via the use of component models based on well-understood scientific principles that are product-independent – a crucial feature for obtaining unbiased scoping and sizing estimates. Level 3 employs a high degree of fidelity in that its models impose actual physical limits and are based on data from real technologies.

This dissertation concludes with two chapters based on studies published as journal articles that used OVEM to address key issues facing the development of EVs and HEVs. The first study used OVEM to make the novel comparison between high-speed flywheels, batteries, and ultracapacitors on the bases of cost and fuel consumption while functioning as the energy storage systems in an HEV. The second study applied OVEM towards a novel examination of the CO_2 emissions from plug-in HEVs (PHEVs) and compares their CO_2 emissions to those from similar EVs and ICE-based vehicles.

Nomenclature

Roman Letters

A	Point of contact between front tires and road
A_f	Frontal area
a	Acceleration
B	Point of contact between rear tires and road, or when used as a subscript – part of the backwards simulation of Level 3 or backwards (as in the backwards flow of information in a simulation)
b	Exponent used in modeling the nature of the switch resistance in the Level 2 power electronics model
C	Capacitance
C_D	Drag coefficient
E	Energy
E_{EO}	Energy consumption by a plug-in hybrid electric vehicle in electric-only mode
E_{EV}	Energy consumption by an electric vehicle
E_{exp}	Voltage in the battery model at the end of the exponential zone of the constant current discharge curve
E_{full}	Terminal voltage in the battery model when it is fully charged
E_{nom}	Voltage in the battery model at the end of the nominal zone of the constant current discharge curve
E_{OC}	Open-circuit voltage
e	Emissions
F	Force, or when used as a subscript – part of the forwards simulation of Level 3
F_{accel}	Acceleration force
F_D	Aerodynamic drag force
F_g	Gravitational force
$F_{inertia}$	Resistive force due to inertia of the wheels
$F_{max\ front}$	Maximum force capable of being applied at the front wheels
$F_{max\ rear}$	Maximum force capable of being applied at the rear wheels
F_{out}	Force output from a particular block
F_{RF}	Rolling resistance force acting on the front tires
F_{RR}	Rolling resistance force acting on the rear tires
F_{rr}	Rolling resistance force
F_{TF}	Force from vehicle acting on the front wheels
F_{TR}	Force from vehicle acting on the rear wheels
$F_{tire\text{-}road\ max}$	Maximum force capable of being applied at the tire-road contact patch
$Fuel_{used}$	Amount of fuel consumed by the alternative power unit
$F_{veh\ reqd\ avg}$	Force requested of the vehicle
f_o	Coefficient in determining rolling resistance coefficient
f_s	Coefficient in determining rolling resistance coefficient
g	Gravitational acceleration
h	Height of the vehicle's center of mass
H_{2used}	Amount of hydrogen consumed by the fuel cell
I	Current
I_{CO2}	Carbon dioxide intensity
i_G	Gear ratio of the highest gear in a multi-speed transmission
I_{max}	Maximum current rating of an alternative power unit
in	Denotes an input
m_{wheel}	Mass of the wheels and tires
N	Gear ratio
N_{wheels}	Number of wheels
out	Denotes an output
P	Power
$P_{conduction}$	Power electronics conduction losses
P_{copper}	Copper losses
$P_{ESS\ cond}$	Energy storage system conduction losses
$P_{PE\ reqd}$	Power requested by the energy storage system
P_{in}	Power input to a particular block
P_{iron}	Iron losses
P_{max}	Maximum power of an alternative power unit
$P_{motor\ reqd}$	Power requested by the motor
P_{out}	Power out from a particular block
$P_{PE\ reqd}$	Power requested by the power electronics
P_{req}	Power requested
$P_{switching}$	Switching losses
Q	Charge
Q_{cap}	Battery capacity
Q_{exp}	Charge in the battery model at the end of the exponential zone of the constant current discharge curve
Q_{nom}	Charge in the battery model at the end of the nominal zone of the constant current discharge curve
$Q_{removed}$	Charge removed from the battery
R	Resistance
r	Tire radius
$reqd$	When used as a subscript, it denotes a request
T	Torque
$T_{GB\ reqd}$	Torque requested by the gearbox block
$T_{ICE\ reqd}$	Torque requested by the internal combustion engine
T_{in}	Torque input to a particular block
T_{max}	The higher of the torque ratings between the motor and internal combustion engine in a parallel or series-parallel hybrid electric vehicle
$T_{max\ motor}$	Maximum torque rating of the electric motor
$T_{max\ wheel\text{-}axle}$	Maximum torque request passed from the wheel-axle block to the gearbox block over the course of a simulation run
T_{out}	Torque output from a particular block
T_{rated}	Rated torque
T_{rms}	Root mean square of the torque output from the gearbox block over one complete drive cycle
$T_{wheel\text{-}axle\ reqd}$	Torque requested by the wheel-axle block
t	Time
t_i	Time at the beginning of the current time step
t_{i+1}	Time at the end of the current time step
t_{i+2}	Time at the end of the next time step
t_{i-1}	Time at the beginning of the previous time step
V	Voltage

i_{nom}	Nominal discharge current in the battery model
J	Inertia
J_w	Inertia of the wheels
j	Imaginary number
K	Polarization voltage
k_b	Coefficient for bearing losses in the gearbox block
K_{BF}	Proportion of braking energy capable of being recouped by the front brakes in an ideal braking scenario
K_{BR}	Proportion of braking energy capable of being recouped by the rear brakes in an ideal braking scenario
k_c	Coefficient of copper losses
$k_{conduction}$	Coefficient of conduction losses in the power electronics
$k_{ESS\ cond}$	Coefficient of energy storage system conduction losses
k_i	Coefficient of iron losses
k_m	Coefficient for meshing losses in the gearbox block
k_{seal}	Coefficient for seal losses in the gearbox block
$k_{switching}$	Coefficient of switching losses
L	Wheelbase
L_1	Distance between center of mass and front wheel along longitudinal axis
L_2	Distance between center of mass and rear wheel along longitudinal axis
m	Vehicle mass
v	Velocity
$v_{ach,i}$	Velocity achieved at the end of the previous time step
$v_{ach,i+1}$	Velocity achieved at the end of the current time step
$v_{current}$	Current speed of the vehicle in a speed-based energy management strategy
v_{max}	The vehicle speed at or above which the APU or secondary ESS no longer needs to recharge the primary ESS in a speed-based EMS
v_{out}	Velocity output from a particular block
$v_{req,i}$	Velocity requested at the beginning of the current time step
$v_{req,i+1}$	Velocity requested at the end of the current time step
$v_{req,i+2}$	Velocity requested at the end of the next time step
$v_{req,i-1}$	Velocity requested at the end of the previous time step
$v_{veh\ in}$	Linear speed input to the forwards vehicle block
$v_{veh\ reqd\ avg}$	Velocity requested of the vehicle
W_F	Normal force acting on the front axle
W_R	Normal force acting on the rear axle
x	Distance
Z	Impedance
Z_W	Warburg impedance
z	Number of speeds in a transmission

Greek Letters

μ_b	Coefficient of road adhesion
μ_{rr}	Rolling resistance coefficient
η	Efficiency
η_{ESS}	Energy storage system efficiency
η_{fc}	Fuel cell efficiency
η_{GB}	Gearbox efficiency
H_{ICE}	Internal combustion engine efficiency
$\eta_{max\ motor}$	Maximum motor efficiency
η_{motor}	Motor efficiency
η_{pe}	Power electronics efficiency
$\eta_{wheel\text{-}axle}$	Wheel-axle efficiency
θ	Ground slope
ρ	Density of air
ω	Angular frequency or angular velocity
$\omega_{GB\ reqd}$	Angular velocity requested by the gearbox block
$\omega_{ICE\ reqd}$	Angular velocity requested by the internal combustion engine
ω_{in}	Angular velocity input to a particular block
ω_{avg}	Average angular velocity output from the gearbox block over a complete drive cycle
ω_{out}	Angular velocity output from a particular block
$\omega_{wheel\text{-}axle\ reqd}$	Angular velocity requested by the wheel-axle block

Acronyms

AC	Alternating current
ACDC	Artemis Combined Drive Cycle
ADVISOR	Advanced vehicle simulator
APU	Alternative power unit
AVG	Average
BEV	Battery electric vehicle
CAFÉ	Corporate average fuel economy
CAPSIM	Center for Automotive Propulsion Systems
CO_2	Carbon dioxide
CS	Charge-sustaining mode
CVT	Continuously variable transmission
DC	Direct current
EGT	Epicyclic gear train
EMS	Energy management strategy
EPA	Environmental Protection Agency
ESS	Energy storage system
EV	Electric vehicle
FTP	Federal Test Procedure
FW	Flywheel
GB	Gearbox
H_2	Hydrogen
HEV	Hybrid electric vehicle
ICE	Internal combustion engine
ICERT	Institute for Carbon and Energy Reduction in Transport
LHV	Lower heating value
M-G	Motor-generator
NEDC	New European drive cycle
OEM	Original equipment manufacturer
OVEM	Oxford Vehicle Model
PE	Power electronics
PEMFC	Proton exchange membrane fuel cell
PHEV	Plug-in hybrid electric vehicle
PSAT	Powertrain Systems Analysis Toolkit
RMS	Root mean square
SOC	State of charge
SUV	Sports utility vehicle
UDDS	Urban Dynamometer Driving Schedule
VESYM	Vehicle simulation model

Table of Contents

1 Introduction

This dissertation addresses the challenges of scoping and sizing components and modeling the tank to wheel energy flows in new and rapidly evolving classes of automotive vehicles. It introduces a system of computer models, known collectively as the Oxford Vehicle Model (OVEM), which provide for the novel simulation of the powertrains of electric (EV) and hybrid electric vehicles (HEV). OVEM has a three-level structure that makes a unique contribution to the field of vehicle analysis by enabling a user to proceed from performing scoping and sizing exercises through to accurately simulating the energy flows in powertrains of electric and hybrid vehicles utilizing existing and emerging technologies based on real world data.

1.1 The Motivation for Advanced Vehicle Research

In 2010, an estimated 1 billion cars and light trucks were in existence around the world, and their widespread use has had far-reaching environmental and economic impacts [1]. The energy to power all of those passenger vehicles comes almost exclusively (94%) from a CO_2 intensive source, oil [2]. This has led road transport to be responsible for approximately 17% of annual global CO_2 emissions – emissions that are leading to widespread pollution and global climate change [2] [3]. The fossil fuels upon which transport is largely based are also a finite resource, and the extraction and production of many of these fuels are likely to become increasingly challenging and expensive due to both human and natural factors [3].

It has been projected that by 2050, 3 billion cars will populate the world's roads, an increase of 2 billion cars over the next 40 years [4]. Much of this growth is projected to occur in developing countries – by 2050 China and India are expected to have 570 and 370 million passenger vehicles respectively, which combined would be nearly as many as the worldwide fleet in 2010 [4].

In an effort to mitigate the environmental, economic, and security dilemmas posed by transport's continued growth and reliance on fossil fuel based automobiles, targets have been set by regulatory bodies to reduce the consumption of fossil fuels by automobiles. For instance, the European Union has set a target for 2020 that the fleet average CO_2 emissions for passenger vehicles will be 95 gCO_2/km [5]. The USA has set a corporate average fuel economy (CAFE) standard of 54.5 mpg for 2025 [6]. China has set a fleet average fuel economy target of 42.2 mpg for 2015 [7]. Currently, only the most advanced commercially available automobiles reach these targets. In order to satisfy the legal, environmental, and economic constraints of the future, vehicles will have to be more efficient and able to utilize energy from alternative sources.

1.2 Alternative Vehicle Powertrains

EVs and HEVs are regarded as options to enable automobiles to reduce or even eliminate the fossil fuel dependency of automobile transport, and hence improve automobile transport's environmental and economic sustainability [8]. Electric and hybrid electric vehicles have a higher tank-to-wheel efficiency than conventional vehicles based on ICEs due to the higher efficiency of their powertrains and their ability to recapture energy during braking [9]. Also, as they store energy on-board in a form other than fossil fuels (such as with batteries), they are not necessarily solely reliant on fossil fuels to power them.

Electric and hybrid electric vehicles have only recently begun to be considered as legitimate alternatives to conventional vehicles. This is due in part to technological developments and in part to a growing consciousness regarding the need to mitigate the negative effects of conventional automobiles powered solely by fossil fuels [8]. As such, electric and hybrid electric vehicle development is still in its nascent stages. The Toyota Prius, the first mass-produced hybrid electric vehicle, was first sold in Japan in 1997 and internationally in 2000. The first mass-produced (highway-certified) electric passenger car of the modern era was the EV-1 from GM which was produced from 1996-1999 before being discontinued by its manufacturer due in part to technological limitations [10]. Since that time several attempts have been made to widely sell electric vehicles (e.g., G-Wiz, Tesla Roadster, Nissan Leaf [11]); however these attempts have been met with limited success due in large part to technological limitations and high cost. A decade since the release of the first mass-produced hybrid electric car may seem like a long time, but when the length of the development cycle of new vehicles is considered – typically on the order of five to seven years – then it becomes clear that even the most advanced hybrid electric vehicles are only in their second or third generation. The development of mass-produced electric vehicles is similarly immature. Yet given the speed at which the technologies that make up these vehicles are evolving, the bounds that were once perceived as the technological limitations of these vehicles must continually be reassessed.

In the field of EV and HEV development, there are few, if any, powertrain technologies, topologies, and energy management strategies that outperform all other alternatives across every metric that is of interest to industry, consumers, and governments. This means that there is often a great deal of uncertainty regarding what might be called the "optimal" powertrain for a particular vehicle or application. Compounding the issues of uncertainty regarding electric and hybrid electric vehicles is the fact that they are complex systems that can utilize many different technologies, and these technologies can be arranged and managed in many different ways. Additionally, new technologies are constantly emerging, and assessing their potential impact on EVs and HEVs is an important challenge.

For clarity of thought and discussion, the range of possible electric and hybrid electric powertrains are generally categorized by four main topologies: pure electric, series HEV, parallel HEV, and series-parallel HEV [12]. The following sections (1.2.1 through 1.2.4 and 1.3) provide an overview for understanding the complexity of the different electric and hybrid electric powertrain topologies.

1.2.1 Electric Vehicle Powertrain

A pure electric vehicle uses an electric motor for traction and that motor is powered by an energy storage system (ESS). In 2011, the energy storage system on-board electric vehicles most commonly takes the form of a battery array, though the battery array has the potential to be hybridized with other technologies such as ultracapacitors or high-speed flywheels [13]. Two of the main strengths of electric vehicles are that they have a tank-to-wheel energy consumption that can typically be at least three to four times lower than conventional vehicles that rely solely on internal combustion engines, and they produce no tailpipe emissions [9]. One of the main weaknesses of electric vehicles is that in order to achieve a range comparable to a conventional, internal combustion engine-based vehicle they need an energy storage system with a high energy capacity [14]. Given the state of energy storage system technology in 2011, such a system is heavy and expensive, especially if it is made large enough to enable an electric vehicle to achieve a range approaching that of a conventional vehicle [14].

The Tesla Roadster (available since 2008) from Tesla Motors is an example of a pure electric vehicle. It uses a lithium-ion battery pack weighing 450 kg, which accounts for 36% of the curb weight of the vehicle, to achieve a range of 220 miles on the EPA combined city/highway drive cycle [11]. Figure 1.1 shows a schematic of a common powertrain topology for an EV.

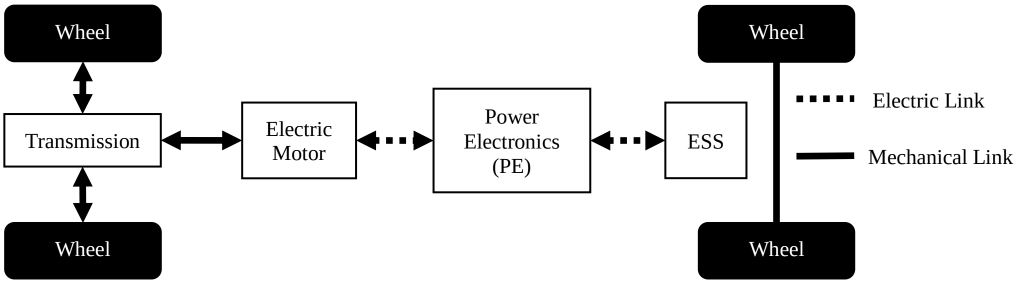

Figure 1.1: Schematic of an EV powertrain

1.2.2 Series Hybrid Electric Vehicle Powertrain

A series hybrid electric vehicle is similar to a pure electric vehicle in that an electric motor provides all of its tractive force, and that motor is powered by an energy storage system [12]. However, a series hybrid also has an on-board power generator that can be used to recharge the energy storage system or supplement the energy storage system's power while the vehicle is driving [9]. The on-board power generator, also known as an alternative power unit (APU), typically takes the form of a fuel cell or an internal combustion engine connected to a generator. The alternative power unit in a series hybrid can often be downsized and operated at its most efficient point since it only has to recharge the energy storage system, and it does not have to provide traction [15]. The energy storage system can also be designed to meet the transient driving loads while the alternative power unit supplies the average power. This means the energy storage system can often be downsized since it shares the energy storage and power production load with the alternative power unit [16]. The presence of the electric traction motor and energy storage system can improve the efficiency of the vehicle by enabling regenerative braking [16]. The energy storage system of a series hybrid can also be charged from the electric grid. Such a vehicle is known as a plug-in hybrid electric vehicle (PHEV).

The Chevrolet Volt (available since December 2010) is an example of a series PHEV that uses an ICE as its APU [17]. The Volt has a reported range of 40 miles in electric-only mode before it has to resort to using its alternative power unit, a four-cylinder internal combustion engine [18]. According to EPA testing on the combined city/highway drive cycle, the Volt will achieve an equivalent of 2.4 L/100 km in electric-only mode and 6.4 L/100 km once its internal combustion engine is engaged. Figure 1.2 shows a schematic for a common series hybrid topology.

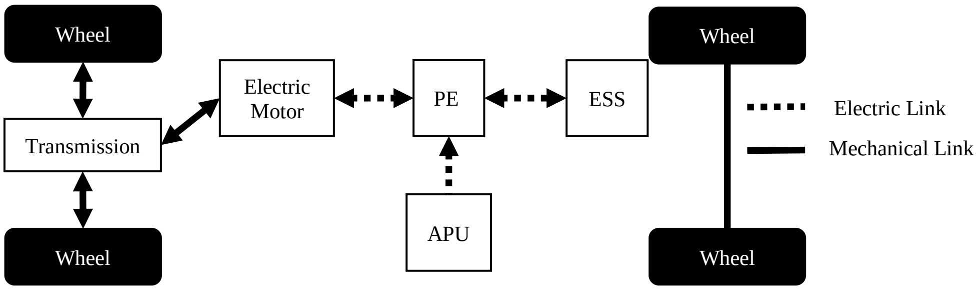

Figure 1.2: Schematic of a series HEV powertrain

1.2.3 Parallel Hybrid Electric Vehicle Powertrain

In a parallel hybrid electric vehicle, both an internal combustion engine and an electric motor can directly provide a vehicle's tractive force. In this configuration an electric motor typically propels the vehicle at low speeds since it has a higher efficiency than an internal combustion engine during the stop-and-go pattern characteristic of urban driving [14]. The internal combustion engine is typically used to power the vehicle during high speed driving where there is less speed fluctuation, and it has to deviate less frequently from operating at its most efficient point [12]. Also the internal combustion engine, electric motor, and energy storage system can be downsized since none of them are solely responsible for the total power output of the vehicle [9]. Parallel hybrids can also be plug-in hybrids; though this is less common since their energy storage systems generally have a lower energy capacity since they are usually only designed to power low-speed, start and stop driving. The Honda Civic Hybrid and the Ford Escape Hybrid are examples of parallel HEVs [19] [20]. Figure 1.3 shows a schematic for a common parallel hybrid topology.

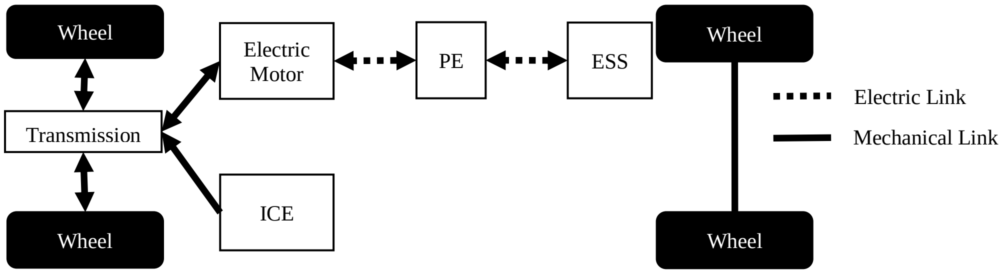

Figure 1.3: Schematic of a parallel HEV powertrain

1.2.4 Series-Parallel Hybrid Electric Vehicle Powertrain

A series-parallel, also known as a dual or power split, hybrid electric vehicle combines elements from both the series and parallel hybrid configurations. Like a parallel hybrid, the road load can be shared between the motor and the internal combustion engine [21]. Like a series hybrid, the engine can also function as an alternative power unit to generate additional power to recharge the energy storage system while the vehicle is driving [12]. A series-parallel vehicle can also be a PHEV. The Toyota Prius implements a series-parallel powertrain topology [22]. Figure 1.4 shows a schematic of a common series-parallel hybrid topology.

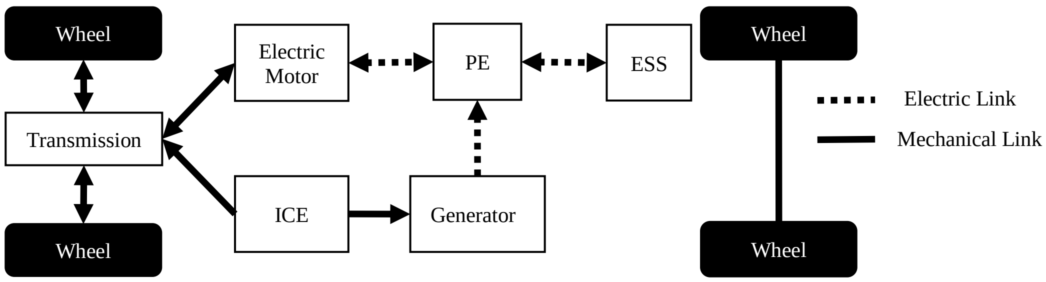

Figure 1.4: Schematic of a series-parallel HEV powertrain

1.3 Electric and Hybrid Electric Vehicle Complexity

The previous section presented a high-level overview of the topologies and component types that usually make up electric and hybrid electric vehicle powertrains, and this section disaggregates those broad categories to present a glimpse into the potential for complexity in crafting these powertrains. Each component class is comprised of numerous variants, and these components can be arranged according to four broad categories of topologies and managed according to two broad categories of energy management strategies. Table 1.1 presents an overview of the technological options available in each of these classes. Note that Table 1.1 is not intended to be an exhaustive list of all possible technology and product combinations that may find a place in electric or hybrid electric vehicles, it is only meant to be indicative of the degree of combinatorial complexity possible in these vehicles.

Table 1.1: Technologies, topologies, and energy management strategies with variants that may be utilized by EVs and HEVs [12] [23]

<table>
<tr><th></th><th colspan="6">Variations</th></tr>
<tr><td>Topology</td><td>EV</td><td>Series HEV</td><td colspan="2">Parallel HEV</td><td colspan="2">Series-Parallel HEV</td></tr>
<tr><td>Transmission</td><td>Fixed Gear Ratio</td><td>Multi-Speed</td><td>Continuously Variable</td><td>Epicyclic Gear Train</td><td></td><td></td></tr>
<tr><td>Motor</td><td>Asynchronous AC</td><td>Switched Reluctance</td><td>Brushless DC</td><td>Synchronous AC</td><td></td><td></td></tr>
<tr><td rowspan="2">ESS</td><td rowspan="2">Ultracapacitor</td><td rowspan="2">Flywheel</td><td colspan="4">Battery</td></tr>
<tr><td>Lithium-Based</td><td>Nickel-Based</td><td>Lead-Based</td><td>Other chemistries</td></tr>
<tr><td rowspan="2">APU</td><td rowspan="2">Fuel Cell (typically with only proton membrane used in light-duty vehicles)</td><td colspan="2">Internal Combustion Engines</td><td></td><td></td><td></td></tr>
<tr><td>Petrol</td><td>Diesel</td><td></td><td></td><td></td></tr>
<tr><td>EMS</td><td>Thermostat</td><td>Speed-Based</td><td></td><td></td><td></td><td></td></tr>
</table>

As it is currently presented, Table 1.1 shows that there are in excess of 10,000 possible combinations (when hybridized energy storage systems are included). A closer examination shows that the number of possible combinations increases as the specificity of Table 1.1 increases. For instance, there are multiple sub-variations of each of the different battery chemistries such as lithium-ion, lithium-polymer, lithium-cobalt-dioxide, lithium-manganese-dioxide. Additionally, Table 1.1 makes no mention of the sizing options for all of these components. The energy management strategies also include numerous parameters that can be tuned to optimize energy consumption. Within each of the technological classifications in Table 1.1, many distinct products actually exist with new products constantly being introduced, further compounding the complexity of possible powertrain configurations. Given all of these other sources of combinatorial complexity, the number of possible electric and hybrid electric vehicle combinations escalates rapidly. The exact number of possible combinations is nearly impossible to determine as new technologies and products are constantly emerging; however, the number of possible combinations is conservatively in excess of 10^7.

By comparison, conventional vehicles have far fewer possible combinations. Table 1.2, presents the primary options available to a conventional vehicle in a similar manner to Table 1.1.

Table 1.2: Technology options for broad component classes in conventional vehicles

<table>
<tr><th></th><th colspan="2">Variations</th></tr>
<tr><td>Transmission</td><td>Multi-Speed</td><td>Continuously Variable</td></tr>
<tr><td>Motor</td><td colspan="2">None</td></tr>
<tr><td>ESS</td><td colspan="2">None</td></tr>
<tr><td rowspan="2">APU</td><td colspan="2">Internal Combustion Engines</td></tr>
<tr><td>Petrol</td><td>Diesel</td></tr>
<tr><td>EMS</td><td colspan="2">None</td></tr>
</table>

While Table 1.2 has additional sub-variations not reflected in it (just as additional sub-variations are not reflected in Table 1.1), it can be seen that conventional vehicles have far fewer combinations possible in their technological makeup.

Building and testing each of these possible combinations in electric and hybrid electric vehicles in order to characterize their performance would be prohibitively time, labor, and resource intensive. Fortunately, computer models can help to analyze how a vehicle will perform without the cost and time that would go into building a physical prototype for every possible vehicle [24] [25].

1.4 Electric and Hybrid Electric Vehicle Simulation

Computer modeling can be a valuable resource in the design and analysis of electric and hybrid electric vehicles for it has the capacity to answer many questions regarding their development at a fraction of the time and cost that would go into actually building and testing prototypes of the array of possible powertrain combinations [24] [25]. The very nature of modeling requires a program to decide what it will and will not attempt to model, since physical systems (especially ones as complex as electric and hybrid vehicles) are too complex to completely represent via a model. Therefore, a vehicle simulation program must know where it is willing to set its ambitions and recognize its limits. This section seeks to illuminate the noteworthy concerns in vehicle modeling.

1.4.1 Issues in Vehicle Simulation

Models are approximations of the physical systems they seek to represent. Since they cannot include all of the effects that characterize a system, they must understand the characteristics that they seek to represent [26]. This requires that simulations strike a balance between fidelity, uncertainty, and accuracy [27]. For clarity of discussion, fidelity, in the context of modeling, refers to the degree to which a model reproduces the characteristics and effects of the physical system it is representing. Uncertainty, in this context, refers to the degree to which certain system characteristics cannot be known or are not desired to be specified for use within a model. Accuracy refers to how well the outcome of a model aligns with the outcome of the physical system.

When simulations contain more uncertainty, they cannot have a high fidelity, and are less accurate. This is usually manifested by simple modeling techniques based on sparse data. As the uncertainty decreases, the fidelity and accuracy usually improves. More complex models are implemented with the aim of enhancing a simulation's fidelity and accuracy; yet, these complex models require more information which typically requires more computational resources (to run the models) and experimental capabilities (to extract the parameters that high-fidelity models require). Different simulation techniques, particularly in vehicle simulation, are used depending on the questions the simulation is trying to answer [28].

The question of timescales and conditions are often of particular concern in many modeling efforts. The model should seek to represent effects that occur over the timescales and conditions that are of interest for that particular effort given the model's objectives [15].

The determination of what timescales are of interest is often not capable of being expressed as a single definite value. Instead, the timescales of interest are usually thought of as an approximate range. It is then incumbent on the discretion of the model's designer to develop a model appropriate for those timescales and conditions.

1.5 Criteria for a Novel Electric and Hybrid Electric Vehicle Modeling Effort

With the knowledge that any modeling effort must understand what it is attempting to model before it can proceed, this section explores the criteria that would guide a novel vehicle modeling effort. In order to navigate the current vehicle modeling landscape to systematically identify where opportunities for novel contributions exist, a list of modeling criteria for assessing the current vehicle landscape based on the unmet needs of likely users of this program was needed.

To develop this list, key sets of potential users of this new program were consulted. The first of these users was the Institute for Carbon and Energy Reduction in Transport (ICERT) at the University of Oxford. The second set was partners in industry (including vehicle manufacturers and OEMs), government, and academia. This section will explain the key issues identified by each of these groups as to how their vehicle modeling needs were not being met by the current vehicle modeling landscape.

ICERT is a long-term research project operating at the University of Oxford across the Transportation Studies Unit in the Department of Geography and the Energy and Power Group in the Department of Engineering Science. ICERT's mission is to use a whole-systems approach to analyze the interface between technology, economics, and society, in order to develop useful approaches for industry and government that aim to increase the rate and effectiveness of carbon reduction in transport. Figure 1.5 presents a diagram of the information flows in the broader ICERT model. Note that a novel vehicle simulation program addresses the challenge of simulating the performance of existing and emerging electric and hybrid electric vehicle types.

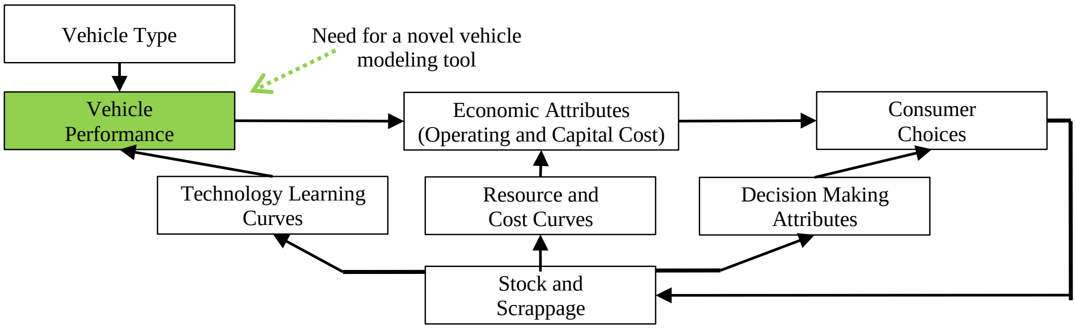

Figure 1.5: Diagram of the information flows in the broader ICERT Model

A crucial part of ICERT's research is that it needed a vehicle simulation tool with several key capabilities. One of the aims of ICERT's research is to generate a comprehensive list of current technologies that could potentially work towards reducing the carbon intensity of automobile operation. In order to generate this list, certain target component specifications needed to be established based on constraints such as future carbon reduction standards. Once this list was generated, ICERT would need a way to analyze this list of potentially useful technologies to see how they would perform in a vehicle. Coping with such a list of existing technologies, and recognizing that new technologies were constantly emerging, spurred ICERT to seek a vehicle simulation program that would be able to produce accurate, rapid results by utilizing data from existing and emerging technologies and capabilities. It should also be emphasized that one of the key questions that ICERT is seeking to answer is how to get the public to increase its rate of adoption of low-carbon vehicles. This has four implications.

The first implication is related to the vehicle characteristics that ICERT would like to ascertain from a vehicle modeling program. ICERT is concerned with the vehicle specifications that are seen to be the key drivers of electric and hybrid electric vehicle adoption: cost (as a proxy for component sizing), range, emissions, and energy consumption.

Therefore any novel vehicle modeling program that ICERT would use would need to be able to be structured in such a way that these figures could be produced with a sufficient degree of accuracy (a discussion of what sufficient accuracy means for ICERT is included below).

The second implication pertains to the types of timescales which ICERT would need to see reflected in a novel vehicle modeling program. ICERT is largely concerned with the types of light-duty vehicles and suburban, highway, and urban driving patterns typically experienced by light-duty vehicles. For instance, it is not interested in more specialist areas such as racing, hill-climb, or off-road where high-fidelity models capturing rapid transient performance is a priority. ICERT is also not interested in predicting effects taking place over long timescales such as degradations in vehicle performance over the course of years. This means that ICERT is concerned with the type of timescales and conditions seen during the types of driving events customary of typical light-duty urban, suburban, and highway driving. These timescales can be thought of as encompassing typical light-duty acceleration and braking events (usually on the order of seconds) to lengthy trips (usually on the order of several hours). Therefore, the timescales of interest to OVEM are those between approximately 1 s to 10^4 s.

The third implication concerns the driving conditions with which ICERT is concerned. ICERT is primarily concerned with delivering information to decision-makers capable of influencing the future of transport. These decision-makers value results that allow for standardized comparisons to be made across a wide array of vehicle types for values such as a range, energy consumption, and emissions. For historical, political, and legacy reasons as well as concerns over standardization and ease of implementation, vehicle testing to obtain these values is typically done by assuming the vehicle travels in a straight line over a widely-used drive cycle. Therefore, ICERT is concerned with simulating vehicles over these "industry standard" conditions: straight-line travel typically over a widely-used drive cycle.

By extension, ICERT is not concerned with extremely aggressive acceleration and braking maneuvers – the kind that are seen in racing and not in normal light-duty vehicle operation. This ability to account for the types of driving patterns normally experienced by light-duty vehicles is available in existing vehicle modeling programs. However, existing vehicle modeling programs disregard the ability to account for changes in elevation while driving. ICERT is aware that existing widely-used drive cycles and vehicle modeling programs cannot account for changes in elevation. ICERT also realizes that changes in elevation are an unavoidable part of normal driving conditions. Changes in slope are of particular interest to electric and hybrid vehicles given their sensitivity to issues regarding energy consumption and range and their capability to utilize regenerative braking during descents. For these reasons, ICERT sought the novel functionality of being able to model the effect that slope would have on electric and hybrid electric vehicles.

The fourth implication relates to ICERT's accuracy objectives from a novel vehicle modeling tool. ICERT is aware that as it is a broad study concerned with many technological, economic, and social parameters that are difficult to know precisely, it will inevitably have high uncertainty across many dimensions of its analysis. It will obviously seek to reduce uncertainty wherever possible, and vehicle modeling is one area where that uncertainty can reasonably be reduced, at least such that the uncertainty is less than in the other less quantifiable and precise areas of its research. ICERT does not have a specific accuracy target, only that it should provide credible results while still adhering to ICERT's other objectives.

In consultations with other partners in academia, government, and industry, a similar but slightly different set of needs from a new vehicle modeling program was identified. The first of these concerns was obtaining a modeling program that would facilitate rapid scoping exercises to quickly determine technologies of particular interest. For instance, one industrial partner had an inchoate conception for a new electric vehicle, but could not find a useful tool to enable the sizing and performance benchmarking of cutting-edge component technologies. Like ICERT these other partners also expressed an interest in a program that would be able to rapidly simulate and scope existing and emerging technologies and capabilities. Also like ICERT, these partners were concerned with obtaining figures for the drivers that are perceived to be key in spurring electric and hybrid electric vehicle adoption: cost, sizing, range, emissions, and energy consumption. These partners were also interested in having simulations that were of a high degree of accuracy; however their accuracy objectives came from a slightly different rationale than ICERT's. These partners wanted to see accuracy as high as possible while still meeting their other concerns regarding rapidity of implementation and simulation. This was because these partners felt that once sufficient scoping had been performed such that a reasonable degree of certainty had been obtained regarding the performance of particular technologies, there was little point in further improving simulation accuracy, as more advanced, real world testing would now be warranted. Their accuracy objective did not have a single, uniform quantitative target; however, it was gathered from these consultations that an accuracy of within approximately 2-5% of real world values would be sufficient.

To summarize, the parties consulted about their vehicle modeling needs proposed the following criteria. These criteria could now be used to survey the current vehicle modeling landscape to identify if and how a novel contribution could be made with the development of a new vehicle modeling program.

1. The program should be able to rapidly simulate and incorporate existing and emerging technologies and capabilities.
2. The program should be able to facilitate sizing and scoping exercises across a wide spectrum of component technologies and sizes in order to understand the relationship between technological options (including those that currently exist and have the

potential to exist in the future) and key EV and HEV characteristics, such as cost, emissions, energy consumption, and range.

3. The program should be concerned with timescales and conditions that align with widely used vehicle testing protocols for ascertaining values such as emissions, energy consumption, and range. The relevant timescales are approximately on the order of 1 to 10^4 s. The conditions are straight-line travel, typically over widely-used drive cycles representing urban, highway, or suburban driving (in order to enable comparison with other studies and reported vehicle characteristics). This excludes racing applications or other similarly extreme off-road or hill climb applications. The simulation should also have the ability to account for changes in elevation.
4. The program should be capable of obtaining a degree of accuracy that warrants reasonable justification to begin with experimental testing. This was suggested by industrial partners to be approximately between 2-5% of real world figures.

1.6 Vehicle Simulation Techniques

A survey of the current vehicle modeling landscape was conducted to see if any single existing modeling packages sufficiently addressed the enumerated design criteria for a novel vehicle modeling effort. In keeping with the philosophy that any modeling effort must have boundaries depending on its objectives, it follows that different vehicle simulation tools focus on different areas of vehicle performance. The array of vehicle modeling efforts can be grouped into two broad categories – those concerned with vehicle dynamics and those concerned with energy flows. Figure 1.6 presents a diagram showing the classification structure of the types of vehicle modeling. This section presents an overview of these modeling techniques and then assesses them against the criteria enumerated in Section 1.5 to determine their suitability for inclusion in a novel vehicle modeling effort.

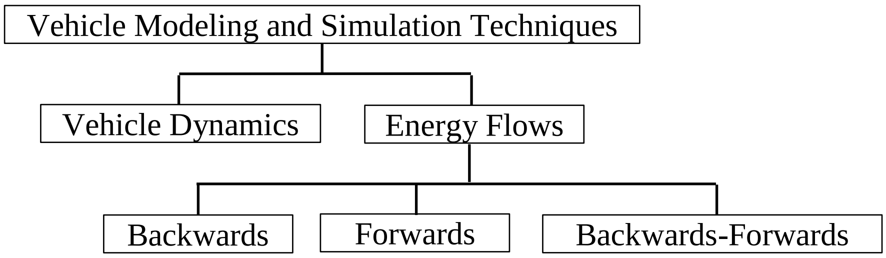

Figure 1.6: Tree diagram of vehicle modeling techniques

1.6.1 Vehicle Dynamics Modeling

Simulators concerned with vehicle dynamics are usually used to simulate properties affecting the dynamic movement of the vehicle such as body flex, cornering, handling, directional stability, vibration, wheel slip, and ride quality. Advanced programs can even be used to perform crash test analysis. Commercially available versions of vehicle dynamics simulators include tools such as CarSim [29] and VESYM [30].

Vehicle dynamics simulators are not meant to model the energy flows in powertrains. As such, they do not meet Criteria #2 set out in Section 1.5 which states that a new vehicle modeling program should be able to scope new technologies to determine figures such as energy consumption, range, emissions, and cost. Additionally, vehicle dynamics simulators would not be relevant to the novel vehicle modeling effort given Criteria #1, since as a class of simulators they are not meant to simulate existing and emerging powertrain technologies. This class of simulators also does not align with Criteria #3, since much of the usefulness of vehicle dynamics simulators would be lost on simulations concerned with straight-line driving. In regard to Criteria #4, this class of simulators would not even produce estimates (accurate or not) for the type of powertrain components of interest in this study. Therefore, vehicle dynamics simulators were not deemed suitable as a class of simulators that might play a role in the new vehicle modeling effort of interest in this study.

1.6.2 Energy Flow Modeling

The other class of simulators is broadly concerned with the energy flows within powertrains (tank to wheel). Typically, this means that the simulation accounts for sources of power losses according to whatever timescales, conditions, and physical effects are of interest to that modeling effort. This class of simulator is generally used to produce figures for values such as range, emissions, energy consumption, and component cost and sizing [28]. Energy flow simulations can typically be subdivided into one of three categories: backwards, forwards, and backwards-forwards. Each of these categories is characterized by a different compromise between uncertainty and fidelity, and each category can be used to illuminate different types of information related to electric and hybrid electric vehicle design and analysis.

1.6.2.1 Backwards Modeling

Backwards modeling is a method of energy flow simulation that is primarily used to predict the component sizing requirements of a vehicle and to estimate a vehicle's energy consumption [31]. Its usefulness in component sizing is made possible by the fact that the key characteristic of backwards models is that they impose no performance limits. It is a technique that is generally used when uncertainty around vehicle design and analysis is high, and as a result of the high uncertainty, the fidelity of backwards models is typically low. Backwards models that are concerned with modeling energy flows primarily use quasi-steady-state models. Quasi-steady-state models are used in order to model the most relevant effects for determining figures such as energy consumption, range, emissions, and component sizing without requiring the extensive computational and experimental resources that are required to build a more dynamic model that can account for rapid transient effects. This is typically appropriate for backwards simulations because they are used when uncertainty regarding component specifications is high and dedicating resources to building a more dynamic model would not align with the high degree of uncertainty typical of the stage in the vehicle analysis process when backwards simulations are typically used.

Figure 1.7 presents the information flows in a common backwards simulation for an EV. Note that in a backwards model, the simulation begins with the user inputting a drive cycle (a trace of velocity as a function of time) along with certain vehicle parameters to enable the calculation of the forces the vehicle must overcome in order to perfectly meet the drive cycle [32]. The simulation takes these inputs and calculates the amount of power (and torque and speed where appropriate) that must be produced by each successive component – from the wheels to the gearbox to the motor to the energy storage system, in the case of an electric vehicle for instance. The simulation progresses by moving backwards from the wheels through the rest of the powertrain, and at each component the simulation factors in the efficiency of that component before sending a power or torque and speed request to the next component [31]. Each component in the powertrain requires a means for determining its efficiency. The efficiency can be fixed, in which case it is usually set by the user in advance, or varying, in which case it is usually determined over the course of the simulation via a modeling process.

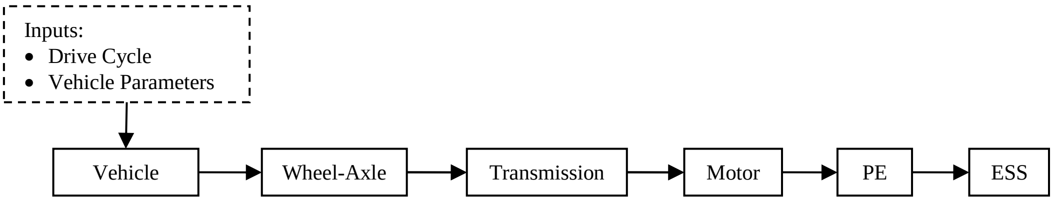

Figure 1.7: The information flows in a backwards simulation for an EV

The primary strength of backwards modeling is that it can determine how different drive cycles, vehicle parameters, and component efficiencies affect component sizing and vehicle energy consumption [32]. The components do not impose any limits on the simulation. Rather, they merely record what was asked of them before passing along a request that accounts for their own losses to the next component. The fact that backwards simulations do not impose any limitations on the performance of their components may appear to be a deficiency, but actually it is a unique advantage because it allows the user to obtain each component's maximum sizing requirements. For example, through a backwards simulation the user will gain an understanding as to what torque and speed ratings the motor will need and what power and energy specifications the energy storage system will need. This can enable the user to then select technologies that meet these criteria. If technologies do not exist that would meet these criteria, then backwards modeling can help to estimate how the technologies will have to improve to meet current design objectives or how the design criteria will have to be modified to work within current technological constraints.

The primary weaknesses of backwards simulations are that they cannot enforce performance limits, and they do not allow for control. Real components certainly have performance limits, and their absence in a model is unrealistic. However the absence of performance limits is a necessary tradeoff such that backwards models can provide component sizing estimates. This often means that higher-fidelity models are less useful in backwards models, given the fact that backwards models are intended for use in scoping generally across broad technological categories, and not with narrowly simulating a specific product highly accurately. The inability of backwards models to allow for sophisticated control stems from the fact that backwards simulations run in an open loop with no feedback. This weakness is also a necessary compromise in order for the backwards models to handle the high level of uncertainty at the early stages of the vehicle design and analysis process, which is when backwards simulations are typically used [33]. In fact, the simplified models in backwards simulations can be viewed as a strength when issues such as minimizing the computational and experimental complexity necessary to run and derive these models is a priority.

At the time OVEM was completed, as far as the author was aware, there were no commercially available backwards simulation packages. Several groups had designed backwards simulation techniques for their own research purposes [31] [34]; however, they have never been readily available. Therefore, the lack of a widely available tool for performing backwards simulations of EVs and HEVs made it difficult to obtain the type of component scoping and vehicle performance estimates that backward modeling is well-suited to provide.

Backwards simulations had the potential to meet several of the criteria set forth in Section 1.5. Foremost, backwards simulations meet Criteria #2 in that they facilitate scoping exercises across many different component technologies and sizes. As a class of simulations, they enable estimates for figures such as energy consumption, range, cost, and emissions to be obtained. By extension, backwards simulations meet Criteria #1 in that they can rapidly simulate existing and emerging technologies. Backwards simulations also meet criteria #3 in that their component models are well-suited to the timescales and conditions of interest. Backwards simulations will likely not meet the accuracy objectives of Criteria #4. Backwards simulations are built to sift through high uncertainty to perform component scoping and sizing estimations. Therefore, they are not built to obtain results that necessarily meet stringent accuracy requirements. Nevertheless, given that backwards simulations strongly meet three of the criteria set forth in Section 1.5, they will have a place in the novel vehicle modeling program considered in this study.

It should be noted that in late 2010, once OVEM was completed [35] [36] [37], Argonne National Laboratory announced the release of a new program called Autonomie that incorporated elements of a backwards modeling approach [38]. While precise details regarding the inner workings of Autonomie were unable to be obtained, the fact that OVEM now had a competitor in the backwards modeling space was viewed as a testament to its value as an advanced powertrain modeling tool.

1.6.2.2 Forwards Modeling

Forwards vehicle modeling simulates the flow of information as it actually occurs in vehicles on the road [39]. It begins with a drive cycle which is fed into a driver model that is meant to represent a human driver. The driver model responds to the speed requests of a drive cycle just like an actual driver would respond to road conditions – by applying the throttle and brake in appropriate measure [31]. The throttle command gets sent to a motor model which uses it to compute the amount of torque it will output and the amount of energy it will consume. The torque produced is passed along to the transmission which factors in its own efficiency and gearing effects. Finally the amount of torque that the vehicle can supply is passed to a model for the wheels which outputs the speed the vehicle was able to achieve. Figure 1.8 shows a diagram for the information flows in a common forwards-looking model for an EV.

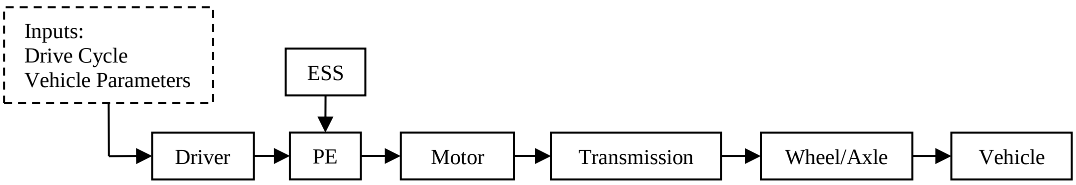

Figure 1.8: The information flows in a forwards simulation for an EV

The strength of forwards simulations is their ability to account for the dynamic processes taking place in a vehicle. They allow for the analysis of the transient response of powertrain components as they react to throttle and brake inputs. This enables the development and testing of effective vehicle controllers with a high degree of resolution [32].

However, accounting for the dynamic processes in a vehicle is also the source of the weaknesses of forward-looking simulations. Forwards simulations rely on solving a system of ordinary differential equations to model the dynamic processes in a vehicle [31]. Obtaining accurate data for the dynamic processes of all the components in a powertrain is typically expensive and time-intensive [26], especially when developing a library of components that can be arranged in different configurations and tested against each other is a priority. Such detailed models, while accurate, can often be inflexible which can be a detriment when attempting to model new technologies which weren't envisioned when the program was designed. Additionally, having to solve systems of differential equations and complex models concerned with small-timescale transient effects adds significantly to the computational complexity of forwards modeling. It is common for the runtime of forwards simulations to be several orders of magnitude higher than other energy flow simulation methods [40]. While forwards simulation is a useful tool, in applications where its high-resolution capabilities are not necessary for tasks such as controller design, its high degree of fidelity can be a detriment that can make the program inflexible and overly computationally and experimentally demanding. Examples of forward-looking simulation tools are CAPSIM (Center for Automotive Propulsion Simulation) [41], PSAT (Powertrain Systems Analysis Toolkit) [42], and AVL Cruise [33] [43].

In assessing forwards simulations against the criteria in Section 1.5, the following conclusions were drawn. Forwards simulations fail to meet Criteria #1 on the grounds that they struggle to *rapidly* simulate component technologies. The runtimes for forwards simulations can be orders of magnitude longer than other energy flow simulation techniques, especially without extensive computational resources. Additionally, the parameters generally required by their component models are not readily available (especially for new technologies) and must therefore be experimentally obtained. Such experiments require time and resources which would work against the goal of rapid simulation. Forwards simulations also have a limited ability to cope with new technologies which may not have been envisioned when the program was designed. Forwards models could meet Criteria #2 in that they would be able to provide estimates for figures such as emissions, energy consumption, and range. However, their ability to scope across an array of existing and emerging technologies is limited given the difficulties explained above in adding new technologies and capabilities to their functionality. Forwards simulations generally don't meet Criteria #3 because their timescales are usually orders of magnitude smaller than those of interest to a novel vehicle modeling effort. Forwards simulations should be able to meet Criteria #4 in that they should be able to produce figures to within 2-5% of real-world accuracy.

Given that forwards simulations failed to meet several key aspects of the criteria for a novel vehicle modeling program, it was decided that they should not be included in the novel vehicle modeling effort.

1.6.2.3 Backwards-Forwards Modeling

Backwards-forwards modeling is a method for simulating the energy flows in a vehicle that operates as a type of hybrid between backwards and forwards modeling. Its goal is to simulate actual vehicle performance using high-fidelity models without requiring lengthy computation times [28]. A backwards-forwards simulation uses information flows similar to those in a backwards simulation; however it imposes actual physical constraints on the performance of its powertrain components and can calculate the components' efficiency using either a fixed or varying approach. A backwards-forwards simulation also combines elements of a forwards simulation, in that it can perform realistic energy flow modeling (with high-fidelity models and performance limits) and high-level controller design. Yet unlike forwards simulation, backwards-forwards simulation is not used for more detailed controller design.

A backwards-forwards simulation begins identically to a backwards simulation in that the torque and speed needed to be produced by the wheels are calculated and then passed to the transmission where losses and gearing effects are applied before the torque and speed requests are passed to the motor [28]. This process continues, with each component factoring in its losses and physical limits, until the simulation can proceed no further in the backwards direction. For an electric vehicle, this occurs at the energy storage system. The forwards part of the simulation begins when the energy storage system outputs how much power it is actually capable of producing. The forwards part of the simulation carries the amount of power the vehicle was able to produce through the powertrain with each component once again factoring in its own efficiency and physical limitations until the speed the vehicle was capable of achieving is outputted from the forwards vehicle block. Figure 1.9 shows the information flows for a common backwards-forwards simulation for an electric vehicle.

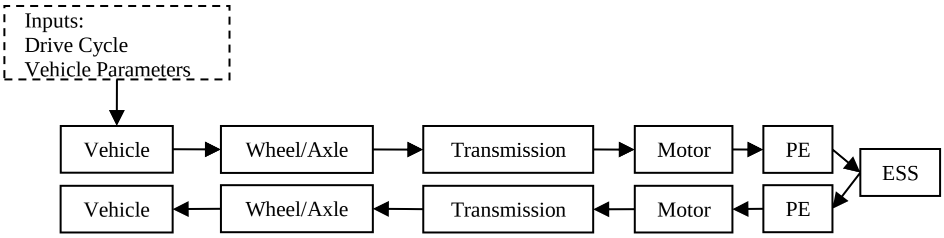

Figure 1.9: Schematic of a backwards-forwards simulation for an EV

The primary strength of backwards-forwards simulation is that it has the advantage of being able to realistically model powertrain performance without the computational and experimental demands of forwards models [31]. Backwards-forwards models can be based on data from real components. This enables them to be flexible and updatable. Backwards-forwards simulations are also useful for producing figures for energy consumption, emissions, range, and cost without having to handle the additional fidelity required by simulations concerned with high-resolution controller design.

Backwards-forwards modeling has several weaknesses. It generally uses a quasi-steady-state simulation method to facilitate its more rapid runtimes and use of models without parameters requiring extensive experimental resources; so it may overlook transient processes that happen on small timescales. Thus, a backwards-forwards simulation may not capture all of the transient effects that would be modeled by a forwards simulation. This means that backwards-forwards simulations generally cannot be used in high-resolution controller design [26]. However, if the user is not concerned with a level of detail that will facilitate detailed controller design, and is content with still being able to model the high-level behavior of the controllers [31], then backward-forwards modeling can be a useful technique.

Backwards-forwards simulations were assessed against the criteria outlined in Section 1.5. Backwards-forwards simulations meet Criteria #1 because they can rapidly simulate and incorporate existing and emerging technologies and capabilities. The runtimes for backwards-forwards simulations are low, thereby mitigating the need for extensive computational resources. Their component models do not need parameters that would typically have to be derived experimentally. Since backwards-forwards simulations have a flexible structure, they can be useful in component sizing and capability scoping. As an energy flow modeling technique, they can produce estimates for emissions, energy consumption, cost, and range. Therefore, backwards-forwards simulations meet Criteria #2. Backwards-forwards simulations, with their quasi-steady-state structure, are well-suited to the timescales and conditions set forth in Criteria #3. Backwards-forwards simulations also have a record of delivering results that meet the accuracy objectives of Criteria #4 [40].

Given that backwards-forwards simulations meet all four of the criteria from Section 1.5, it was determined that a novel vehicle modeling program would benefit from incorporating a backwards-forwards modeling approach. However, existing backwards-forwards vehicle modeling programs exist – most notably, ADVISOR. So the question for a novel vehicle model becomes one of trying to identify areas where ADVISOR is deficient in meeting the listed criteria. A thorough analysis of ADVISOR showed that it was in fact deficient in several areas that affect its suitability with the listed criteria.

ADVISOR’s first area of deficiency concerns Criteria #1 and #2. ADVISOR has limited ability to incorporate new technologies and capabilities that are not already a part of its existing library and structure. As an example of its limited ability to handle new technologies, ADVISOR does not have a high-speed flywheel model, and trying to incorporate one as a retrofit would be prohibitively difficult. New capabilities – such as hybridized energy storage systems, advanced energy management strategies, in-wheel motors, and front, rear, all-wheel driving, and the ability to account for load transfer – are also something that is beyond the functionality of ADVISOR. Trying to add such capabilities would also be prohibitively difficult. Since all of these components and capabilities are beyond ADVISOR's scope, there is clearly room for a novel vehicle modeling program to better meet Criteria #1 and #2.

ADVISOR largely meets Criteria #3 in that its timescales and conditions are in line with those that would be sought from a novel vehicle modeling effort. However, ADVISOR does not have the ability to account for changes in elevation. Given the role that changes in elevation can play in affecting the range, energy consumption, and emissions of electric and hybrid electric vehicles, a new vehicle modeling program would make a novel contribution by including such functionality.

ADVISOR's capacity to meet Criteria #4 is limited and varied. For ADVISOR either does not have models or has models of insufficient fidelity in key areas that detract from its ability to meet the Criteria #4 accuracy goal for a wide range of technologies and capabilities. For instance, ADVISOR assumes that the efficiency of its fixed gearbox and epicyclic gear train is constant, when existing literature shows that this assumption is overly simplified [44] [45]. ADVISOR also makes a simplifying assumption in calculating the final speed a vehicle will achieve based on the amount of power it generated in order to avoid using more complicated equations. ADVISOR employs a number of other simplifying assumptions particularly in its energy storage system models that will be identified in detail in the dissertation (Sections 4.6.1 and 4.6.2). Making improvements in these areas where

ADVISOR makes simplifying assumptions by making the models more complex will constitute a novel contribution to energy flow simulation accuracy. They key for a novel vehicle modeling effort using a backwards-forwards approach is to improve upon the accuracy deficiencies of ADVISOR while still upholding the other listed criteria.

For the reasons outlined above, it appeared that a novel vehicle modeling contribution could be made by incorporating a backwards and backwards-forwards approach. The following section will examine the steps behind creating this new vehicle modeling program.

1.7 Constructing a Novel Vehicle Modeling Program

In the preceding section it was concluded that a novel vehicle modeling program seeking to best meet the listed criteria of Section 1.5, should include both backwards and backwards-forwards models. The next step was then to determine the optimal manner in which a single program could incorporate both backwards and backwards-forwards model(s).

In order to guide the thinking about how to best integrate these two modeling approaches into a single package, it is helpful to imagine these modeling approaches as existing along a spectrum going from high uncertainty and low fidelity on one end to low uncertainty and high fidelity on the other end. At the high uncertainty, low fidelity end, the ability to conduct scoping and sizing exercises to reduce that uncertainty is key – making it well-suited for a backwards simulation. At the other end of the spectrum, where fidelity is high and uncertainty is low, a backwards-forwards approach would be more appropriate since the focus is on utilizing the low uncertainty to produce accurate results.

From the user’s perspective, backwards simulations are most useful in performing technology scoping and component sizing estimations across an array of technologies and components. At this stage in the vehicle design and analysis process, uncertainty is high, and the user is seeking to gain a greater understanding about which technologies and components, and in what sizes, will enable a vehicle to meet its performance objectives (in this case in regards to energy consumption, emissions, and range). At this stage in the vehicle analysis process, the user values a model's ability to cope with a large degree of uncertainty in order to guide future thinking about vehicle analysis. When a user has progressed to using backwards-forwards models, uncertainty regarding component specifications has been reduced, and the user is now interested in accurately modeling specific technologies and products in a powertrain to credibly see how such a powertrain would actually perform. In such a case, the user values credible results using real-world data. This section will explore how OVEM balanced both the technical capabilities of backwards and backwards-forwards models with their ability to add value to the user in order to arrive at a single package that best met the objectives set forth in Section 1.5.

First, the issue of how to best integrate backward model(s) into a single package was addressed. The component models in backwards simulations can be based on either a fixed or varying efficiency [32]. Representing components as fixed efficiencies is obviously the simpler case. It may appear to be overly simple; however, during initial design stages, uncertainty regarding component specification and selection can be high and having a simple model to match that high uncertainty can be advantageous for representing technologies in an approximate manner. For these reasons, it was determined that a backwards models with fixed user-specified component efficiencies would be included in the novel vehicle simulation package.

Yet as was noted above, representing components as having fixed efficiencies is a simplification of actual component behavior. Fixed efficiencies would be suitable and valuable when uncertainty regarding vehicle design and analysis was at its highest, but given that backwards models can represent component efficiencies as varying, the opportunity to develop a backwards model with varying component efficiencies was explored.

A backwards model with varying component efficiencies would theoretically be able to produce more credible results than a backwards model with fixed efficiencies; though these more credible results would require a reduced uncertainty in order to meaningfully model the varying efficiencies of the components. This lead to the key question in the development of a backwards model with varying efficiencies: how to best vary the component efficiencies.

The efficiencies needed to vary in a physically meaningful way if they were to produce useful results. Thus, three options were available. The varying efficiencies could either be determined by being based on readily available product data, experimentally obtained data, or through modeling the physical principles governing a component's efficiency [46]. Basing the efficiencies on readily available product data was problematic because of the fact that the purpose of backwards simulations is to refrain from modeling specific products. Committing to specific products violates the mission of backwards simulations which are meant to be used in scoping and sizing exercises to estimate which types of technologies would ultimately be used in a vehicle. For instance, a backwards model imposes no performance limits so that component sizing estimates can be obtained. For a motor, this would mean imposing no torque and speed limits. However, data from an existing motor would naturally have performance limits which would clash with the objectives of backwards modeling. Varying the efficiencies based on experimentally-obtained data requires a measure of experimental resources that is not commensurate with the high degree of uncertainty still present at this stage in the simulation process. On the other hand, models based on well-understood physical principles would be able to simulate the behavior of components across broad technological categories in a meaningful way without committing to specific products. Such an approach would enable the user to take only a vague conception of the component and apply its general physical principles in a physically meaningful way to rapidly arrive at approximate sizing and scoping estimates. This is valuable for a backwards simulation because it allows the model to maintain a product-independent structure that is valuable for backwards simulations (and the stage in the vehicle design process when backwards simulations are used).

For these reasons, it was decided that another backwards model should be created in the novel vehicle modeling program – where the efficiencies vary based on general, well-understood physical principles. This would enable this varying-efficiency backwards model to simulate components with a higher fidelity than the fixed-efficiency approach while still retaining its scoping and sizing capability by not committing to data from specific products.

From the user's perspective, a simulation approach that models physical effects in a technologically-relevant but product-independent manner is valuable in a backwards simulation. It allows the user to take the initial sizing and scoping estimates obtained from Level 1 – when uncertainty was highest – and refine those estimates using a physically-meaningful approach without committing to a specific technology or product. A backwards approach that varies its component efficiencies in this manner clearly has value in the vehicle design and analysis process, and it was thus included into the novel vehicle modeling program.

With a basis for implementing both a fixed and varying efficiency backwards model, the focus then turned to the issue of constructing an optimal backwards-forwards model. From the user's perspective a backwards-forwards model adds value by being able to model component efficiencies with high fidelity and accuracy in order to produce credible results. A backwards-forwards model is typically utilized once the backwards models have been used to obtain an estimate as to the types of technologies and products that would enable a vehicle to meets its design objectives.

The primary question governing the development of a novel backwards-forwards simulation was the manner in which it should model component efficiency. A backwards-forwards simulation is typically used when uncertainty is low and the need for accuracy is high. So for a backwards-forwards simulation, representing component efficiencies as being fixed is too simple. Instead, the component efficiencies need to vary based on the vehicle's characteristics and the manner in which it is being driven (similar to how component efficiencies actually vary). At this point, the listed criteria for a novel vehicle modeling tool were called upon to guide the thinking behind crafting the new backward-forwards component models. Criteria #1 stated that it was a priority for the program to rapidly incorporate and simulate existing and emerging technologies and capabilities, and Criteria #4 specified that this program needs to do so accurately. There are two broad options available to derive the parameters necessary to accurately model real technologies. The first is to rely on information about these technologies that is generally readily available. This enables the technologies to be incorporated and simulated quickly and accurately without requiring extensive experimental and computational resources [26]. The second option is to experimentally derive the parameters necessary to operate a model with a varying efficiency. Experimentally deriving these parameters can be costly and time-consuming, perhaps prohibitively so, especially when data from cutting-edge and expensive components is sought. Therefore, experimentally deriving these parameters clashes with the larger goal of being able to quickly incorporate and simulate new technologies and capabilities. For this reason, it was determined that the component models in the backwards-forwards simulation should be based on readily available data.

A backwards-forwards model based on readily available data from real components can add significant value to the user. When such a backwards-forwards model is integrated into a single package with the two types of backwards models explained above, this single package would meet the criteria outlined in Section 1.5 and would be a significant, novel contribution to the vehicle modeling landscape.

1.8 The Oxford Vehicle Model (OVEM)

In the preceding section, the basic philosophy and structure of three distinct modeling approaches were identified that together met the listed criteria of Section 1.5 in a way that has the potential to add significant value to the landscape of vehicle modeling. The first modeling approach was a backwards simulation based on component models with fixed efficiencies. The second was a backwards simulation with component models where the efficiencies vary based on general physical principles. The third was a backwards-forwards simulation where the component efficiencies would be drawn from models based on readily available data. These modeling approaches were named Levels 1, 2, and 3, respectively, in what came to be known as the Oxford Vehicle Model (OVEM).

As OVEM was built, it was imperative that each level maintained a consistent philosophy throughout so that each level adhered to the relevant initial criteria that spurred its development in the first place. Implicit in the application of the four criteria of Section 1.5 to the construction of the novel program spelled out in Section 1.7 are three non-criteria that deserve special mention as they run in opposition to the four criteria of Section 1.5. These non-criteria are modeling issues that fall outside of the scope of OVEM given its primary four criteria. Since these three non-criteria will be applied to all three levels of OVEM, it is most appropriate to discuss them at this stage.

The first non-criterion is that the component models will not directly account for thermal effects. This non-criterion was implemented because information on the thermal behavior and properties of powertrain components is rarely readily available. It was thus determined that thermal behavior could not be accounted for the interest of aligning with the Criteria #1 objective of facilitating rapid simulation of existing and emerging components.

The second non-criterion is that the component models will only model the bulk properties of each powertrain component and will not be concerned with individual variations that might occur in the various sub-components. For instance, the battery model will assume that each cell in the module will behave in exactly the same manner. This is a simplification, as manufacturing imperfections and operating conditions can lead individual sub-components to behave in a manner that is out of line with their bulk component properties. However, information on sub-component performance variations and manufacturing tolerances is rarely readily available. Since such information is not readily-available, directly accounting for sub-component variations was deemed beyond the scope of OVEM.

The third non-criterion is concerned with accessory loads. Accessory loads are those power losses that are incurred by powering the ancillary equipment in a vehicle that is not directly responsible for the tractive force generated by the vehicle. For instance, the pumps that serve a fuel cell would be an accessory load. Information on accessory loads for powertrain components is rarely readily available, thus directly accounting for them was deemed to be outside of the scope of OVEM.

With the non-criteria established, the remainder of this section revisits the four criteria that motivated the development of OVEM to present how these four criteria governed the creation of each level in OVEM.

1.8.1 Level 1

Level 1 utilizes a backwards modeling approach where the component models are based on a fixed efficiency which is set by the user based on the user’s particular component sizing and scoping questions. The fixed efficiency approach enables the component models to rapidly assess an array of technologies (Criteria #1) especially at a stage in the analysis process when uncertainty is likely to be high. The fixed efficiency approach enables the calculation of energy flows affecting values such as vehicle energy consumption, emissions, range, and component sizing and cost (Criteria #2). The fixed efficiency approach of the component models is in line with the timescales and conditions of interest (Criteria #3). The primary downside to the Level 1 model is that its accuracy can be low (Criteria #4) since it employs models with such low fidelity. But as was noted above, obtaining highly accurate results via high-fidelity models is not the focus of the Level 1 model. Instead, its focus is on scoping and sizing a wide array of components.

1.8.2 Level 2

Level 2 uses a backwards modeling approach where the component models use a varying efficiency which is based on an application of general physical principles regarding broad technology types. The fact that the models are based on general physical principles governing an array of technologies enables for the rapid simulation of different technologies (Criteria #1). As a backwards model, it is suited towards performing component scoping to help determine parameters such as energy consumption, range, emissions, cost, and sizing (Criteria #2). The models are built so as to reflect the timescales and conditions of interest (Criteria #3). As a backwards simulation, accuracy is not a priority; therefore, the program is not concerned with meeting the Criteria #4 accuracy objective. However the models still seek to model the efficiency of the components in a physically meaningful yet product-independent way that should have a higher fidelity and accuracy and lower uncertainty than Level 1. The fact the models in Level 2 are product-independent is also crucial during the scoping and sizing exercises for which backwards simulations are primarily employed.

1.8.3 Level 3

Level 3 is a backwards-forwards model, and as such it is the modeling approach in OVEM with the lowest uncertainty and highest accuracy. Level 3 enables the rapid simulation of existing and emerging technologies by basing its component models on readily-available data from actual products and systems (Criteria #1). In meeting this criterion, Level 3 seeks to reduce computational and experimental complexity to facilitate the rapid simulation of these powertrains. Level 3 is constructed in such a way that it allows for a library of components and capabilities so that scoping across many different dimensions can be performed to deliver figures for energy consumption, emissions, range, cost, and sizing (Criteria #2). The Level 3 component models are based around the timescales and conditions of interest (Criteria #3). Accuracy is an important criterion for Level 3, so it was developed in such a way as to meet the accuracy objective of Criteria #4.

1.9 Overview of Dissertation

This introduction has described the motivation for constructing a novel vehicle modeling program, OVEM, capable of simulating the energy flows in a new and rapidly evolving class of automobiles. Based on a survey of the existing vehicle modeling landscape, it has identified the criteria that OVEM should adhere to in order for it to make a novel contribution to the field. OVEM's unique modeling structure consisting of three distinct "levels" – incorporating backwards and backwards-forwards modeling techniques – was proposed to enable OVEM to meet these criteria. Levels 1, 2, and 3 are each based on their own modeling philosophy, and the following three chapters (Chapters 2, 3, and 4, respectively) explore the rationale behind the construction of the constituent parts of each level's models as well as presenting the inner workings of the three levels.

Chapter 2 presents Level 1 which is a backwards model where components are represented as fixed efficiencies. Chapter 3 describes Level 2 which is a backwards model where the components are modeled by efficiencies that vary in physically meaningful ways that are independent of any specific technology. Chapter 4 presents Level 3 which incorporates models based on data from real-world components to simulate how an actual vehicle would perform with high-fidelity models enforcing performance limits. Chapters 2, 3, and 4, each present a case study where OVEM was used to provide concrete examples of its capabilities. At the end of Chapters 2, 3, and 4, a summary of the novel contributions made by each of the levels is also presented. The following section in this chapter (Section 1.9.1) provides an overview of the novel contributions made throughout this thesis.

Following the thorough description of OVEM's operational characteristics and capabilities, Chapters 5 and 6 present detailed case studies based on two of the three journal-published articles by the author that demonstrate the novel contributions to knowledge made possible by applying OVEM towards the analysis of electric and hybrid electric vehicles [35] [36] [37]. The criteria spurring OVEM's creation called for a vehicle modeling program capable of rapidly simulating new and existing technologies – partly to facilitate scoping comparisons across metrics of interest such as energy consumption, emissions, and range. Chapter 5 does just that by using OVEM to make the novel comparison between high-speed flywheels, ultracapacitors, and lithium-based batteries functioning as the energy storage system in a fuel cell based series hybrid. It was ultimately shown that high-speed flywheels merit consideration alongside of lithium-based batteries and ultracapacitors as feasible options for onboard energy storage in series hybrids. Chapter 6 demonstrates OVEM's ability to provide accurate scoping comparisons for vehicles using advanced technologies across a range of topologies. In this study, OVEM was used to compare the tank to wheel CO_2 emissions from advanced electric and plug-in hybrid powertrains to those from a conventional vehicle based on an internal combustion engine by using a single vehicle platform. The key results of this study quantitatively demonstrated the novel insight that plug-in hybrids have the potential to have fewer tank to wheel emissions than electric and conventional vehicles in regions where the grid-generated electricity is CO_2 intensive.

Chapter 7 is the final chapter of this thesis, and it provides a recapitulation of the work presented throughout the thesis. It also recounts the specific contributions made in this thesis along with how these contributions were developed, and presents an outlook for future work that can be done with OVEM.

1.9.1 Overview of the Specific Contributions of this Dissertation

The novel contributions of this dissertation span the breadth of OVEM. This section provides an overview of these novel contributions in advance, with reference to where a more detailed discussion of them can be found in the body of the text, so that they can be more easily identified and understood during a reading of the entire dissertation.

This section will first discuss the novel contributions made by the constituent component and capability models of OVEM and how these contributions were developed. Then this section will discuss how these individual contributions combine into the broader contribution of OVEM – providing a view on the novel contribution of OVEM as a whole program. This section will then conclude with a discussion of the contributions made via the application of OVEM to real-world questions.

Level 1 makes four unique contributions with its capability and component modeling techniques. All four of these contributions appear in Levels 2 and 3 as well (with a degree of fidelity commensurate with the rest of that level's vehicle model). However, since the first incarnation of these techniques appears in the Level 1 program, they will be discussed as part of Level 1.

The first two novel capabilities of the Level 1 program are the ability to model multiple tractive electric motors (Sections 2.4, 3.4, and 4.4) and hybridized energy storage systems (Sections 2.6, 3.6, 4.6, and 4.9). Both of these capabilities are concepts that are recently emerging alongside the rise in electric and hybrid electric vehicles – as they were largely unexplored in a field dominated by the internal combustion engine. Though both of these capabilities have been discussed in the literature as concepts, no energy flow vehicle modeling programs have been built with these functionalities [40]. Thus, the novel work in this study came in turning these new concepts into a series of algorithms and modeling techniques that could be used in OVEM. For instance, the author did novel work in creating Equation 4.73, which was used to control the energy flow between hybridized energy storage systems in a speed-based energy management system.

The other two novel capabilities introduced in the Level 1 program came with the rolling resistance model and the ability to account for slope in the drive cycle (refer to Section 2.1 for a more detailed discussion on these topics). With both of these functionalities, an existing knowledge base was leveraged to turn the concepts into practical realities in OVEM. In the case of modeling rolling resistance, existing energy flow vehicle models had incorporated some means of accounting for rolling resistance; however, their approach was overly simplified and did not account for the effect that vehicle speed has on rolling resistance [40]. A survey of the literature was conducted, and empirical work on measuring rolling resistance was found. The results of this existing empirical work (Equation 2.11 and Figure 2.4) had never been adapted for use in an energy flow vehicle model [26] [40], so the author's contribution of deriving this work into an algorithm capable of functioning within the structure of OVEM was novel. This required novel programming to create the interpolation techniques and coding loops in the model to enable these empirical findings to actually work towards more accurately modeling rolling resistance.

Existing energy flow vehicle modeling programs did not include the ability to account for slope [26]. This is an important omission as electric and hybrid electric vehicles have the ability to benefit from modeling slope since they can recapture energy during descents. To incorporate slope into OVEM, standard Newtonian equations of motions were derived (Equations 2.5, 2.6, 2.8, 2.10, 2.12, and 2.13) and then adapted for use within OVEM. The novel work came in adapting these derivations for use within OVEM. A particularly unique feature of this adaptation came from the author's realization that these equations accounting for slope needed to be a function of distance traveled, rather than time elapsed, to account for a scenario in which the vehicle was not able to meet the sloping drive cycle requested of it. Structuring these functions in this way was unique in that it ran counter to the structure of the rest of OVEM and other existing energy flow vehicle modeling programs [40].

Level 2 has its own set of novel component modeling contributions. The first of these was the gearbox model. Existing energy flow vehicle modeling programs had gearbox models; however, they made the simplifying assumption that the efficiency of the gearbox was constant [26] [40]. Empirical evidence shows that this is not the case, and that gearbox losses are affected primarily by its design (gear ratio and seal, bearing, and meshing losses) and the load it is transmitting [44] [57]. So OVEM leveraged this empirical evidence to devise the backwards gearbox modeling technique explained in Section 3.3. The novel work in this regard came in creating Equation 3.2 based on this existing empirical work and in programming the algorithms required to enable Equation 3.2 to function with OVEM.

The rest of the novel component modeling techniques in the Level 2 program came from the motor, power electronics, and energy storage system models (Sections 3.4, 3.5, and 3.6, respectively). The existing body of knowledge on each of these components was leveraged to understand how their primary loss mechanisms could be modeled in a manner that was physically meaningful yet general enough to be product-independent (in accordance with the objectives of Level 2). However, understanding the primary loss mechanisms was only the first step in devising the models. Novel work was conducted by the author to create the equations to actually model these components' efficiency (Equations 3.6, 3.11, and 3.12) – for while the concepts upon which they are based are well-understood, their derivation was entirely novel since it was done to enable physically meaningful efficiency calculations across a range of products. Novel work was also done to create the methodology, in its entirety, that enables the coefficients for Equations 3.6, 3.11, and 3.12 to be calculated (refer to Sections 3.4.1, 3.5.1, and 3.6.1 for more information).

The Level 3 model features eight novel contributions from its component and capability models. The first of these capabilities is the load transfer model (for more information refer to Section 4.1.1.3). Load transfer in vehicles is a well-understood phenomenon with an existing body of knowledge. However, it is a phenomenon that has been overlooked by energy flow vehicle models. Load transfer can significantly impact electric and hybrid electric vehicles – namely via the amount of energy capable of being captured through regenerative braking. For this reason, the Level 3 model in OVEM was designed with the capability to model load transfer. In building this capability into OVEM, the existing body of knowledge on load transfer was leveraged – the derivation of Equations 4.22 to 4.30 existed in the literature. However, the author performed the novel task of accounting for inertia in this derivation. The author also performed the novel task of combining the derivations from Equations 4.22-4.35 with Equations 4.36 and 4.37 to yield Equations 4.38 and 4.39 which enable the energy capable of being recaptured via braking to be calculated (and which are additionally novel in that they also account for inertia). Programming Equations 4.38 and 4.39 into an algorithm capable of functioning within OVEM was also a novel achievement as it had never been done before in an energy flow vehicle modeling program [26] [40].

The second novel contribution of the Level 3 program was concerned with improving the accuracy of calculating the final speed achieved by the vehicle at the end of each time step. Existing energy flow vehicle models made a simplifying assumption on this topic to avoid dealing with the complex quadratic that results from the Newtonian dynamics describing the final speed achieved by the vehicle [26] [40]. OVEM did not want to use this assumption in its attempt to achieve greater accuracy. To go beyond this simplifying assumption, the author performed a novel derivation, based on first principles from the standard Newtonian equations of motion (first described in Section 2.1), in order to improve the accuracy of the calculation to determine the final speed achieved by the vehicle at the end of each time step. This novel derivation required solving the complex quadratic referenced above and is reflected in Equations 4.8 through 4.20. To the best of the author's knowledge, this derivation has not been performed before, thus making it a novel contribution to the field of vehicle modeling. For more information on this novel derivation, refer to Section 4.1.1.2.

The third and fourth novel contributions of the Level 3 model have to do with the gearbox and epicyclic gear train models. Existing energy flow vehicle models included models for a gearbox and epicyclic gear train. However these models, made the simplifying assumption that the efficiency of these components was constant. Empirical evidence shows that the efficiency of these components is not constant and depends on its design (gear ratio and seal, bearing, and meshing properties) and the load it is transmitting [44] [57]. Thus, novel work was done to adapt this existing empirical work into a series of equations and modeling principles that could be integrated into OVEM. For the gearbox, the efficiency equations (Equations 4.40 and 4.41) were novel contributions derived by the author based on the existing empirical findings (Section 4.3). For the epicyclic gear train (Section 4.8), the efficiency relationship shown in Figure 4.39 was a novel contribution derived by the author also based on empirical findings. Turning these equations in programmable algorithms also required novel work, since these relationships had not previously been reflected in energy flow vehicle models [26] [40].

The fifth novel contribution came from the Level 3 ultracapacitor model. Existing empirical and theoretical work on ultracapacitor modeling served as the foundation for the ultracapacitor model in OVEM. For example, the models in Figure 4.12 and Figure 4.14 existed previously and were used to initially frame the structure of the ultracapacitor model.

A truncated version of these existing models was integrated into OVEM (refer to Figure 4.18), such that the model would meet OVEM's computational and experimental complexity criteria [47]. The novel work came in combining this truncated model with the relationship described in Figure 4.20 and Figure 4.21, which models how the capacitance of an ultracapacitor varies with its state of charge. This is a phenomenon which had heretofore not been included in existing ultracapacitor models in energy flow vehicle modeling, so developing the equations to merge the model in Figure 4.18 with the relationships in Figure 4.20 and Figure 4.21, and then translating those equations into a programmable code for an energy flow vehicle modeling program was novel. Refer to Section 4.6.1 for more information on the ultracapacitor model.

The sixth novel contribution of the Level 3 program comes from the battery model. With the battery model, an existing modeling technique (shown in the derivation of Equations 4.64 through 4.69) served as the foundation for the model integrated into OVEM. The novel work consisted firstly of converting these equations into programmable code capable of functioning within OVEM. The novel work also consisted of characterizing an array of battery technologies for use in this model (e.g. the characterized battery chemistries of Figure 4.28 and Figure 4.29). Refer to Section 4.6.2 for more information on the battery model.

The seventh novel contribution came with the high-speed flywheel model. Though non-high-speed flywheel models exist, high-speed flywheel models have not been seen before [31], likely due to the fact that high-speed flywheels are themselves a novel technology. Existing flywheel models were not suitable for describing the losses of high-speed flywheels because they make simplifying assumptions regarding the speed-dependent nature of high-speed flywheel efficiency. Since there were no existing templates on high-speed flywheel models which could be leveraged, OVEM built one from scratch. The author obtained empirical data on high-speed flywheel efficiency through collaborations with a high-speed flywheel manufacturer (Figure 4.30). All of the work to then translate the nature of high-speed flywheel efficiency (described in Figure 4.30) into an OVEM model was novel. This consisted firstly of deriving the algorithms that: input the power request to the high-speed flywheel, assess the operating efficiency of the high-speed flywheel based on its operating conditions, and then output the power the high-speed flywheel was capable of delivering. Then the novel work also consisted of deriving the algorithms to allow the high-speed flywheel to be either mechanically or electrically integrated into the powertrain. Refer to Section 4.6.3 for a more detailed explanation of the novel work required to create the high-speed flywheel model.

The eighth novel contribution of the Level 3 model came as a result of work done to support the fuel cell model (refer to Sections 4.7.2 and 5.2.2 for more information). The author conducted a survey of an array of commercially available fuel cells. From this survey, the author was able to derive two things. The first was a description of the relationship between fuel cell power rating and mass (Figure 5.4). The second was the observation that the power-current and efficiency-current curves describing fuel cell behavior had similar shapes and values across a range of fuel cell sizes when these curves were normalized by the maximum power and current ratings of the fuel cell (Figure 5.2 and Figure 5.3). Both of these observations were novel, and they enabled the fuel cell model in OVEM to be constructed to allow for the continuous scaling of fuel cell size (within realistically defined bounds) rather than relying on the discrete sizes of a few products [40]. This capability made OVEM a more useful component sizing tool - the effects of which can be seen in the case study of Chapter 5.

The above enumeration of the novel constituent parts of OVEM should indicate the degree of novelty underpinning OVEM's development. But OVEM's novelty is more than just the sum of its parts. Each level in OVEM represents a novel modeling approach that was developed to address a current shortcoming of the vehicle modeling landscape. Levels 1 and

2 were the only backwards energy flow vehicle models available at the time of the development of OVEM. With no pre-existing template to follow, novel work was required to develop the modeling philosophies and overarching structures for both Levels 1 and 2. Novel work was also required to define the overall architecture for Level 3 given the extent of new components and capabilities that it introduced (e.g. high-speed flywheel and hybridized energy storage systems). OVEM as a whole also represents a novel achievement for vehicle modeling, as it is capable of addressing a broad array of questions by incorporating models of varying degrees of fidelity and accuracy into a single package to cope with inputs of varying degrees of certainty.

Applications of OVEM's models also produced several new and important contributions. These contributions were presented in three journal-published articles, two of which were presented in this dissertation, as Chapters 5 and 6. The first of these journal-published studies (Chapter 5) made the first published comparison between high-speed flywheels, batteries, and ultracapacitors functioning as the energy storage system in a light-duty hybrid electric vehicle [35]. This study showed that high-speed flywheels could be competitive with batteries and ultracapacitors on the bases of cost and fuel economy.

The second study (the one not presented in this dissertation due to page limit constraints) made the novel contribution of quantitatively comparing the tank to wheel CO_2 emissions for a range of electric vehicles (with varying battery array sizes) to the CO_2 emissions from comparable ICE-based vehicles. This study demonstrated quantitatively that EVs have the potential to have higher tank to wheel emissions relative to similar ICE-based vehicles in regions where the CO_2 intensity of grid-generated electricity is high.

The third study (Chapter 6) used OVEM to predict the CO_2 intensity of electric and hybrid electric vehicles relative to conventional vehicles given the CO_2 intensity of the electric grid in four key countries around the world [37]. OVEM's novel contribution in this regard came in that it was able to make a comparison using a standard vehicle platform across conventional, electric, and hybrid electric vehicles by virtue of its simulation capabilities, even though no single vehicle platform that has conventional, electric, and hybrid variants exists. In this study, OVEM also demonstrated, in a quantitative way, the novel observation that in regions where the CO_2 intensity of grid electricity is high, plug-in hybrids can have lower CO_2 emissions across their entire range than electric and conventional ICE-based vehicles.

2 Level 1 Simulation

The Level 1 simulation in OVEM addresses the challenge of performing scoping and sizing exercises across broad technological categories that could have an application in electric and hybrid electric vehicles. Level 1 is based on a backwards modeling approach where the component efficiencies are fixed. This technique allows for the rapid attainment of first order estimates for figures such sizing, energy consumption, range, emissions, and cost. The Level 1 simulation is concerned with the timescales (approximately 1 s to 10^4 s) and conditions of interest to OVEM (refer to Section 1.5 for more information). It accounts for these timescales by modeling the bulk efficiency of the powertrain components as a fixed value over the course of the drive cycle. It accounts for these conditions by employing straight-line drive cycles (that are normally widely-used in the field) with the ability to account for changes in slope.

The Level 1 simulation employs a low-fidelity approach in order to handle the high uncertainty that typically is customary during early stages in the vehicle design and analysis process (which is when backwards simulations are generally used). As such, it is not as concerned with producing results that meet OVEM's accuracy criteria. Nevertheless, as will be demonstrated in a case study at the end of this chapter (Section 2.8), the results obtained from Level 1 are useful in guiding electric and hybrid electric vehicle design and analysis

Level 1 is based around modular component models. All of the component efficiencies are set by the user and are constant throughout one simulated run through a drive cycle. The models do not attempt to account for the thermal behavior or accessory loads of any of the components. Also, the components are only modeled by their bulk efficiency and no direct consideration is given to the sub-components or accessory loads that may comprise the respective components. This was done in order to ensure that the Level 1 models facilitate the rapid simulation of broad technological categories without committing to any particular technology or product.

Since Level 1 is only backwards looking, it places no constraints on vehicle performance. Instead, it only records the power, and where appropriate torque and speed, requested from each component for each time step over the course of the drive cycle. This facilitates the use of Level 1 in determining component sizing requirements. Figure 2.1 shows a diagram for the Level 1 simulation of an EV. A range of typical efficiency values, inclusive of an array of technologies, for each component in an EV is shown in Table 2.1 [9] [12] [24]; however, the user can enter any efficiencies that may be relevant to the particular set of technologies of interest.

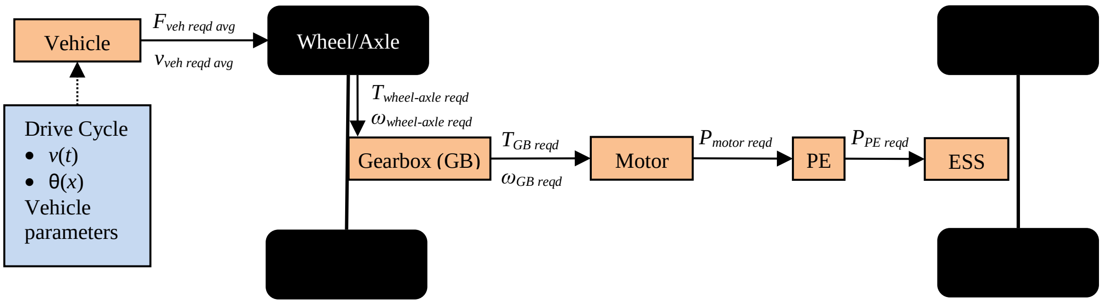

Figure 2.1: Diagram of the Level 1 simulation for an EV

Table 2.1: Typical range of efficiency values for the components in an EV

	Wheel-axle	Gearbox	Motor	PE	ESS
Efficiency Range	98%-99%	95%-98%	50%-95%	90%-98%	70%-95%

The Level 1 simulation has the ability to simulate vehicles with and without regenerative braking. It can also simulate vehicles with one, two, or four tractive motors functioning with or without gearboxes. Below is a description of each block and the information flows between those blocks in the Level 1 simulation for a two wheel drive electric vehicle with one motor (currently the most common form of EV).

2.1 Vehicle Block

The purpose of the vehicle block is to model the forces acting on the vehicle and calculate the force and speed the vehicle needs to produce to meet a given drive cycle.

The vehicle block begins by accepting the drive cycle as a user-specified input. The drive cycle is selected by the user from an easily-updatable library. In keeping with OVEM's timescale criteria, its default time step is one second. One second is also the standard time step for industry standard drive cycles. For more information on drive cycles, refer to Section 2.1.1.

The vehicle block calculates the linear speed the vehicle must achieve, $v_{veh\ reqd\ avg}$, by averaging the velocity requests at the beginning and end of the current time step

$$v_{veh\ reqd\ avg} = \frac{v_{req,i} + v_{req,i+1}}{2}. \tag{2.1}$$

The acceleration the vehicle must achieve over each time step is calculated according to

$$a = \frac{v_{req,i+1} - v_{req,i}}{t_{i+1} - t_i} \tag{2.2}$$

as seen in Figure 2.2. The velocity and acceleration requested by the vehicle block are calculated in this manner in order to negotiate an appropriate balance between computational runtime and accuracy. For instance, it would be possible to divide the velocity requested by the drive cycle into finer timescales; however, past work has shown that for backwards and backwards-forwards simulations such timescales add to the runtime without adding to the simulation's accuracy [40] – especially when considering the timescales and driving conditions of interest to OVEM. On the other hand, stretching the timescales such that

$$v_{veh\ reqd\ avg} = v_{req,i+1} \tag{2.3}$$

and

$$a = \frac{v_{req,i+2} - v_{req,i}}{t_{i+2} - t_i} \quad 2.4$$

positions the simulation to not fully account for the transient fluctuations in velocity requested by the drive cycle. As can be seen in Figure 2.2, an approach based on Equations 2.3 and 2.4 would send an acceleration request that would miss the spike in velocity occurring at t_{i+1}.

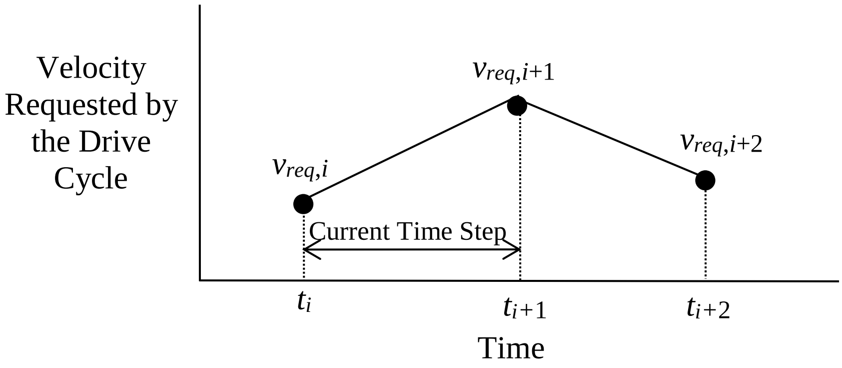

Figure 2.2: Discrete velocity steps in the drive cycle

To determine how to model the forces acting on the vehicle, the vehicle model returned to the criteria set forth in Section 1.5. Since OVEM is only concerned with straight-line travel, the vehicle block was only concerned with forces acting longitudinally on the vehicle. The primary external longitudinal forces a vehicle must overcome are aerodynamic drag, rolling resistance, and slope [12] [47] [48].

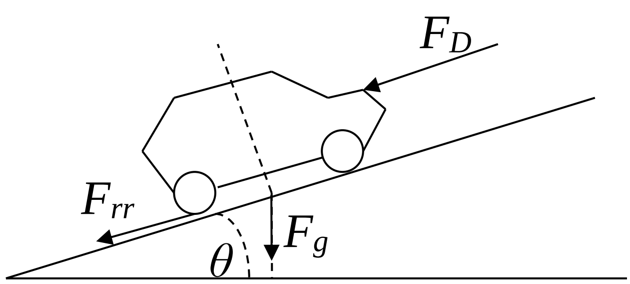

Figure 2.3: Free body diagram of the primary external forces acting on a moving vehicle

Aerodynamic drag is a complex function of air flow acting against the structures making up the external shape of the vehicle. Fully modeling air resistance in a high-fidelity manner would add a prohibitive computational and experimental load to OVEM [47].

Instead, the force due to aerodynamic drag, F_D, can be modeled by the following semi-empirical equation

$$F_D = \frac{1}{2}\rho C_D A_f \left(v_{veh\,reqd\,avg}\right)^2 \qquad 2.5$$

where the drag coefficient, C_D, is an empirically determined constant for a particular vehicle shape, ρ is the density of the ambient air, and A_f is the frontal area of the vehicle [12] [47] [48]. Manufacturers often publish the drag coefficient and frontal area information for their vehicles, and there is a large body of literature regarding drag coefficients and frontal areas for different vehicle types. Thus, this equation conforms with OVEM's goal of facilitating rapid simulation (Criteria #1) in part by using data that is readily available for many different vehicle types.

The force due to gravity is expressed as

$$F_g = mg\sin(\theta)\ . \qquad 2.6$$

where m is the mass of the vehicle, g is the acceleration due to gravity, and θ is the angle of the slope. Note from Figure 2.1, that the requested slope (θ) is calculated as a function of the distance the vehicle has traveled (x) whereas the velocity requested ($v_{veh\,reqd\,avg}$) is computed as a function of time (t). Velocity is expressed as a function of time because that is the customary method in vehicle modeling and real world testing [40] [42]. Slope is calculated as a function of distance because the slope over which a vehicle will be traveling depends more accurately on the vehicle's distance from its origin than on the time elapsed since it departed from its origin (a more comprehensive discussion on slope is included below in Section 2.1.1). This is more relevant in Section 4 when the backwards-forwards simulation imposes physical limits on the powertrain, and the possibility arises that a vehicle may not be able to completely meet the drive cycle. For the Level 1 simulation, this issue is less relevant since all that is being calculated are the requirements placed on the powertrain if it were to completely meet the given drive cycle and slope profile.

The inertia of the rotating components in EVs and HEVs also deserves consideration. OVEM is not concerned with inertia from the perspective of handling since it is only concerned with straight-line travel; instead it is concerned with inertia from the perspective of modeling the forces the vehicle must overcome insofar as they effect vehicle energy consumption, and hence range and emissions. It is difficult if not impossible to fully and accurately account for all sources of inertia in a vehicle. Additionally, the contribution of many sources of inertia in a vehicle are small to the point where their marginal contribution to overall vehicular inertia is negligible, so the user must understand how accounting for inertia aligns with the objectives of the user's current modeling effort [49]. Prior work has shown that in EVs and HEVs the primary sources of rotating inertia are the wheels and tires [49]. Assuming that the moment of inertia of the wheel and tire (J_w) can be modeled as a solid rotating cylinder,

$$J_w = \left(\frac{m_w r^2}{2}\right) n_{wheels} \qquad 2.7$$

where m_w is the mass of the wheel and tire and r is the radius of the tire. The moment of inertia of a single wheel and tire must be multiplied by the number of wheels (n_{wheels}) on the vehicle. The force required then to overcome this inertia is

$$F_{inertia} = \frac{J_w}{r^2} a \qquad 2.8$$

If the user desires to account for additional sources of rotating inertia, OVEM can accommodate that. For instance, depending on the user's application and topology of interest, the inertial properties of the vehicle may more closely resemble those of a conventional, ICE-based vehicle. In such a case, a common technique derived to account for the inertia of a conventional vehicle's rotating components by treating them as an effective mass that scales the curb mass of the vehicle can be used. The equation below is a common technique used to sum the inertia of a vehicle's moving parts and treat them as an effective mass (m_e, which becomes the new mass of the vehicle in the simulation) for a conventional vehicle

$$m_e = m\left(1 + 0.04 + 0.0025{i_G}^2\right) \tag{2.9}$$

where i_G is the highest gear ratio used in the vehicle [12]. This equation is not relevant for pure electric vehicles as the number of moving parts in an electric vehicle is significantly less than in a conventional vehicle. For that reason, if an electric vehicle is being examined, then accounting for the inertia of the wheels has been shown to be sufficient [49]. However it is ultimately incumbent on the user to ensure that OVEM's accounting of inertia aligns with the user's objectives, and OVEM has been built with a structure to facilitate changes to inertial specifications made by the user.

The resistive force due to rolling resistance is a complex function of tire structure, tire material, road surface conditions, tire temperature, vehicle speed, and tire inflation pressure [12]. The complexity and interrelatedness of the factors affecting rolling resistance combine to make it difficult, if not impossible, to account for all of them [47]. The literature was examined to assess different techniques for modeling rolling resistance. In many applications, the rolling resistance force (F_{rr}) is simply modeled by

$$F_{rr} = \mu_{rr} m g \cos(\theta). \tag{2.10}$$

where μ_{rr} is the rolling resistance coefficient, and it is treated as being constant for a particular vehicle over a drive cycle. A common modeling technique is to model the rolling resistance coefficient as a fixed value and tire manufacturers may publish these fixed coefficients for their products. However, this approach does not account for the fact that rolling resistance varies for a particular vehicle, chiefly with speed, so a more advanced representation of rolling resistance was sought.

Similar to aerodynamic drag, the complex nature of rolling resistance can be simplified via a semi-empirical approach where the rolling resistance coefficient varies as a function of tire properties and vehicle speed (note that OVEM assumes that road surface conditions do not affect rolling resistance since OVEM is only interested in travel over dry asphalt as per its interest in industry standard testing conditions) [47]. The rolling resistance coefficient has been demonstrated to vary in a general way across many different light-duty vehicle types according to the semi-empirical equation

$$\mu_{rr} = f_o + 3.24 f_s \left(0.0044704 v_{veh\ reqd\ avg}\right)^{2.5}. \qquad 2.11$$

where the dimensionless coefficients f_o and f_s (though the coefficient 0.0044704 has units of s/m) are used in calculating the rolling resistance coefficient and $v_{veh\ reqd\ avg}$ is expressed in m/s. In the case when f_o and f_s are known, perhaps through estimates based on readily available tire specifications, then those figures can be used. In instances where such information is not available, f_o and f_s can be assumed to vary as a function of tire inflation pressure for a wide array of light-duty vehicles according to the semi-empirical relationship seen in Figure 2.4 [47].

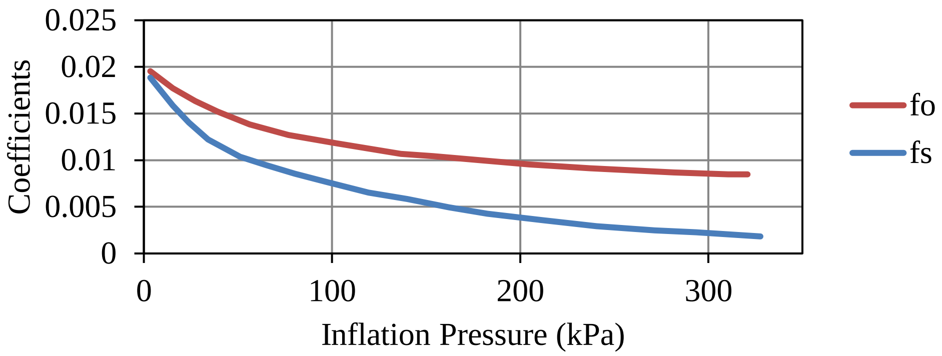

Figure 2.4: Coefficients affecting rolling resistance coefficient as a function of tire inflation pressure

Figure 2.5 shows how the rolling resistance coefficient ultimately varies with speed according to a tire inflation pressure of 250 kPa. Note that the rolling resistance coefficient is relatively constant for speeds less than approximately 40 km/h. It is important to note that the user has the option of tuning the values of f_o and f_s in order to directly specify the relationship between the rolling resistant coefficient and speed for the vehicle of interest. Once the rolling resistance coefficient has been determined via this method, then Equation 2.10 can be used to calculate the rolling resistance force.

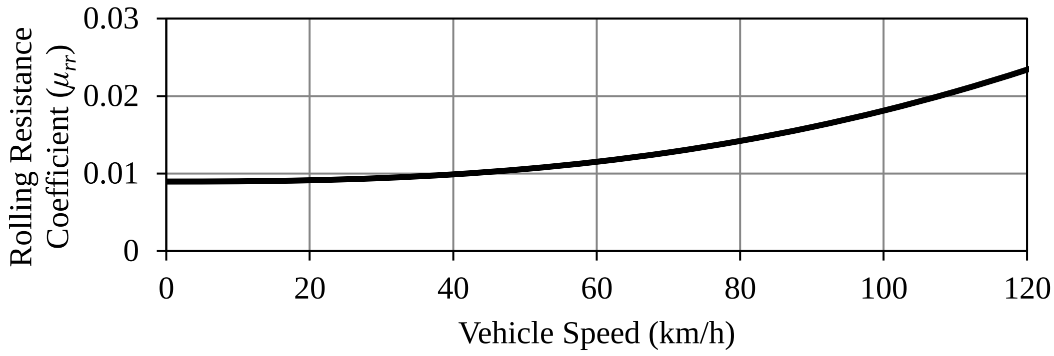

Figure 2.5: An example of how rolling resistance varies with speed with a tire inflation pressure of 300 kPa, according to Equation 2.11 and Figure 2.4

The vehicle must also generate additional force to accelerate and decelerate

$$F_{accel} = ma = m\frac{v_{req,i+1} - v_{req,i}}{t_{i+1} - t_i} \ . \qquad 2.12$$

The total force that the vehicle must generate is

$$F_{veh\ reqd\ avg} = F_D + F_g + F_{rr} + F_{accel} + F_{inertia} \ . \qquad 2.13$$

The force request ($F_{veh\ reqd\ avg}$) and the speed request ($v_{veh\ reqd\ avg}$) are the outputs of the vehicle block that are passed to the wheel-axle block. If the vehicle has multiple motors, then the force request is divided by the number of motors and can be governed by a proportional power split as set by the user.

2.1.1 Drive Cycles

The drive cycle is a key input to the vehicle block, and as such it serves as the basis for all of the torque, speed, and power requests calculated by the simulation. For that reason, the role of drive cycles in OVEM warrants a brief discussion.

A drive cycle is typically expressed as a velocity versus time trace. Drive cycles usually arise out of academic studies or legislative mandates in order to assess vehicle performance (usually in terms of emissions, range, or energy consumption) over different driving conditions. Drive cycles can have varied objectives. For instance, one drive cycle may be focused on replicating urban driving, another may focus on highway driving, and another may seek to blend elements of both urban and highway driving.

OVEM has compiled a library of drive cycles, including many of the most common ones used for vehicle testing purposes around the world. The New European Drive Cycle (NEDC) is an example of a drive cycle that seeks to model both urban and highway travel. The New European Drive Cycle, as seen in Figure 2.6, is used as the basis for emissions and fuel consumption testing of commercial vehicles in Europe. The EPA Combined (Figure 2.7) is a drive cycle that is commonly used in the United States that also seeks to capture elements of both urban and highway driving.

OVEM can easily incorporate any new drive cycle that the user may wish to use. One of the additional unique features of OVEM is that it can handle slopes, so that the user can understand how a realistic drive cycle with changes in altitude will affect the simulated vehicle.

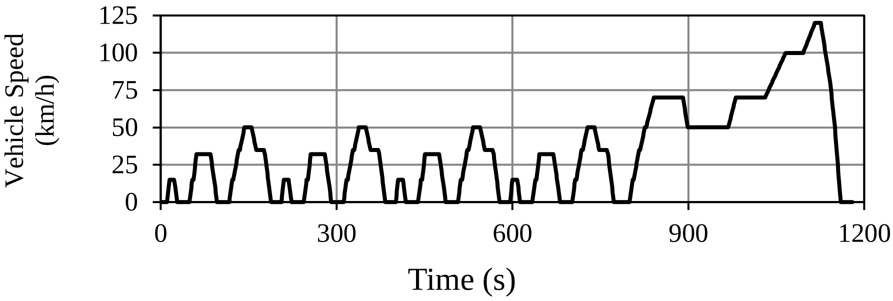

Figure 2.6: The New European Drive Cycle

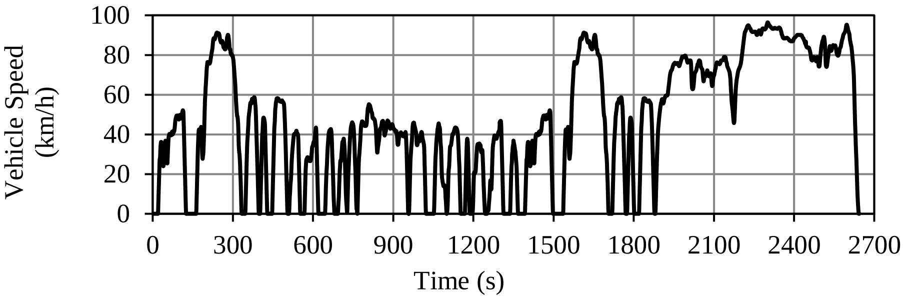

Figure 2.7: EPA Combined Drive Cycle

Drive cycles are ultimately only approximate representations of real-world driving. Drive cycles that could be defined as "industry standards" given their widespread use in determining official ratings for values such as range, energy consumption, and emissions, typically make two primary simplifying assumptions: vehicles only travel in a straight line and only travel over flat terrain. These drive cycles came to be used as industry standards because of political, historical, and technical reasons in order to simplify and standardize testing procedures for a range of vehicle types. Drive cycles may at times be criticized for portraying real-world driving as less demanding than or not representative of normal driving. This may be true for certain drive cycles (such as for the New European Drive Cycle); however, there are widely used drive cycles that are more realistic representations of real-world driving such as the Artemis Combined Drive Cycle (ACDC) shown in Figure 2.8.

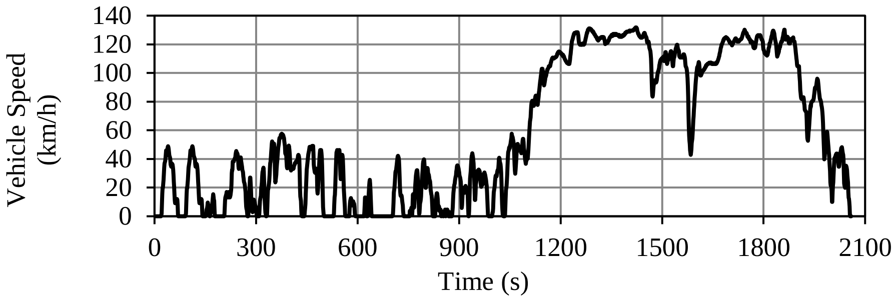

Figure 2.8: Artemis Combined Drive Cycle (ACDC)

Slope is not accounted for in these industry standard drive cycles. Yet, slope can have a significant impact on figures such as range, emissions, and energy consumption, and the fact that most drive cycles do not account for it has more to do with political and legacy reasons than rigorous technical fundamentals. Since slope has the capacity to appreciably affect values such as emissions, range, and energy consumption (the kind of values with which OVEM is concerned), OVEM was built with the capacity to model a slope profile alongside a drive cycle. No standard slope profiles exist, as far as the author is aware, that accompany widely-used drive cycles. However, the user can create a slope profile in OVEM to examine its effect on the vehicle.

2.2 Wheel-Axle Block

The wheel-axle block accepts the force and speed requests calculated by the vehicle block as inputs, accounts for the losses in the wheel and axle, and outputs torque and angular velocity requests, to the gearbox block.

The wheel and axle experience power losses due to friction in their bearings and seals. As the Level 1 model is just a first order approximation, the efficiency ($\eta_{Wheel\text{-}Axle}$) of the wheel-axle block is treated as a fixed value throughout the drive cycle, and this efficiency is entered by the user. The wheel-axle block also accepts the user-defined parameters of tire radius (r) to convert the linear force and speed to torque and angular velocity. For a motoring case (constant velocity or positive acceleration), the torque request ($T_{Wheel\text{-}Axle\ reqd}$) is obtained by dividing the force request from the vehicle block by the wheel-axle efficiency (which is between 0 and 1). This is based on the premise that during motoring as the power requests move from the wheel and axle back through the powertrain to arrive at the energy storage system (in the case of an EV) each component must ask the next component for more power than it was asked for due to its own internal losses

$$T_{Wheel-Axle\,reqd} = \left(F_{veh\,reqd\,avg}r\right)\frac{1}{\eta_{Wheel-Axle}}\,. \qquad 2.14$$

During a braking event (deceleration), the wheel-axle block multiplies the torque request by the efficiency because as the power flows from the wheels back towards the energy storage system (in the case of an EV) each component will reduce the amount of power that is passed to the next component due to its own internal losses

$$T_{Wheel-Axle\,reqd} = \left(F_{veh\,reqd\,avg}r\right)\eta_{Wheel-Axle}\,. \qquad 2.15$$

Angular velocity is calculated by dividing the linear velocity requested of the vehicle by the radius of the tire. Note that the wheel-axle losses have already been accounted for when calculating the torque requirements so they do not need to be factored in again

$$\omega_{Wheel-Axle\, reqd} = \frac{v_{veh\, reqd\, avg}}{r} \quad . \qquad 2.16$$

The wheel-axle block produces these torque and speed requests as outputs, and they are passed to the gearbox block.

2.3 Gearbox Block

The gearbox block receives the torque and speed requests from the wheel-axle block as inputs, applies the torque reduction and speed multiplication effect of the gears, accounts for the losses in the gears, and outputs speed and torque requests which are typically sent to the motor block.

As a Level 1 model, the gearbox block treats the gearbox as having a fixed efficiency for a particular vehicle across its simulated drive cycle. When the vehicle is motoring, the gearbox block applies the effect of the gear ratio (*N*) to reduce the torque request according to

$$T_{GB\, reqd} = \frac{T_{wheel-axle\ \, reqd}}{N} \frac{1}{\eta_{GB}} \qquad 2.17$$

where η_{GB} is the fixed, user-specified efficiency of the gearbox. During braking, Equation 2.17 becomes

$$T_{GB\, reqd} = \frac{T_{wheel-axle\ \, reqd}}{N} \eta_{GB} \qquad 2.18$$

to account for the fact that less power is available to the components further upstream from the gearbox due to the losses in the gearbox. The speed outputted to the motor ($\omega_{GB\, reqd}$) is

$$\omega_{GB\, reqd} = N\omega_{wheel-axle\, reqd}. \qquad 2.19$$

Note that the gearbox efficiency has already been accounted for in the torque calculation so it did not need to be included in calculating the speed output. In order to model a gearbox where the gear ratio varies, the user merely has to specify the gear ratios and at what speeds the gear shifts should occur. In order to model direct-drive motors with no gearbox, the user sets the gear ratio to 1 and the efficiency of the gearbox to 100%.

The torque and speed requests from the gearbox block are sent as outputs, typically to the motor block. The torque and speed versus time traces inputted to and outputted by this block provide an approximation for the required torque and speed ratings of the gearbox.

2.4 Motor Block

The motor block takes the torque and speed requests from the gearbox block as inputs, accounts for the efficiency of the motor, and outputs a power request, typically to the power electronics (PE) block.

The motor block converts the torque and speed requests into a power request to pass to the power electronics. The torque, speed, and power versus time traces inputted to this block provide an estimate for the required torque, speed, and power ratings of the motor. In the motoring case, the fixed, user-specified efficiency is accounted for by

$$P_{motor\ reqd} = \left(T_{GB\ reqd}\,\omega_{GB\ reqd}\right)\frac{1}{\eta_{motor}} \qquad 2.20$$

and in the braking case, the efficiency is accounted for by

$$P_{motor\ reqd} = \left(T_{GB\ reqd}\,\omega_{GB\ reqd}\right)\eta_{motor}\,. \qquad 2.21$$

This power request ($P_{motor\ reqd}$) is sent as an output, typically to the power electronics block. The motor block can also model multiple motors where each motor shares a part (either equal amounts or subject to a fixed proportional split) of the overall power and torque demands.

2.5 Power Electronics Block

The power electronics block receives the power request from the motor(s) as an input, accounts for the efficiency of the power electronics, and then outputs an updated power request, typically to the energy storage system block. The power versus time input into this block also provides an approximation for the required power rating of the power electronics. The power electronics model accounts for its losses via the constant, user-defined efficiency, in the motoring case,

$$P_{PE\ reqd} = P_{motor\ reqd}/\eta_{PE} \qquad 2.22$$

and in the braking case

$$P_{PE\ reqd} = P_{motor\ reqd}\eta_{PE}. \qquad 2.23$$

This power request is then sent as an output, typically to the energy storage system block.

2.6 Energy Storage System Block

The energy storage system block receives the power request from the power electronics block as an input, accounts for the efficiency of the energy storage system, and outputs the amount of power requested by the energy storage system. The power input into the energy storage system block can be used to determine the required power rating of the energy storage system. The energy storage system model factors in the constant, user-defined efficiency to determine the amount of power that must be supplied to the energy storage system, typically in the form of power from the grid, in the motoring case,

$$P_{ESS\ reqd} = P_{PE\ reqd}/\eta_{ESS} \qquad 2.24$$

and in the braking case

$$P_{ESS\ reqd} = P_{PE\ reqd}\eta_{ESS}\ . \qquad 2.25$$

In the Level 1 energy storage system block, it is assumed that the efficiency of the energy storage system is the same during charging and discharging. By taking the power ($P_{ESS\ reqd}$) versus time curve that is outputted by the energy storage system and integrating it with respect to time, an approximation for the energy rating of the energy storage system can be obtained. This figure can be divided by the range achieved by the vehicle to arrive at an estimate for the vehicle's tank-to-wheel energy consumption. The power demands on the energy storage system can also be split between multiple devices functioning as a hybridized energy storage system, such as with batteries and ultracapacitors.

2.7 Series, Parallel, and Series-Parallel Hybrid Electric Vehicle Models

The Level 1 simulation also includes models for series, parallel, and series-parallel HEVs. Information flows in these models in the same way as in the EV simulation. All of the component blocks still rely on a user-defined, fixed value to account for their efficiency. A diagram showing the information flows in the series HEV model can be seen in Figure 2.9.

In the series HEV model, the rest of the powertrain behaves exactly as in an electric vehicle simulation with the added alternative power unit (APU) now receiving a power request from the energy storage system. The alternative power unit accounts for its losses and outputs a power versus time trace over the entire drive cycle identical to the manner in which the energy storage system block operates. This enables the user to determine values that may be of interest such as the average and peak power required from the alternative power unit.

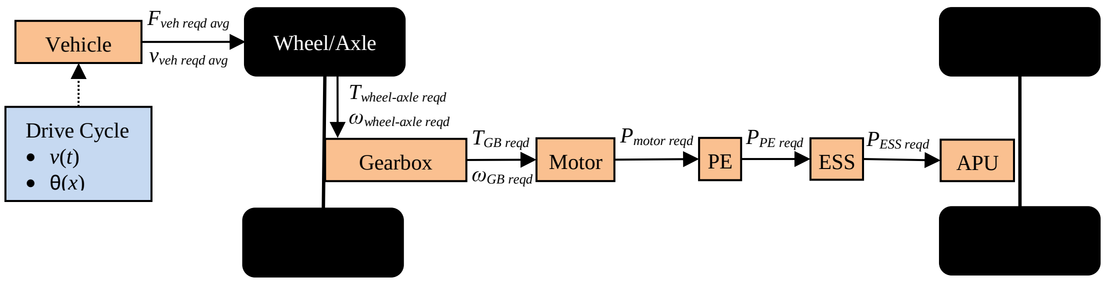

Figure 2.9: Diagram of the information flows in the Level 1 series HEV model

Figure 2.10 and Figure 2.11 present the information flows in the Level 1 parallel and series-parallel models. In the parallel and series-parallel HEV simulations, an additional parameter known as the hybridization ratio needs to be specified. The hybridization ratio denotes how the power requirements are split between the motor and the internal combustion engine (ICE). For instance, with a hybridization ratio of 20% the electric motor will handle

20% and the internal combustion engine will handle 80% of all the vehicle's power requirements to meet the road load for every time step over the drive cycle. This is a simplification of how motors and ICEs generally share the road load in parallel and series-parallel HEVs, but it is a simplification that is aligned with the aims (to obtain approximate scoping and sizing estimates) and limitations (backwards models cannot employ sophisticated control techniques) of the Level 1 model.

In the Level 1 series-parallel model, the ability of the ICE to generate extra power to recharge the energy storage system is not factored in for several reasons. The first is that the sizing of the ICE will nearly always be determined by the demands placed on it by the road load and not by the much smaller energy storage system charging requirements. The second is that there is no way to implement a meaningful energy management strategy which would tell the ICE when to turn on and off since the Level 1 simulation is an open loop with no feedback. This makes it impossible to, for instance, turn on the internal combustion engine once the energy storage system reaches a certain state of charge (SOC) since the energy storage system has no record of its state of charge in this purely backwards looking simulation. Yet, as this does not interfere with the aim of the Level 1 simulation – sizing technologies to estimate figures such as energy consumption, range, emissions, and component sizing – this is not an issue.

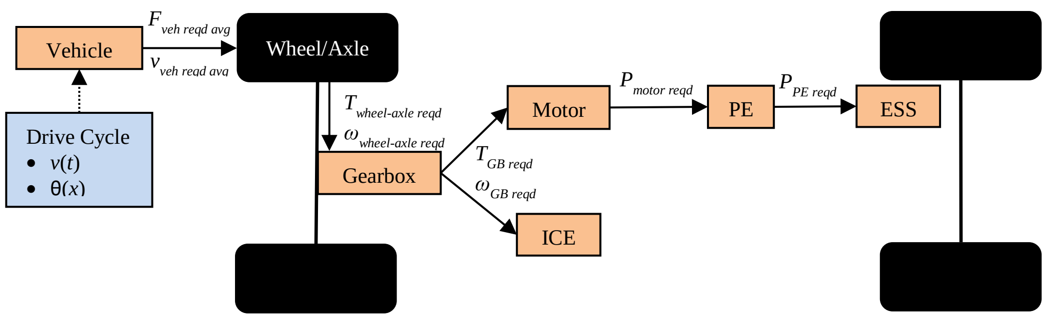

Figure 2.10: Diagram of the Level 1 parallel HEV model

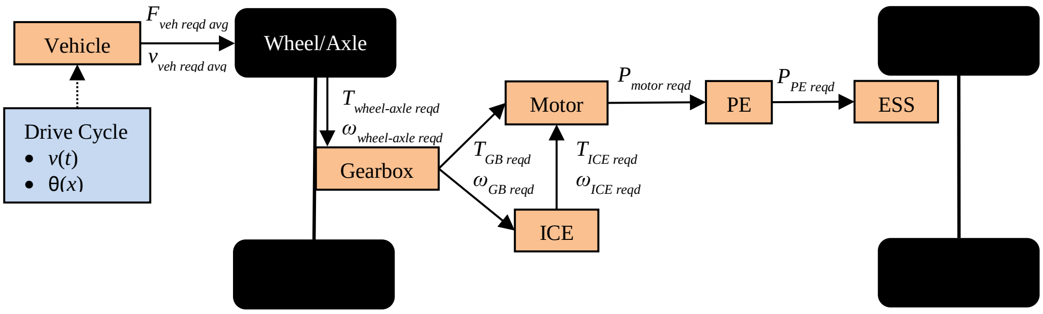

Figure 2.11: Diagram of the Level 1 series-parallel HEV model

2.8 Level 1 Case Study: Milk Float Modeling

The following is a case study that provides an illustration of the ability of the Level 1 model to address problems related to the scoping of new technologies and capabilities to address concerns over range and energy consumption in an analysis environment with high uncertainty.

2.8.1 Introduction

A milk distributor, whose primary means of delivering milk in urban settings is via electric milk floats, approached the author seeking advice on ways to improve the range of its milk float fleet. Currently, the majority of its milk floats are propelled by DC motors. These floats achieve a 56 km (35 mi) range on a single charge over a standard milk delivery route. A small percentage of the fleet has been equipped with more efficient AC motors that enable the floats to achieve a 72 km (45 mi) range. Currently none of the milk floats employ regenerative braking. The milk distributor speculated that their floats could benefit from incorporating regenerative braking, and they calculated that if their floats could achieve a range of roughly 105 km (65 mi), then it could result in substantial cost savings by streamlining their delivery routes. It was speculated that the floats might be able to achieve that target range by employing regenerative braking, and this case study tested that hypothesis by using the Level 1 models.

2.8.2 Methods

Before the milk float could be simulated, it needed the external shape, mass, and rolling resistance parameters to model the forces acting on it. The simulation also required a drive cycle, so one was implemented that was representative of the type of driving the milk floats generally experience. The constant efficiencies of the components were estimated. And lastly, a strategy was devised to model the milk floats as though they were traveling over an actual delivery run.

2.8.2.1 Drive Cycle Selection

The process of determining how far the range of the floats could be extended began by understanding their current driving patterns. In order for the Level 1 simulation to work, it first needed a drive cycle that was representative of the type of driving experienced by the floats. The floats are delivery vehicles operating in urban environments, so their drive cycle is characterized by frequent stops and starts. The milk distributor also noted that the floats have a maximum speed of 40 km/h. The drive cycle selected was relatively representative of the sort of driving pattern that an average float would undergo. This 2.6 km long drive cycle (Figure 2.12) was originally measured by Wipke et al. [26] on a city bus. It is likely that the floats may have longer stop times than those depicted in this cycle; however, that should not affect the Level 1 energy consumption calculations since the default setting in Level 1 assumes that the vehicle does not consume energy when it is not moving. It should also be noted that this study assumed the floats traveled over flat terrain which was a simplifying assumption that was deemed both necessary – in the absence of any terrain data – and reasonable – since the floats generally travel over the relatively flat landscape of urban Oxford.

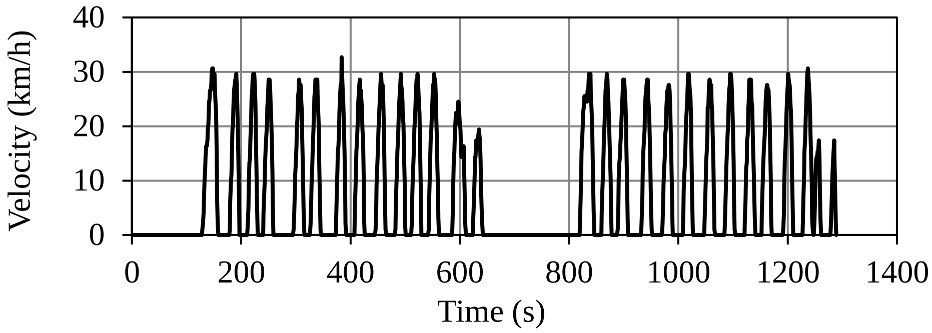

Figure 2.12: Drive cycle used to represent the milk floats' driving pattern

2.8.2.2 Milk Float Specifications

The characteristics of the powertrain's components along with the mass and shape parameters of the float had to be determined. The floats' battery pack is comprised of 36 cells each with a nominal charge capacity of 585 Ah. The floats use lead-acid batteries. The terminal voltage of lead-acid batteries typically remains relatively constant during discharge [50]. Therefore, it is reasonable to assume, based on a terminal voltage of 2 V, that the batteries contain 151 MJ (42 kWh) of energy. The milk floats also do not employ regenerative braking. Table 2.2 displays the amount of energy stored in the energy storage system along with other key vehicle parameters. The tire radius was provided by the milk distributor, and the rest of the parameters were based on figures obtained from similar vehicles [12].

Table 2.2: Parameters of the milk float

C_D	A_f (m^2)	f_o	f_s	r (m)	Mass, Fully Loaded (kg)	Mass, Empty (kg)	ESS Capacity (MJ)
0.7	3	0.01	0.002	0.41	5000	2700	151

2.8.2.3 Vehicle Simulation

When a milk float is fully loaded with cargo, its mass is 5000 kg, and over the course of a delivery run its mass decreases as the cargo is delivered, so that when it is empty, its mass is 2700 kg. In modeling the vehicle, it is important to account for this decrease in mass over the vehicle range. This was done by running the simulated vehicle through the 2.6 km long drive cycle as many times as it took for it to achieve its range. Floats powered by the DC motor went through 22 iterations of the drive cycle to achieve their 56 km range, and floats powered by the AC motor went through 28 iterations to achieve their 72 km range. At the beginning of the first iteration, the mass of the simulated vehicle was always set to 5000 kg, signifying a fully laden float. At the end of each iteration, the mass of the vehicle was reduced by a constant amount so that for the last iteration in the simulation, the vehicle's mass had decreased to 2700 kg. It was known how much energy the energy storage system had to provide during each of these iterations. The net energy used in each iteration was summed to yield the total energy used by the milk float during a simulated delivery run. Of course, this approach is only an approximation of the actual route and delivery pattern undertaken by a given float. To improve the accuracy of the simulation, actual drive cycle and delivery data would need to be obtained. However, since this study was looking at the floats' driving patterns on average across the entire fleet, this was a reasonable assumption.

2.8.2.4 Component Efficiencies

The next step in characterizing the modeled milk float was to obtain estimates for its components' efficiencies. Table 2.3 and Table 2.4 present the initial efficiency estimates for the milk float powertrains with DC and AC motors, respectively. These initial estimates were based on a review of the literature for the types of components used in the floats [9] [12] [23]. Note that the only parameter that differs between the two types of floats is the motor, so that is the only component where the efficiencies differ.

Table 2.3: Initial component efficiency estimates for a milk float with a DC motor

	Wheel-Axle	Gearbox	Motor	PE	ESS
Efficiency	99%	96%	70%	96%	85%

Table 2.4: Initial component efficiency estimates for a milk float with an AC motor

	Wheel-Axle	Gearbox	Motor	PE	ESS
Efficiency	99%	96%	90%	96%	85%

These initial estimates allowed the simulation to be run to produce estimates for the energy consumption, and hence, the range of the floats assuming there was no regenerative braking.

The initial estimate for the range of the floats using a DC motor and an AC motor was 52 km and 67 km, which differed from the actually ranges of 56 km and 72 km, respectively.

Since this study's goal was to closely characterize the existing powertrains (obviously given the constraints and limitations of the Level 1 model), the efficiencies of the powertrain's components were tuned slightly from their initial estimates. The tuned efficiencies for the components still remained within the range agreed upon in the literature as outlined in Table 2.1. The updated values are shown in Table 2.5 and Table 2.6. These updated values enabled the modeled floats to achieve ranges, assuming no regenerative braking, for the powertrains with DC and AC motors of 56 km and 72 km, respectively. The exact efficiency values for each of these components are not of critical importance; rather they are primarily useful insofar as they allow the Level 1 model to approximate the behavior of the floats' powertrains as they currently exist so that the effect that regenerative braking would have on the floats' range could be better estimated.

Table 2.5: Tuned component efficiency estimates for a milk float with a DC motor

	Wheel-Axle	Gearbox	Motor	PE	ESS
Efficiency	99%	96%	76%	96%	87%

Table 2.6: Tuned component efficiency estimates for a milk float with an AC motor

	Wheel-Axle	Gearbox	Motor	PE	ESS
Efficiency	99%	96%	93%	96%	87%

2.8.3 Results and Discussion

The milk floats do not currently use regenerative braking. Yet given their operation with frequent starts and stops, they would likely benefit from regenerative braking [51]. So the next step looked at the potential impact that regenerative braking could have on the floats' range. Table 2.7 shows the improvement in range predicted by the Level 1 simulation if the floats were able to capture 50% and 100% of the energy available to their energy storage systems (note that this is the energy *available* to the energy storage system, therefore, it reflects the losses from the components that the energy passed through prior to reaching the energy storage system).

It should be noted that while it is rare for an electric vehicle to recapture all of the energy available to its energy storage system, the milk float, because of its design and driving characteristics, likely has the potential to recapture a high percentage of its energy. Most electric vehicles are designed so that their bus voltage enables their maximum speed. For instance, a vehicle with a maximum speed of 150 km/h will likely have a high bus voltage that allows it to attain that speed. Yet when that vehicle is braking at 15 km/h, the voltage generated by its motor during regenerative braking may only be 10% of the bus voltage. It can be technically difficult and inefficient to step that low motor voltage up to the high bus voltage to enable full regenerative braking, so typically that energy is not recaptured. However, the milk float presents a slightly different scenario. It has a low maximum speed and hence likely has a lower bus voltage. So even when braking at low speeds, the voltage generated by its motor can still constitute a useful fraction of the bus voltage. This makes it more likely for the motor's voltage to be able to be efficiently stepped up to the bus voltage, facilitating the recapture of the float's energy. While the float will still not capture 100% of the energy available to its energy storage system, it could reasonably be expected to come closer to that theoretical upper bound than many other electric vehicles.

Table 2.7: Simulated range with no regenerative braking and assuming 50% and 100% of the energy available to the ESS was in fact recaptured

	Range with no regenerative braking (km)	Estimated range with ESS capturing 50% of energy available to it (km)	Estimated range with ESS capturing 100% of energy available to it (km)
DC motor	56	66	77
AC motor	72	92	122

Several conclusions were drawn from this analysis. The first was that the DC motor will likely not allow the floats to achieve a 105 km range. Granted this study was based on simplifying approximations about the driving pattern, shape and mass parameters, and component efficiencies of the floats, but the simulations showed that even if 100% of the energy available to the ESS was in fact recaptured by the ESS in the floats with DC motors, they would still be significantly short of reaching the target range of 105 km. On the other hand, the Level 1 model showed that the more efficient AC motors could have the potential to reach a 105 km range if they adopted regenerative braking. Of course, the exact range achieved would depend on the nature of the regenerative braking strategy that was employed. And the range could vary from one float to another depending on the drive cycle of a particular float.

To gain a better understanding of how the chosen parameters affected the range (and by extension, energy consumption) of the simulated milk floats, a sensitivity analysis was performed (Figure 2.13). In the sensitivity analysis, each of the vehicle parameters that could be varied was varied by ±5% and the corresponding change in the floats' range was recorded. A sensitivity analysis was done for both floats using both the DC and AC motors. The data presented in Figure 2.13 is the average of the absolute values of the percent changes in range caused by either the 5% increase or decrease in the vehicle input parameters. In this analysis, it was assumed that the energy storage systems recaptured 50% of the energy *available* to them. This condition was selected in order to provide a conservative and representative snapshot of the floats by avoiding modeling them at the upper or lower limits of their regenerative braking possibilities. Also note that this sensitivity analysis was done for these specific floats over a specific drive cycle, and any conclusions drawn from this analysis regarding the sensitivity of the model to the input parameters cannot be uncritically applied to any vehicle in any context. Parameters such as the drive cycle and cargo offloading pattern were not included in this sensitivity analysis since they are merely approximations of the actual float's behavior and it is impossible to vary them in a systematic manner that would provide meaningful insight into their effect on the floats' energy consumption.

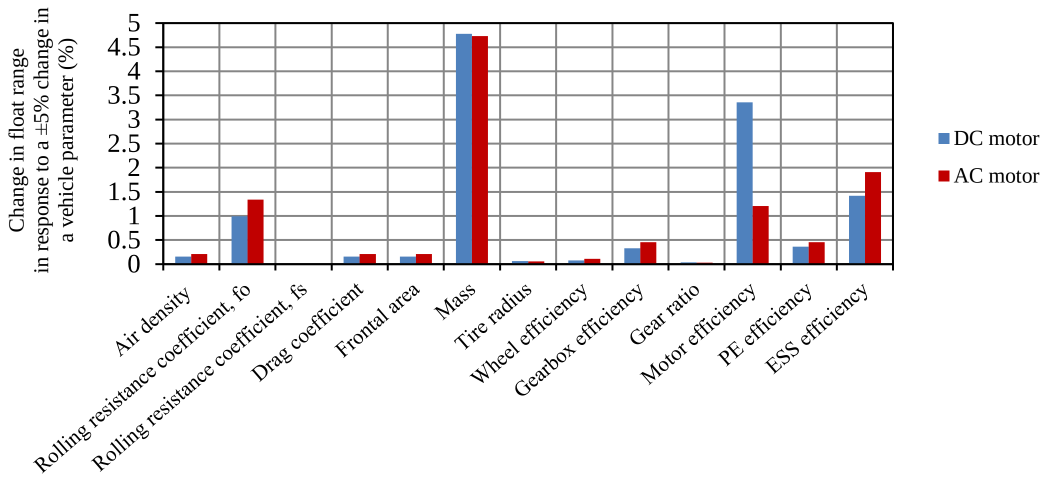

Figure 2.13: Level 1 sensitivity analysis for the milk floats with DC and AC motors

The sensitivity analysis in Figure 2.13 revealed several insights. All of the parameters that play a role in determining aerodynamic drag had little effect on the range of the floats. This was expected given the low speeds at which the floats travel. Given the low-speed travel of the floats, it was also unsurprising that rolling resistance had a greater impact on the floats' range than aerodynamic drag. However, it is interesting to disaggregate the constituent factors of rolling resistance to analyze the role they played. The rolling resistance coefficient f_s, which varies with speed (Equation 2.11), had a negligible effect on range. This was also largely due to the low-speed travel of the floats. On the other hand, the rolling resistance coefficient that is independent of speed (f_o) had a comparatively greater impact than those values effecting vehicle load which are dependent on speed. The energy consumption of the floats was most sensitive to the mass. This is understandable given that the floats' are heavy vehicles undergoing frequent acceleration cycles. The fact that the model is so sensitive to mass is means two things for the model. On the one hand, mass is a parameter that is actually known with a high degree of certainty for the floats so it this may appear to be a source of strength for the model. On the other hand, the manner in which the cargo mass is offloaded from the floats requires a number of assumptions that may not be entirely accurate. It is possible that the lack of knowledge about the exact cargo offloading patterns of the floats could be a significant contributor to any disagreement between the model's predictions and the actual data.

Tire radius and gear ratio both had a negligible impact on the floats' range. This is because these two parameters mediate the balance between the torque and speed demands seen by the upstream components. However, in the Level 1 simulation, the distinct torque and speed demands are less relevant in affecting range since the power requests are only scaled by constant, scalar efficiencies.

The relationship between the efficiency of the powertrain components follows a pattern that is understandable given the nature of the Level 1 model. It was observed that the less efficient a component is relative to the other components in its powertrain, then the greater its proportional impact in affecting the powertrain's range. This follows from the constant scalar efficiencies of the Level 1 model, and it illuminates two interesting points. The first point informs a broad observation regarding vehicle modeling: it is important to have a higher degree of confidence in the efficiency values used for those components with the lowest efficiencies as they have the greatest ability to influence outputs like energy consumption and range. The second point builds on this observation by noting that even small gains in improving the efficiency of the least efficient components can have proportionally higher impacts in improving the tank to wheel efficiency of the powertrain.

The sensitivity analysis showed that the greatest sources of potential error in simulating the floats (aside from the inherently low-fidelity modeling approach) likely came from the values for rolling resistance, mass, motor efficiency, and energy storage system efficiency. The drive cycle and cargo offloading pattern are also likely responsible for introducing error between the actual and simulated results given that they are only approximations of the driving patterns experienced by the actual floats.

2.9 Summary of Level 1 Contributions

This section provides a synthesis of the novel contributions made in the Level 1 program and how these contributions were developed, i.e. what new knowledge was required to make Level 1 a working vehicle modeling program. The contributions range from the broad – the fundamental structure of the Level 1 program – through to the detailed – specific innovations made in individual component blocks.

The fundamental structure of the Level 1 program as a backwards vehicle model constitutes a novel contribution to knowledge. Though the theory of backwards vehicle energy flow simulations existed [31], it had not been applied towards the development of an actual backwards program. Thus, a novel contribution of the Level 1 model is that it was a practical application of the backwards vehicle modeling theory. The primary impact of the Level 1 model was the rapid component scoping and sizing that it enabled (OVEM Criteria #1 and #2, Section 1.5), especially when integrated with Levels 2 and 3 in OVEM.

To construct the Level 1 program, the theory of backwards simulations had to be adapted into a practical program capable of functioning within the objectives and constraints of OVEM. This required developing novel structures and algorithms to enable the Level 1 program to function as theorized. For instance, each component model in the Level 1 program leverages a fixed efficiency value to calculate its power demand. Calculating a power demand based on an efficiency value is an established technique. However, novel work was required to create and program the set of algorithms that enable these efficiency calculations to be carried out for each component within the overall program (Section 1.8.1).

Several of the constituent models making up the Level 1 program made a novel contribution to the field of vehicle modeling. It should be noted that these contributions originated in the Level 1 program (with a degree of fidelity commensurate with the Level 1 aims and constraints) and were then carried through (in more complex incarnations) to the

Level 2 and Level 3 programs. Yet since these capabilities had their origins in the Level 1 program, they will be discussed here.

The first of these contributions has to do with the Level 1 program's ability to model multiple tractive electric motors. The notion of using multiple tractive electric motors in automobiles is an emerging idea that has been gaining acceptance in the field. It is considered an attractive idea because of the potential of multiple tractive motors to provide superior handling, acceleration, and energy recapture during braking. Its emergence as a viable concept has been spurred by the increasing use of tractive electric motors in automobiles – a notion which itself has led to a widespread rethinking of many long-standing notions of powertrains limited by the constraints of ICEs. However the concept of multiple tractive motors is still a new concept and as such there are no vehicle modeling programs currently available that account for it [26] [40].

Thus, in order to implement the concept of multiple tractive motors in OVEM, novel work was done by the author to translate the theory into a practical reality. This meant that devising the algorithms for allocating power demands between the multiple motors and implementing these algorithms into OVEM code was the novel work of the author. For instance, developing the algorithm that would control how power should be split between variously sized motors during acceleration and braking was the novel work of the author.

The second novel contribution in the Level 1 component models is that of the hybridized energy storage systems. The concept of hybridized energy storage systems in automobiles is new, having only surfaced recently alongside the growing interest in EVs and HEVs. Since it is a new concept, existing vehicle modeling programs have not been built with this functionality [26] [40]. OVEM recognized that hybridized ESSs could play a role in EV and HEV development, and so this functionality was built into OVEM. To build this functionality, the author had to develop a series of novel equations and algorithms to control the energy flow between different ESSs. For instance, Equation 4.73 and its integration into OVEM was the product of novel thinking by the author to implement a speed-based strategy to control energy flow between hybridized ESSs (refer to Sections 2.6 and 4.9 for more information on this topic).

The third novel contribution to originate from the Level 1 program was the manner in which the Level 1 program accounted for rolling resistance. Existing energy flow vehicle modeling programs calculate rolling resistance according to Equation 2.10 where the coefficient is constant [26] [40]. Yet despite the pervasiveness of this assumption, the literature shows that it is overly simplified. To more accurately account for the effects of rolling resistance, the speed-dependence of rolling resistance should be included in the model. To do this, the author performed the novel task of creating a programmable algorithm based on existing experimental work (the relationships described in Equation 2.11 and Figure 2.4) to account for the effect of speed on rolling resistance in OVEM. A more detailed explanation of this work is contained in Section 2.1.

The fourth novel contribution from the Level 1 program is the ability to account for slope as a part of the drive cycle. A survey of the vehicle modeling landscape showed that energy flow modeling programs could not account for slope as part of their drive cycle inputs [26] [40]. Slope is an unavoidable feature of real-world driving, and the energy consumption of electric and hybrid electric vehicles has the potential to be appreciably affected by accounting for slope given their potential to recapture energy during descents. To account for slope in OVEM, the author used Newtonian equations of motion to derive how the vehicle would be affected by a changing slope (Equations 2.5, 2.6, 2.8, 2.10, 2.12, and 2.13). The novel work came in adapting these derivations for use within OVEM. A particularly unique feature of this adaptation came from the author's realization that these equations accounting for slope needed to be a function of distance traveled, rather than time elapsed, to account for a scenario in which the vehicle was not able to meet the sloping drive cycle requested of it. Structuring these functions in this way was unique in that it ran counter to the structure of the rest of OVEM and other existing energy flow vehicle modeling programs [40].

3 Level 2 Simulation

The Level 2 simulation in OVEM further addresses the challenge of performing sizing and scoping exercises across arrays of technologies that could have an application in electric and hybrid electric vehicles. It does this by employing a method that builds on the Level 1 approach by varying the component efficiencies according to general physical principles. This allows for higher-fidelity simulations of powertrain components while still coping with a large degree of uncertainty such that product-independent scoping and sizing can be performed.

Level 2 uses a backwards modeling approach like Level 1, and as a backwards model, Level 2 imposes no power, torque, and speed limits. Both Levels 1 and 2 merely calculate and record the power, torque, and speed that each component must produce to enable the vehicle to completely meet the given drive cycle. However, Level 2 differs from Level 1 in the way its component models calculate their efficiency. The component models in Level 2 employ higher fidelity component models with the aim of producing more refined estimates for component sizing and vehicle energy consumption.

In Level 2, the efficiencies are not constant, user-specified values. Instead, the efficiencies are calculated based on modeling the primary loss mechanisms for certain general technological categories. This method enables the simulation to account for a technology's general physical principles while avoiding simulating specific real-world products. This enables the efficiency of the powertrain's key components to vary based on how the vehicle is being driven. And it allows the backwards simulation to be used as a component sizing tool that is independent of any specific product which is useful when component scoping and sizing is the primary priority of the simulation. An understanding, even if only a simple and general one, of how the changing efficiency of each component affects its power, energy, torque, and speed demands, provides a more realistic estimate for component sizing, energy consumption, and range than could be attained from Level 1 alone.

It should be noted that Level 2 is not meant to be a precise predictor of vehicle performance or characteristics. It is a backwards simulation and as was explained in Chapter 1, Level 2 is primarily intended to enable scoping and sizing estimates, and not to provide highly accurate results. Therefore, meeting OVEM's 2-5% accuracy criteria (Section 1.5) is not a priority for Level 2. This is the outcome of the deliberate choice to make the models general enough so that they can apply to an array of technologies and sizes for each component in an effort to cope with the uncertainty regarding component and capability specifications that characterize the early and less precise stages of the vehicle design and analysis process.

The Level 2 component models meet the criteria of Section 1.5 in the following ways. First, the models are built such that they account for component losses that are relevant to the timescales of interest to OVEM. The loss mechanisms modeled in Level 2 are accounted for such that a consistent degree of fidelity is applied throughout the simulation to produce figures for values such as vehicle energy consumption, emissions, range, and component sizing. Level 2 is also structured such that it is concerned with the timescales and conditions relevant to OVEM.

One of the issues faced by the Level 2 model is that by using models based on general physical properties, it can be more difficult to create models for less well-understood technologies that may be novel or for technologies that behave nonlinearly as a function of many factors that can be difficult to model. Nevertheless, the Level 2 approach works reasonably well for components such as electric motors, power electronics, and gearboxes – which are all relatively mature and well-understood. Yet, for that reason, the Level 2 model was thus far only developed for an electric vehicle. The following is a description of each component block in a Level 2 electric vehicle.

3.1 Vehicle Block

In the Level 2 electric vehicle model, the vehicle block is the same as in Level 1. This was done because both Levels 1 and 2 account for the same effects: drag, rolling resistance, slope, and acceleration. As in Level 1, the Level 2 vehicle block takes a drive cycle and certain vehicle parameters as inputs, calculates the force and linear speed that the vehicle must achieve, and outputs the force and linear speed requests to the wheel-axle block.

3.2 Wheel-Axle Block

The wheel-axle block in Level 2 is also the same as in Level 1. This was considered to be sufficient because the wheel-axle losses are usually small relative to the rest of a powertrain's losses [52]. Additionally, there was little evidence that the wheel-axle losses varied significantly based on the way in which the vehicle was driven [12] [40]. Just as in Level 1, the Level 2 wheel-axle block accepts the force and speed inputs from the vehicle block, converts the force and linear speed requests to torque and angular speed requests, accounts for the losses in the wheel and axle, and then outputs the updated torque and angular speed requests to the gearbox block.

3.3 Gearbox Block

The Level 2 gearbox block takes the torque ($T_{in\ GB}$) and speed ($\omega_{in\ GB}$) requests from the wheel-axle block as inputs, calculates the efficiency of the gearbox over a time step, accounts for the effects of the gear ratio, and outputs an updated torque and speed request, typically to the motor block.

A survey of the literature revealed that most vehicle modeling programs simply treat a given gear ratio as having a fixed efficiency [26] [53] [54]. Additionally, literature on the topic of gear design and analysis either does not discuss gear efficiency or assume that it can be modeled as a constant value for a given ratio [55] [56]. However, it was gathered from consultations with practitioners in the field that the efficiency of gearboxes does in fact vary based on the driving patterns of the vehicle. So a means for modeling that varying efficiency in a physically-meaningful yet product-independent manner, consistent with the goals of Level 2, was sought. Given the lack of availability of a varying efficiency gearbox model in the literature that could be applied to Level 2, it was decided that Level 2 would employ a version of the general gearbox efficiency model in Equation 4.40 (discussed in Section 4.3) to calculate the gearbox efficiency. This equation is based on empirical observations that were obtained via work done by Hewland [44] [57]. The key point to bear in mind when adapting Equation 4.40 for use in Level 2 is that the maximum torque rating of the drive motor is not known in Level 2, whereas it is known in Level 3. This is due to the fact that Level 2 is a backwards simulation and the maximum limits of its components are not known in advance due to the backwards model's objective of outputting sizing estimates. In order to adapt Equation 4.40 for use in Level 2, the assumption was made that

$$\frac{T_{\max GB\ in}}{N} = T_{\max motor} \tag{3.1}$$

where $T_{max\ motor}$ is the rated torque of the motor, N is the gear ratio, and $T_{max\ GB\ in}$ is the highest single torque request received by the gearbox block over the course of the entire drive cycle. This assumption is akin to assuming that the motor is exactly sized to meet the maximum torque demands placed on the vehicle. It is a simplifying assumption, but one that still enables the Level 2 model to be used effectively for component sizing purposes. It also requires that the simulation proceeds entirely though the gearbox block before any torque and speed demands are passed to the motor block.

Equation 4.40 assumes that the losses in the gearbox are due to friction in the meshing between the gear teeth and in the seals and bearings where k_m, k_{seal}, and k_b represent the coefficients of those loss terms respectively [44]. Note at this point (Equation 3.2) that the losses due to the seals have been assumed to scale with the torque rating of the gearbox as a result of the assumption in Equation 3.1. While this is a simplifying assumption in order to enable Equation 4.40 to function in the Level 2 model, it is one that was deemed reasonable based on literature and data from and consultations with gearbox manufacturers [44] [52] [57].

The assumption implicit in Equation 3.1 is that the small (but non-negligible) gearbox losses do not impact the motor sizing, at least insofar as the assumption is applied towards approximating Equation 3.1 so that Equation 3.2 can be used in Level 2. This was deemed reasonable given the minor impact that this assumption has on calculating gearbox efficiency and given the generally high degree of uncertainty that is embedded in the Level 2 model.

In addition to the seal losses, the meshing and bearing losses scale with the power transmitted by the gearbox – all of which is based on empirical observations [44] [52] [57]. By substituting the assumption in Equation 3.1 into Equation 4.40, the equation that expresses the efficiency of the Level 2 gearbox is

$$\eta = \frac{T_{in\ GB}\omega_{in\ GB}}{T_{in\ GB}\omega_{in\ GB} + k_{seal}T_{\max GB\ in}\omega_{in\ GB} + (k_m + k_b)T_{in\ GB}\omega_{in\ GB}} \qquad 3.2$$

where T_{in} and ω_{in} are the torque and speed inputs, respectively, to the gearbox block from the wheel-axle block. Note from this equation that the speed terms cancel out, showing that the efficiency only varies with torque. The speed terms were included in this presentation of Equation 3.2 in order to more clearly show how the losses varied with power.

The coefficients of the loss terms can assume a range of values, but k_{seal} and k_b are generally set to 0.00103 and 0.005, respectively [57]. The coefficient due to meshing losses is difficult to know precisely, but it is generally held to be between 0.015 and 0.02 [52] [57]. This holds true for a gearbox of most any size or ratio that would reasonably be found in a light-duty automobile [52] [57]. This also meets the OVEM objective of using models that can rapidly compare a range of technologies and topologies.

An efficiency map for a gearbox generated from a vehicle based on the Nissan LEAF, a commercially available electric vehicle, (parameters in Table 3.1) is shown in Figure 3.1.

Table 3.1: Parameters for the modeled Nissan LEAF

C_D	A_f (m^2)	m (kg)	r (cm)	f_o	f_s
0.29	2.3	1678	31	.01	.002

Figure 3.2 contains an efficiency map from an actual one-speed gearbox [44]. In Figure 3.1 and Figure 3.2, the torque and speed axes have been scaled by the maximum torque and speed values of the simulated and actual gearboxes, respectively. While the model does not completely represent the losses in the actual gearbox, and the two maps are for different types of vehicles, there is a qualitative similarity between the Level 2 model and the actual gearbox and a quantitative similarity in that the model approximates the average efficiency of the gearbox over its speed range. Both figures show that the efficiency is primarily dependent upon torque, and that the efficiency increases as torque increases. The Level 2 model does not fully account for an increasing speed-dependence seen in the actual efficiency data at higher efficiencies. Nevertheless, it was deemed to be an acceptable model for the Level 2 simulation given the physically-meaningful and product-independent fidelity objectives and uncertainty characteristics of Level 2, as set forth in Chapter 1.

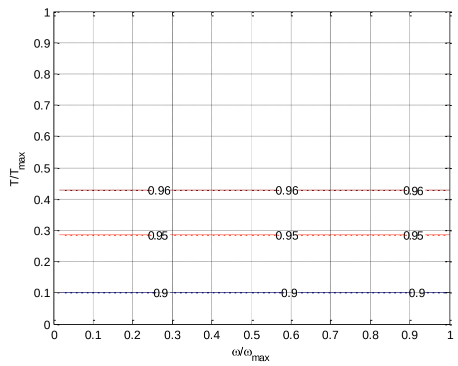

Figure 3.1: Efficiency map generated using the Level 2 gearbox model for the Nissan LEAF over the LA-4 drive cycle; k_m=0.015, k_{seal}=0.00103, and k_b=0.005

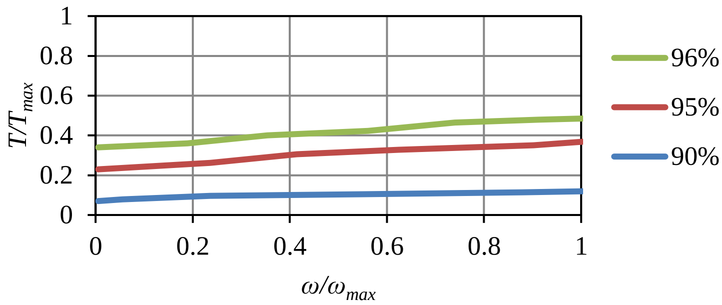

Figure 3.2: Efficiency map from an actual single speed gearbox [44]

Once the gearbox efficiency for a given time step is calculated, it is applied, along with the gear ratio, according to Equations 2.17 and 2.18, towards calculating the updated torque request that will be the gearbox block's output. The updated speed request is calculated just as in Level 1 according to Equation 2.19. The gearbox block outputs these updated torque and speed requests, typically to the motor block.

3.4 Motor Block

The electric motor model takes the torque ($T_{in\ motor}$) and speed ($\omega_{in\ motor}$) requests from the gearbox as inputs, calculates the efficiency of the motor, and then applies that efficiency towards providing a power request sent as an output, typically to the power electronics block. In a real electric motor, the efficiency varies depending on the torque and speed at which the motor is operating. The Level 2 motor model seeks to simulate that. The motor model makes the assumption that a motor's losses stem solely from two sources: copper and iron losses. This assumption is true for nearly all types of electric motors [24].

Copper losses are the losses due to the resistance of the conducting wires within the motor. Since they are a resistive loss, the power loss, P, due to copper losses is modeled as

$$P = I^2R \ . \tag{3.3}$$

where I is the current and R is the resistance. In an electric motor, the torque is generally proportional to the current so the copper losses, P_{copper}, in an electric motor can be assumed to be proportional to the square of the torque as made equivalent by the proportionality constant, k_c [46],

$$P_{copper} = k_cT^2 \ . \tag{3.4}$$

Iron losses encompass two types of losses: hysteresis and eddy current losses. Hysteresis losses stem from the additional amount of energy required to continuously magnetize and demagnetize the metal in the motor [24]. Eddy currents are currents generated in the motor's ferromagnetic material by the rotating magnetic field [58]. Eddy currents are subject to the same resistive losses modeled by Equation 3.3. The eddy current and hysteresis losses both arise from the fluctuating magnetic field which varies with the speed of the motor. Therefore, the iron losses, P_{iron}, are proportional to the speed of the motor as made equivalent by the proportionality constant, k_i,

$$P_{iron} = k_i\omega \ . \tag{3.5}$$

The overall efficiency of the motor can then be modeled as

$$\eta_{motor} = \frac{T_{in\,motor}\omega_{in\,motor}}{T_{in\,motor}\omega_{in\,motor} + k_cT_{in\,motor}{}^2 + k_i\omega_{in\,motor}} \ . \tag{3.6}$$

Once the motor efficiency over a given time step is determined, the power requested by the motor is calculated according to Equations 2.20 and 2.21. For more information on how the coefficients for the copper and iron losses are calculated, refer to Section 3.4.1 below. The motor block's power request is then passed along as an output, typically to the power electronics block. It should also be noted that the Level 2 motor block can account for multiple tractive and in-wheel motors.

3.4.1 Determining the Coefficients in the Level 2 Motor Model

When the simulation begins, the coefficients for the loss terms are unknown, and to generate a simulated efficiency map for the motor that depends on torque and speed they must either be calculated or entered in manually. If they are entered in manually, then the simulation does not need to calculate them. However, if the user does not enter the coefficients directly, in order to calculate the loss coefficients the user must still enter an approximation for the maximum efficiency of the motor. This maximum efficiency is usually guided by the range of component efficiencies contained in Table 2.1. It was assumed that the motor operates most efficiently when the copper losses equal the iron losses [59]. The gearbox block runs through the entire drive cycle, and the root mean square of the torque and the average speed requested of the motor by the gearbox block are determined. It was then assumed that the maximum efficiency of the motor occurs at the root mean square of the torque and the average speed requested of the motor by the gearbox block – which serves as an approximation for assuming that the motor is ideally sized for the road load requested of it. With these assumptions, Equation 3.6 now appears as

$$\eta_{max\ motor} = \frac{T_{rms}\omega_{avg}}{T_{rms}\omega_{avg} + k_c {T_{rms}}^2 + k_i \omega_{avg}} \qquad 3.7$$

where $\eta_{max\ motor}$ is the user-specified maximum motor efficiency, and T_{rms} and ω_{avg} are the root mean square torque and average angular velocity, respectively, requested of the motor block over the entire drive cycle. Since the iron and copper loss terms are equal and T_{rms} and ω_{avg} are known, then k_c and k_i can be obtained. Once all of the loss coefficients have been determined, then Equation 3.6 can be used to generate an efficiency map for the vehicle to use throughout the simulated drive cycle. Figure 3.3 shows an efficiency map obtained from using the Level 2 simulation to model the motor of the Nissan LEAF. The map in Figure 3.3 combines the efficiency of the motor and power electronics since this is a common way to present electric motor efficiency maps.

3.5 Power Electronics Block

The power electronics block receives the torque ($T_{in\ PE}$) and speed ($\omega_{in\ PE}$) requests from the motor as an input, calculates the efficiency of the power electronics, applies that efficiency to an updated power request, and outputs that power request, typically to the energy storage system block. The power electronics block creates an efficiency map to determine the efficiency of the power electronics based on the way the vehicle is being driven.

In power electronics, the two primary losses are conduction and switching losses [60]. Conduction losses are due to the resistivity of the wires, electronic switching components, and connections [46]. The aim of Level 2 was to model the losses from each of its components in a manner that is physically meaningful in the way it accounts for losses but also general enough to account for an array of technologies. With that in mind, it is known that the conduction losses ($P_{conduction}$) in power electronics switches can in the most simple case be modeled as purely Ohmic where

$$P_{conduction} \propto I^2 \ . \qquad 3.8$$

However, the conduction losses are not always purely Ohmic for all power electronic switch technologies [60]. Thus, given the design criteria for Level 2, which was to be able to scope across an array of technologies in a general yet physically meaningful and product-independent way, it was determined that building in the capacity to model switches where the losses were not purely Ohmic was a necessary function. For such switches where the conduction losses are not purely Ohmic, the conduction losses are proportional to the current raised to an exponent (β), where the exponent varies between 1.8-2.2 [60]. As current is proportional to torque, torque (T) was substituted in for current in the relationship in Equation

3.8 thus making torque proportional to the conduction losses. In order to account for unit dimensionality issues when factoring in these non-Ohmic loss characteristics, the following equation was used where the normalizing value (T_0^{β}) was used as a factor in the coefficient equating the conduction losses to the torque

$$P_{conduction} = \frac{k_{conduction}}{{T_0}^{\beta}} T^{\beta} \quad . \tag{3.9}$$

This normalizing factor eliminates the dimensionality issue posed by the exponent β. Switching losses, $P_{switching}$, are approximately linearly proportional to torque [44]. They can be made equivalent by the proportionality constant, $k_{switching}$,

$$P_{switching} = k_{switching} T \quad . \tag{3.10}$$

The overall expression for the efficiency of the power electronics is modeled as

$$\eta_{PE} = \frac{T_{in\ PE}\,\omega_{in\ PE}}{T_{in\ PE}\,\omega_{in\ PE} + \frac{k_{conduction}}{{T_0}^{\beta}} {T_{in\ PE}}^{\beta} + k_{switching} T_{in\ PE}} \tag{3.11}$$

The power electronics block assumes that the loss mechanisms are the same during motoring and regenerative braking.

3.5.1 Determining the Coefficients in the Level 2 Power Electronics Model

Just as with the motors, the assumption was made that the peak efficiency is obtained when the two loss terms – switching and conduction losses – are equal. The user must set the maximum efficiency, and it was assumed that the maximum efficiency occurs at the root mean square of the torque and the average speed of the vehicle as outputted by the gearbox block over the entire drive cycle. This enables the power electronics block to calculate the $k_{conduction}\ /T_0^{\beta}$ and $k_{switching}$ coefficients (which can also be inputted manually by the user). Once the coefficients are obtained, Equation 3.11 can be used to produce an efficiency map for the power electronics. The efficiency map of the power electronics is applied to the power request outputted by the block according to Equations 2.22 and 2.23. Figure 3.3 shows the combined efficiency map for the motor and power electronics produced by the Level 2 model based on the Nissan LEAF. Figure 3.4 presents an efficiency map for an actual motor and power electronics system [61]. The Level 2 motor and power electronics models simplify the loss mechanisms actually experienced by real motors and power electronics. Nevertheless, the agreement between Figure 3.3 and Figure 3.4 show that the Level 2 motor and power electronics blocks are sufficiently representative (for the purposes of Level 2) in simulating the efficiency of the components they attempt to model.

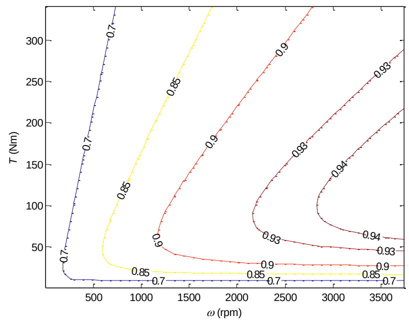

Figure 3.3: Combined efficiency map from the motor and power electronics in the Level 2 model, note that the Level 2 map does not impose any torque or speed limits

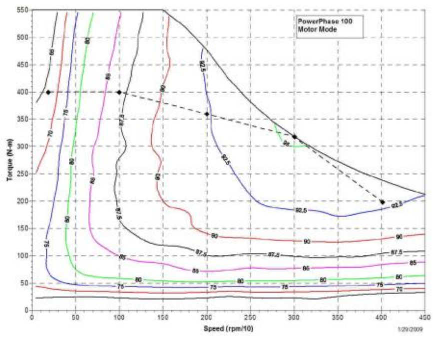

Figure 3.4: Combined efficiency map for an actual motor and power electronics system [61]

3.6 Energy Storage System Block

The energy storage system block is the last block in the Level 2 EV simulation. It accepts the power request from the power electronics block, calculates the efficiency of the energy storage system over a given time step, applies that efficiency to the power request of the energy storage system, and outputs the energy storage system's power request. Energy storage systems such as batteries and ultracapacitors can both be modeled as voltage sources in series with an internal resistance [62]. The internal resistance dissipates power as a pure resistor would, as seen in Equation 3.3. Since current is proportional to torque, the energy storage system efficiency can be modeled as

$$\eta_{ESS} = \frac{T_{in\ ESS}\omega_{in\ ESS}}{T_{in\ ESS}\omega_{in\ ESS} + k_{ESS\ cond}T^2}\ . \qquad 3.12$$

This is a simplification of the actual loss mechanisms in energy storage systems of different technologies. Yet, this simplification is in line with the methods and aims of the Level 2 model.

3.6.1 Determining the Coefficients in the Level 2 ESS Model

The user must set the peak efficiency of the energy storage system in order to proceed. The peak efficiency is assumed to occur at the root mean square of the torque and the average speed of the vehicle as requested by the gearbox over the entire drive cycle. With this assumption, $k_{ESS\ cond}$ can be calculated. Then the energy storage system block proceeds to apply the efficiency to the energy storage system’s power request according to Equations 2.24 and 2.25. Once the efficiency has been applied, the power request is sent as an output. These power requests can be plotted over time and integrated to yield the estimated energy consumption of the vehicle.

3.7 Level 2 Case Study: Milk Float Modeling

The following is a case study that builds on the Level 1 case study of the milk floats (Section 2.8). It provides an illustration of how the Level 2 model can be used to produce more refined estimates for range and energy consumption for a number of technologies and capabilities in an analysis environment with high uncertainty.

3.7.1 Introduction

The case study with the milk floats was continued with the Level 2 simulation. The goal in this study was to refine the initial estimates concerning the prospects for extending the range of the milk floats to 105 km (65 mi) by utilizing regenerative braking.

3.7.2 Methods

This study first had to establish that the Level 2 model was closely characterizing the actual performance of the floats. This study used the same vehicle parameters (seen in Table 2.2) and drive cycle (seen in Figure 2.12) as the Level 1 study. This study also followed the same methodology as in Level 1 where the cargo mass of the float was linearly reduced as the float was run through 22 iterations of the drive cycle for the DC motor and 28 iterations for the AC motor.

The Level 2 simulation requires that the maximum efficiencies for the gearbox, motor, power electronics, and energy storage system models be set by the user. The estimate for the efficiency of the wheel-axle is fixed throughout the simulation. The estimated maximum efficiencies were based on values reported in the literature [9] [12] [21]. At the end of the simulation, the average efficiencies for the components over the course of the drive cycle were obtained.

It should be noted that the loss coefficients for the motor, power electronics, and energy storage system models are not recalculated each time the cargo mass is reduced. They are fixed based on what they were determined to be for the first iteration when the float was fully laden. This is a necessary condition because the characteristics of the motor, power electronics, and energy storage system will not change as a float sheds its cargo. Table 3.2 and Table 3.3 show the average efficiencies and where applicable the maximum efficiencies for each of the components in the DC and AC motors respectively.

Table 3.2: Estimated maximum component efficiencies for a powertrain with a DC motor

	Wheel-Axle	Gearbox	Motor	PE	ESS
Maximum	99%	98%	80%	95%	94%

Table 3.3: Estimated maximum component efficiencies for a powertrain with an AC motor

	Wheel-Axle	Gearbox	Motor	PE	ESS
Maximum	99%	98%	95%	95%	94%

3.7.3 Results and Discussion

Table 3.4 and Table 3.5 show the average efficiency of the components over the course of an entire delivery run for a milk float with a DC and AC motor, respectively.

Table 3.4: Average efficiency of each component over a delivery run in a float with a DC powertrain

	Wheel-Axle	Gearbox	Motor	PE	ESS
Average	99%	97%	68%	94%	90%

Table 3.5: Average efficiency of each component over a delivery run in a float with an AC powertrain

	Wheel-Axle	Gearbox	Motor	PE	ESS
Average	99%	97%	87%	94%	90%

Table 3.6 shows the predicted range of the floats if they were able to recapture 0%, 50% and 100% of the energy available to their energy storage systems when braking (note that this is the energy *available* to the energy storage system, therefore, it reflects the losses from the components that the energy passed through prior to reaching the energy storage system).

Table 3.6: Range of the floats with no regenerative braking and the predicted range given two different regenerative braking scenarios

	Range with no regenerative braking (km)	Estimated range with ESS capturing 50% of energy available to it (km)	Estimated range with ESS capturing 100% of energy available to it (km)
DC	56	66	79
AC	72	92	127

Most notably for this study, the Level 2 simulation showed that if a milk float with an AC motor was able to use regenerative braking, it could have the potential to exceed the target range of 105 km. While it is impossible for a milk float's energy storage system to capture 100% of the energy available to it, for reasons discussed in Section 2.8.3, it is likely that a milk float's energy storage system could capture a significant portion of the energy available to it. Though the exact amount of energy it could recapture is still unknown at this point. It is also interesting to note that, even with regenerative braking, floats with the less efficient DC motors would likely be unable to achieve the target range of 105 km. The Level 2 simulation showed results similar to those from the Level 1 simulation. All of the respective range predictions were within 4% of each other (refer to Table 2.7).

To gain a better understanding of how the chosen parameters affected the range of the simulated milk floats, a sensitivity analysis was performed (Figure 3.5). Just as in Section 2.8.3, each of the vehicle parameters that could reasonably be varied were varied by ±5% and the corresponding change in the float's range was recorded. A sensitivity analysis was done for both floats using both the DC and AC motors. The data presented in Figure 3.5 is the average of the absolute values of the percent changes in range caused by either the 5% increase or decrease in the vehicle input parameters. In this analysis, it was assumed that the energy storage systems recaptured 50% of the energy *available* to them. This condition was selected in order to provide a conservative and representative snapshot of the floats by avoiding modeling them at the upper or lower limits of their regenerative braking possibilities. Also note that the results in this sensitivity analysis were done for these specific floats over a specific drive cycle, and any conclusions drawn from this analysis regarding the sensitivity of the model to the input parameters cannot be uncritically applied to any vehicle in any context.

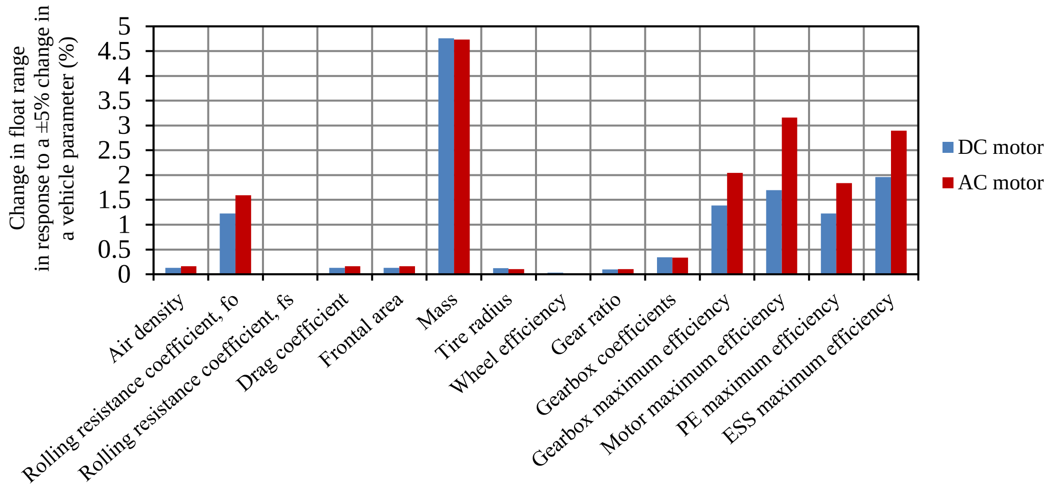

Figure 3.5: Level 2 sensitivity analysis for the milk floats with DC and AC motors

The Level 2 sensitivity analysis shows many similarities to the analysis done for the milk floats in Level 1. As in Level 1, the parameters affecting aerodynamic drag have little impact on the floats' range due to the fact that the floats do not travel at high enough speeds for drag to have a significant effect. The floats' low speed also leads the rolling resistance coefficient (f_s) that is scaled by speed to have little effect on the floats' range while the rolling resistance coefficient that is not influenced by speed (f_o) has a comparatively greater effect on vehicle load than those parameters affecting the resistive forces that are dependent on speed. Once again, the model is highly sensitive to the mass of the floats, which is expected given that the floats are heavy vehicles undergoing frequent accelerations and decelerations along their delivery routes. The fact that the model is so sensitive to mass means two things for the model. On the one hand, mass is a parameter that is actually known with a high degree of certainty for the floats which appears to add credibility to the results. On the other hand, the manner in which the cargo mass is offloaded from the floats requires a number of assumptions that may not be entirely accurate. It is possible that the lack of knowledge about the exact cargo offloading patterns of the floats could be a significant contributor to any disagreement between the modeled and actual results.

The tire radius and gear ratio both have little effect on the floats' range. This is likely because the tire radius and gear ratio both primarily affect how the required power from the vehicle will be disaggregated into torque and speed. Yet this has less significance in affecting vehicle range in the Level 2 model since the motor (the component whose efficiency is ordinarily most sensitive to the torque and speed combinations produced by a given driving pattern) is optimally sized for a particular vehicle given the nature of the Level 2 model (Section 3.4).

The component efficiencies – wheel, gearbox, motor, and energy storage system – demonstrate an effect on the floats similar to the one seen in Level 1. The range of the floats appears to be most sensitive to those components that have the lowest maximum efficiency (refer to Table 3.2 and Table 3.3). Just as in Level 1, this has two implications. The first is that it is more imperative to have a high degree of confidence regarding the maximum efficiencies inputted for those components with the lowest maximum efficiencies. The second is that small gains in efficiency for the least efficient components can lead to proportionally higher gains in tank to wheel powertrain efficiency than can gains in the efficiency of the more efficient components.

3.8 Summary of Level 2 Contributions

This section provides a synthesis of the novel contributions made in the Level 2 program and how these contributions were developed, i.e. what new knowledge was required to implement them into a working vehicle modeling program. The contributions range from the broad – the fundamental nature of the Level 2 program – to the detailed – specific innovations made in individual component blocks.

The fundamental structure of the Level 2 program as a functioning backwards vehicle model where the component efficiencies vary in a product-independent yet physically-meaningful way constitutes a novel contribution to knowledge. As was the case with the

Level 1 program, the theory of backwards energy flow vehicle modeling programs existed, but that theory had not been translated to an actual computer model. Novel thinking outlined throughout Chapter 1 identified that a backwards energy flow vehicle model where the component efficiencies varied in a product-independent but physically meaningful manner would constitute a novel contribution. Once this opportunity was identified, novel work was then conducted to turn the theory of backwards energy flow vehicle modeling into an actual computer model. Translating the theory into a reality required novel work from the author to develop and build the framework for the entire model as well as the intricacies of its constituent parts. In the case of the Level 2 model, it is most effective to explain the novel contribution of the entire program by looking at the novel contributions of each of its parts (gearbox, motor, power electronics, and energy storage system) and how those novel contributions were developed.

Gearbox models could be found in existing energy flow vehicle models. However, these models had made the simplifying assumption that the efficiency of the gearboxes could be treated as constant [26] [40]. This assumption is overly simplified as it disregards empirical data from the literature which shows that gearbox efficiency varies based on its design (gear ratio and seal, bearing, and meshing losses) and upon the load it is transmitting. In order to build a gearbox model where the efficiency would vary in a product-independent yet physically meaningful way, existing empirical work was leveraged by the author [44] [57]. The novel work came in creating Equation 3.2 and then turning it into a programmable algorithm (described in detail in Section 3.3) based on this existing empirical work.

The motor, power electronics, and energy storage system models in the Level 2 program also constitute a novel contribution to knowledge. While each component's model represents a unique contribution, the manner in which each model was developed is similar enough such that it makes sense to combine the discussion on how each component model was developed. The body of knowledge on the primary loss mechanisms for electric motors, power electronics, and energy storage systems is well-established. The novel work came in adapting this existing knowledge on the primary loss mechanisms for each component given the unique focus of Level 2 on providing product-independent yet physically meaningful simulations. This required deriving the efficiency equations (Equations 3.6, 3.11, and 3.12) for each of these components – where both the derivations and the resulting efficiency equations were novel. Novel work was also required to develop the modeling principles that enable the coefficients of the efficiency equations to be calculated in a product-independent manner. These principles are explained in detail in Sections 3.4.1, 3.5.1, and 3.6.1. For more information on the novel work behind these component models, refer to Section 3.4 for the motor, Section 3.5 for the power electronics, and Section 3.6 for the energy storage systems.

4 Level 3 Simulation

OVEM's Level 3 model addresses the problem of rapidly simulating existing and emerging technologies, arranged and managed in many different ways, with a sufficient degree of accuracy (approximately within 2-5% of real-world values). Level 3 uses a backwards-forwards simulation technique, which builds on Levels 1 and 2 by capitalizing on reduced uncertainty and high-fidelity models to make more accurate predictions regarding figures such as range, emissions, energy consumption, and component sizing.

Level 3 was constructed such that it aligned with the criteria set forth for OVEM in Section 1.5. Level 3 was intended to rapidly simulate emerging and existing technologies and capabilities, and that intent is reflected throughout Level 3. As was discussed in Chapter 1, the *rapid* simulation of existing and emerging technologies and capabilities is enabled by the fact that the component models in Level 3 are based on readily-available data from specific products. As such, the Level 3 component models were built so that they could allow for the incorporation of readily-available information on existing and emerging products without requiring extensive experimental or computational resources to obtain and process that simulation's data. This chapter will explain in detail the types of readily available data for the different powertrain components and how this data was incorporated into models built to handle data for an array of technological variations. The fact that the Level 3 component models employ readily-available data also means that they do not incorporate data that is generally not readily available. This means that certain physical effects and characteristics are not accounted for – as was outlined in the non-criteria enumerated in Section 1.8.

The Level 3 models were built around the timescales and conditions of interest to OVEM. The timescales of interest are approximately from 1 s to 10^4 s, and the remainder of this chapter will demonstrate how the component models reflect that. The condition of OVEM's interest in straight-line travel is also reflected in Level 3, and Level 3 has the capacity to incorporate slopes alongside of the drive cycles.

In addition to meeting all of the other criteria set out above and in Chapter 1, Level 3 was designed to meet an accuracy objective of being within approximately 2-5% of real-world figures. This chapter and a validation in Section 6.3 provide illustrations to demonstrate that Level 3 ultimately meets this accuracy objective.

For each powertrain topology, the Level 3 simulation begins with a backwards-looking information flow. During the backwards phase of the simulation, the torque, speed, and power requested of each component is calculated with each component factoring in its own losses and performance limits before passing its torque, speed, and power requests along to the upstream components. Once the simulation can proceed no further in the backwards direction, and the simulation records how much power it was able to produce/accept, the forwards phase of the simulation begins. During the forwards phase of the simulation, the torque, speed, and power that each component can produce is calculated based on the amount of power the vehicle was actually able to produce in response to the request calculated during the backwards phase.

Below is a discussion of the four powertrain topologies currently implemented in Level 3: EV, series HEV, parallel HEV, and series-parallel HEV. Figure 4.1 outlines the high-level information flows in the Level 3 electric vehicle simulation. The electric vehicle model is the foundation of the Level 3 simulation. Many of the component blocks and modeling principles used in the electric vehicle model serve as the basis for the models in the other topologies. The electric vehicle model begins by proceeding in the backwards direction with each component factoring in its losses and performance limits. Once, the simulation reaches the energy storage system blocks, the energy storage system blocks calculate how much power they are able to accept or produce in response to the backwards power request. With the information on how much power the energy storage system can accept or produce, the simulation then proceeds in the forward direction with each component making use of the vehicle's available power and/or torque and speed to try to meet the initial power, torque, and speed requests of the backwards run. The Level 3 electric vehicle model has unique capabilities that will be highlighted in the following sections, chief among them is the ability to rapidly and accurately incorporate data from new technologies into its component models and to arrange these models in innovative ways, such as in a hybridized energy storage system.

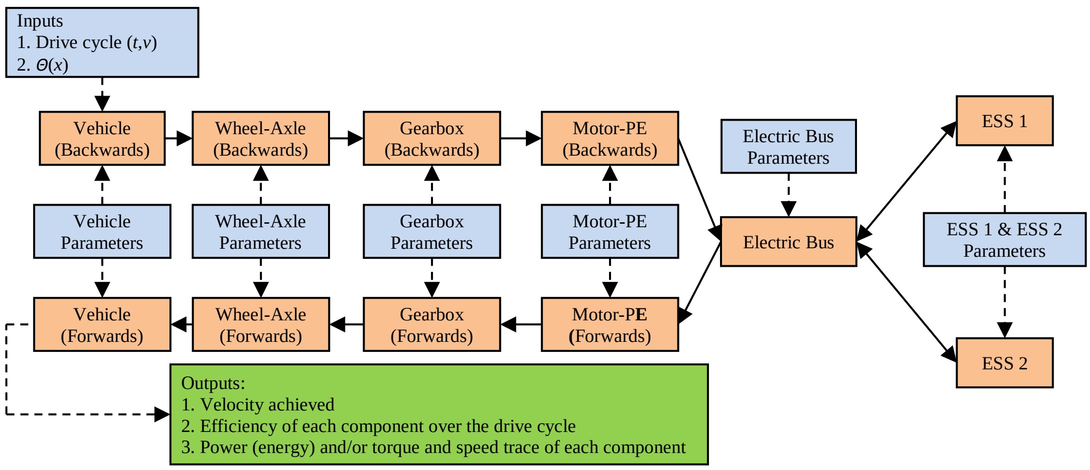

Figure 4.1: Information flows in the Level 3 EV model

The primary difference between the Level 3 series hybrid model and the Level 3 electric vehicle model is that the series hybrid model contains an alternative power unit that connects to the electric bus. As was noted in Chapter 1, the alternative power unit usually takes the form of an internal combustion engine or a fuel cell. Figure 4.5 provides a representation of the information flows within the series HEV model. The alternative power unit's function can be envisioned as a third energy storage system that is capable of delivering power via the consumption of a fuel. Though unlike an energy storage system, an alternative power unit is not capable of accepting power and storing energy. The exact role the alternative power unit plays in the vehicle depends on the nature of the alternative power unit and the vehicle's energy management strategy.

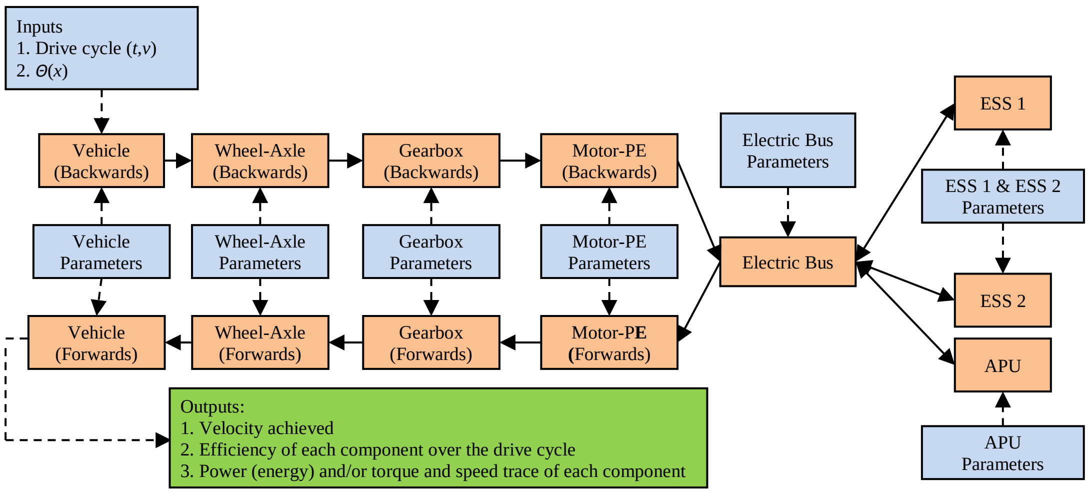

Figure 4.2: Information flows in the Level 3 series HEV model

As was explained in Sections 1.2.3 and 1.2.4, parallel and series-parallel hybrids have an internal combustion engine that shares the road load with an electric motor. In both a parallel and series-parallel hybrid, the power supplied by the motor and internal combustion engine is blended together by a transmission that typically takes the form of an epicyclic gear train (EGT). In a parallel hybrid, the internal combustion engine does not produce extra power to recharge the energy storage system; whereas in a series-parallel HEV, the internal combustion engine can produce extra power to recharge the energy storage system [12]. Since this small difference is primarily what distinguishes a parallel from a series-parallel HEV, the models are similar. The series-parallel HEV just has the ability to request extra power from the internal combustion engine, and then it is able to pass that power through the epicyclic gear train and the motor/generator to recharge the energy storage system. Figure 4.3

and Figure 4.4 illustrate the information flows within the parallel and series-parallel hybrid models, respectively.

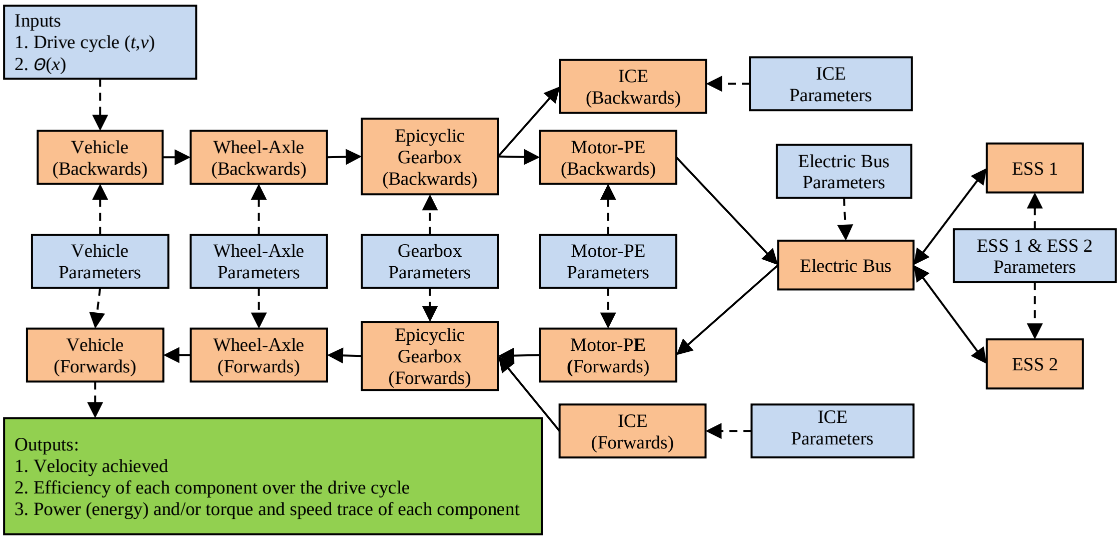

Figure 4.3: Information flows in the Level 3 parallel HEV model

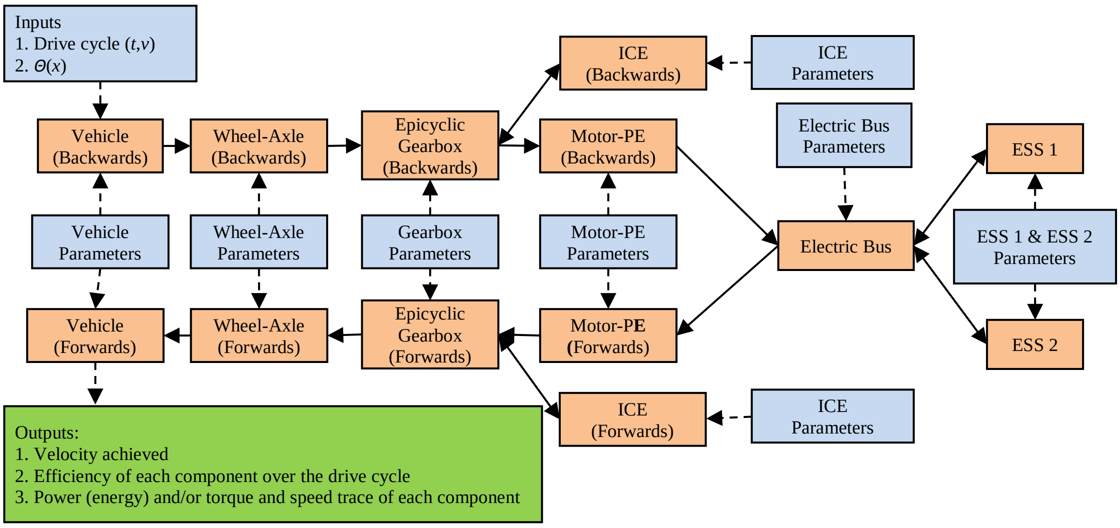

Figure 4.4: Information flows in the Level 3 series-parallel HEV model

For more insight into how Level 3 can be used, refer to the case study in Section 4.10 and to the author's original journal-published articles in Chapters 5 and 6.

4.1 Vehicle Blocks

The vehicle blocks serve as the interface between the vehicle and its environment. The purpose of the backwards vehicle block is to model the external forces acting on the vehicle in order to provide the rest of the simulation with the force and speed targets that the vehicle must strive to meet. The purpose of the forwards vehicle block is to take the force and speed that the vehicle is able to produce at its wheels and then determine what the final speed of the vehicle will be at the end of every time step as it moves along the road. The vehicle blocks account for the forces resulting from drag, rolling resistance, slope, and acceleration. These are the primary longitudinal forces acting on a vehicle when it travels in a straight line, which is why they were included in this study. No lateral forces were included as it was assumed that the vehicle only travels in a straight line. The vehicle model also assumes that the resistive forces it does account for can be accurately modeled by the equations and approach outlined in Section 2.1.

4.1.1.1 Backwards Vehicle Block

The backwards vehicle block operates similarly to the vehicle blocks in Levels 1 (Sections 2.1) and 2 (Section 3.1). The main difference stems from the fact that Level 3 is a backwards-forwards simulation where the real-world performance limits of the component models mean that a vehicle may not be able to completely meet the requested drive cycle. In order to account for this, the Level 3 vehicle block substitutes the value $v_{ach,i}$ which represents the velocity achieved at the end of the previous time step, for $v_{req,i}$, the velocity requested at the end of the previous time step. In Level 3, the term $v_{ach,i}$ is calculated as the output of the forwards vehicle block during the previous time step and reflects the vehicle's best attempt to meet the requested drive cycle given the limitations of its components. For the first time step in a Level 3 simulation (that is when $v_{ach,i}$ has not been calculated yet) $v_{req,i}$ is still used, and the speed and force outputted by the backwards vehicle block are calculated just as in Equations 2.1 through 2.13 in Section 2.1. However for all time steps after the first time step (that is once $v_{ach,i}$ has been calculated by the forwards vehicle block), $v_{ach,i}$ is substituted for $v_{req,i}$ in Equations 2.1 through 2.13 producing

$$v_{veh\ reqd\ avg} = \frac{v_{ach,i} + v_{req,i+1}}{2} \quad 4.1$$

$$F_D = \frac{1}{2}\rho C_D A_f \left(v_{veh\ reqd\ avg}\right)^2 \quad 4.2$$

$$F_g = mg\sin(\theta) \quad 4.3$$

$$F_{rr} = \mu_{rr} mg\cos(\theta) \quad 4.4$$

$$F_{inertia} = \frac{J_w}{r^2}a \quad 4.5$$

$$F_{accel} = ma = m\frac{v_{req,i+1} - v_{ach,i}}{t_{i+1} - t_i}. \quad 4.6$$

where μ_{rr} is calculated according to Equation 2.11. The total force the vehicle must produce is still calculated based on

$$F_{veh\ reqd\ avg} = F_D + F_g + F_{rr} + F_{inertia} + F_{accel}\ . \quad 4.7$$

Just as was explained in Section 2.1, the velocity and force requested by the backwards vehicle block are calculated in this manner in order to negotiate a reasonable balance between computational runtimes and accuracy.

It is important to emphasize that the $v_{ach,i}$ term implies that it is possible for the vehicle to not fully meet the requested drive cycle due to realistic performance limits in the other component models in the powertrain. If during a given time step the vehicle is not able to meet the drive cycle, then at the beginning of the next time step the vehicle will be traveling at a speed less than the speed that is being requested of it. In this case, the vehicle will be called upon to try to make up for its deficient velocity output in an effort to close the gap between the speed it has obtained and the speed requested of it. Figure 4.5 provides an illustration of the relationship between the velocity requested and velocity achieved by a vehicle in a case when the vehicle is not able to exactly meet the drive cycle. As shown in

Figure 4.5, the most common instances when the velocity achieved will deviate from the velocity requested will come when the vehicle is requested to undergo high accelerations, attain high speeds, or ascend steep hills. Generally such extreme driving conditions fall outside of the scope of OVEM. Yet, the simulation keeps a record of how much the achieved velocity deviates from the requested velocity. Powertrains that have significant discrepancies between the requested and achieved velocities are deemed failures, and only powertrains that actually meet the drive cycle are considered to be viable.

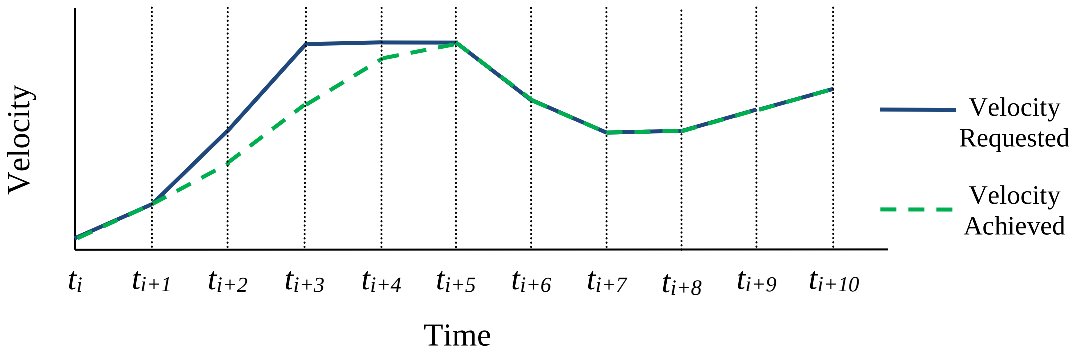

Figure 4.5: Qualitative illustration of a potential relationship between the velocity requested and achieved, demonstrating circumstances where the vehicle would not be able to completely meet the drive cycle

The force request ($F_{veh\ reqd\ avg}$) and the speed request ($v_{veh\ reqd\ avg}$) are the outputs of the vehicle block, and they are passed to the backwards wheel-axle block.

4.1.1.2 Forwards Vehicle Block

The vehicle speed achieved at the end of each time step is limited by either the amount of torque or the amount of speed the powertrain could produce [26]. Therefore, the forwards vehicle block takes the linear force and speed outputted from the forwards wheel-axle block to determine which one will determine the final speed the vehicle achieves at the end of each time step.

To calculate the speed-limited case, the forwards vehicle block begins with the speed it received as an input from the wheel-axle block, $v_{veh\ in}$, which represents the speed that the vehicle can produce in its best attempt to meet the drive cycle. That speed is taken to be the average of the speed achieved at the end of the previous time step, $v_{ach,i}$, and the speed that will be achieved at the end of the current time step, $v_{ach,i+1}$

$$v_{veh\ in} = \frac{v_{ach,i+1} + v_{ach,i}}{2}\,. \qquad 4.8$$

This can be rearranged to yield an expression for the speed attained at the end of the current time step

$$v_{ach,i+1} = 2v_{veh\ in} - v_{ach,i}\ . \qquad 4.9$$

The torque limited case is derived from Newton's equations of motion (Equations 2.5 through 2.13) except that now the speed achieved at the end of the current time step ($v_{ach,i+1}$) has been substituted into the place of the speed requested at the end of the current time step ($v_{req,i+1}$)

$$F_{ach} = \frac{1}{2}\rho C_D A_f \left(\frac{v_{ach,i+1} + v_{ach,i}}{2}\right)^2 + \mu_{rr} mg\cos(\theta) + mg\sin(\theta) + \frac{(v_{ach,i+1} - v_{ach,i})}{\Delta t}\left(m + \frac{J_{wheel}}{r^2}\right) \qquad 4.10$$

All of the vehicle's shape, mass, and rolling resistance parameters are known, as is the velocity already achieved by the vehicle at the end of the previous time step ($v_{ach,i}$). So Equation 4.10 can be turned into a quadratic equation that can be solved to yield the road speed of the vehicle at the end of the current time step

$$A{v_{ach,i+1}}^2 + Bv_{ach,i+1} + C = 0 \qquad 4.11$$

where

$$A = \frac{1}{8}\rho C_D A_f \qquad 4.12$$

$$B = \frac{1}{4}\rho C_D A_f v_{ach,i} + \frac{\left(m + \frac{J_w}{r^2}\right)}{\Delta t} \qquad 4.13$$

$$C = \frac{1}{8}\rho C_D A_f {v_{ach,i}}^2 - \frac{\left(m + \frac{J_w}{r^2}\right) v_{ach,i}}{\Delta t} - F_{ach} + \mu_{rr} mg\cos(\theta) + mg\sin(\theta) \qquad 4.14$$

An analysis of Equation 4.11 is warranted. The first step is to apply the quadratic formula to Equation 4.11

$$v_{ach,i+1} = \frac{-B \pm \sqrt{B^2 - 4AC}}{2A} \qquad 4.15$$

In order for Equation 4.15 to not have any complex roots,

$$B^2 > 4AC \qquad 4.16$$

must be true. Substituting Equations 4.12 through 4.14 into Equation 4.16 produces

$$\frac{\left(m + \frac{J_{wheel}}{r^2}\right)^2}{\Delta t^2} > \rho C_D A_f \left[\frac{mg}{2}(\mu_{rr}\cos\theta + \sin\theta) - \frac{F_{ach}}{2} - \frac{\left(m + \frac{J_w}{r^2}\right) v_{ach,i}}{\Delta t}\right] \qquad 4.17$$

where in practice, the term on the left hand side of the inequality ensures that for any realistic values the inequality will be true and there will be no complex roots. The only way that the inequality would not be true is if the F_{ach} term were to be sufficiently negative and/or the mass of the vehicle and wheel inertia were sufficiently small. However, if realistic values for these terms are used, this never occurs. For instance, using the Nissan Leaf specifications shown in Table 3.1, Figure 4.6 plots the values for right hand side of the inequality (denoted as RHS) subtracted from the left hand side of the inequality (denoted as LHS) as a function of F_{ach} for five different values of $v_{ach,i}$. The inequality of Equation 4.15 has no complex roots when the LHS-RHS in Figure 4.6 is positive – which as can be seen in Figure 4.6 is true for these, and all other, realistic vehicle parameters.

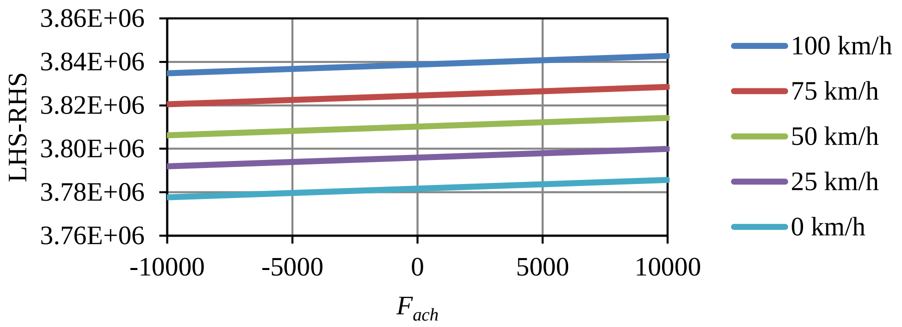

Figure 4.6: Difference between the left hand side and right hand side of the inequality in 4.17 as a function of the force achieved by the vehicle at different speeds. The inequality of Equation 4.15 has no complex roots when LHS-RHS is positive

Since in practice Equation 4.15 produces no complex solutions, it follows that it produces one negative solution and then either an additional negative solution or a positive or zero solution depending on the value of the discriminant relative to *B*. It will be shown that while it is theoretically possible to arrive at two negative solutions or a negative and zero solution, in practice this never happens given realistic values in Equations 4.12 through 4.14.

In order to arrive at a positive and negative solution to Equation 4.15, the following inequality must be true since *B* is always positive

$$B < \sqrt{B^2 - 4AC} \tag{4.18}$$

If both sides of this inequality are squared, it can be simplified to show that in order to arrive at a positive and negative solution to Equation 4.15, the following inequality must be true

$$4AC < 0 \tag{4.19}$$

Since *A* is always positive (refer to Equation 4.12) then the only way for the term 4*AC* to be negative is for the term *C* to be negative. In order for *C* to be negative, this inequality would have to be true

$$\frac{1}{8}\rho C_D A_f {v_{ach,i}}^2 + \mu_{rr} mg\cos(\theta) + mg\sin(\theta) < \frac{\left(m + \frac{J_w}{r^2}\right) v_{ach,i}}{\Delta t} + F_{ach} \tag{4.20}$$

For realistic vehicle parameters (for the types of vehicles of interest to OVEM), the sum of the terms on the right hand side of Equation 4.20 is much larger than the sum of the terms on the left hand side of the expression and the inequality does holds true. The inequality in Equation 4.20 will only be violated if the force achieved is impractically negative (especially given that such a high negative braking force would also have to accompany a low speed) and/or the vehicle mass and wheel inertia is unrealistically low. Thus Equation 4.11 in practice produces one positive and one negative solution and has done so for every realistic vehicle type ever simulated over any drive cycle in OVEM. Figure 4.7 plots *C* from Equation 4.14 as a function of F_{ach} for various values of $v_{ach,i}$ for the LEAF. Note that for all realistic parameters *C* is negative and hence Equation 4.15 produces one positive and one negative solution. The only condition where C is positive is when a braking force is applied to the vehicle once it has already stopped. This is clearly impossible. Thus for all realistic vehicle parameters C is negative and Equation 4.15 produces one positive and one negative solution.

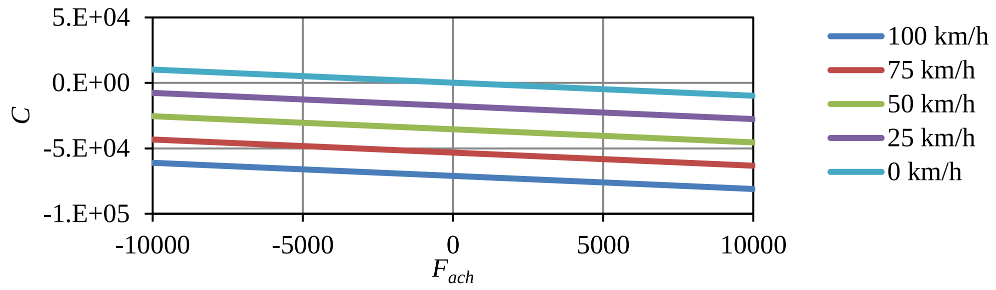

Figure 4.7: C from Equation 4.14 as a function of F_{ach} at various $v_{ach,i}$

The negative solution is rejected since a velocity in OVEM cannot be negative, as OVEM is not concerned with modeling a vehicle traveling in reverse, and the positive solution is retained as the final speed achieved at the end of the time step, $v_{ach,i+1}$, through the torque limited case. This approach is more accurate than the method used in ADVISOR [40]. ADVISOR makes the assumption that the speed achieved at the end of the previous drive cycle is equal to the speed achieved at the end of the current drive cycle

$$v_{ach,i+1}{}^2 = v_{ach,i} \times v_{ach,i+1} \qquad 4.21$$

in order to avoid dealing with the quadratic in Equation 4.11. This oversimplification introduces the likelihood of errors being made in calculating the final speed achieved by the vehicle.

In OVEM, the values for the final speed achieved from both the speed and torque limited cases are compared, and the lowest value for the final speed achieved is taken as the limiting case. Therefore, it is outputted as the speed the vehicle attained at the end of that time step. By knowing the speed achieved at the end of every time step, the user can track how well the modeled powertrain was able to meet the drive cycle.

4.1.1.3 Vehicle Load Transfer

The vehicle block can also account for load transfer in a vehicle. Load transfer is typically an issue that is handled more by programs concerned with vehicle dynamics, which is not OVEM's primary focus. However, load transfer can be of interest in analyzing the effect of how different vehicle constructions affect the ability of an electric or hybrid electric vehicle to capture energy through regenerative braking. Since regenerative braking is a key factor influencing electric and hybrid electric vehicle tank to wheel energy consumption, it was determined that incorporating the ability to model load transfer insofar as it affects regenerative braking capacity was a useful addition for OVEM that was aligned with OVEM's design criteria. Modeling the effect of load transfer on regenerative braking is also a novel contribution made by OVEM to the vehicle modeling landscape.

Load transfer is the physical shift in the amount of load supported by the front and rear axles as the vehicle accelerates and experiences changes in slope [47]. During positive acceleration and hill climb, the rear axle supports an increasing proportion of the vehicle's load. During deceleration and hill descent, the front axle supports a greater proportion of the load. The default setting for the Level 3 vehicle block does not account for the load transfer that takes place within the vehicle when the acceleration and slope are nonzero. This suffices when the user either does not have knowledge of the vehicle's mass distribution or is not concerned with load transfer within the vehicle; however, the Level 3 simulation allows for this more complex consideration of the forces acting on the vehicle.

By accounting for the load transfer taking place in the vehicle, the simulation can determine the maximum tractive forces capable of being applied at the wheels. This has two implications. First, it means that the torque produced by the tires, responsible for accelerating and decelerating the vehicle, will be limited to the maximum force that the tire-road contact surface can handle. Second, since the load transfer within the vehicle is known then the amount of energy capable of being captured through regenerative braking given the drive type (front wheel drive, rear wheel drive, or four wheel drive) can be determined.

Figure 4.8 shows the free body diagram used in modeling the load transfer effects on the vehicle. F_D is the drag force and is modeled according to Equation 2.5. The mass of the vehicle is represented as m and the acceleration of the vehicle is denoted by a, which is calculated according to Equation 4.6. F_{RR} and F_{RF} are the forces due to rolling resistance acting on the rear and front wheels respectively. F_{TR} and F_{TF} are the forces acting on the rear and front wheels respectively from the vehicle's internally generated torque which is positive in the case of acceleration and constant, nonzero speed and negative in the case of deceleration. Points A and B are the location of contact between the front and rear tires, respectively, and the road. L is the wheelbase of the vehicle. L_1 and L_2 are the distances from A and B respectively to the center of gravity along the vehicle's longitudinal axis. The height of the center of gravity is denoted by h. The normal forces acting on the front and rear axles are represented by W_F and W_R, respectively. The inertia of the front and rear wheels is represented by $J_F\alpha$ and $J_R\alpha$, respectively, where α is the angular acceleration of the wheels, and $\alpha=a/r$, where r is the radius of the wheels.

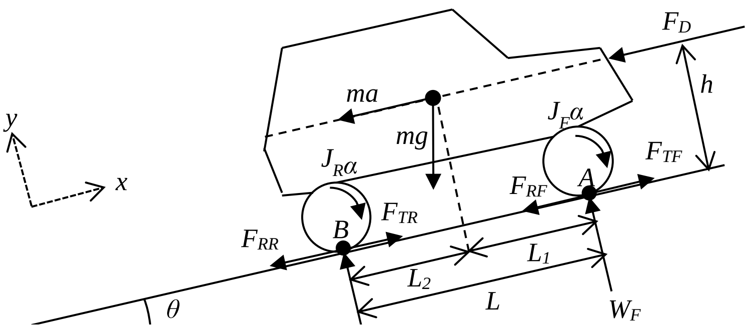

Figure 4.8: Diagram showing the forces acting on the vehicle in the Level 3 load transfer model

In order to analyze the load transfer taking place in a vehicle, W_R and W_F must be determined. W_R and W_F are derived by considering the moments acting in equilibrium around point A [12] [48]

$$\sum M_A = W_R L - mgh\sin\theta - mgL_1\cos\theta - mah - F_D h + J_F\alpha + J_R\alpha = 0 \quad 4.22$$

and by considering the forces acting in equilibrium along the y-axis

$$\sum F_y = W_F + W_R - mg\cos\theta = 0\,. \quad 4.23$$

Note that in this derivation the drag force was assumed to act at height h [47]. This is the default setting in the Level 3 simulation, though the user can change this. Also, all transverse load transfers were not included as per the criteria set forth in Section 1.5 regarding straight-line travel [48]. Solving Equations 4.22 and 4.23 for W_F and W_R,

$$W_F = \frac{mgL_2\cos\theta - mgh\sin\theta - mah - F_D h + J_F\alpha + J_R\alpha}{L} \quad 4.24$$

$$W_R = \frac{mgL_1\cos\theta + mgh\sin\theta + mah + F_D h - J_F\alpha - J_R\alpha}{L} \quad 4.25$$

In order to calculate the amount of braking energy that can be recaptured from each axle, the forces acting in equilibrium along the x-axis must also be considered

$$\sum F_x = F_{TF} + F_{TR} - F_{RF} - F_{RR} - ma - mg\sin\theta - F_D = 0. \quad 4.26$$

Substituting Equation 4.26 into Equations 4.24 and 4.25, yields the following expressions for the normal forces acting on each axle

$$W_F = \frac{mgL_2\cos\theta - h(F_{TF} + F_{TR} - F_{RF} - F_{RR}) + J_F\alpha + J_R\alpha}{L} \quad 4.27$$

$$W_R = \frac{mgL_1\cos\theta + h(F_{TF} + F_{TR} - F_{RF} - F_{RR}) - J_F\alpha - J_R\alpha}{L} \quad 4.28$$

where the rolling resistance force acting on the tires at each axle is

$$F_{RF} = \mu_{rr} W_F \quad 4.29$$

$$F_{RR} = \mu_{rr} W_R \quad 4.30$$

where μ_{rr} varies as explained in Section 2.1 [47] [48].

With expressions for the normal force acting on each axle, the issues of the maximum force capable of being sustained by the tire-road contact and the maximum amount of braking energy capable of being recovered from either axle can be calculated. First the issue of determining the maximum force capable of being sustained by the tire-road contact patch will be addressed.

Many techniques exist that attempt to model the complex relationship between the speed of the tire, the surface the tire is traveling over, and the force the tire is capable of applying (either in braking, acceleration, and/or cornering) [63] [64] [65] [66] [67] [68]. The spectrum of dynamic tire models can generally be thought of as spanning from experimental to theoretical – i.e. from a basis in full scale tire experiments on one end to a basis in the theory of the behavior of the physical structure of the tire [69]. The more theoretical models are used to aid in tire design. However, tire design is beyond the scope of OVEM and thus these models were not considered further for implementation into OVEM. The experimentally-based models are based on parameters that are obtained through extensive experimental measurements, and are generally used to model tire performance under a range of vehicle driving conditions and maneuvers. Perhaps the most well-known of these experimentally-based models is "The Magic Formula" tire model [63]. This model consists of a series of parameters and a set of equations that relate slip, load, slip angle, and camber angle to longitudinal force, lateral force, and aligning moment [63]. This model has a proven track record of delivering accurate results, and it was thus considered for implementation into OVEM.

However, The Magic Formula tire model and other experimentally-based models have traits that clash with several of the design criteria set forth for OVEM. One of the primary drawbacks of The Magic Formula tire model is that it requires extensive experimental resources in order to characterize a tire for use in the formula [70].

Additionally, data on existing and emerging tires that can be used by The Magic Formula is not readily available [70]. This leads The Magic Formula tire model to clash with the first of OVEM's criteria - which was that any component model implemented in OVEM should facilitate the rapid simulation of existing and emerging technologies and should be able to be based on readily available data for a range of products. The Magic Formula tire model and other complex experimentally-based tire models are also primarily concerned with representing properties of vehicle dynamics such as those experienced during aggressive braking, acceleration and cornering. In order to fully capture these aggressive driving events, advanced models such as these are needed; however, as was set forth in OVEM's third design criteria, OVEM is only interested in straight-line travel and the less aggressive driving conditions typically experienced during ordinary urban, suburban, and highway driving. Since, OVEM is only interested in straight-line travel and does not consider lateral movement or lateral forces, it has no need for much of The Magic Formula's capability – that is its ability to model the effect of lateral motion and forces on tires [63]. Due to the conflict of the Magic Formula tire model and other experimentally-based tire models with two of OVEM's key design criteria, they were ultimately not implemented in OVEM.

Instead, an alternative model that borrowed from elements of the Magic Formula model was used in order for the model to better align with OVEM's objectives. Given the more ordinary driving conditions with which OVEM was concerned, it was determined that the following assumptions could be made. OVEM was only concerned with longitudinal travel; hence laterally-acting forces, and slip angles were not included. As part of OVEM's interest in "industry-standard" testing conditions, it was also only concerned with travel over dry asphalt and could thus disregard any variations in tire-road interaction caused by different road surfaces (ice, loose gravel, etc.).

The maximum force capable of being sustained at the tire-road contact patch can be modeled as [49] [67]

$$F_{F\ tire-road\ max} = \mu_b W_F \qquad 4.31$$

$$F_{R\ tire-road\ max} = \mu_b W_R \qquad 4.32$$

where μ_b is the coefficient of road adhesion and $F_{F\ tire\text{-}road\ max}$ and $F_{R\ tire\text{-}road\ max}$ are the maximum forces capable of being sustained by the tire-road contact patch for a given time step at the front and rear tires, respectively. The coefficient of road adhesion is a function of the slip (λ) between the wheel and ground at the tire contact patch [47] [49] [69], where slip in the context of OVEM is defined as

$$\lambda = \frac{v_{req,i+1} - v_{ach,i}}{max\{v_{req,i+1}, v_{ach,i}\}} \qquad 4.33$$

The coefficient of road adhesion varies nonlinearly as a function of slip for various road conditions – for example, icy, wet, and dry asphalt roads. Since OVEM is concerned only with travel over dry asphalt roads, that was the only condition over which the slip dependence of the coefficient of road adhesion was assessed. Figure 4.9 presents a curve that shows how the coefficient of road adhesion varies with longitudinal slip. This curve is representative of the curve experienced by an array of light-duty vehicles and tire types [47] [48] [67] [71]. Note that this curve is a generic curve, and that the user can adjust this curve to suit specific modeling needs.

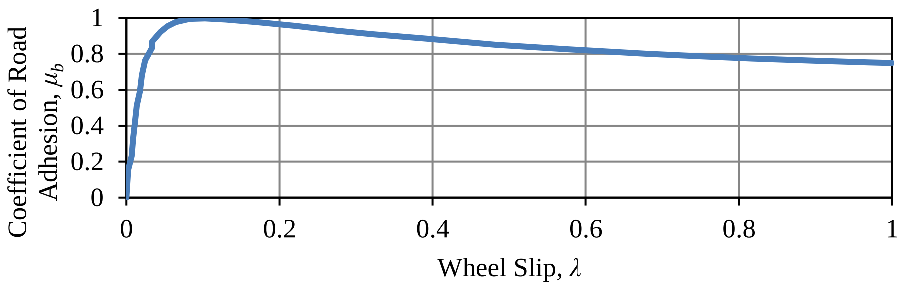

Figure 4.9: Representation of dependence of the coefficient of road adhesion on wheel slip

This approach met OVEM's criteria in several ways. First, it facilitates the rapid simulation of new and existing technologies. More complex tire-road interface models require extensive experimental resources to obtain complex model parameters as these parameters are rarely readily available [70]. OVEM's model can apply to a range of tire and vehicle types thus avoiding the burden of needing extensive experimental resources to obtain the parameters for many different possible vehicle and tire combinations. This approach also accounts for the longitudinal effects taking place on the vehicle. Thus, this was the approach implemented in OVEM to determine the maximum force capable of being applied at the tire-road contact patch.

The next issue that the load transfer model was built to address was determining the amount of energy that could be recovered given regenerative braking taking place at either the front or rear axle. The following demonstrates how this was derived. By substituting Equations 4.23, 4.29, and 4.30, into Equations 4.27 and 4.28 where the tractive force is made equal to the maximum braking force that can be applied, and by summing the inertia of the front and rear tires into a single term, J_w, rearranging yields

$$W_F = \frac{mg\cos\theta\,[L_2 + h(\mu_b + \mu_{rr})] + J_w\alpha}{L} \quad 4.34$$

$$W_R = \frac{mg\cos\theta[L_1 - h(\mu_b + \mu_{rr})] - J_w\alpha}{L} \quad 4.35$$

For a constant road surface (such as dry asphalt), the ideal proportion of braking force applied between the front and rear axles can be assumed to be equal to the maximum braking force capable of being applied at each axle (Equations 4.31 and 4.32) divided by the total braking force that is capable of being applied [47] [48]

$$K_{BF} = \frac{W_F}{(W_F + W_R)} \quad 4.36$$

$$K_{BR} = \frac{W_R}{(W_F + W_R)} \quad 4.37$$

where K_{BF} and K_{BR} are the ideal proportion of braking force applied at each axle [47] [48]. The ideal braking proportions are important because braking applied in this measure ensures the maximum braking forces on the front and rear axles are generated at the same time which prevents the wheels from locking, thereby allowing the vehicle to retain directional stability [48]. Substituting Equations 4.34 and 4.35 into 4.36 and 4.37 yields the expressions for the ideal braking proportions for the front and rear axle which in turn determine the upper limit for the amount of braking energy that can be recovered given regenerative braking at either axle

$$K_{BF} = \frac{L_2 + h(\mu_b + \mu_{rr}) + J_w \alpha}{L} \tag{4.38}$$

$$K_{BR} = \frac{L_1 - h(\mu_b + \mu_{rr}) - J_w \alpha}{L} \tag{4.39}$$

Note that K_{BF} and K_{BR} are only the proportion of the total braking energy that is capable of flowing back into the powertrain given regenerative braking at the front and rear axles, respectively. The backwards vehicle block outputs these braking proportions as limits to the amount of energy that will be allowed to pass to the upstream blocks in the powertrain in the event of regenerative braking on the wheels of a particular axle. The subsequent losses from the gearbox, motor, energy storage system, and other components handling energy in the powertrain will further reduce the amount of energy that will ultimately go on to be recaptured and stored in the energy storage system.

4.2 Wheel-Axle Blocks

The purpose of the wheel-axle blocks is to account for the losses in the wheel and axle and to account for the effect of the radius of the tires by converting between the linear force and velocity requests handled by the vehicle blocks and the torque and angular velocity requests handled by the rest of the components in the powertrain. The default setting for the wheel-axle model is to treat the wheels and axles as having a fixed efficiency. This is obviously a simplification, but one that is reasonably accurate since wheel-axle losses are generally relatively low compared to the losses experienced by other components in the powertrain and are generally proportional to the power passing through the wheels and axles [72]. The default setting on the wheel-axle blocks is to impose no power, torque, or speed limits; however, such limits for the wheel and axle can be specified.

4.2.1 Backwards Wheel-Axle Block

The backwards wheel-axle block accepts the force and speed requests coming from the backwards vehicle block as inputs. The backwards wheel-axle block in the Level 3 model operates identically to the wheel-axle blocks in Levels 1 (Section 2.2) and 2 (Section 3.2). The backwards wheel-axle block outputs torque and speed requests, typically to the backwards gearbox block.

4.2.2 Forwards Wheel-Axle Block

The forwards wheel-axle block takes the torque and speed supplied by the forwards gearbox block as inputs and converts them to linear force and speed. It also accounts for the efficiency of the wheel and axles during both motoring and braking cases. If the amount of negative torque produced by the motor in regenerative braking is insufficient to decelerate the vehicle enough for a particular braking event, the forwards wheel-axle block will apply mechanical brakes to provide the remaining negative torque. The forwards wheel-axle block outputs the linear force and speed produced by the vehicle to the forwards vehicle block.

4.3 Gearbox Blocks

The purpose of the gearbox block is to account for the losses in the gears and to apply the effect of the gear ratio. The Level 3 gearbox model in OVEM is based on an empirical model where the losses are a function of the torque rating of the gearbox and the power flowing through the gearbox. This gearbox model was selected because it aligns with OVEM’s goals for the Level 3 model in that it has the appropriate combination of being flexible enough to apply to an array of fixed gearbox sizes while still providing accurate predictions for the efficiency of the gearbox. More advanced gearbox modeling tools exist that enable the user to discern the effect that measures such as changing the gears' geometry, lubrication, orientation, materials, and thermal environment has on their efficiency [73] [74]. But any gains in accuracy achieved by these types of models were outweighed by the models' complexity (both experimentally and computationally) which would have been too high for implementation in OVEM, as OVEM was intended to be a platform based on models derived from readily available data in order to facilitate rapid simulation of existing and emerging technologies. Nevertheless, OVEM could quickly incorporate an efficiency map or analytical equation for gearbox efficiency derived from a more complex gearbox modeling tool.

4.3.1 Backwards Gearbox Block

The backwards gearbox block receives the torque ($T_{GB,in,B}$) and speed ($\omega_{GB,in,B}$) requests from the backwards wheel-axle block as inputs. The gearbox model assumes that its losses come from the following sources: meshing between the gear teeth and friction between the seals and bearings [75]. These assumptions and the efficiency equation that they yield are based on empirical observations from a range of gearboxes [52] [57]. The losses due to friction in the seals are proportional to the product of the square of the gear ratio, the maximum rated torque of the motor, $T_{max\ motor}$, and the speed from the wheel-axle block, ω_{in}. This loss term has the coefficient k_{seal} [44]. The losses due to the bearings and meshing are approximately proportional to the power currently handled by the gearbox, and they have the coefficients of $k_{bearing}$ and k_{mesh} respectively [57]. The coefficients k_{seal} and k_b are generally set to 0.00103 and 0.005, respectively [57]. The coefficient due to meshing losses is difficult to know precisely, but it is generally held to be between 0.015 and 0.02 [52] [57]. This holds true for a gearbox of most any size or ratio that would reasonably be found in a light-duty automobile

[52] [57]. This helps meet the OVEM objective of using models that can rapidly compare a range of technologies and topologies. The efficiency of the gearbox can then be expressed as

$$\eta = \frac{T_{GB,in,B}\omega_{GB,in,B}}{T_{GB,in,B}\omega_{GB,in,B} + k_{seal}NT_{\max motor}\omega_{GB,in,B} + (k_{mesh} + k_{bearing})T_{GB,in,B}\omega_{GB,in,B}} \; . \qquad 4.40$$

The backwards gearbox applies this efficiency to the torque request and reduces the torque and multiplies the speed as shown in Equations 2.17 and 2.19 before the speed and torque requests get passed to the backwards motor block.

4.3.2 Forwards Gearbox Block

The forwards gearbox block takes the torque ($T_{GB,in,F}$) and speed ($\omega_{GB,in,F}$) that the forwards motor block supplies as inputs. It uses a rearranged form of Equation 4.40 so that the efficiency is based on the torque and speed inputs coming from the motor during the forward phase of the simulation.

$$\eta_{GB} = \frac{T_{GB,in,F}\omega_{GB,in,F} - k_{seal}T_{\max motor}N\omega_{GB,in,F}}{(1 + k_{mesh} + k_{bearing})T_{GB,in,F}\omega_{GB,in,F}} \; . \qquad 4.41$$

For the motoring case, the forward gearbox block applies the gear ratio and the efficiency according to

$$T_{GB,out,F} = \eta_{GB}T_{GB,in,F}N \qquad 4.42$$

and for the braking case

$$T_{GB,out,F} = \frac{1}{\eta_{GB}}T_{GB,in,F}N \; . \qquad 4.43$$

The speed outputted by the gearbox is calculated according to

$$\omega_{GB,out,F} = \frac{\omega_{GB,in,F}}{N} . \qquad 4.44$$

since the efficiency has already been accounted for in the torque calculation. The forwards gearbox block outputs the torque ($T_{GB,out,F}$) and speed ($\omega_{GB,out,F}$) produced by the gearbox, typically to the forwards wheel-axle block.

4.4 Motor-Power Electronics Blocks

The primary purpose of the motor-power electronics block is to model the losses and performance limits of the motor and its power electronics. It imposes performance limits based on the maximum torque and speed curves of the motor and power electronics, and it calculates the efficiency of the motor and power electronics based on an efficiency map. The torque and speed curves along with the efficiency map are usually contained in the literature for a commercially available motor-power electronics package. Thus, the Level 3 motor model meets the OVEM criteria for being able to be rapidly implemented using data that is typically readily available while still providing accurate results. Computational tools exist that are capable of modeling motor and power electronics behavior in much more detail. Typically, these packages involve finite element analysis and are used to determine the performance and efficiency of different motor and power electronics designs [76]. Since OVEM is not concerned with such detailed questions of design, these modeling techniques were not implemented in OVEM. However, OVEM could easily incorporate an efficiency map generated by such a program.

In the Level 3 simulation, the motor and power electronics are combined into one block because manufacturers commonly report their efficiency as one system, or if the efficiency maps for a motor and power electronics module are reported separately, they can usually be combined to produce an efficiency map for the motor and power electronics as one system.

The Level 3 motor block also has the ability to model multiple tractive motors (direct-drive or with a gearbox). This is something that, to the best of the author's knowledge, is unique to OVEM.

4.4.1 Backwards Motor-Power Electronics Block

The backwards motor-power electronics block takes the torque and speed requests from the gearbox as inputs. The motor-power electronics model enforces the motor's torque and speed limits. The motor-power electronics block determines its efficiency based on an efficiency map where the efficiency of the motor and power electronics varies with torque and speed. Figure 4.10 shows one such efficiency map [61]. The efficiency is then used to calculate the power that the motor will produce as an output. The power request is computed according to Equations 2.20 and 2.21. This power request is then typically outputted to the energy storage system via the electric bus.

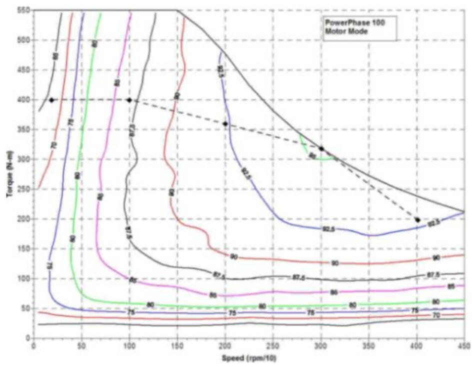

Figure 4.10: Efficiency map for a commercially available 100 kW permanent magnet electric motor and power electronics system [61]

The maximum torque curve in Figure 4.10 warrants a brief discussion as it demonstrates principles that are common across a range of motors used in OVEM. The maximum torque of the motor is generally set by the current limit imposed by the power electronics. This results in the constant torque seen until approximately 1500 rpm. For further speed increases beyond the base speed (1500 rpm, for this motor), the output voltage from the power electronics becomes limited, and field weakening is required. This causes the maximum torque of the motor to decrease, though at this stage (between 1500-2000 rpm, for this motor) the torque decreases in such a way relative to the speed increases that the power still increases. Eventually the motor reaches its maximum power limit where power is held constant (at approximately 2000 rpm, for this motor) and the torque continues to decrease proportionally as speed increases. The maximum power limit is commonly imposed by the power electronics, and a constant power region (seen at speeds greater than 2000 rpm, for this motor) produces a hyperbolic relationship between maximum torque and speed.

4.4.2 Forwards Motor-Power Electronics Block

The electric bus block passes the amount of power it can supply to the forwards motor-power electronics block. The backwards motor-power electronics block calculated the ratio between the amount of torque requested from it by the backwards gearbox block and the amount of power it requested from the bus. The forwards motor-power electronics model multiplies this ratio by the amount of power it receives from the electric bus to determine the amount of torque it can generate. It is assumed that the speed of the motor is the same as was calculated during the backwards phase of the simulation. The updated torque and speed values are used to determine the new efficiency of the motor on its efficiency map. The incoming power from the electric bus ($P_{motor,in,F}$) is scaled by this efficiency (η_{motor}) and divided by the speed input from the backwards motor-power electronics block ($\omega_{motor,in,F}$) to produce the torque of the motor. During the motoring case, the torque ($T_{motor,out,F}$) is calculated according to

$$T_{motor,out,F} = \frac{P_{motor,in,F}}{\omega_{motor,in,F}} \eta_{motor} \tag{4.45}$$

where $P_{motor,in,F}$ is the power input coming from the electric bus and $\omega_{motor,in,F}$ is the speed input coming from the backwards motor-power electronics block. Note that during the forwards part of the simulation for the motoring case, the upstream power is multiplied by the efficiency because the components downstream from the motor block will have less power available to them due to the motor's internal losses. During the braking case, the torque output is divided by the efficiency to reflect that the downstream components will actually have more power passing through them than the upstream components due to the internal losses of each component

$$T_{motor,out,F} = \frac{P_{motor,in,F}}{\omega_{motor,in,F}} \frac{1}{\eta_{motor}}. \quad 4.46$$

The amount of torque and speed the motor can actually produce or accept is then outputted to the forwards gearbox block.

4.5 Electric Bus Block

The electric bus serves as the interface between the motor-power electronics blocks and the energy storage system and alternative power unit blocks. The electric bus block manages this interaction by controlling the vehicle's energy management strategy (EMS), which is discussed in Section 4.9. Level 3 has the ability to simulate two different types of energy storage systems simultaneously being used to power the vehicle – which is a feature unique to OVEM in the vehicle modeling landscape. OVEM can be a valuable tool to analyze how hybridizing the energy storage system, such as with batteries, ultracapacitors, or an alternative power unit, such as an ICE or fuel cell, can affect the vehicle's performance. The models governing the behavior of the energy storage system are complex, and a discussion of the component models and their energy management strategies appears below. The electric bus block receives the power capable of being produced or accepted by the energy storage system which it turns into an output that gets passed to the forwards motor-power electronics block.

4.6 Energy Storage System Block

The energy storage system block is comprised of three different technologies – ultracapacitors, batteries, and high-speed flywheels – with each technology having multiple products comprising its library thus far in OVEM. The technologies can be arranged to function alone or in combination with another technology. OVEM's capacity to hybridize energy storage systems is something that is not available in other vehicle modeling packages [40]. This is a significant contribution to the field as the ability to hybridize energy storage systems, particularly of different technologies in order to capitalize on their unique strengths, has the potential to be a key advancement for electric and hybrid electric vehicles.

The size and technology of the energy storage system(s) are set by the user and the power flows between the energy storage system(s) and the rest of the vehicle are managed by the electric bus's implementation of an energy management strategy. Below is a description of the different models that make up the energy storage system block.

4.6.1 Ultracapacitor Model

Ultracapacitors are a promising technology for storing electrical energy aboard electric and hybrid electric vehicles [77]. Their high specific power (on the order of 8 kW/kg) and high cycle life (on the order of 10^6 cycles) make them well-suited for the type of frequent and intense charging and discharging commonly demanded from the energy storage systems in electric and hybrid electric vehicles [78] [79] [80] [81] [82]. For these reasons, an ultracapacitor model was essential for OVEM. Section 4.6.1.1 presents the review of the ultracapacitor modeling landscape that was conducted. And as Section 4.6.1.2 explains, an ultracapacitor model that met OVEM's criteria was derived and ultimately implemented.

4.6.1.1 Overview of Existing Ultracapacitor Models

Ultracapacitors store charge on the electric double-layer that forms between an electrode typically made of highly porous activated carbon and an electrolyte [83] [84]. The high surface area of the porous carbon electrode allows for a great deal of charge to be stored along the electric double layer. Figure 4.11 provides a diagram illustrating the principle behind how charge is distributed throughout the electrode-electrolyte interface and how that charge must travel through the porous structure of the electrode in order to reach the ultracapacitor's terminals [85]. The unique structure of ultracapacitors gives them two characteristics that must be accounted for in their modeling. The first of these characteristics is that their voltage and capacitance vary as a nonlinear function of the state of charge. The second of these characteristics is that their impedance and charge storage dynamics are a function of frequency. Ultracapacitor modeling programs must account for these factors in a manner that is appropriate given the objectives of the modeling effort.

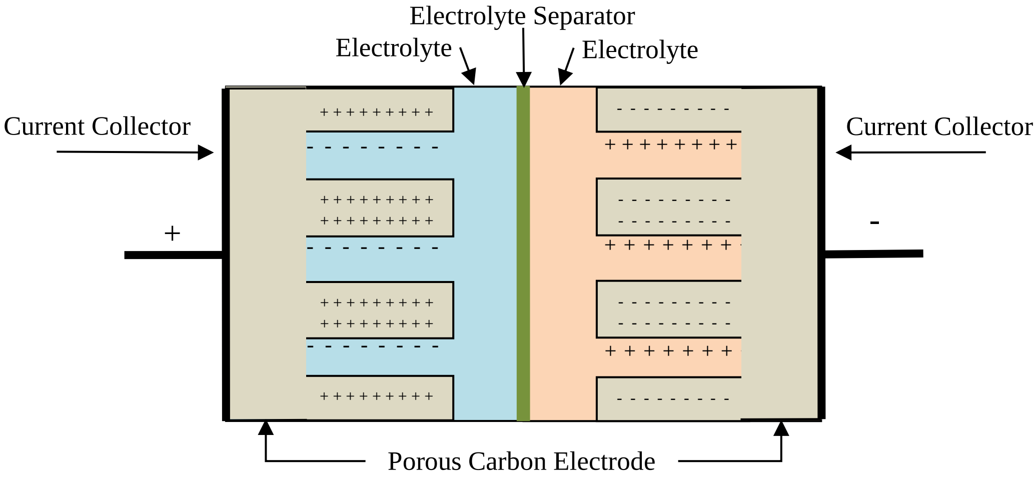

Figure 4.11: Schematic of the electrode and electrolyte inside an ultracapacitor

Existing ultracapacitor models can generally be lumped into two categories: physics-based and circuit-based. Physics-based models are typically concerned with the internal dynamics of the ultracapacitor that generally happen over small timescales [78] [86] [87] – timescales that are smaller than those of interest to OVEM. Additionally, physics–based models tend to require extensive experimental and computational resources to generate and process their necessary parameters. Given the inability of these models to facilitate rapid simulation of existing and emerging technologies by being able to be based on readily available product data and since they were concerned with timescales outside of OVEM's range of interest, they were not considered further for implementation into OVEM.

However, circuit-based models are an established technique that is more suited to the timescales and conditions of interest to OVEM [88]. Thus, they were investigated further as a potential basis for OVEM's ultracapacitor model. A common approach in modeling ultracapacitor behavior is to construct an equivalent circuit that represents the physical processes taking place within the device. This typically leads to an equivalent circuit model consisting of repeating resistor and capacitor (RC) branches that simulate the distributed nature of the resistance and capacitance within an ultracapacitor [89]. Each of the RC branches contributes a time constant to the overall RC network. These time constants combine to represent the series of charge storage effects created by the electrode's porosity. Figure 4.12 demonstrates a branched RC circuit [85]. In principle, any number of RC branches could be used to describe the distributed nature of charge storage in ultracapacitors – with more branches theoretically enabling a better representation of the distributed nature of the charge storage. However, the interdependence between the equivalent circuit parameters means that calculating the parameters for more than four or five branches can rarely be done efficiently [90]. Equivalent circuit models in the literature generally only consist of four to five branches [85] [89] [90] [89]. For that reason the ultracapacitor model initially examined in OVEM (Figure 4.14) has four RC branches.

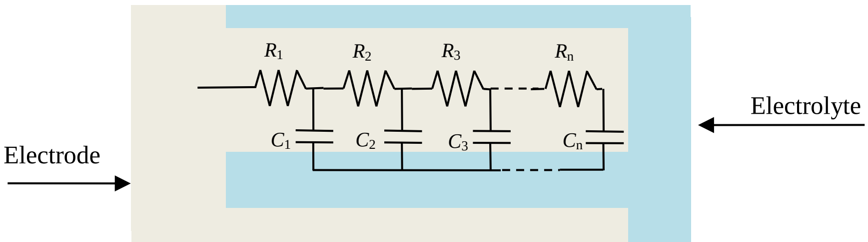

Figure 4.12: Ultracapacitor equivalent circuit model

Ultracapacitors have only been designed with automotive applications in mind for roughly the past ten years, and ultracapacitors have yet to find their way into a mainstream commercially available automobile [91]. The technology is constantly evolving, and while this model has successfully modeled ultracapacitor behavior in the past, ultracapacitor behavior is highly sensitive to the electrode's pore structure and materials [89]. This study wanted to verify that it was valid for the newest ultracapacitor releases by testing it against experimental results.

Ultracapacitor behavior is a function of frequency [89]. So in order to find the values of the elements in the equivalent circuit in Figure 4.12, a technique known as impedance spectroscopy was employed. Impedance spectroscopy is a well-established technique that is frequently used to characterize electric devices [92]. It uses the fact that the impedance of a device, Z, is defined as

$$Z(j\omega) = \frac{V(j\omega)}{I(j\omega)} \tag{4.47}$$

where V is the voltage and I is the current and V, I, and Z are dependent on frequency, ω. To determine the impedance from Equation 4.47, either the voltage or current across the device must be varied (usually sinusoidally) at a known frequency while the change in the other parameter is observed. In practice, it is simpler to control the current for ultracapacitors [93], so in this study the discharge current was varied sinusoidally with a controlled frequency and amplitude, and the resulting alternating voltage across the ultracapacitor was measured. A schematic of the experimental apparatus that was built to carry out this test is shown in Figure 4.13.

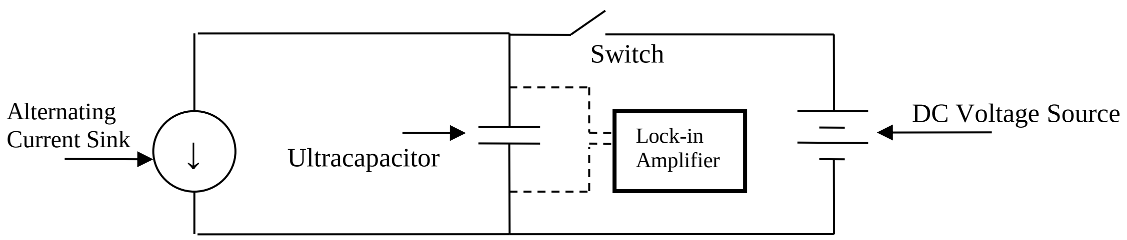

Figure 4.13: Schematic of the impedance spectroscopy experimental apparatus

A 2600 F (Maxwell) ultracapacitor was first charged by the voltage source to a DC bias of 2.5 V which was the upper limit of its operating range. The switch was then opened so that the ultracapacitor was no longer connected to the DC voltage source. The current sink began to slowly discharge the ultracapacitor by withdrawing a current of a known amplitude and frequency. The discharging current produced a small oscillating voltage signal across the ultracapacitor. This signal was measured by a lock-in amplifier (Stanford Research Systems, SR830). Lock-in amplifiers are able to extract small signals (on the order of 10^{-9} V) from noisy environments where the noise may be thousands of times larger than the signal of interest. By using a technique called phase-sensitive detection, the lock-in amplifier is able to identify a signal at a specified frequency and determine its magnitude and phase relative to a reference signal [94]. In this case, the reference signal was the signal driving the current sink and the measured signal was the voltage across the ultracapacitor. The root-mean-square of the AC voltage and current were inserted into Equation 4.47 and the impedance of the ultracapacitor at that particular frequency was obtained. This process was repeated for a range of frequencies from 10 mHz – 100 Hz.

Once the experimental data was obtained, it appeared that the measured impedance of the ultracapacitor was affected by the inductance of the connections between the ultracapacitor and the rest of the experimental apparatus as indicated by the tendency of the impedance's phase to move towards 90° at high frequencies. In order to account for this, a serial inductor, *L*, was added to the model in Figure 4.12, and this revised equivalent circuit appears in Figure 4.14 [93].

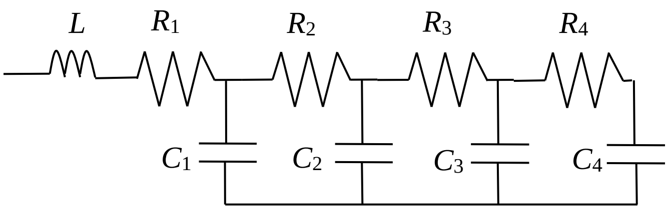

Figure 4.14: Revised four branch model

The impedance (Z) of the revised four branch model seen in Figure 4.14 is expressed by the Laplace transform (assuming the inductor and capacitors had no initial current or voltage, respectively) [93].

$$Z = Ls + R_1 + \cfrac{1}{C_1 s + \cfrac{1}{R_2 + \cfrac{1}{C_2 s + \cfrac{1}{R_3 + \cfrac{1}{C_3 s + \cfrac{1}{R_4 + \cfrac{1}{C_4 s}}}}}}} \quad 4.48$$

This expression for the impedance is substituted into the transfer function in Equation 4.47, and just as in the experimental impedance spectroscopy procedure, the model varies the input current sinusoidally and its effect on the voltage across the modeled ultracapacitor is observed.

The parameters in the four branch model were arrived at through an analysis of the break points in the experimental data. Table 4.1 shows the values used for the parameters in the revised four branch model seen in Figure 4.14.

Table 4.1: Values of the parameters in the four branch model

R_1	210 μΩ	C_1	90 F	L	44 nH
R_2	50 μΩ	C_2	1600 F		
R_3	190 μΩ	C_3	110 F		
R_4	30 μΩ	C_4	700 F		

Figure 4.15 shows the agreement between the experimental data and the predictions of the four branch model from Figure 4.14.

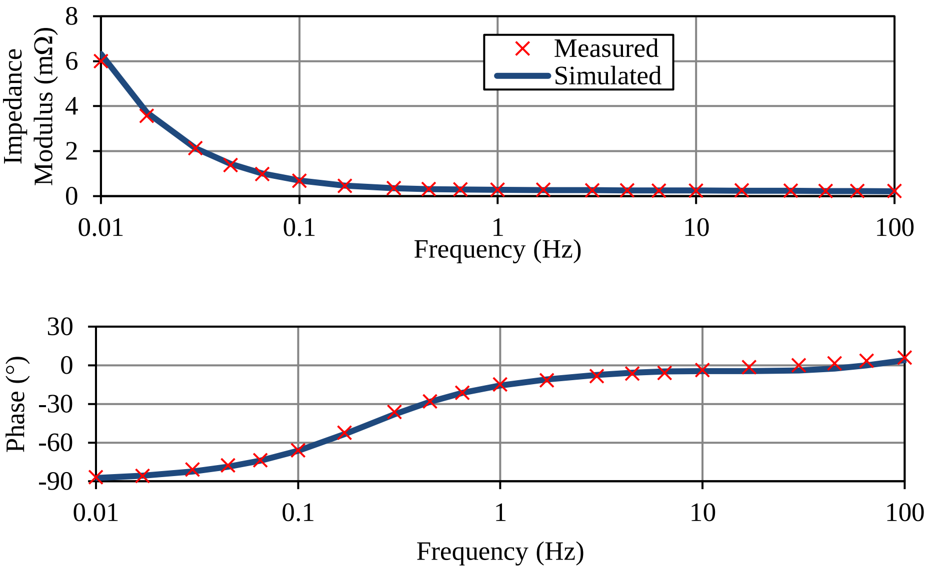

Figure 4.15: Comparison between the four branch model's prediction and the experimental measurement of ultracapacitor impedance

The four branch model shows an agreement to within 3μΩ of the experimental results on the impedance modulus. The agreement on the impedance modulus for most of the frequency range is actually closer than 5% with the largest disagreement occurring toward the low end of the frequency range, near 10 mHz (corresponding to a time constant of 100 s). The largest disagreement between the experimental and simulated results on the phase was 3°, and it occurred around 60 Hz (corresponding to a time constant of 16 ms). Due to the small disagreement between the model and the experimental results, it was apparent that the four branch model accurately modeled ultracapacitor behavior.

However, the drawback of the four branch model was that while it was accurate, it was experimentally and computationally intensive. Deriving the model parameters through impedance spectroscopy requires a great deal of time and experimental resources. The computational runtimes for this model were also long enough to impinge upon OVEM's goal of being able to rapidly compare many different powertrains. The time step of the rest of the vehicle simulation is set to 1 second. The four branch model accurately predicts ultracapacitor behavior up to 100 Hz. Therefore, it accounts for transient processes with time constants on the order of 10 ms (100 Hz^{-1}). This made it a less than ideal choice for implementation into OVEM. Such a degree of resolution is not necessary given the longer time step (1 s) used throughout the rest of the Level 3 simulation. In order to rectify these issues, an alternative model was sought that was more experimentally and computationally efficient and appropriate given OVEM's objectives.

It was observed that the RC time constants from Table 4.1 for R_1C_1, R_3C_3, and R_4C_4 were all similar: 52 s, 48 s, and 48 s, respectively. Thus, it was concluded that they might be redundant and could be combined into a single branch. A two branch model was constructed as shown in Figure 4.16.

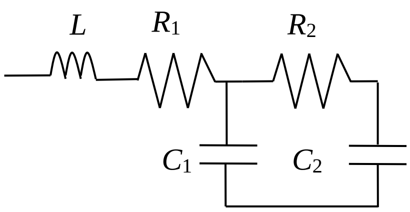

Figure 4.16: Revised two branch ultracapacitor model

The parameters for the two branch model were set as shown in Table 4.2.

Table 4.2: Parameters for two branch ultracapacitor model

R_1	280 μΩ	C_1	1100 F	L	65 nH
R_2	50 μΩ	C_2	1500 F		

The comparison between the measured experimental results and the results from the two branch model are shown in Figure 4.17.

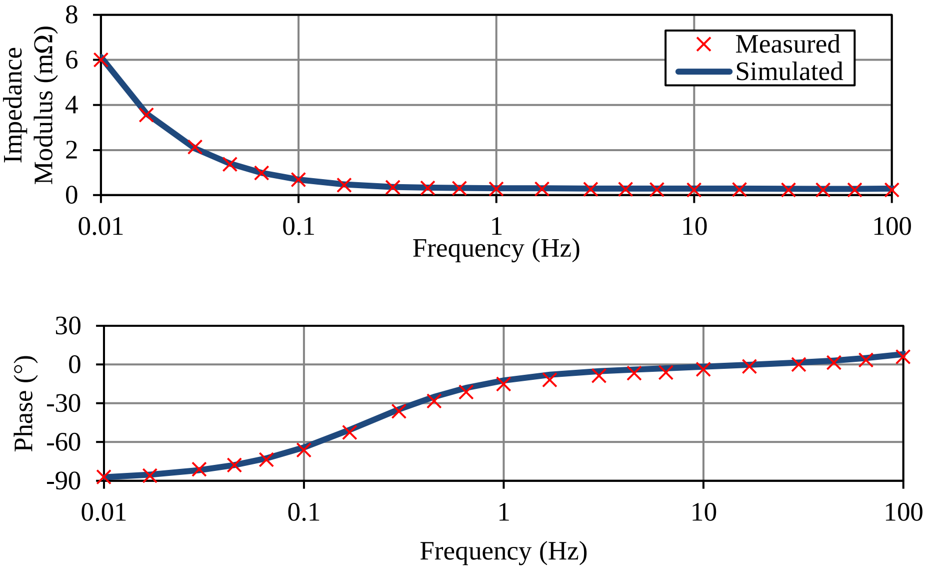

Figure 4.17: Comparison between the two branch model's prediction and experimental measurement of ultracapacitor impedance

The greatest difference between the measured and simulated impedance modulus and phase occurs at 100 Hz where they vary by 9 μΩ and 4°, respectively. Over the timescales of interest to OVEM (1 Hz – 0.01 Hz), the simulation produces results for the impedance modulus to within 5% of the measured results. However, the two branch model still required extensive computational and experimental resources as impedance spectroscopy still had to be employed to derive its parameters.

4.6.1.2 Ultracapacitor Model Used in OVEM

R.A. Dougal et al. identified that a multi-branch model could be truncated based on the simulation's accuracy requirements [89]. Thus, the effect of removing all but one of the RC branches from the four branch model was examined. The serial inductor was also removed as its time constant was outside the range of interest for the Level 3 simulation. Figure 4.18 shows the simplified model.

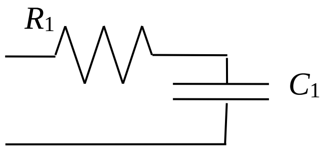

Figure 4.18: Simplified equivalent circuit with one RC branch

The impedance of the simplified model can be expressed by a Laplace transform which was substituted into the transfer function in Equation 4.47

$$\frac{V(s)}{I(s)} = Z(s) = R_1 + \frac{1}{C_1 s} \ . \qquad 4.49$$

The simplified model was then compared to the experimental data for a 2600 F ultracapacitor. R_1 was set to 330 μΩ which was the manufacturer's rated equivalent series resistance and C_1 was set to the rated capacitance of 2600 F [95]. Figure 4.19 shows the simplified model's ability to predict the experimental data based on the rated internal resistance and capacitance.

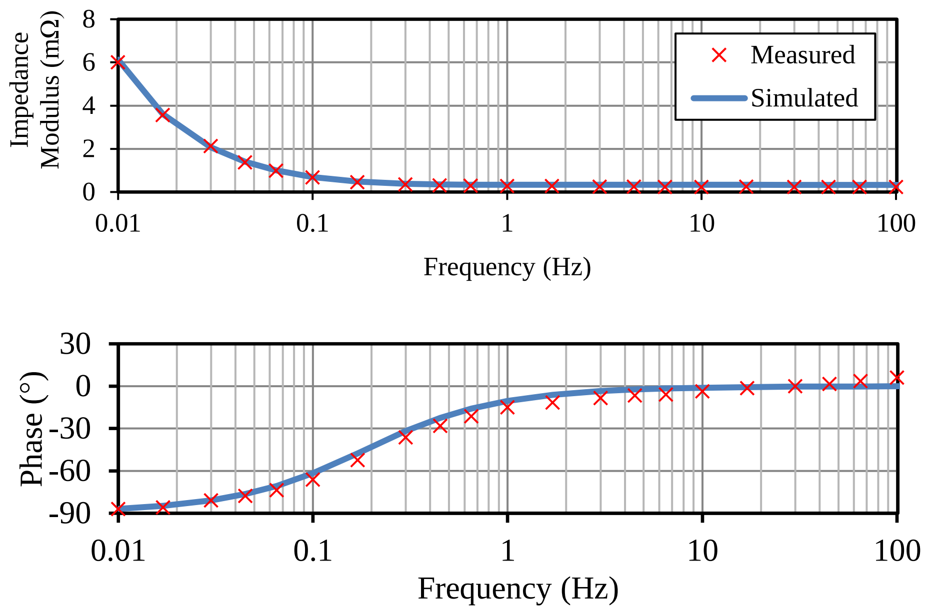

Figure 4.19: Comparison between the simplified model's (one RC branch) prediction and the experimental measurement of ultracapacitor impedance

The simplified model predicts the impedance modulus of the ultracapacitor to within 80 μΩ with the largest difference between the experimental data and modeled results occurring at 100 Hz (corresponding to a timescale of 10 ms). The fact that the first-order model deviates the most from the data at 100 Hz is understandable given that as a first order model with one RC branch and no inductor it has a more limited ability to accurately account for a wide frequency range. Yet, timescales on the order to 10 ms are outside of the timescale range of interest to OVEM. For the timescales relevant to OVEM (approximately 1-10^4 s), the simplified, first-order model is within OVEM's accuracy range. So while the four and two branch models are more accurate across a wider frequency range, the simplified model is sufficiently accurate for OVEM. The marginal gain in accuracy obtained through the four and two branch models was, in the estimation of the author, overshadowed by the reduced need for experimental resources and computational runtimes made possible via the one branch model, as the one branch model was able to utilize readily available data which aligned with OVEM's goal of enabling rapid simulation of existing and emerging technologies.

With the one RC branch model characterizing the ultracapacitor across its frequency range, the ultracapacitor then need to account for the nonlinearity of its voltage and capacitance as a function of the ultracapacitor's state of charge. One of the fundamental equations describing ultracapacitor behavior is

$$E_{OC} = \frac{Q}{C} \tag{4.50}$$

where E_{OC} is the open-circuit voltage of the ultracapacitor, C is its capacitance, and Q is the amount of charge the ultracapacitor contains. Note that Q is proportional to the state of charge (SOC varies from 1 to 0 with 1 being fully charged and 0 being fully discharged) of the ultracapacitor. In an ideal capacitor, the capacitance remains constant regardless of the state of charge. However, in actuality the capacitance of an ultracapacitor varies as a function of its stage of charge, which has been overlooked by existing vehicle modeling packages – notably, ADVISOR [40]. Figure 4.20 shows an example of how the capacitance varies as a function of the state of charge for a 350 F ultracapacitor [96].

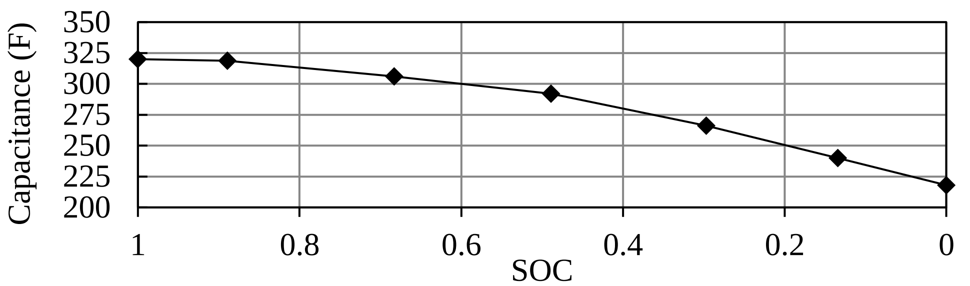

Figure 4.20: Variation in capacitance as a function of SOC for a 350 F ultracapacitor

This means that according to Equation 4.50, the open-circuit voltage of an ultracapacitor does not vary linearly with the stage of charge. Figure 4.21 shows the relationship between E_{OC} and stage of charge for a Maxwell 350 F ultracapacitor [96]. Note that this relationship is typical for a range of ultracapacitor sizes, and this data is usually available as part of the literature on an ultracapacitor. Thus, all of the parameters necessary to construct this ultracapacitor model can be obtained from readily available sources – a key criteria for implementation into OVEM.

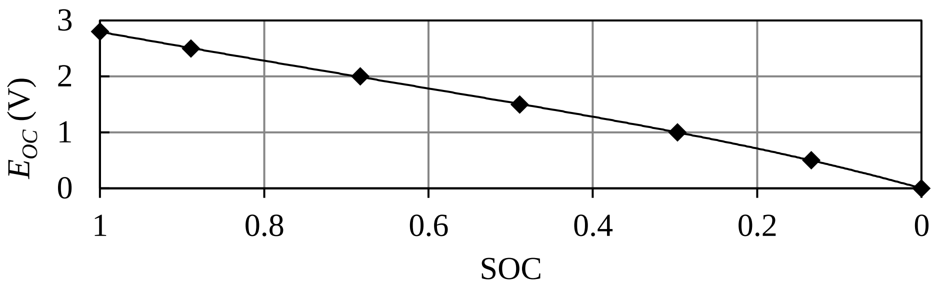

Figure 4.21: Relationship between the open-circuit voltage and SOC of a 2600 F ultracapacitor

4.6.1.3 Integration into OVEM

The one RC branch model was modified once again based on the knowledge of the relationship between the capacitance, open-circuit voltage, and state of charge of an ultracapacitor so that it could be integrated into OVEM. The ultracapacitor could now be modeled as an open-circuit voltage source, E_{OC}, and take the place of the capacitor in the one branch RC equivalent circuit. The open-circuit voltage source was then placed in series with the resistor, R. This was ultimately the model that was integrated into OVEM. A schematic of this model is shown in Figure 4.22, and a derivation of how it integrates with the rest of the vehicle model is shown below.

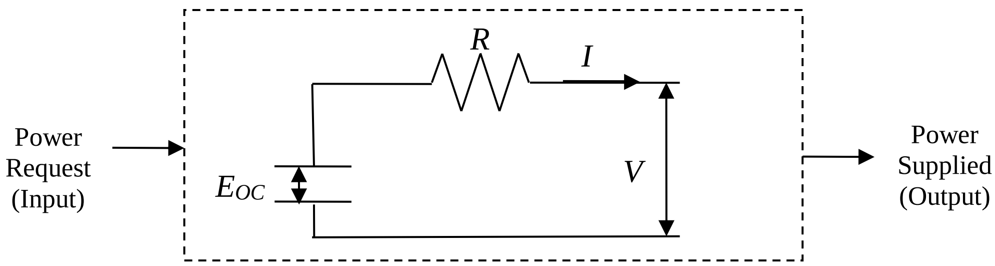

Figure 4.22: Equivalent circuit model for an ultracapacitor implemented in the Level 3 simulation

The model works by first taking a power request (which it receives from the electric bus block) as an input (note that this based in part on derivations from [24] [46]). The power, P, which the ultracapacitor can deliver (positive value) or receive (negative value) is given by

$$P = IV \tag{4.51}$$

where I is the current entering or exiting the ultracapacitor and V is the voltage across the terminals of the ultracapacitor. R is the series internal resistance and E_{OC} is the open-circuit voltage of the ultracapacitor. For the case when the ultracapacitor is discharging, the open-circuit voltage is expressed as,

$$E_{OC} = V + IR \tag{4.52}$$

and for the case when the ultracapacitor is charging, it is expressed as

$$E_{OC} = V - IR. \tag{4.53}$$

By substituting Equation 4.51 into Equations 4.52 and 4.53 the quadratic expressions are obtained for discharging

$$RI^2 - E_{OC}I + P = 0 \tag{4.54}$$

and charging

$$RI^2 + E_{OC}I - P = 0 \tag{4.55}$$

the ultracapacitor. By applying the quadratic equation to Equations 4.54 and 4.55, the following expressions can be obtained for the current leaving (during discharging)

$$I = \frac{E_{OC} \pm \sqrt{{E_{OC}}^2 - 4RP}}{2R} \tag{4.56}$$

and entering (during charging)

$$I = \frac{-E_{OC} \pm \sqrt{{E_{OC}}^2 + 4RP}}{2R}\ . \tag{4.57}$$

the energy storage system. In order to ensure that there are no complex roots in Equations 4.56 and 4.57, a maximum power limit is set on the power request such that

$$|P| < \frac{{E_{OC}}^2}{4R} \tag{4.58}$$

Any power request passed to the energy storage system that violates this inequality is limited by the model so that the inequality holds true.

Given that the discriminant in both equations is positive, as ensured by the limitation imposed in Equation 4.58, in the discharging case (where the power requests are labeled as positive) and charging case (where the power requests are labeled as negative) the following inequality is true

$$E_{OC} > \sqrt{E_{OC}{}^2 - 4RP}\ . \qquad 4.59$$

This means that the discharging case (Equation 4.56) has two positive solutions, and the charging case (Equation 4.57) has two negative solutions.

For the discharging case, this means that one of the positive solutions has a higher numeric value than the other positive solution – meaning that one solution requires a higher current to meet the power request than the other solution. For the charging case, one solution has a lesser negative value than the other negative solution – meaning that one solution requires more current than the other solution in order to deliver the specified power charge to the energy storage system.

Figure 4.23 provides a visual example of this concept. Figure 4.23 plots the two positive solutions (high current and low current) for the discharge case for a range of power requests for a representative energy storage system: a 2600 F ultracapacitor array (consisting of 2000 cells each with an internal resistance of 300 μΩ) at a state of charge such that its E_{OC} is currently 2.5 V/cell.

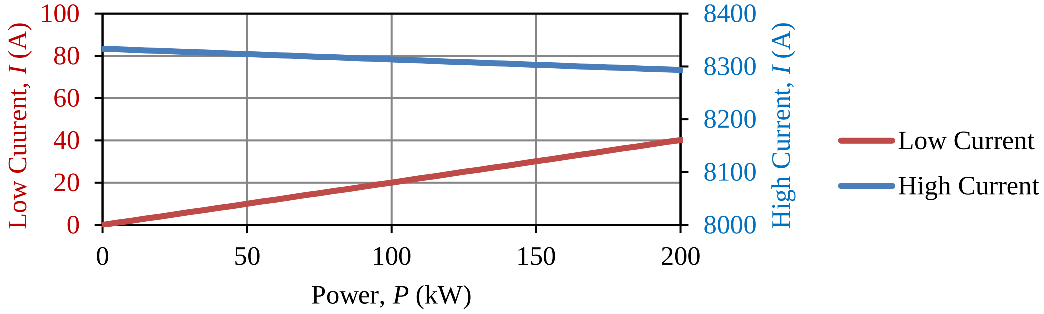

Figure 4.23: Plot of high and low positive currents in the discharge case for a 2600 F ultracapacitor

The question of which solution to use is answered by using the solution in both the charging and discharging cases where the absolute value of the current is closest to zero. This is done for two reasons: to reduce the strain on the energy storage system posed by high current charges and discharges and to prevent the energy storage system's state of charge from draining needlessly by meeting power demands with a higher than necessary current. Therefore for both the discharging and charging cases, the only solution that is used is the solution where the absolute value of the current is closest to zero: so for discharging

$$I = \frac{E_{OC} - \sqrt{{E_{OC}}^2 - 4RP}}{2R} \tag{4.60}$$

and charging

$$I = \frac{-E_{OC} + \sqrt{{E_{OC}}^2 + 4RP}}{2R} \; . \tag{4.61}$$

If the amount of current entering or exiting the ultracapacitor is greater than the maximum amount it can handle as specified by the manufacturer's datasheet, then the model limits the current to the maximum allowable limit. Once the model knows the amount of current entering or exiting the ultracapacitor, it can multiply that value by the length of the time step to determine the amount of charge removed during that time step. The amount of charge added to and removed from the ultracapacitor is tracked, and at the end of each time step the cumulative amount of charge removed is compared to the charge capacity of the ultracapacitor to determine its state of charge (SOC)

$$SOC = 1 - \frac{Cumulative\ Charge\ Removed}{Capacity} \, . \tag{4.62}$$

The terminal voltage is then computed from

$$V = E_{OC} - IR \tag{4.63}$$

since the current is computed to be negative during charging and positive during discharging. Once the terminal voltage is known it can be multiplied by the current to determine the power supplied or accepted by the energy storage system, and this power is ultimately the output from the ultracapacitor model.

4.6.2 Battery Model

Batteries are currently the most common means for storing electricity onboard commercially available electric and hybrid electric vehicles [11] [97]. Therefore, any effort to simulate EVs and HEVs must incorporate a way to model battery behavior. The battery model used in OVEM aligns with OVEM's goals of incorporating component models that are sufficiently experimentally and computationally efficient and able to be based on readily available data. Sections 4.6.2.1 through 4.6.2.3 present the process that went into formulating the battery model that was ultimately integrated into OVEM.

4.6.2.1 Existing Battery Models

Modeling battery behavior is a difficult task, as batteries behave as a function of many complex electrochemical processes. To compound the challenge of modeling battery behavior, there are an array of battery chemistries, each with its own distinct processes and traits that can require detailed models to fully capture their nuances. Different types of battery models have been devised to try to model battery behavior, and these models generally fall into two main categories: physics-based and circuit-based.

Physics-based models are typically concerned with the internal electrochemical processes taking place inside a battery [98] [99] [100] [101] [102] [103] [104]. They attempt to model these processes in great detail, usually with the aim of better understanding existing batteries or creating better batteries in the future. These types of models are require a measure of experimental resources to obtain their necessary parameters that make them poorly suited for the more systems-level modeling endeavor of Level 3 [88]. Therefore, they were not considered further for implementation into OVEM.

Circuit-based models, similar to what was investigated for the ultracapacitors, are also widely used. With circuit-based models, there is a strong relationship between complexity and accuracy. Simple circuit-based models often do not account for the effect that discharge rate and state of charge have on the capacity and voltage of the battery. More complex circuit-based models attempt to account these effects by incorporating nonlinear circuit elements to model the complex electrochemical processes taking place within a battery. These nonlinear elements have the potential to improve the accuracy of the model; however, they dramatically increase the experimental and computational demands of the model.

Figure 4.24 shows the equivalent circuit of one such circuit-based model for a lead-acid battery derived by Mauracher and Karden [105]. In this model, E_{OC} is an open-circuit voltage source that depends on the state of charge of the battery. R_0 is a constant resistance representing all the conductive elements of the battery. R_D is a charge-transfer resistance, and Z_{WI} and Z_{WL} are Warburg impedances that model diffusion in the electrolyte. C_D accounts for the double-layer capacitance. V is the terminal voltage of the battery, and I is the current entering or exiting the battery.

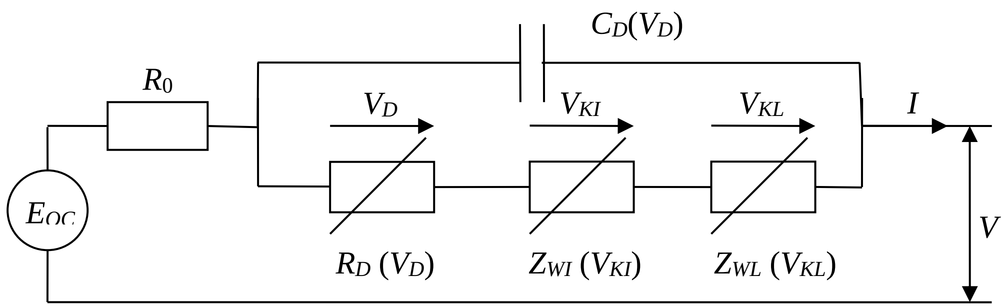

Figure 4.24: Complex equivalent circuit model for a lead-acid battery

This model was shown to produce accurate results – within 1% agreement with experimental data. However, it has a host of disadvantages that clash with OVEM's selection criteria for a battery model. C_D, R_D, Z_{WI}, and Z_{WL} are all nonlinear elements which are derived through impedance spectroscopy. As was learned during the formulation of the ultracapacitor model, impedance spectroscopy is an experimentally demanding process that would impede the model's ability to rapidly incorporate the parameters from new battery products. For instance, it would take weeks to obtain the parameters necessary to model a new battery in order to observe the effect that it might have on a vehicle's energy consumption. In an environment where new battery technologies are constantly emerging, this time penalty is prohibitively costly. Additionally, models using these complex parameters require long computational runtimes which also hurts OVEM's ability to rapidly assess different powertrain topologies. These circuit elements also primarily model processes that occur outside of the timescales of interest to OVEM [105]. And this particular model is only applicable to a lead-acid battery chemistry, and thus is not well-suited to meeting OVEM's goal of having a battery model that could serve as a flexible tool capable of rapidly simulating many different battery chemistries.

Figure 4.25 shows an equivalent circuit model for a lithium-ion battery [106]. In this model, L is an inductor, R_i is an Ohmic resistance, Z_{ZARC} consists of an arbitrary number of branched resistor-capacitor circuits (similar to the branched RC circuit in the complex ultracapacitor model), and Z_W is a Warburg impedance.

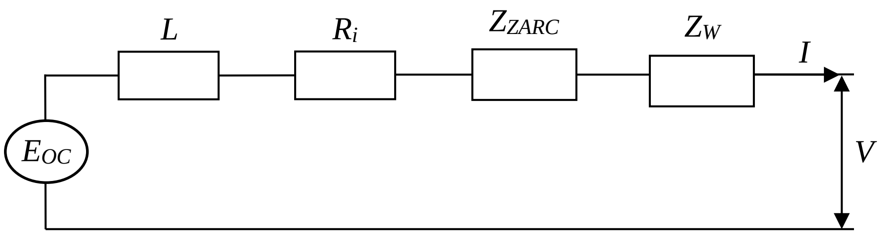

Figure 4.25: Complex equivalent circuit model for a lithium-ion battery

Just as with the equivalent circuit model for the lead-acid battery, this model requires impedance spectroscopy to characterize the nonlinear circuit elements, Z_{ZARC} and Z_W. These nonlinear elements add significantly to the model's computational runtime. The complexity of this lithium-ion model further shows that conducting impedance spectroscopy for every battery across all of the different chemistries of interest to OVEM would consume a prohibitive amount of resources and time.

4.6.2.2 Battery Model Used in OVEM

Given the challenges presented by the aforementioned battery modeling techniques, an alternative was sought that would be able to provide sufficient accuracy across a range of chemistries and products while minimizing the need for experimental and computation resources by being based on readily available data. Based on the success of formulating a simplified ultracapacitor model, this study ventured to develop an accurate battery model in order to meet the design criteria of Level 3.

Treating batteries as an open-circuit voltage with a series resistance, as seen in Figure 4.26, is a commonly used method to model battery behavior [62].

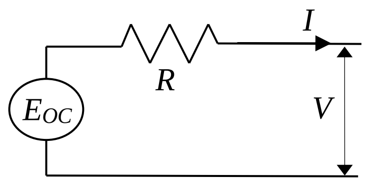

Figure 4.26: Simplified battery model

In this model, E_{OC} represents an open-circuit voltage source, R is a series resistance that represents the internal resistance of the battery, I is the current exiting or entering the battery, and V is the terminal voltage of the battery. Ordinarily, this model would be too simple to capture many of the effects necessary to ensure a satisfactory level of accuracy for the OVEM battery model. However, based on the work of Tremblay et al. [107] and Shepherd [108], which derived an algorithm that expresses E_{OC} as a function of the state of charge of the battery, this model can be used to provide accurate results using data that can be readily obtained.

This algorithm uses the constant current discharge curves typically provided by battery manufacturers on their datasheets to ascertain E_{OC} and R [107]. In this approach, E

varies with the state of charge of the battery, and R is constant. This is a simplification of real battery behavior as E_{OC} is not solely dependent on state of charge and the internal resistance of batteries can vary based on the state of charge and the discharge rate. However, it has been shown that for most battery chemistries generally the state of charge dependence of the internal resistance only has a significant effect when the battery is less than 10% discharged or more than 90% discharged [105]. During typical real world operation, vehicular battery states of charge of more than 90% and less than 10% are avoided to help prolong battery life [97]. So for most batteries, over the bulk of their operating range, it is reasonable to assume that R is constant. Note that this model also does not account for any leakage current or self-discharge losses in the battery since those effects generally happen over time scales that are significantly longer than those considered in OVEM.

A generic constant current discharge curve for a battery is shown in Figure 4.27. The curve in Figure 4.27 is from a sealed nickel-zinc battery which was chosen because it is qualitatively similar to the constant current discharge curves for a range of battery chemistries [109]. In a constant current discharge, the terminal voltage of the battery initially experiences an exponential decline, denoted in Figure 4.27 as the exponential zone. As charge is withdrawn, the terminal voltage of the battery enters a period where the voltage remains relatively flat. This interval is known as the nominal zone and the terminal voltage in this range is usually reported as the battery's rated voltage. Finally, once the charge removed from the battery passes a certain point the voltage begins to drop off rapidly.

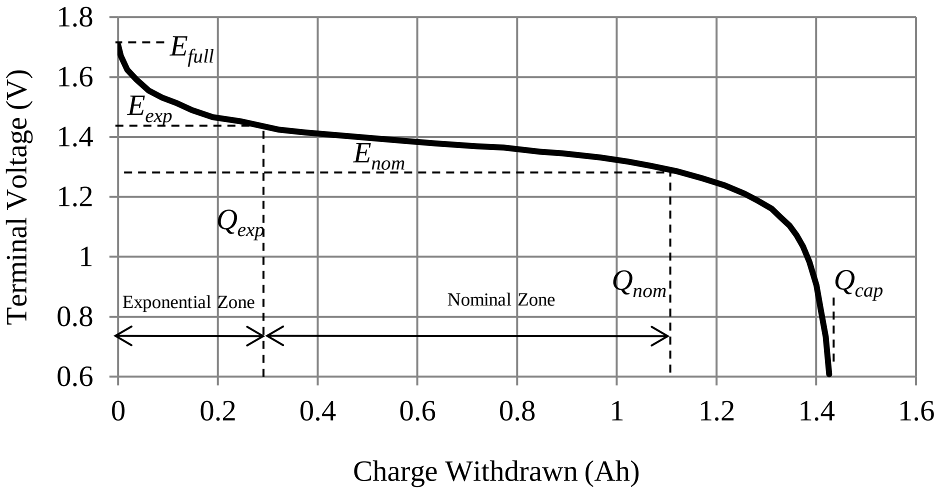

Figure 4.27: A generic constant current discharge curve obtained from a sealed nickel-zinc battery [109]

Figure 4.27 is also labeled with several key parameters which will play a role in deriving the expressions for E_{OC} and R. E_{full} is the terminal voltage of the battery when it is fully charged. E_{exp} is the terminal voltage of the battery when enough charge has been withdrawn that it is at the end of its initial exponential voltage drop. Q_{exp} is the amount of charge withdrawn from the battery when the voltage reaches E_{exp}. E_{nom} is the voltage at the end of the nominal zone, just before the voltage drops off sharply. Q_{nom} is the amount of charge withdrawn at the end of the nominal zone. Q_{cap} is the battery's capacity. The derivation to follow is based on the work of Tremblay et al. [107] and Shepherd [108], and it encompasses Equations 4.64 to 4.69. In this derivation, it will be seen how the values described above interact to predict the discharge behavior of a battery. The exponential zone of the discharge curve is modeled by the expression

$$Ae^{(-B \cdot Q_{removed})} \qquad 4.64$$

where $Q_{removed}$ is the cumulative charge removed from the battery during a discharge and

$$A = E_{Full} - E_{Exp} \qquad 4.65$$

and

$$B = \frac{3}{Q_{Exp}} \ . \qquad 4.66$$

The polarization at the anode and cathode of the battery as current flows into or out of it can be accounted for by

$$K = \frac{\left(E_{full} - E_{nom} + A(e^{-BQ_{nom}} - 1)\right)\left(Q_{cap} - Q_{nom}\right)}{Q_{nom}} \qquad 4.67$$

where K is the polarization voltage. It is assumed that the battery has a constant potential E_0

$$E_0 = E_{full} + K + Ri_{nom} - A \qquad 4.68$$

where i_{nom} is a value for the current that can be changed to yield an improved fit. Ultimately the open-circuit voltage is obtained from

$$E_{OC} = E_0 - K\frac{Q_{cap}}{Q_{cap} - Q_{removed}} + Ae^{(-B \cdot Q_{removed})} \ . \qquad 4.69$$

It should be noted that the expression for E in Equation 4.69, while based on values meant to represent physical parameters, is a quasi-empirical formula where the values influencing the determination of E_{OC} are often tuned over multiple iterations in order to yield an expression for E_{OC} that produces the best fit with the data [108]. Through the iterative curve-fitting process these parameters may lose elements of their physical significance, in an attempt to obtain a better fit, and obtaining the better fit is ultimately the higher priority [108].

Figure 4.28 and Figure 4.29 show the result of implementing the expression obtained for E_{OC} and the value determined for R into Equation 4.52 for the discharge curves of batteries of different chemistries. The experimental curve (points labeled “exp”) represent values that were taken from the batteries’ datasheets. Figure 4.28 and Figure 4.29 show that this model (curve labeled “sim”) predicts the discharge behavior to within 3%. Table 4.3 contains the key parameters in the battery model that were used to obtain the model’s curves. The modeled curves were fit so as to minimize the disagreement between their predictions and the experimental data across the entire curve. Thus, the location on the curves where the greatest discrepancy occurs is not necessarily consistent for every type of battery simulated. For instance, in Figure 4.28 the greatest difference between the modeled and experimental curves occurs in the region where the battery has a low state of charge. And in Figure 4.29

the greatest difference occurs on the 10 A curve. If the user is particularly interested in having the model align with a particular segment of the experimental data, the model can be adjusted to do that. However, the default approach (as pictured in Figure 4.28 and Figure 4.29) is to have the model minimize the difference between itself and the experimental data across the entire length of all the discharge curves.

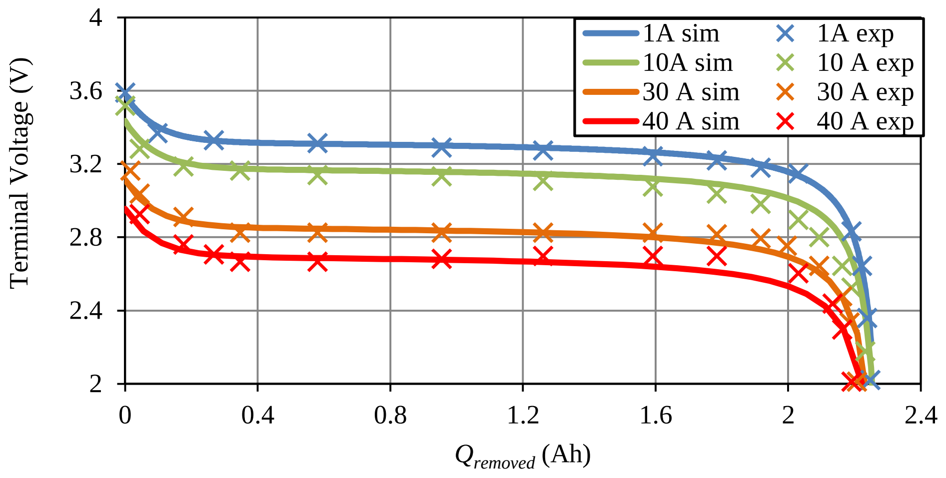

Figure 4.28: Experimental [110] and Level 3 simulated discharge curves for a lithium-ion battery

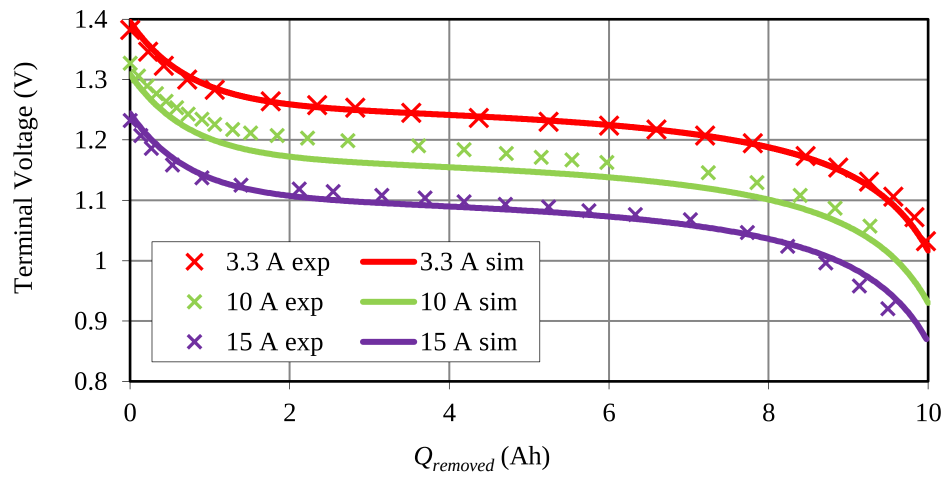

Figure 4.29: Experimental [111] and Level 3 simulated discharge curves for a nickel-metal hydride battery

Table 4.3: Parameters for the modeled nickel-metal hydride and lithium-ion batteries

	Lithium-Ion Battery Modeled in Figure 4.28	Nickel-Metal Hydride Battery Modeled in Figure 4.29
E_0 (V)	3.3583	1.325
R (Ω)	0.016	0.013
K (V)	0.0241	0.02628
A (V)	0.2604	0.14
B (Ah^{-1})	11.195	1.363

This was the battery model implemented in OVEM due to its sufficient level of accuracy, low computational and experimental demands, and the fact that it is based on data that is generally readily available.

4.6.2.3 Integration into OVEM

The battery model was integrated into OVEM in a manner identical to the way in which the ultracapacitor model was integrated – refer to Section 4.6.1.3, particularly Equations 4.51 through 4.63. Just as with the ultracapacitor model, the battery model receives a power request from the energy storage system block, determines the amount of power it can accept or reject based on its state of charge, and then outputs the power it accepted or rejected back to the energy storage system block.

4.6.3 High-Speed Flywheel Model

Flywheels are a mature technology that, due to advances in high-strength and low density materials, have now found an application as high-speed flywheels as a potential means for storing energy onboard electric and hybrid electric vehicles [13] [35] [112]. The specific power and cycle life traits of high-speed flywheels make them well-suited for automobile energy storage system applications where frequent charging and discharging is common – such as in electric and hybrid electric vehicles. Thus, any attempt to model electric and hybrid electric vehicles should incorporate a high-speed flywheel model. OVEM is, to the best of the author’s knowledge, the only vehicle simulation package to incorporate a high-speed flywheel model.

4.6.3.1 Existing High-Speed Flywheel Models

Prior vehicle simulation packages have largely not included high-speed flywheels and where they have been incorporated, the models often assume that flywheels only experience friction losses that are a fixed percentage of the power entering or exiting the flywheel [13]. This oversimplified approach does not account for many of the loss mechanisms taking place in a high-speed flywheel. Other studies that have modeled flywheels have generally been confined to buses, rail, or even stationary applications [113] [114] [115]. Since those types of applications generally use more massive flywheels, their models have generally failed to model the high speeds and the subsequent loss behaviors that are seen in high-speed flywheels. Therefore, a new high-speed flywheel model was developed that aligned with OVEM's objectives.

4.6.3.2 High-Speed Flywheel Model Used in OVEM

Energy, *E*, is stored in a flywheel according to

$$E = \frac{1}{2} J \omega^2 \qquad 4.70$$

where *J* is the moment of inertia and ω is the angular velocity. The spin-down loss curve seen in Figure 4.30 shows that high-speed flywheels experience losses proportional to the square of their speed [116]. A spin-down loss curve plots the power losses experienced by a flywheel throughout its operating speed range. Such a curve is generated by letting a flywheel spin freely down from its maximum speed. The speed of the flywheel is sampled in small time intervals, and at each of these intervals the amount of energy stored in the flywheel can be determined from Equation 4.70. The power losses taking place at each of these speeds can then be computed by dividing the difference in stored energy from one step to the next by the length of the time interval in between samples. Experimentally-derived spin-down loss curves are generally part of the literature accompanying a commercially produced high-speed flywheel (the caveat here is that few high-speed flywheels are commercially available as they are a cutting-edge technology). OVEM can accept any spin-down loss curve for a flywheel, and incorporate it into the model. As was stated previously, a primary concern in building component models in OVEM was to develop models based on reliable and accurate data that is relatively easy to obtain to facilitate rapid implementation and simulation. Since the spin-down loss curve meets those criteria, it was chosen to serve as the basis for OVEM's high-speed flywheel model. Note that the crosses in Figure 4.30 are the experimental data and the black line is the best-fit curve to that data.

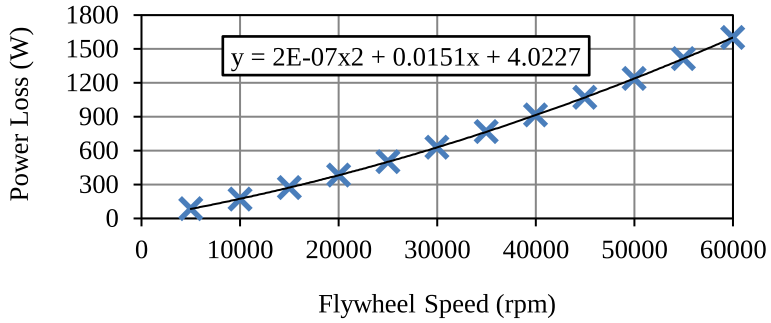

Figure 4.30: High-speed flywheel spin-down loss curve with best-fit curve [116]

Just as with the other energy storage system models, the high-speed flywheel model begins by receiving a power request to either charge or discharge. If the power request is above the maximum power rating of the flywheel, then the model limits that request to the maximum level that the flywheel can handle. The model then converts that power request to an energy request by multiplying the power request by the time step of the simulation. Given the current state of charge, the model calculates how much energy is currently stored in the flywheel, and the model determines how it will respond based on the energy request it just received. In the case of a discharge request, the flywheel model ensures that more energy will not be delivered than is currently being stored in the device. In the case of a charge request, the model ensures that more energy will not be taken in than can be stored in the flywheel.

A flywheel experiences losses as long as it is spinning regardless of whether or not it is receiving charge or discharge requests, and the model accounts for these losses. The model assumes that the time step used in the simulation is sufficiently small such that the losses can be computed based on the average of the speed of the flywheel at the beginning and end of each time step. Once the losses are computed, they are deducted from the amount of energy currently stored in the flywheel and the state of charge of the flywheel is updated to reflect the amount of energy it is currently storing.

4.6.3.3 Integration into OVEM

A high-speed flywheel can be integrated into a vehicle as an energy storage system in one of two ways: electrically or mechanically [13]. Both integrations have advantages and disadvantages. Simulating a high-speed flywheel's performance in both types of integrations can be a useful step in determining which integration is the most effective for a particular application.

In an electrical integration, the flywheel is connected to the electric bus through a motor/generator. A fixed ratio gearbox or an alternative type of transmission can be used to bring the flywheel's operating speed down to a range the motor/generator can handle. Figure 4.31 illustrates how an electrically integrated high-speed flywheel would appear in a series HEV.

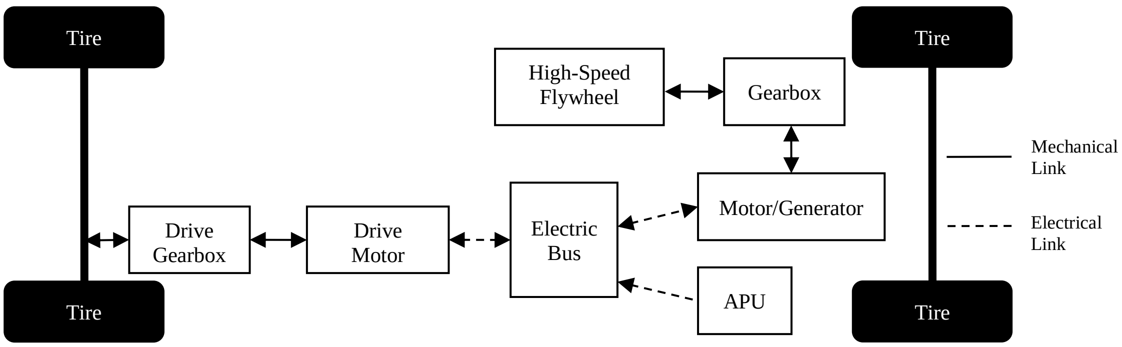

Figure 4.31: Schematic of an electrically integrated high-speed flywheel in a series HEV

Electrically integrating flywheels offers several advantages. The first is that by connecting the flywheel directly to the electric bus it interfaces with the rest of the vehicle as if it were a more traditional energy storage system such as a battery or ultracapacitor. While electrically integrating a flywheel still requires additional control efforts, it does not require extensively reengineering the powertrain [13]. Also, since the flywheel-motor/generator-gearbox unit is connected to the electric bus via wires, it has more flexibility with its packaging in the powertrain. The primary disadvantage of electrically integrating a flywheel is that it can be a relatively inefficient way to transmit and store power since the losses of the wheel-axle, tractive gearbox, and tractive motor along with those losses from the motor/generator, gearbox, and flywheel all detract from the overall efficiency [13].

The electrically integrated flywheel model adheres to the backwards-forwards nature of the Level 3 simulation. Figure 4.32 illustrates the information flows of an electrically integrated flywheel. The backwards power request originates at the electric bus just as it does for a battery or ultracapacitor. That power request gets passed to the backwards motor/generator block (which works in the same way as the motor block described in Section 4.4) that determines the torque-speed combination with which to handle that power request given the current speed of the flywheel. The efficiency of the motor/generator at that torque and speed is applied to the power request (with the request being multiplied by the efficiency in the case of charging, and divided by the efficiency in the case of discharging). The torque and speed request is then passed along to the backwards gearbox block (identical to the gearbox block described in Section 4.3.1) which accounts for its own efficiency and converts its torque and speed requests to a power request before passing it along to the high-speed flywheel block. The flywheel block then outputs the power it was able to accept or produce to the forwards gearbox. The forwards gearbox block (Section 4.3.2) uses the current speed of the flywheel and the power accepted or produced by the flywheel to compute the torque at which it must operate. The forwards gearbox block accounts for its losses and then passes the torque and speed to the forwards motor/generator block. The forwards motor/generator block (which works identically to the block described in Section 4.4.2) takes the outputs from the forwards gearbox and computes the efficiency corresponding to those torque and speed conditions based on its efficiency map. The forwards motor/generator block applies that efficiency to the torque and speed passing through it and then multiplies those torque and speed figures to obtain the power. The power is then ultimately outputted to the electric bus.

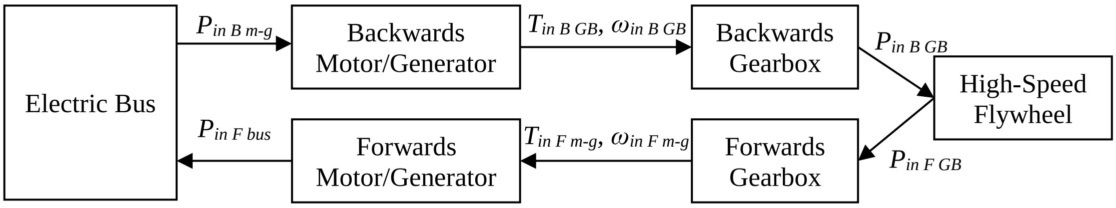

Figure 4.32: Information flows in the electrically integrated high-speed flywheel model

In a mechanical integration, the flywheel is connected directly to the drivetrain through a clutch and transmission which usually takes the form of a continuously variable transmission (CVT). Figure 4.33 shows how a flywheel could be mechanically integrated into a series HEV.

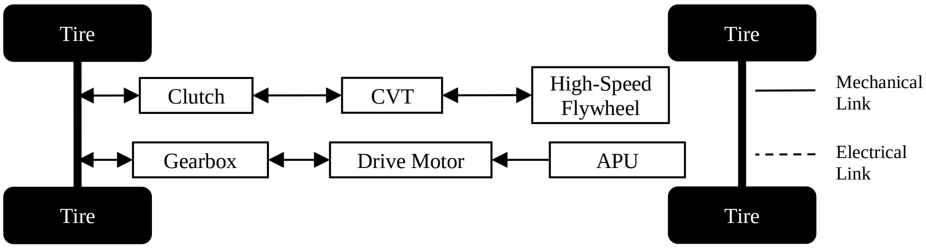

Figure 4.33: Schematic of a mechanically integrated high-speed flywheel in a series HEV

Mechanically integrating the flywheel tends to be more efficient than electrically integrating it since there are fewer components involved to contribute to the overall losses. Yet, a mechanical integration allows for less flexibility in the packaging since the flywheel has to be mechanically connected to the drivetrain.

The mechanically integrated flywheel model also proceeds according to the backwards-forwards simulation method. Figure 4.34 shows the information flows in the model. The backwards continuously variable transmission block receives the torque and speed request calculated by the backwards wheel-axle block. It applies its efficiency, which by default is assumed to be constant [117]. The backwards continuously variable transmission block then converts its torque and speed request to a power request that gets passed to the high-speed flywheel block. The high-speed flywheel block calculates the amount of power it can accept or produce given the power request and its current state of charge. It passes its power output onto the forwards continuously variable transmission block which accounts for its efficiency before passing its torque and speed outputs along to the backwards gearbox block. Since, the backwards gearbox block is connected to the drivetrain, the speed input it receives is identical to the speed output from the backwards wheel-axle block. During a motoring event, the torque input that the backwards gearbox block receives will be less than the torque output from the backwards wheel-axle block if the high-speed flywheel was able to supply power, thereby reducing the load on the drive motor. During a braking event, if the high-speed flywheel was able to accept power, then the regenerative braking load on the drive motor or friction brakes will be reduced.

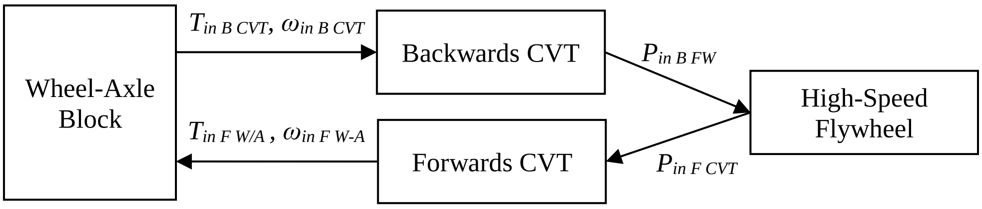

Figure 4.34: Information flows in the mechanically integrated high-speed flywheel model

4.7 Alternative Power Unit Block

In the series hybrid model, the alternative power unit interfaces with the electric bus in a manner similar to the energy storage system blocks. The alternative power unit block receives a power request (only discharge, since an alternative power unit cannot recharge) from the electric bus and then seeks to meet that request to the best of its ability. Its primary outputs include the amount of power it was able to produce and the amount of fuel it consumed to produce that power. The alternative power unit is governed by the same energy management strategies (Section 4.9) as the energy storage system. Below is a more detailed explanation of the two alternative power unit technologies for which Level 3 models have been developed.

4.7.1 Internal Combustion Engine Model

In 2011, internal combustion engines are the most commonly used power converter in automobiles. It is likely that internal combustion engines will continue to be installed in more than 90% of all new vehicles sold in developed economies through 2015, and they will continue to play a dominant role through 2030 even as EVs and HEVs likely become more prevalent [118]. Therefore, modeling internal combustion engines is an essential part of any hybrid vehicle simulation effort.

4.7.1.1 Existing Internal Combustion Engine Models

Many branches of internal combustion engine modeling exist, each with their own objectives. Most of these models take a detailed look at ICEs, often taking a physics-based approach by focusing on particular components and processes within engines, typically with the aim of either being able to better understand current engine designs or of designing better engines in the future [119] [120] [121] [122]. These types of modeling packages are concerned with physical processes with timescales outside of OVEM's range of interest. They also require a measure of physical parameters that need extensive experimental and computational resources that impinge on the simulation's ability to deliver rapid results for existing and emerging technologies. The Level 3 simulation is more concerned with rapidly implementing and simulating the efficiency of a range of existing and emerging internal combustion engine technologies. Therefore, this class of ICE simulators was not included in developing OVEM.

4.7.1.2 Internal Combustion Engine Model Used in OVEM

Given the objectives of OVEM, and the larger Level 3 modeling structure, the established method of using an internal combustion engine's efficiency map was deemed appropriate to use as the basis for the ICE model [123]. Efficiency maps are generally available as part of the literature on many different engine types. And having a model based around these efficiency maps ensures that OVEM will be able to rapidly assimilate data for existing and emerging engine technologies. Such a model will also be able to effectively simulate the efficiency of the engine which is ultimately the output most relevant for OVEM's objectives of determining values such as emissions, range, component sizing, and energy consumption. Similar to an electric motor, an internal combustion engine's efficiency map plots its efficiency as a function of its torque and speed. Figure 4.35 shows an efficiency map for a 1.9L Volkswagen TDI engine [124].

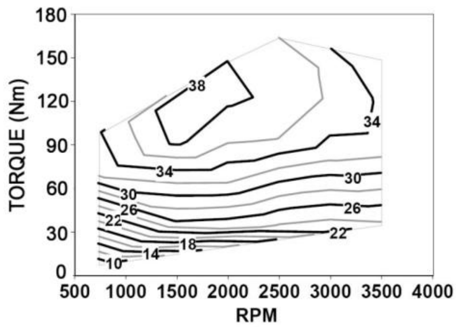

Figure 4.35: An example of an efficiency map for a 1.9L Volkswagen TDI diesel engine [124]

An important benefit of using an internal combustion engine in a series hybrid is that the engine does not have to provide traction for the road wheels and hence doesn't have to provide the power for the transient demands of realistic road driving [12]. Since the internal combustion engine is only being used to recharge the energy storage system, it can be operated more efficiently by running at torques and speeds that produce the highest possible efficiency [15]. This concept is fundamental to the way in which the internal combustion engine model proceeds.

The internal combustion engine also produces mechanical power that must be converted to electrical power before it can interface with the electric bus to recharge the energy storage system. This is accomplished by passing the torque and speed produced by the internal combustion engine through a generator, usually with a gearbox as an intermediate step to bring the output from the internal combustion engine into a more optimal range for the generator. The Level 3 model includes the generator for the internal combustion engine along with an optional gearbox.

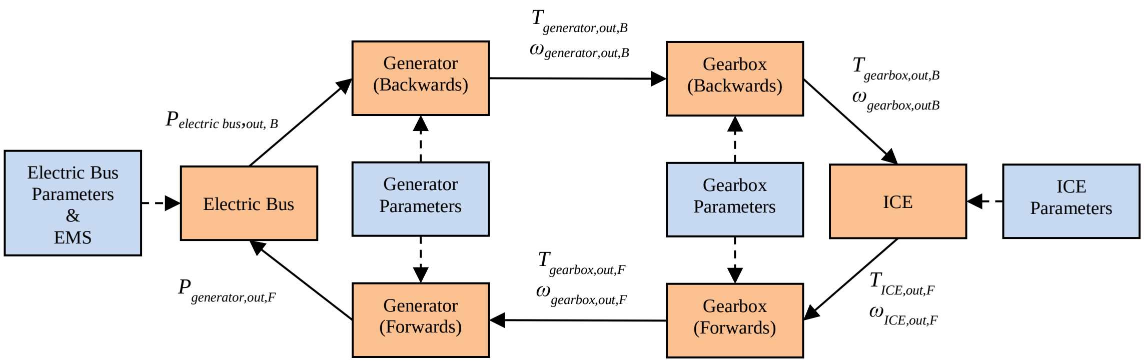

Figure 4.36: Information flows in the Level 3 ICE APU model

The information flows between the generator, gearbox, and ICE are structured in a backwards-forwards fashion in keeping with the larger Level 3 architecture. The internal combustion engine alternative power unit model begins by receiving a power request from the electric bus block. If the power request is higher than either the generator or internal combustion engine can tolerate, then the request is limited to whichever maximum power rating is lower between the generator and internal combustion engine. The model then creates a list of the possible torque and speed combinations (in user specified increments) for the generator that would be able to meet the power request, making sure to disregard any torque and speed combinations, that fall outside of the generator's operating region. The efficiency of each of these torque and speed combinations in the generator is recorded and stored. Each of the generator's torque and speed combinations is passed through the gearbox model (identical to the backwards and forwards gearbox models described in Sections 4.3.1 and 4.3.2, respectively). The gearbox applies its gear ratio to the torque and speed requests and then applies its own efficiency calculations to each one of the different requests. The efficiency of each of these combinations in the gearbox is also stored. The list of torque and speed requests is then passed along to the internal combustion engine model which records the efficiency achieved by each of the physically permissible combinations. The alternative power unit model then determines its overall system efficiency by multiplying the efficiencies from the generator, gearbox, and engine together for each torque and speed combination. Whichever torque and speed combination produces the highest overall efficiency is the combination that is used. This achieves the effect of enabling the internal combustion engine and the alternative power unit to operate in its most efficient region, as it would strive to do in an actual series hybrid. It should also be noted that the internal combustion engine's alternative power unit model includes a parameter that can be set by the user so that the torque and speed of the generator and internal combustion engine do not vary too much from one time step to the next. For instance, it is unrealistic for the internal combustion engine serving as an alternative power unit to go from 0 to 100 kW in a single 1 second time step. So the user can set parameters that will limit the amount the speed and torque of the system can change in a single time step. If this constraint is utilized, then only torque and speed combinations that satisfy it will be allowed.

Once the torque and speed used by the ICE is known, the fuel consumption of the engine can be calculated

$$Fuel_{used} = \frac{P_{req}}{LHV_{fuel}\eta_{ICE}}\Delta t \tag{4.71}$$

where P_{req} is the product of the torque and speed produced by the ICE, LHV_{fuel} is the lower heating value of the fuel, η_{ICE} is the efficiency of the engine during a given time step, and Δt is the length of the time step. The lower heating value of the fuel was used because that is the most common practice in both the ICE and fuel cell modeling literature [125] [126] [127] [128].

4.7.2 Fuel Cell Model

Fuel cells have characteristics that make them desirable as onboard power generation systems for hybrid electric vehicle applications [129]: their efficiency is typically higher than that of internal combustion engines [130], and they can utilize an array of fuels such as pure hydrogen, diesel, gasoline, methanol, and carbon monoxide [131]. Depending on the fuel and the manner in which it is processed, fuel cells may emit zero or significantly fewer emissions than comparably sized internal combustion engines [125]. Though fuel cells are not currently widely used in commercial vehicles, they have the potential to play an increasingly important role in the future, and thus they merit inclusion in OVEM's simulation effort.

4.7.2.1 Existing Fuel Cell Models

Fuel cell models can generally be grouped into one of two categories: physics-based or systems-level. Physics-based models are concerned with the detailed modeling of small-timescale processes of the fuel cell as a system, usually with the aim of better understanding existing fuel cell designs or with the aim of improving these designs in the future [132] [133] [134] [135] [136]. These models need detailed parameters which require extensive experimental and computational resources to obtain and process. This leads these types of models to conflict with OVEM's goal of being able to use models based on readily available data to facilitate rapid simulations across different technology categories. Therefore, a different modeling approach was sought.

4.7.2.2 Fuel Cell Model Used in OVEM

The Level 3 fuel cell model ultimately implemented in OVEM utilized the fact that fuel cell performance is primarily characterized by two curves [137]. This is particularly true for proton exchange membrane fuel cells (PEMFCs) which are the type most commonly used in vehicle applications [23] [131]. The first curve is known as a current-power (*I*-*P*) curve. This curve plots the relationship between the current and power produced by a fuel cell. Figure

4.37 shows an example of an *I-P* curve for a PEMFC [138]. The second curve is known as an efficiency curve, and it plots the efficiency of a fuel cell as a function of the amount of current the fuel cell is producing. This approach was used because it met OVEM's criteria of using readily-available data that would facilitate rapid implementation and simulation of existing and emerging technologies. It also met the condition of being relevant to the timescales of interest to OVEM.

Figure 4.38 shows the efficiency curve for the same fuel cell whose *I-P* curve was shown in Figure 4.37 [138]. In addition to being accurate characterizations of fuel cell performance, the efficiency and *I-P* curves are relatively simple to obtain as they are generally included in the literature on most commercially available fuel cells. Chapter 5 (Section 5.2.2 in particular) contains an in depth example for how the fuel cell model can be used in an actual series HEV.

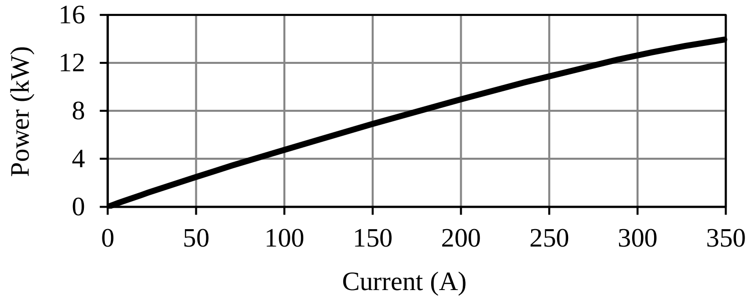

Figure 4.37: *I-P* curve for a PEMFC [138]

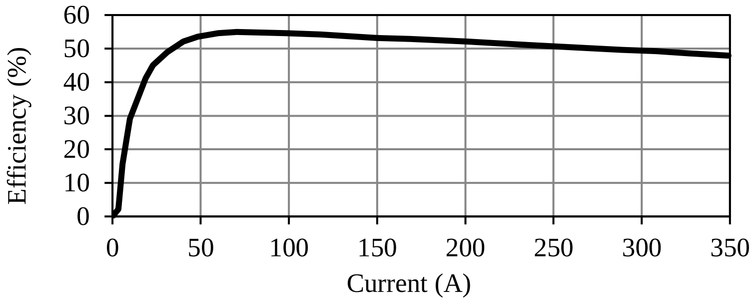

Figure 4.38: Efficiency curve for a PEMFC [138]

4.7.2.3 Integration into OVEM

The rest of the fuel cell model was built around the *I-P* and efficiency curves in a manner similar to the other energy storage system and alternative power unit models. The fuel cell model receives a power request. It then limits the power request to the maximum amount the fuel cell can handle. This power request is used to find the corresponding current on the *I-P* curve. This current is used to locate the efficiency (η_{FC}) of the fuel cell from the efficiency curve. The amount of hydrogen used by the fuel cell ($H_{2\,used}$) to meet the power request (P_{req}) is calculated by

$$H_{2\,used} = \frac{P_{req}}{LHV_{H_2}\eta_{FC}}\Delta t \qquad 4.72$$

where LHV_{H2} is the lower heating value of hydrogen fuel and Δt is the time step of the simulation.

4.8 Epicyclic Gear Train Block

In parallel and series-parallel HEVs, the electric motor and internal combustion engine are frequently coupled together by an epicyclic gear train (EGT), sometimes also referred to as a planetary gear train [12] [139]. The EGT enables the ICE, the motor, or both to provide tractive power to the vehicle. EGTs can be configured to allow power to flow from the ICE to the motor/generator and then to the energy storage system in order to recharge it as is the case in series-parallel hybrids [139].

4.8.1.1 Existing Epicyclic Gear Train Models

In surveying the literature on EGTs, it was found that many of the existing models made assumptions that were either overly simple or based on weak or impractical experimental evidence. For instance, ADVISOR assumes the epicyclic gear train is 100% efficient [26]. Several other models assume that the efficiency of the EGT does not depend on the load it is bearing [53] or assume that the efficiencies for each interaction between all of the different elements in the gear train are constant and are known in advance without being based on real-world data [53] [140] [54].

Experimental results showed that these assumptions were largely invalid, and that EGTs do in fact experience load-dependent losses [45]. Formulating assumptions about the efficiency of each individual interaction between the different gear elements based on no experimental results required incorporating a degree of uncertainty into the model that was not commensurate with the level of fidelity being sought in the Level 3 models. Therefore, a new type of EGT modeling approach was developed for the Level 3 simulation.

4.8.1.2 Epicyclic Gear Train Model Used in OVEM

The EGT model used in the Level 3 parallel and series-parallel HEV models is based on empirical work conducted on several different EGTs tested over a range of loads [45]. Bearing, meshing, churning, and windage losses that vary with the load handled by the EGT were accounted for by using these empirical results; whereas they were not accounted for by many analytical and numerical models in the literature. It was also shown in the literature that the efficiency can be assumed to vary with the ratio between the backwards input torque and the maximum torque of the tractive devices attached to the gear (T/T_{max}) [45]. This approach is especially suited to the purpose of backwards-forwards modeling because the efficiency can be assumed to vary only as a function of the backwards input torque (the torque transferred between the wheel-axle and the EGT during the backwards phase of the simulation) [45]. Figure 4.39 shows the results from this experimental study conducted for EGTs of two different sizes tested over an array of loads. Since the trend in efficiency for two different EGTs over a range of loads followed the same qualitative pattern and were both within 3% of each other, the average efficiency curve of the two different EGT sizes was ultimately used as the basis for determining the efficiency of the Level 3 EGT model. Note that T_{EGT} is the output torque of the gear train, and T_{max} is the higher value between the maximum torque of the ICE and motor. This approach is based on an empirical approach that cannot necessarily be assumed to apply to all potential EGT sizes and scenarios; however, this data clearly shows that assuming a constant efficiency EGT is insufficient. This approach provides an accurate means for accounting for EGT efficiency based on readily available data over the timescales of interest to OVEM.

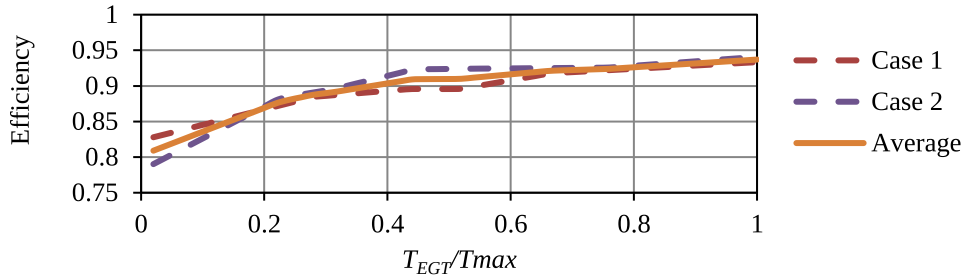

Figure 4.39: Empirical results from a range of EGTs tested over different loads and the average result used in the Level 3 parallel and series-parallel HEV simulation

4.8.1.3 Integration into OVEM

Initially, the EGT model proceeds identically in both the parallel and series-parallel HEV models. The torque and speed requests calculated by the backwards wheel-axle block are fed into the backwards EGT block. The EGT model uses the average curve in Figure 4.39 to calculate its efficiency based on the torque request it receives from the backwards wheel-axle block relative to the maximum torque capable of being provided by whichever device has the highest torque rating between the ICE and electric motor ($T_{EGT}/T_{\max}$). The model assumes that the EGT retains that efficiency throughout the time step. In cases when the vehicle is accelerating or traveling at a constant speed, the EGT model accounts for its losses and gear ratio (specified by the user) and then sends the torque and speed requests to the ICE. The ICE determines how much torque and speed it will produce in response to the requests it receives (for more information see Section 4.9.3.1) and outputs the torque and speed it supplies to the second phase of the EGT model.

The second phase of the EGT model takes the torque and speed supplied by the ICE and compares it to the requests that the first phase of the EGT model sent to the ICE. If the ICE produced less power than was requested of it, then the second phase of the EGT model asks the motor to make up the difference. If the ICE produced more power than was requested of it, then the second phase of the EGT model sends the excess power to the motor/generator where it will be used to recharge the ESS (note that the ICE will only generate excess power if it is a series-parallel HEV). For any excess power going from the ICE to recharge the ESS, the second phase of the EGT factors in its own internal losses.

The third phase of the EGT model is purely forward-looking. It receives as its input the torque and speed supplied from the forwards motor and ICE blocks. It synthesizes the power supplied by the ICE and motor, accounts for its losses (retaining the same previously calculated efficiency), and outputs the torque and speed it could supply to the wheel-axle block.

In instances when the vehicle is braking, the energy flows from the ICE are not involved since it cannot receive power. The torque and speed requests pass back from the wheel-axle block to the EGT block. The EGT block applies its efficiency to the torque signal and then passes the updated torque and speed signals to the motor/generator where they go on to recharge the energy storage system.

4.9 Energy Management Strategies

The interactions between the energy storage system(s), the alternative power unit (in the case of HEVs), and the rest of the vehicle are governed by an energy management strategy (EMS). Energy management strategies balance the technologies, topologies, and operating conditions of the application usually in an effort to achieve a result such as minimized energy consumption or emissions [141]. For instance, a series HEV delivery van with an ICE-based APU and batteries traveling in suburban areas will likely have a different optimal EMS than the same vehicle traveling in an urban area. And its optimal EMS will almost certainly be different than the EMS best suited for an EV or HEV sports car. OVEM handles the complexity of EMSs by grouping them into two categories: thermostat and speed-based. Each of these broad categories contain different parameters that can be tuned in order to enable the vehicle to best meet its goals.

4.9.1 Thermostat

The objective of the thermostat EMS is to maintain the state of charge of the ESS in a set region. In the thermostat EMS, when the state of charge of the ESS drops below a certain threshold, either the other ESS (in the case of a hybridized ESS) and/or the APU is called upon to recharge it. This threshold is known in the Level 3 simulation as the *charge on level*. Once the ESS's SOC has dropped below the *charge on level*, the ESS will continue to be recharged until it reaches its upper threshold at which point the ESS and/or APU are no longer needed to supply power to the ESS, and they are switched off. This upper SOC limit is known in the Level 3 simulation as the *charge off level*.

Figure 4.40 shows how the SOC of the ESS varies in a plug-in hybrid electric vehicle (PHEV) when it is run with a thermostat EMS. This PHEV is a series HEV with an ICE serving as the APU. The vehicle was run over multiple iterations of the NEDC, and the ICE was programmed to turn on when the ESS's SOC reached 20% and turn off when the SOC had returned to 80%.

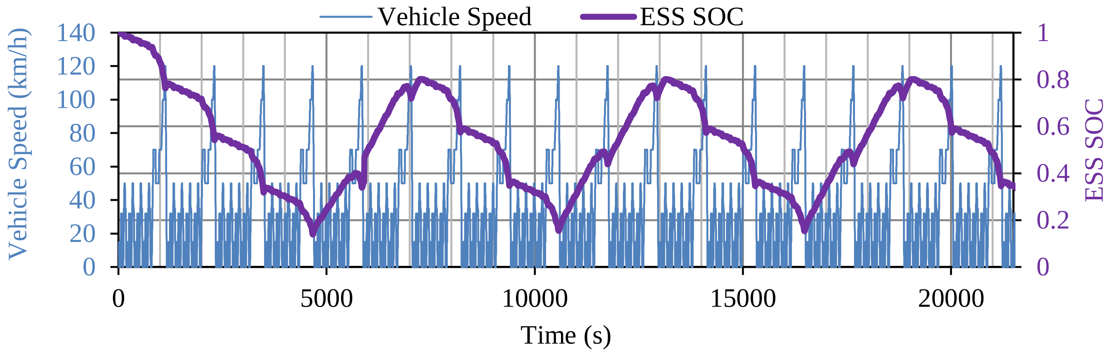

Figure 4.40: Illustration of the thermostat EMS in a PHEV over the NEDC

The thermostat approach also incorporates a contingency known as a power-follower. The power-follower comes into operation when the power request from the vehicle exceeds the capacity of the first ESS and additional power must be drawn from other ESSs and/or the APU [142].

The *charge on level* and *charge off level* parameters tell the other ESS and the APU when to produce extra power, but the ESS and APU must also be told how much power to produce. The Level 3 simulation provides the user with two different ways to control the charging rate. The first works by specifying a fixed charge rate that is independent of the size of the ESS or APU. The second approach makes the charging rate proportional to the power rating of the ESS or APU.

4.9.2 Speed-Based

Speed-based energy management strategies seek to keep the state of charge of the energy storage system inversely proportional to the kinetic energy of the vehicle. The speed-based EMS used in the Level 3 simulation is based on the concepts established by S. Barsali et al. [141]. This EMS is based on the premise that at low speeds it is likely that the vehicle will accelerate in the near future, and the ESS should have a high SOC so that it can power that acceleration. At high speeds, it is likely that the vehicle will be braking soon so the ESS should have a low SOC which will allow it to accept as much of the regenerative braking energy as possible.

Whenever the inequality below is true, the APU or secondary ESS is called upon to provide extra power to recharge the primary ESS

$$(1 - SOC) > \frac{v_{current}}{v_{max}} \qquad 4.73$$

where $v_{current}$ refers to the current speed of the vehicle and v_{max} refers to the vehicle speed at or above which the APU or secondary ESS no longer needs to produce power to recharge the primary ESS. Figure 4.41 shows how the state of charge of the energy storage system in a PHEV varies when governed by the speed-based EMS. In this simulation v_{max} was set to

100 km/h. Notice that when the speed of the vehicle increases the SOC is allowed to drop, and when the vehicle speed decreases, the SOC is brought back up by switching on the APU.

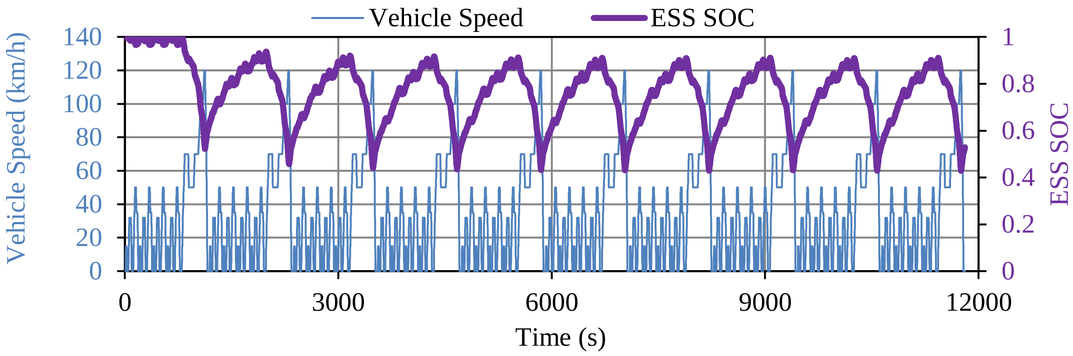

Figure 4.41. Illustration of the speed-based EMS for a PHEV over the NEDC

The speed-based EMS also allows for a power-follow contingency. In cases where the power requests exceed the maximum power rating of the first ESS, the other ESS and/or APU can be called upon to deliver extra power to satisfy the request.

4.9.3 Parallel and Series-Parallel Hybrid Electric Vehicle Energy Management Strategies

The parallel and series-parallel HEV models employ the same energy management strategies as the series HEV model: thermostat and speed-based. The logic and rationale for these EMSs remains the same in the parallel and series-parallel case with the ICE functioning in the role of the APU. Yet, the parallel and series-parallel models do have an additional level of complexity that controls the operating range of their ICEs. This is done so as to make sure that their ICEs utilize their hybridized electric motors in order to operate as efficiently as possible. In the parallel and series-parallel HEV models when the ESS requires power for recharging, the ESS sends a signal to the ICE model telling it to produce additional power. If the ICE is capable of producing extra power, it does so under the framework and constraints explained in Section 4.9.3.1. The power then flows out from the ICE, through the EGT model, through the motor/generator model, and then finally to the ESS.

4.9.3.1 Parallel and Series Parallel Internal Combustion Engine EMS

In a parallel and series-parallel HEV, the ICE is coupled to the wheels. This means that the ICE cannot always operate at its most efficient point as it would if it were in a series HEV. When a series-parallel HEV is using the ICE solely to recharge the ESS and not to provide a tractive motoring force, then the ICE can operate in its most efficient region. However, in instances where the ICE is called upon to provide a tractive force to the wheels, it has to respond to changes in the road load.

The ICE model begins the same for both the parallel and series-parallel HEV models. The model receives torque and speed requests from the EGT model. First the speed is checked, to make sure that the request does not exceed the limits of the ICE. If the request is greater than the maximum speed the ICE can handle, then the request is reduced so that it falls within the ICE's operating range. Then the model examines the torque request. The maximum amount of torque that an ICE is capable of producing is a function of speed. So at the requested speed, the model determines whether the torque request exceeds the maximum allowable limit. If so, then the torque request is reduced to the maximum amount the ICE can handle at the selected speed.

The efficiency map for an ICE reveals that there are regions over which its operation is relatively inefficient as seen in Figure 4.35. One of the objectives of operating the ICE in parallel and series-parallel HEVs is to confine the ICE's operation to torque and speed regions where it will operate more efficiently. For example, it is often inefficient to have ICEs operating at low speeds and torques [12]. So in the ICE model, the user can set minimum torque and speed thresholds below which the engine will not operate in order to help ensure that the efficiency of the ICE is maximized. Figure 4.42 shows how these regions can be constructed on a generic ICE efficiency map. In the parallel HEV model, whenever the torque and/or speed requests received by the ICE are below these minimum thresholds then the ICE model produces no power and the rest of the power is left to be supplied by the motor. If the torque and/or speed requests are above the minimum thresholds then the ICE model meets them.

The series-parallel HEV model works identically to the parallel HEV model except for situations when the ICE needs to produce extra power to recharge the ESS. In the case when the ESS needs recharging and the speed request to the ICE model is below the minimum threshold, a fixed percentage (set by the user) of the difference between the minimum and maximum speed of the ICE is added to the speed request such that the updated speed request is below the maximum speed and above the minimum threshold value. In instances when the speed request is above the minimum threshold, then no alterations are made to the speed request. Once the speed is determined, the ICE must determine the amount of torque it will produce to cover both the tractive road load and the additional power needed to recharge the ESS. If the tractive torque request is above the minimum torque threshold, then the ICE model increases the torque request by a fixed percentage (set by the user) of the difference between the maximum speed of the ICE and the torque request. If the torque request is below the minimum torque threshold, then the ICE model increases the torque request by a fixed percentage (specified by the user) of the difference between the maximum and minimum torque values for the ICE at that speed.

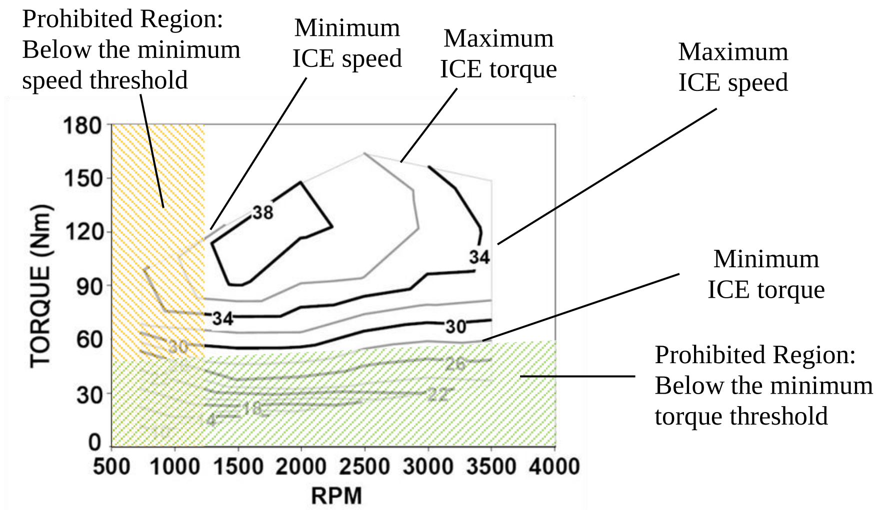

Figure 4.42: Efficiency map of an ICE with minimum torque and speed thresholds as used in the Level 3 parallel and series-parallel HEV models

Once the torque and speed that the ICE will produce has been determined, the model interpolates the efficiency map to determine the efficiency of the ICE at that point. When the efficiency is known, then the fuel consumption of the engine can be determined from Equation 4.71.

4.10 Level 3 Case Study: Milk Float Modeling

The following is a continuation of the milk float case study that builds on the Level 1 and 2 case studies of the milk floats. It provides an illustration of how the Level 3 models can be used to provide credible results based on product data even in an environment where uncertainty regarding component specifications and vehicle driving characteristics is high.

4.10.1 Introduction

The case study concerning the potential of the milk floats to extend their range by incorporating regenerative braking was continued with the Level 3 EV model. The Level 3 models are based on actual data from real components and the simulation imposes realistic physical limits on the performance of the vehicle. This should theoretically lead to more accurate results than those obtained from the studies done using the Level 1 and Level 2 models.

4.10.2 Methods

The mass and external shape parameters for the milk float had already been obtained in the Level 1 (Section 2.8) and 2 (Section 3.7) case studies. So for the Level 3 milk float study, the primary challenge was finding reliable data for the powertrain's components, particularly for the motor and battery. The floats' delivery run was simulated in a manner similar to what was done in the Level 1 and 2 case studies, but with some slight differences to take advantage of the capabilities of the Level 3 simulation.

4.10.2.1 Component Selection

The first step in simulating the milk floats using the Level 3 model was to characterize the components in the powertrain. All of the floats, regardless of their motor type, had the same battery pack. The floats contained 36 Exide 95EPzB585 lead-acid batteries each with a rated capacity of 585 Ah [143]. The discharge data from these batteries was obtained from the manufacturer. Figure 4.43 shows the ability of the Level 3 battery model to predict the discharge curves of the float's battery. The battery model shows agreement to within 2% with the experimental data.

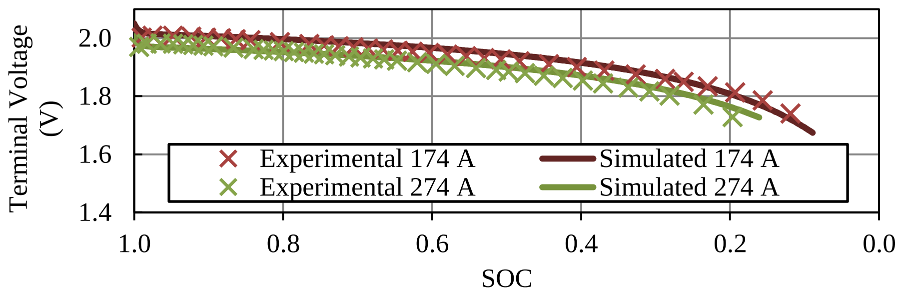

Figure 4.43: Comparison between the experimental data [143] and the Level 3 battery model's predictions for the Exide 95EPzB585 lead-acid battery

The efficiency maps for the DC and AC motors used in the floats could not be located. As a substitute, the motor models were based on 45 kW DC and AC motors with known efficiency maps [61] [144]. Figure 4.44 and Figure 4.45 show the efficiency maps of the DC and AC motors used in this study, respectively. Since these maps are only an approximation of the actual motors' efficiency maps, it is worth reiterating that this study should not be taken as an exact prediction of the floats' performance but rather a reasonable estimate given the available information.

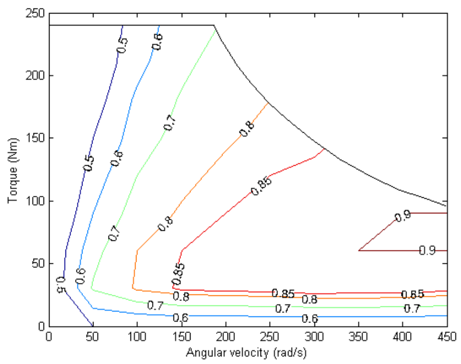

Figure 4.44: Efficiency map for the milk float's modeled DC motor [24]

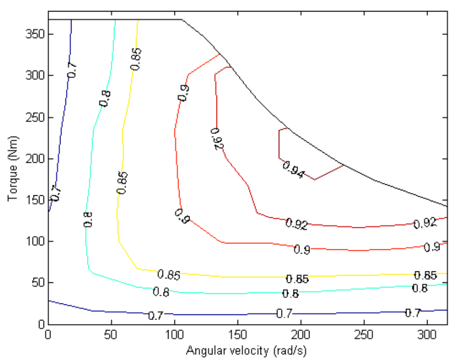

Figure 4.45: Efficiency map for the milk float's modeled AC motor [61]

4.10.2.2 Vehicle Simulation

With the components in the powertrain characterized, the study validated the simulated floats' range against the real floats' range, assuming that the floats' used no regenerative braking. The two types of floats, one with a DC and one with an AC motor, were put through 22 and 28 iterations of the drive cycle, respectively, just as in the case studies for Level 1 and 2. In both of the simulations, a fixed amount of cargo weight was removed from the float during each iteration of the drive cycle as it traveled through its range so that it was fully loaded at the beginning of its delivery run and empty at the end. This study used the same drive cycle and vehicle parameters as had been used in the Level 1 and 2 milk float studies.

Once the range of the floats while operating without regenerative braking had been validated, the next step was to simulate the float's range with regenerative braking in order to see how much of an improvement could be expected from regenerative braking. The principle that a float should linearly offload its cargo over the course of its delivery run was still adhered to; however since the range of the floats was not known in advance, an iterative approach was devised to determine how much cargo to offload during each repetition of the drive cycle. By running multiple iterations of the floats' entire delivery run, the simulation was able to converge at a value for the mass of cargo offloaded before each new iteration of an individual drive cycle within the larger delivery run so that regardless of the ultimate range of the float, it began its run fully loaded with cargo and ended with no cargo.

It should be noted that this assumption concerning the offloading of cargo weight may not be entirely accurate, especially if regenerative braking is introduced, since significant regenerative braking has the potential to change the delivery patterns for the floats. For instance, if a float is able to significantly increase its range by using regenerative braking, then the limiting factor in the amount of milk it can deliver per day may now be the amount of cargo it can hold rather than the distance it can travel in between charges. It is conceivable with an extended range, a float could deplete its cargo and have to return to the depot to pick up another load without having to recharge. If the range of the floats were to increase, the logistics of charging them would have to be determined by the milk distributor. Therefore, that concern is beyond the scope of this study. But it is important to be aware, that the predictions contained in this study are in part a result of several simplifying assumptions that have attempted to account for the important factors affecting the range of the floats, and that the presence of these simplifying assumptions means that the results should not be taken as precise forecasts but rather as reasonable estimations.

4.10.3 Results and Discussion

This study began by attempting to have the Level 3 model characterize the floats as they currently exist. Assuming no regenerative braking, a float with a DC motor was simulated to have a range of 58 km (36 mi) which was within 4% of the reported range of the real DC floats, 56 km. This close level of agreement with the floats appears to be a positive result. However, it is also important to bear in mind that the actual range of the floats is an average value from across the entire fleet. This study, in attempting to model a representative float, may have not actually modeled any one particular float with a high degree of accuracy. So it is important to remember that this study was only concerned with making an approximation regarding the average range of the floats. For it is probable that the range of actual individual floats could vary around this average value given the exact nature of their driving and cargo offloading patterns.

When the DC float was simulated with regenerative braking, its range was estimated to be 90 km (56 mi). This prediction is approximately 16% higher than the projections made by Levels 1 and 2 for the floats with a DC motor. An analysis of the causes of this discrepancy was conducted. The energy flows through each of the component blocks was examined for the Level 1, 2, and 3 models. The Level 1, 2, and 3 models all used the same drive cycle, aerodynamic drag, rolling resistance, mass, tire radius, and gear ratio data so those did not contribute significantly to the discrepancy. It was ultimately determined that the different motor models and motor data between the three levels was the largest factor contributing to the discrepancy. In the Level 1 case study, the fixed DC motor efficiency was set to 76%. In the Level 2 case study, the maximum DC motor efficiency was set to 80%. The efficiency map employed in the Level 3 simulation from an actual DC motor had a maximum efficiency of approximately 90%. Figure 4.46 plots this efficiency map, and overlaid on the map are the torque and speed requests made of the motor as it traversed the drive cycle under three different cargo levels: 5000 kg (full cargo), 3850 kg (half cargo), and 2700 kg (no cargo).

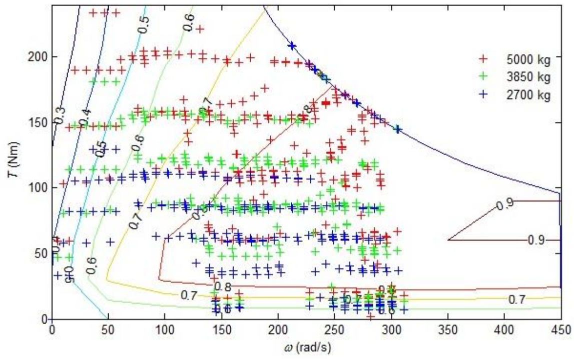

Figure 4.46: Efficiency map of the DC motor used in the milk float study, overlaid with the torque and speed requests from the drive cycle for three different cargo levels

From Figure 4.46 it can be seen that a significant number of the torque and speed combinations requested of the motor lie at an efficiency above 80%. This shows that by using this particular efficiency map, the overall vehicle became more efficient and thus achieved a longer range than was predicted by Levels 1 and 2. The sensitivity analysis presented in Figure 4.47 also shows that the range of the floats is particularly sensitive to the motor because relative to the other components and parameters of the vehicle it is proportionally a source of a high amount of losses. So any change in motor efficiency can produce proportionally high changes in the vehicle's range. Unfortunately, the necessary data could not be found for the exact type of DC motors used in the floats so this map is only an approximation, and the motor models in Levels 1 and 2 are also only approximations. However, what is certain is that between Levels 1, 2, and 3 a range of efficiency values for a DC motor have been examined, and the results across all three levels agree on the larger point that, even when equipped with regenerative braking, a float powered by a DC motor would not achieve the target range of 105 km.

For a float with an AC motor with no regenerative braking, the Level 3 model estimated that the float would have a range of 66 km (41 mi). This was within 9% of the actual range reportedly achieved by the floats with AC motors. This discrepancy can be explained by the uncertainty inherent in this study. The sensitivity analysis presented later in this section shows that the motor efficiency maps and the drive cycle and cargo offloading schedule are the most obvious areas where best estimates are approximating for actual data. If this study had access to the actual efficiency maps for the motors onboard the floats and if the drive cycle and cargo offloading pattern of the floats were more accurately known, the credibility of these results would be improved.

For a float with an AC motor with regenerative braking, the Level 3 model predicted that the range would be 106 km (66 mi) which is above the target of 105 km set forth by the milk distributor. Based on the previous validation of the floats, it is reasonable to assume that this prediction is only accurate to within roughly ±10%. Due to this uncertainty, the prediction that a float with an AC motor and regenerative braking will achieve a range of 105 km should not be taken as an absolute guarantee.

To gain a better understanding of how the chosen parameters affected the range of the simulated milk floats, a sensitivity analysis was performed (Figure 4.47). A sensitivity analysis was done for both floats using both the DC and AC motors. Each of the vehicle parameters that could be varied was varied by ±5% and the corresponding change in the float's range was recorded.

In the Level 3 model, the motor and battery models do not lend themselves to be simply scaled by ±5%. In these instances a slightly different technique had to be employed in order to create a 5% change in the underlying data. There is no single optimal way to do this as these models are more than just scalar values, so the approaches used were compromises deemed to be reasonable by the author based on the objectives of this sensitivity analysis. In the case of the motor efficiency map, the torque and speed axes were each scaled by ±5%. In effect this changes the sizing of the motor and it also affects where the torque and speed points from the drive cycle will fall on the efficiency map. In the case of the battery model, the parameters describing the discharge curves were tuned such that the curves demonstrated an approximately ±5% change from their original positions. Again, these approaches were deemed reasonable in the interest of conducting a sensitivity analysis that could provide a measure of insight into the importance of the parameters affecting vehicle range.

The sensitivities presented in Figure 4.47 are the average of the absolute values of the percent changes in range caused by either the 5% increase or decrease in the vehicle input parameters. In this analysis, it was assumed that the energy storage systems recaptured 50% of the energy *available* to them. This condition was selected in order to provide a conservative and representative snapshot of the floats by avoiding modeling them at the upper or lower limits of their regenerative braking possibilities. Also note that the results in this sensitivity analysis were done for these specific floats over a specific drive cycle, and any conclusions drawn from this analysis regarding the sensitivity of the model to the input parameters cannot be uncritically applied to any vehicle in any context.

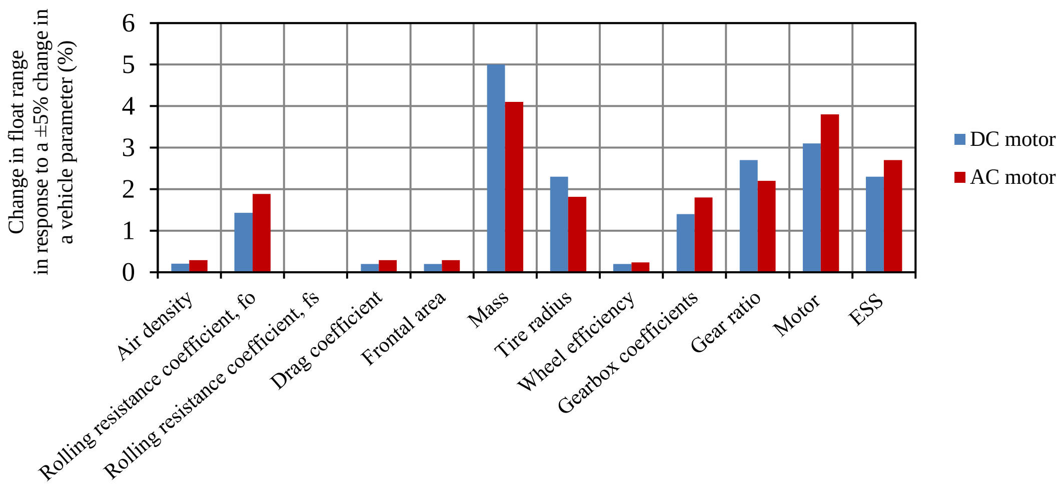

Figure 4.47: Level 3 sensitivity analysis for a milk float with a DC and AC motor

The parameters determining the resistive forces acting on the vehicle affect the range of the floats in a manner similar to what was seen in Levels 1 and 2. The parameters determining aerodynamic drag and the speed component of rolling resistance (f_s) have little effect due to the low speeds at which the floats travel. The constant rolling resistance coefficient (f_o) has a higher effect relative to the other resistive force parameters due to the low speeds experienced by the floats. Just as in Levels 1 and 2, the range of the floats is most sensitive to mass. The beginning and ending values of the floats' mass are known precisely. However, the manner in which the floats offload their cargo is not known precisely, and it is possible that this could be a strong contributor to any disagreement between the modeled and actual figures. The effect of wheel efficiency is low, as wheel efficiency represents a small portion of the collective powertrain losses.

Vehicle range is more sensitive to tire radius and gear ratio in the Level 3 model than it was in the Level 1 and 2 models. The tire radius and gear ratio determine how the power requests are disaggregated into torque and speed requests. This can have significant impacts on range since in the Level 3 model these torque and speed requests are ultimately passed to the motor block where they are subjected to an efficiency map that may not be optimally constructed for them. It is possible that these torque and speed requests may be clustered in areas of higher or lower efficiency on the efficiency maps of the motors which could produce substantive changes in vehicle range. The gearbox coefficients also affect where the torque and speed points will lie on a motor's efficiency map so their effect cannot be discounted; however their effect on the range of the floats was not as great as the gear ratio.

The range of the floats' is also sensitive to the efficiency map of the motor and the battery model. The contours of a motor's efficiency map have significant leverage in determining a powertrain's losses as torque and speed combinations clustered in areas of high or low efficiency can greatly affect the overall vehicle's energy consumption. The battery model also can have a great deal of influence over the range. Though note that in this study, the battery model was based on data from the actual batteries used in the floats and the battery model agreed with the actual data to within 2%, thus its results can be assumed to reflect a high degree of accuracy.

This study showed that a float with an AC motor and regenerative braking will come close to achieving the target range of 105 km. It would therefore be advisable for the milk distributor to convert their floats to AC motors with regenerative braking, if the cost of this conversion across their entire fleet makes sense from an economic standpoint.

4.11 Summary of Level 3 Contributions

This section will enumerate each of eight novel component and capability modeling techniques of the Level 3 model, and provide a discussion as to how the technique was developed, i.e. what new knowledge was required to implement it into a working vehicle modeling program.

The first novel contribution made by the Level 3 model was that of the load transfer model. The dynamics governing load transfer in vehicles are well-understood, and a body of knowledge, replete with equations, exists to describe the phenomenon (refer to the derivation of Equations 4.22 to 4.30). However, existing energy flow vehicle modeling programs have not included the functionality to be able to account for load transfer [31]. Thus, integrating the existing knowledge on load transfer into a working energy flow vehicle model was a novel achievement. Novel work was also done to combine this existing derivation with Equations 4.36 and 4.37 to yield Equations 4.38 and 4.39 (which are also novel in that they account for inertia and indicate how much braking energy can be recaptured from each axle). Programming Equations 4.38 and 4.39 into an algorithm capable of functioning within OVEM was also a novel achievement as it had never been done before in an energy flow vehicle modeling program [26] [40].

The second novel contribution was an improvement upon an oversimplified modeling technique used previously in backwards-forwards vehicle models when calculating the final speed achieved by the vehicle at the end of each time step [26] [40]. Calculating the final speed achieved by the vehicle requires solving a complex quadratic based on the classical dynamics describing the vehicle's motion (refer to Section 2.1 to see the original derivation of the classical mechanics determining the vehicle's motion). Existing programs avoided this complex quadratic by making the simplifying assumption that the difference between the speed at the end of the current time step and the previous time step was effectively negligible. To better align OVEM with its accuracy criteria, the author instead performed a novel derivation that solved the complex quadratic – refer to Equations 4.10 and 4.20 to see this novel derivation. Novel work was also performed in developing the computational algorithms required to program this derivation into OVEM.

The third novel contribution made by the Level 3 model concerns its gearbox model (Sections 4.3.1 and 4.3.2). Existing backwards-forwards vehicle modeling programs included gearbox models; however, these models assumed that the efficiency of a gearbox at a given gear ratio was constant [31]. This assumption disregards the fact that the empirical evidence shows that the efficiency of gearboxes actually varies as a function of its design (gear ratio and seal, bearing, and meshing properties) and the load it is transmitting. OVEM accounted for this varying efficiency by leveraging existing empirical work in the area of gearbox efficiency [44] [57]. The novel work in OVEM's case came in creating Equations 4.40 and 4.41 based on an understanding of the factors affecting gearbox efficiency as expressed in the existing empirical work.

The fourth novel contribution made by the Level 3 model concerns its epicyclic gear train model. Existing backwards vehicle modeling programs included gearbox models; however these models assumed that the efficiency of the gear train was constant. This assumption disregards the empirical work on the topic which shows that the efficiency of epicyclic gear trains actually varies as a function of its design, the sizing of the components attached to it, and the load it is transmitting. Based on a survey of the empirical work done on the efficiency of epicyclic gear trains, it was determined that their efficiency could be expressed as a function of the ratio between the torque demanded of the EGT by the drive axle relative to the torque rating of either the ICE or electric motor (whichever is higher) attached to the epicyclic gear train. The author performed novel derivations (refer to Figure 4.39) based on this existing empirical work to build an epicyclic gear train efficiency model that could be programmed into OVEM (for more information on the EGT model refer to Section 4.8).

The fifth novel contribution came from the Level 3 ultracapacitor model. Existing empirical and theoretical work on ultracapacitor modeling served as the foundation for the ultracapacitor model in OVEM. For example, the models in Figure 4.12 and Figure 4.14 were used to initially frame the structure of the ultracapacitor model. A truncated version of these existing models were integrated into OVEM (refer to Figure 4.18), such that the model would meet OVEM's computational and experimental complexity criteria [47]. The novel work came in combining this truncated model with the relationship described in Figure 4.20 and Figure 4.21, which models how the capacitance of an ultracapacitor varies with its state of charge. This is a phenomenon which had heretofore not been included in existing ultracapacitor models in energy flow vehicle modeling, so developing the equations to merge the model in Figure 4.18 with the relationships in Figure 4.20 and Figure 4.21, and then translating those equations into a programmable code for an energy flow vehicle modeling program was novel. Refer to Section 4.6.1 for more information on the ultracapacitor model.

The sixth novel contribution of the Level 3 program comes from the battery model. With the battery model, an existing modeling technique (shown in the derivation of Equations 4.64 through 4.69) served as the foundation for the model integrated into OVEM. The novel work consisted firstly of converting these equations into programmable code capable of functioning within OVEM. The novel work also consisted of characterizing an array of battery technologies for use in this model (e.g. the characterized battery chemistries of Figure 4.28 and Figure 4.29). Refer to Section 4.6.2 for more information on the battery model.

The seventh novel contribution of the Level 3 model comes from its high-speed flywheel model. High-speed flywheels are a nascent technology that have not been included in any existing energy flow vehicle models [26] [40]. Flywheel models that do exist are often characterized by simplifying assumptions regarding their loss mechanisms. They either assume that the losses are a fixed percentage of the power transmitted by the flywheel or they have not accounted for the unique loss mechanisms faced by high-speed flywheels. The author determined the data that would be necessary to model the losses from a high-speed flywheel, and then collaborated with a high-speed flywheel manufacturer to collect this data. Using this data as the basis for the model, the author then performed the novel work of building a high-speed flywheel efficiency model in OVEM. There was no existing basis for creating a high-speed flywheel model, so all of the author's work in this area (deriving the necessary equations and modeling principles and then programming the model) was novel. The author also ascertained from the literature that flywheels could be integrated into a powertrain either mechanically or electrically. Yet, there were no practical examples of computer models dealing with high-speed flywheel vehicle integration to leverage, so the author undertook the novel task of deriving the algorithms to model both mechanical and electrical integration of high-speed flywheel. For more information on how this was done for the high-speed flywheel model, refer to Section 4.6.3.

The eighth novel achievement of the Level 3 model comes from work done on to fuel cell sizing and efficiency curves (refer to Sections 4.7.2 and 5.2.2 for more information). A survey conducted by the author of a broad array of commercially available fuel cells enabled the author to derive an empirical equation describing the relationship between fuel cell power rating and mass (Figure 5.4). It also allowed the author to make the observation that the power-current and efficiency-current curves describing fuel cell behavior had similar shapes and values across a range of fuel cell sizes when these curves were normalized by the maximum power and current ratings of the fuel cell (Figure 5.2 and Figure 5.3). Both of these observations were novel, and they enabled the fuel cell model in OVEM to be constructed in such a way as to allow for the continuous scaling of fuel cell sizing (within realistically defined bounds) rather than relying on the discrete sizes of a few limited products [40]. This made OVEM a more useful component sizing tool - the effects of which can be seen in the case study of Chapter 5.

5 Case Study 1: A Comparison of High-Speed Flywheels, Batteries, and Ultracapacitors as the Energy Storage System in a Fuel Cell Series Hybrid Electric Vehicle

Batteries are currently the most common form of energy storage aboard commercially available EVs and HEVs [145]. However, they have limitations, such as cost, cycle life, and low energy and power density. High-speed flywheels are an emerging technology that has the potential to address several of the shortcomings of the more traditional forms of energy storage – batteries, and to an extent, ultracapacitors. This chapter presents a study that looked at high-speed flywheels as a potential energy storage system onboard a fuel cell based series HEV, and compared their performance to batteries and ultracapacitors on the bases of cost and fuel economy.

This chapter and the next chapter are based on original journal-published articles by the author that have been included in this dissertation because they illustrate just some of the types of issues OVEM can be used to address. This particular chapter especially highlights two of the unique capabilities of OVEM's Level 3 models. First, it demonstrates OVEM's ability to conduct component-level studies by rapidly comparing cutting-edge energy storage system technologies on the metrics of fuel economy and cost. Second, it shows how OVEM can use flexible and scalable models (particularly for the ESSs and fuel cell) based on readily available data that can produce accurate results without extensive experimental and computational resources. This chapter is based on an article originally published by the author in the *Journal of Power Sources* [35].

5.1 Introduction

Amidst growing concerns over energy security, climate change, air pollution, and fossil fuel reserves, alternatives to conventional automobile powertrains based on internal combustion engines (ICEs) are being investigated [12] [146]. Powertrains based on fuel cells are one such alternative that have the potential to overcome many of the problems endemic to ICEs [12]. Fuel cells typically have a higher tank-to-wheel efficiency than ICEs, and depending on how the hydrogen fuel is generated they have the potential to emit significantly fewer pollutants [146]. However, it should be noted that issues related to fuel cell operation, cost, manufacturing, and refueling infrastructure are all responsible for their current lack of widespread adoption (though a thorough examination of these issues is beyond the scope of this study) [23].

Hybridizing a fuel cell with an ESS can have several positive impacts [141]. The ESS can be designed to meet the transient power demands of normal driving conditions. With the ESS handling the transient loads, the fuel cell only has to provide the average power demands [16]. This enables the fuel cell to be downsized which reduces costs and typically improves efficiency [147]. The ESS provides the additional benefit of being able to store energy captured through regenerative braking [16].

Most of the work done in designing and optimizing series HEVs has only considered batteries and/or ultracapacitors as the ESS [16] [80] [81] [82] [137]. While previous research has produced a great deal of information about optimal ESS technologies and configurations, it has largely neglected high-speed flywheels as an ESS technology that could compete with ultracapacitors and batteries.

Flywheels are a mature energy storage technology, but in the past, weight and volume considerations have limited their application as vehicular ESSs [113]. The energy, *E*, stored in a flywheel is expressed by Equation 4.70 where it can be seen that the energy stored in a flywheel can be increased either by increasing its inertia or speed. In stationary applications, where the mass and size of a flywheel is typically not a primary concern, the energy storage capacity of a flywheel is usually increased by simply adding to its inertia. However, in mobile applications, where the mass and size of a flywheel is of critical importance, increasing the speed of a flywheel is the most effective method for improving its energy storage capacity. Improvements in low friction bearings and high tensile strength and low density materials have now made high speeds attainable hence making lightweight high-speed flywheels a reality [148]. For instance, the high-speed flywheel used in this study weighs 15 kg, has a maximum speed of 60,000 rpm, and is capable of storing 540 kJ. The Ragone plot in Figure 5.1 shows that the specific energy and power properties of high-speed flywheels should make them competitive with existing ESS technologies [96] [149] [150].

High-speed flywheels also have several unique charging properties. Flywheels, as well as ultracapacitors, have the benefit over batteries of a high cycle life over which they experience little degradation in their efficiency [151]. Due to their high specific power, flywheels, along with ultracapacitors, can recharge much quicker than batteries. The most crucial performance drawback of high-speed flywheels is that they experience relatively high internal losses which cause them to self-discharge rapidly compared to batteries and ultracapacitors [152] [153]. For instance, the high-speed flywheel used in this study will go from fully charged to fully discharged in around fifteen minutes with no external power draws. The two primary sources of losses in high-speed flywheels are bearing and windage losses [113] [154]. Windage losses can be significant given the high rotating speeds of these flywheels. High-speed flywheels can avoid windage losses by operating in an evacuated environment. The high-speed flywheel in this study operates in a near vacuum to reduce the windage losses. This also helps preserve the structural integrity of flywheel due to heating of the rotor from the windage forces [117]. The bearing losses can be addressed through the use of more efficient bearings – magnetic or ceramic bearings depending on the speed range [113]. Advanced magnetic and ceramic bearings cost significantly more than more conventional bearings [154]. Since the high-speed flywheel in this study was designed for mainstream adoption, it uses more conventional rolling-element bearings in order to lower its cost which has the consequence of increasing its internal losses.

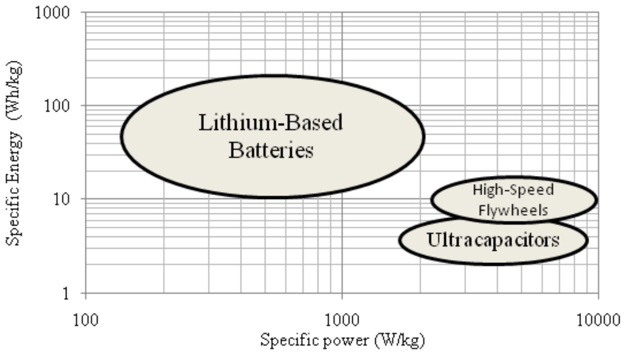

Figure 5.1: Ragone plot of the different ESS technologies considered in this study

Prior studies have examined the modeling and implementation of flywheel systems in vehicles [113] [114] [115]. However, previous research has not provided a direct comparison between high-speed flywheels, ultracapacitors, and batteries functioning as the ESS in an HEV. This study aims to make that comparison by using OVEM’s Level 3 model (Chapter 4). Simulations were run over a range of different ESS configurations utilizing different control strategies over two drive cycles. The performance of the three different technologies was then evaluated for their effect on fuel economy and cost. The reader should also note that though the HEV in this study uses a fuel cell, a fuel cell and an ICE function in largely the same way in producing power for a series HEV (when only high-level power flows are considered), so the results in this study could be expected to be largely applicable to a series HEV based on an ICE as well.

5.2 Vehicle and Component Models

This study used OVEM's Level 3 series HEV model [35] [36] [37] to model the fuel cell HEV with the three different types of ESSs.

5.2.1 Vehicle Simulator

Below is a brief discussion of the assumptions and parameters used in this study's series HEV simulations. For more information on the inner workings of OVEM's Level 3 series HEV model refer to Chapter 4.

Vehicle Blocks: The vehicle blocks require that the drag coefficient, frontal area, rolling resistance coefficient, tire radius, glider mass (curb weight excluding the mass of the ESS, fuel cell, and motor) be specified. In order to obtain these parameters, the author conducted a survey of popular mid-size sedans in the United States for which this data was provided by the manufacturers: 2008 Toyota Camry Solara, 2009 BMW 525, 2008 Mercedes C-Class, 2007 Nissan Altima, 2008 Mazda 6, and 2009 Volkswagen Passat. The average of each of the specifications was ultimately used in this investigation which resulted in the simulated vehicle having a drag coefficient of 0.29, a frontal area of 2.2 m^2, a tire radius of 25 cm, and a glider mass of 1250 kg. The coefficient of rolling resistance was set to 0.01, and the density of the ambient air was set to 1.2 kg/m^3 [12]. For more information on the vehicle blocks, refer to Section 4.1.

Wheel-Axle Blocks: The wheel-axle bearing losses were assumed to be fixed at 1% of the transmitted power, and that was held constant for all the ESS types [52]. For more information on the wheel-axle blocks, refer to Section 4.2.

Gearbox Blocks: The gear ratio in the gearbox block was set to 2. The dimensionless gearbox coefficients (refer to Equations 4.40 and 4.41) k_{seal}, k_{mesh}, and $k_{bearing}$ were set to 0.00103, 0.02, and 0.005, respectively [44]. For more information on the gearbox blocks, refer to Section 4.3.

Motor-Power Electronics Block: The motor-power electronics data used in this study was based on a commercially available permanent magnet topology [61]. For more information on the motor-power electronics blocks, refer to Section 4.4.

ESS Blocks: For information on the modeling behind the three different types of ESSs used in this study, refer to Section 4.6. For more specific information on the ESSs (high-speed flywheel, ultracapacitor, and battery) related to this particular study, refer ahead to Sections 5.2.3, 5.2.4, 5.2.5, respectively.

APU Block: For information on the fuel cell model specific to this study, refer ahead to Section 5.2.2. For more information on the general inner workings of the fuel cell model used in this study, refer to Section 4.7, particularly Section 4.7.2.

5.2.2 Fuel Cell Model

Since this study was only concerned with the overall electrical characteristics and fuel consumption of the fuel cell, the fuel cell model utilized the current-power (*I-P*) and efficiency curves published for fuel cells of different power ratings. A survey of published data for PEM fuel cells agreed with Bauman and Kazerani [137] which showed that it was reasonable to assume that the shape of the *I-P* and efficiency curves for cells of a range of power ratings were similar when the current and power axes were normalized by their maximum values, I_{max} and P_{max}. The *I-P* and efficiency curves used by the model were the average of the scaled curves from an array of commercially available fuel cells with different power ratings [138] [141] [155] [156] [157]. Figure 5.2 and Figure 5.3 show the data obtained from the fuel cells and the average curves used in the model for the *I-P* and efficiency curves, respectively.

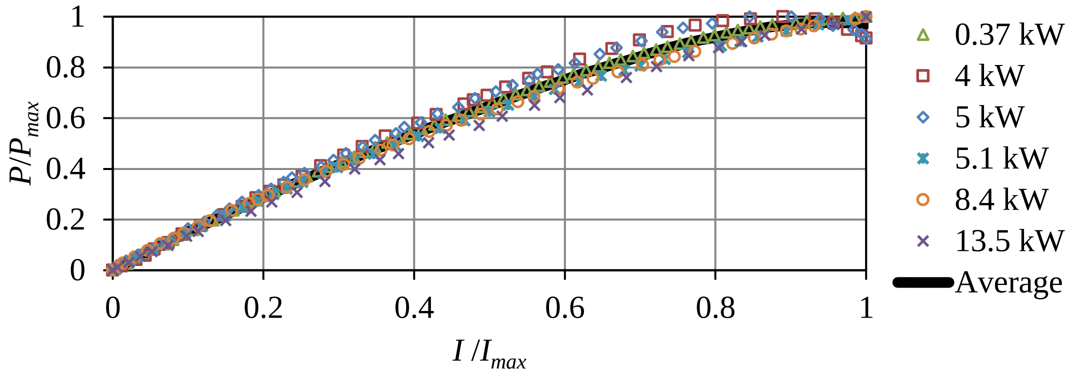

Figure 5.2: Normalized *I-P* curves for an array of commercially available fuel cells [141] [155] [138] [156] [157]

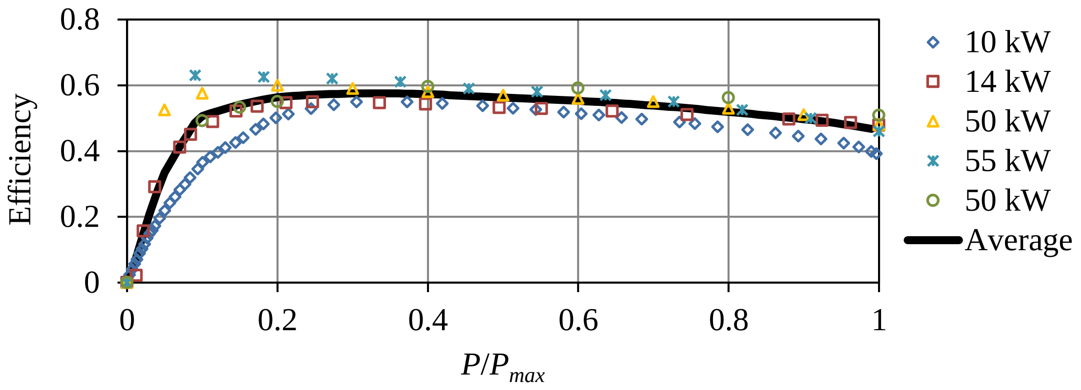

Figure 5.3: Normalized efficiency curves for an array of commercially available fuel cells [141] [138] [156] [157] [155]

The survey of commercially available fuel cells also revealed that the relationship between the mass and the power rating of a fuel cell could be reasonably represented by a power law relationship as seen in Figure 5.4. Thus, the fuel cell model only requires that the maximum power of the fuel cell be specified, and from that the fuel cell mass, *I-P* curve, and efficiency curve can all be determined. When the fuel cell model receives a power request, it determines the mass of the hydrogen that must be consumed in order for it to meet that power request based on the lower heating value of hydrogen, 120 MJ/kg. Fuel cell cost estimates are wide-ranging, as they involve approximations about the cost reductions that fuel cell manufacturing will experience with increased production. With high-volume production, [155], [158], and [159] estimate that PEM fuel cells will cost between \$200-\$400 per kilowatt. This was the cost range used in this study, making fuel cells the most expensive power source in the vehicle.

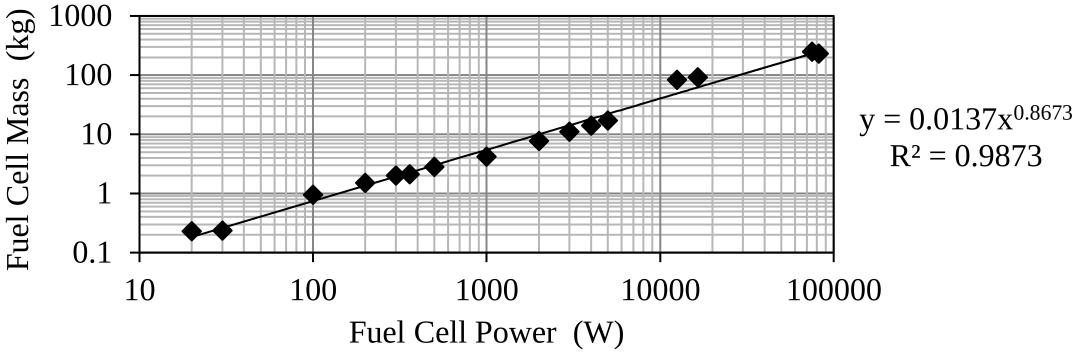

Figure 5.4: Relationship between the mass and maximum power of commercially available PEM fuel cells [138] [141] [155] [156] [157]

5.2.3 High-Speed Flywheel Model

The high-speed flywheel in this study was based on data for a 120 kW flywheel from Flybrid Systems [116]. For more information on the high-speed flywheel model refer to Section 4.6.3.

In this study, the high-speed flywheel was mechanically integrated instead of electrically integrated in order to take advantage of the higher system efficiency characteristic of a mechanical integration. Prior research has shown the efficiency of a continuously variable transmission (CVT) connected to a high-speed flywheel is approximately 85% regardless of the power passing through it [117]. Therefore in this study the CVT model was treated as having a fixed efficiency of 85%. The standard flywheel weighs 15 kg and through correspondence with a Flybrid representative, it was estimated that with high volume production a CVT for a 120 kW flywheel would weigh approximately 48 kg. According to Flybrid's cost estimates based on mainstream automotive market production volume, the high-speed flywheel should cost between $1000-$3000 and the CVT should cost no more than $1500 which brings the total high-speed flywheel system cost to between $2500-$4500 or $21-$38 per kilowatt. Proper packaging for high-speed flywheels is also critically important so that the device is contained in the event of a rupture. In this study, the containment packaging was set at 15 kg [117].

Since this study was comparing ultracapacitor and battery arrays of varying sizes, it also wanted to examine the effect of the three different flywheel sizes. Though the standard high-speed flywheel used in this study weighs 15 kg and stores 540 kJ, the flywheel size can be varied. Through personal correspondence with a Flybrid representative, it was determined that the mass of the flywheel can be decreased by 20%, however the mass of the flywheel cannot be increased because the 15 kg version is the largest that the bearings in this study could handle. If more energy storage is required from the flywheel, then multiple flywheels must be used. If multiple flywheels are used together, the mass, energy storage, cost, and losses are increased by a factor equal to how many flywheels are connected together and added to the fixed cost and mass of the ancillary flywheel equipment. If the mass of the flywheel is reduced by 20%, the cost and mass scale linearly yet the power losses remain the same because the same bearings are used as in the standard flywheel [117].

5.2.4 Ultracapacitor Model

The ultracapacitor model in this study is based on a 350 F ultracapacitor [96]. For more information on the ultracapacitor model refer to Section 4.6.1. The literature quotes ultracapacitors as costing between $0.01-$0.015 per Farad in high-volume production [160]. This puts the cost between $3.50-$14 per cell and between $13-$51 per kilowatt.

5.2.5 Battery Model

The battery model in this study is based on a commercially available lithium-ion cell marketed for use in vehicles [110]. Lithium-ion batteries were used in this study because their specific energy and power ratings are amongst the highest of all battery technologies [161]. For more information on the battery model refer to Section 4.6.2. The battery manufacturer has published a cost of $110 per 6 cells. It has also been reported that through higher volume production the cost could be reduced to $100 per 6 cells [137]. Using this cost range, each cell costs between $17-$18. With a continuous current limit of 70 A, the 3.3 V cells cost between $72 -$79 per kilowatt.

5.2.6 Drive Cycles

The fuel economy of a vehicle is affected to a large degree by the drive cycle over which it is tested. So in order to more completely characterize a given powertrain, it must be examined over different drive cycles. In this study, the vehicle was tested over 12 iterations (82.1 miles) of the New European Drive Cycle (NEDC), seen in Figure 2.6, and 4 iterations (83.5 miles) of the Artemis Combined Drive Cycle (ACDC), seen in Figure 2.8. The NEDC was chosen because it is the basis for emissions testing in Europe. The ACDC was chosen because it is a more aggressive drive cycle with both a demanding urban and highway component that is more representative of real world driving [162]. The ACDC was constructed by placing the motorway Artemis drive cycle immediately following the urban Artemis drive cycle.

5.3 Energy Management Strategies

The energy management strategy selected for an HEV can have a dramatic impact on its performance [141]. Previous studies have examined optimal strategies for fuel cell series HEVs that do not know the drive cycle in advance [15] [141]. Those studies form the basis for the energy management strategy used for the battery and ultracapacitor. However due to the lack of literature on energy management strategies for mechanically integrated high-speed flywheels, one was devised by the author for this study. For more information on energy management strategies in OVEM refer to Section 4.7.

5.3.1 High-Speed Flywheel

The purpose of the high-speed flywheel acting as an ESS is to store energy captured through regenerative braking and release that energy during acceleration. In this study, the high-speed flywheel only charges through regenerative braking. It would be possible for the high-speed flywheel to receive excess power generated by the fuel cell so that it could recharge in the absence of a braking event to prepare for a future acceleration. However, this pathway is inefficient, and charging the high-speed flywheel exclusively through braking was shown in the initial work of this investigation to be a more efficient control strategy. Thus, it was the strategy employed in this study.

During a motoring event (acceleration or constant speed driving), the controller first requests the power from the high-speed flywheel and the high-speed flywheel supplies as much power as it can in an effort to meet that request. If the high-speed flywheel is unable to fully meet that request on its own, then the controller turns to the fuel cell to provide the remaining power. Once the high-speed flywheel is fully discharged, the fuel cell must meet all of the power requests until the flywheel's SOC increases via energy captured through regenerative braking.

5.3.2 Ultracapacitor and Battery

Like the high-speed flywheel, the ultracapacitor and battery modules receive energy from regenerative braking and provide energy during acceleration and constant speed motoring. Yet unlike the high-speed flywheel, they are able to receive power from the fuel cell with lower losses. Hence the efficiency of the powertrain can be improved by recharging the ultracapacitors and batteries with excess power generated by the fuel cell.

In this study, the batteries and ultracapacitors used a speed-based energy management strategy. For more information on this type of strategy refer to Section 4.9.2. In this study, the highest fuel economy was consistently achieved when v_{max} in Equation 4.73 was set to 80 km/h. Therefore, 80 km/h was the v_{max} used throughout the simulations. When the fuel cell was called upon to recharge the ESS, it did so at its point of optimal efficiency which was at 31% of the rated power as seen in Figure 5.3.

5.4 Simulation Results and Discussion

The results of this study can be classified into two areas. The primary focus was to compare the high-speed flywheel, ultracapacitor, and battery functioning as the ESS in a fuel cell HEV, and that comparison is presented in Section 5.4.2. Another ancillary, but important result that affects the overall performance, fuel consumption, and cost of the powertrain was the sizing of the fuel cell required in order for the vehicle to meet the drive cycle given its ESS, and those results are presented in Section 5.4.1.

5.4.1 Fuel Cell Sizing

As the most expensive power source in the powertrain, the power rating of the fuel cell was kept as low as possible to minimize overall powertrain costs. In this study, the goal was to keep the agreement between the velocity requested by the drive cycle and the velocity achieved by the vehicle to be within 2% and to never exceed 3 km/h. Given that constraint, the fuel cell size varied between 29-45 kW for the range of ESS technologies and sizes.

5.4.2 Flywheel, Ultracapacitor, Battery Comparison

The cost of the batteries and ultracapacitors is directly proportional to their number and mass. As an additional cell is added to the array, the cost and mass of the array both increase by the amount of that one cell. The flywheel was examined at its standard specifications (15 kg and 540 kJ), with a 20% reduction in energy storage and mass, and with two and three standard flywheels connected together.

Figure 5.5 and Figure 5.6 plot the fuel economy of the vehicle (measured in kilometers per kilogram of hydrogen gas consumed) against the cost of the ESS (in US Dollars) for the three different ESS technologies. Figure 5.7 and Figure 5.8 plot the fuel economy of the vehicle against the total power source cost (ESS and fuel cell). The ideal ESS would be as close to the top left corner of Figure 5.5 through Figure 5.8 as possible as this would represent an ESS that minimizes costs and maximizes fuel economy.

On the NEDC, the fuel economy of the most fuel efficient high-speed flywheel (standard size) was 4% and 6% lower than the most fuel efficient ultracapacitor and battery arrays respectively. Yet, the most fuel efficient high-speed flywheel costs between 14% to 57% less than the most fuel efficient battery array, and is potentially 2.8 times less expensive than the most fuel efficient ultracapacitor array. Battery arrays costing approximately the same as the most efficient flywheel achieve around 3-4% higher fuel economy. Ultracapacitor arrays costing approximately the same as the most fuel efficient flywheel achieve between 3% higher to 7% lower fuel economy. These results show that though high-speed flywheels may not produce the best fuel economy of the technologies simulated, their fuel economy is within a few percentage points of the best performers, and the flywheels have the potential to be less expensive.

Recall that the error bars in Figure 5.5 through Figure 5.8 come from the cost ranges that were explained for the high-speed flywheels, ultracapacitors, and batteries in Sections 5.2.3, 5.2.4, and 5.2.5, respectively. Recall also that the multiple data points in Figure 5.5 through Figure 5.8 come from differently sized energy storage systems for each of the three technologies as was explained for the high-speed flywheels, ultracapacitors, and batteries in Sections 5.2.3, 5.2.4, and 5.2.5, respectively.

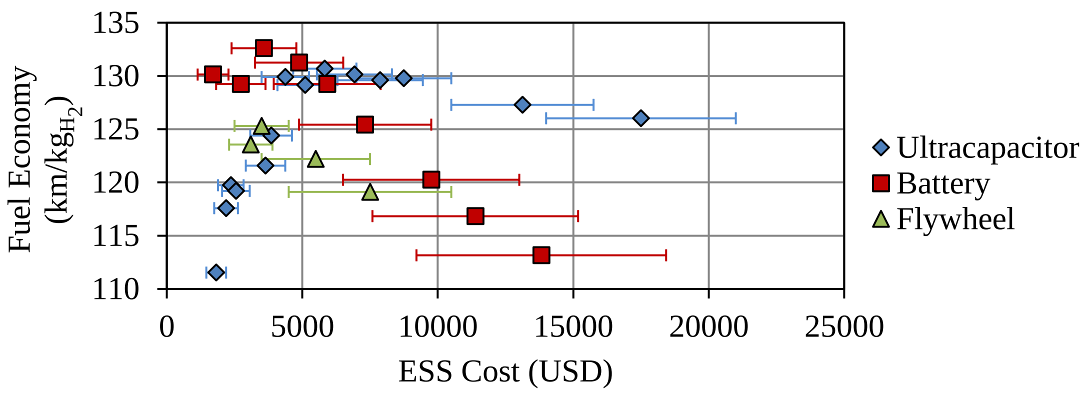

Figure 5.5: Fuel economy as a function of ESS cost on the NEDC

On the ACDC, the most fuel efficient flywheel configuration occurs when two flywheels are used. The most fuel efficient battery array achieves 3% higher fuel economy than the most fuel efficient flywheel and roughly 4% higher fuel economy than the standard flywheel. Yet the two flywheel configuration costs between 1.4 to 3.4 times less, and the standard flywheel costs between 2.4 to 4.7 times less than the most fuel efficient battery array. The most fuel efficient flywheel costs approximately the same as similarly fuel efficient battery arrays. Every flywheel configuration achieved a higher fuel economy than the most fuel efficient ultracapacitor array on the ACDC, and the most efficient flywheel costs approximately the same as the most efficient ultracapacitor array. The results from the simulation run over the more aggressive ACDC show, even more than those from the NEDC, that high-speed flywheels can achieve a fuel economy within a few percentage points of the best performing battery and ultracapacitor arrays with the potential to be cheaper. This shows that high-speed flywheels deserve to be considered as viable options for ESSs aboard HEVs.

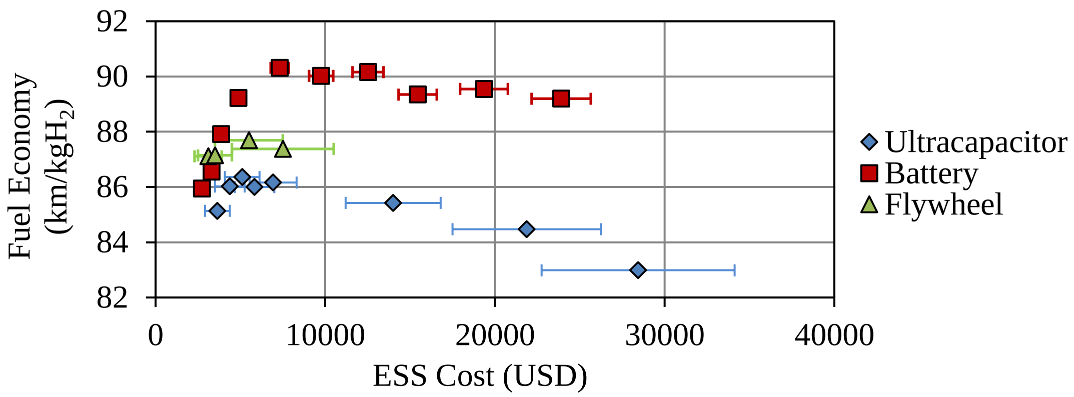

Figure 5.6: Fuel economy as a function of ESS cost on the ACDC

Once the cost of the fuel cell is accounted for, as seen in Figure 5.7 and Figure 5.8, the differences in the cost of the powertrains employing the different ESS technologies were significantly reduced. The small differences in cost between the different ESS technologies become overshadowed by the fuel cell costs. This is due to the high cost of the fuel cells (and the large uncertainty in their cost) relative to the cost of the ESS.

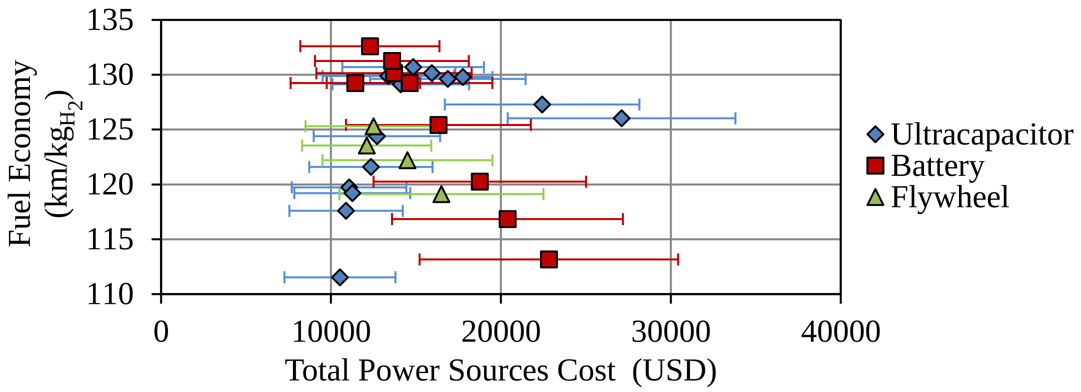

Figure 5.7: Fuel economy as a function of total power source (fuel cell + ESS) cost on the NEDC

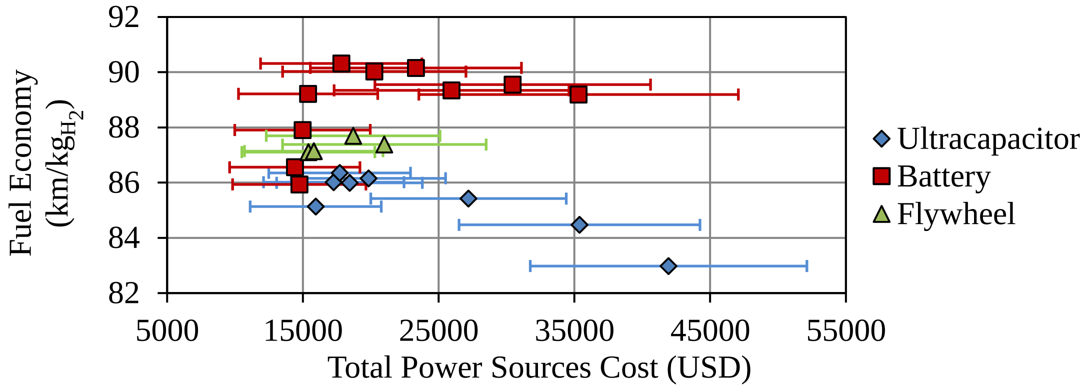

Figure 5.8: Fuel economy as a function of total power source (fuel cell + ESS) cost on the ACDC

5.5 Conclusion for Case Study 1

This chapter provides a comparison between high-speed flywheels (mechanically integrated via a CVT), ultracapacitors, and lithium-ion batteries serving as the ESS in a series HEV with a fuel cell. Powertrains utilizing three different ESS technologies were simulated using OVEM. The data used for the ESSs in the simulation all came from commercially available products. Each of the three technologies was simulated over a range of sizes. A particularly novel contribution here was in determining the sizing relationship between fuel cell mass and power rating.

The results from this study showed that a vehicle with a high-speed flywheel as an ESS never achieved the highest fuel economy of the three ESSs tested on either drive cycle.

Yet on the New European Drive Cycle, the fuel economy of the high-speed flywheel was only 4-6% lower than the most fuel efficient ultracapacitor and battery arrays respectively, and the high-speed flywheel had the potential to offer substantial cost savings. On the Artemis Combined Drive Cycle, the flywheel achieved a higher fuel economy than any of the ultracapacitor arrays simulated and achieved approximately the same fuel economy as similarly priced battery arrays. These results provide the novel insight that in future studies high-speed flywheels merit consideration as alternatives to ultracapacitors and batteries in series HEVs.

Future work could benefit from reducing the uncertainty in the costs of the fuel cells and energy storage system components. In this study, it was shown that once the cost of the fuel cells was accounted for along with the ESS cost, many of the comparatively small differences in ESS costs were eclipsed by the relatively large fuel cell costs. It should be mentioned that these costs do not reflect the lifetime costs of any of these ESS components. It is likely that ESS technologies with higher cycle lives (such as flywheels and ultracapacitors) will be less expensive over the course of the vehicle’s lifetime. Future research efforts should seek to better understand those life cycle costs.

6 Case Study 2: Modeling the Prospects of Plug-In Hybrid Electric Vehicles to Reduce CO_2 Emissions

PHEVs are commonly considered to be a temporary solution that can enable transport to move away from emissions intensive conventional ICE-based vehicles (CVs) until battery technology improves and costs decrease to such an extent that widespread EV adoption is possible. However, this chapter shows that plug-in hybrid electric vehicles – primarily because they don't require as heavy a battery pack as typical EVs and because they can decouple their APU from the road load – have the potential to enable greater tank-to-wheel CO_2 emissions reductions than both EVs and conventional ICE-based vehicles, depending on the nature of the vehicle and the processes used to produce its electrical energy.

This chapter illustrates how the Level 3 models can be used to provide accurate energy consumption comparisons across a range of powertrain topologies and technologies in order to examine the high-level impacts of PHEVs and EVs. These impacts can have important implications for policy decisions regarding the role PHEVs and EVs can play in the future of transport. This study makes use of OVEM's rapidity of implementation in comparing the energy consumption and CO_2 emissions from a range of technologies and topologies. It is based on an original article published by the author in the journal, *Applied Energy* [36]. Another original journal-published article (*Energy Policy*) by the author uses

OVEM to address a similar issue regarding the effective tank to wheel emissions from a range of electric vehicle of varying types relative to conventional ICE-based vehicles. It was not included in this dissertation due to page limit constraints, but can be viewed for further reference on the matter [36].

6.1 Introduction

Plug-in hybrid electric vehicles (PHEVs) have the potential to reduce petroleum use and CO_2 emissions in automobile transport by utilizing more efficient powertrains that obtain at least part of their energy from grid electricity [163]. The ability of PHEVs to attain CO_2 emissions reductions over conventional vehicles based on ICEs while overcoming the range limitations of many EVs has been well documented [164] [165]. However, PHEVs are not just simply a compromise between the low CO_2 emissions of EVs and the long range of conventional vehicles, confined to produce CO_2 emissions somewhere in between those of EVs and conventional vehicles. PHEVs have the potential to be lighter than EVs and operate their ICEs more efficiently than conventional vehicles. A PHEV with these traits has the potential to operate with fewer CO_2 emissions than both an EV and a conventional vehicle. This study models the CO_2 emissions from PHEVs and EVs, and compares them to those from conventional vehicles to gain a better understanding of the ability of PHEVs to lower CO_2 emissions in transport.

Approximately more than 94% of vehicles on the road in 2010 are conventional vehicles based on ICEs [166]. One of the greatest strengths of conventional vehicles is that their oil-based fuels enable them to achieve high performance over a long range [167]. Yet, the greenhouse emissions stemming from their low efficiency and reliance on oil has led to increasing concern over their negative environmental and economic impacts [2]. With the number of cars in the world projected to grow more than fourfold by 2050 to 3 billion, more efficient and less oil-dependent means of transportation are being increasingly investigated [4].

EV and HEVs represent one way to reduce automobile transport's CO_2 emissions and oil dependency [168] [169]. The powertrains of pure EVs are completely electric. EVs generally receive their power from the electric grid, and store that power in an energy storage system (ESS) onboard the vehicle. The energy storage system onboard EVs can take many forms, the most common of which is currently batteries [145]. EVs typically have a higher tank-to-wheel efficiency than conventional vehicles, and they produce no tailpipe emissions [145]. Yet their energy must still be generated in some way, which means that their CO_2 emissions are directly related to the CO_2 emissions of the power generation mix from which they derive their energy. The CO_2 emissions characteristics of a power generation mix can be expressed in a figure known as CO_2 intensity. CO_2 intensity is the average amount of CO_2 emitted per unit of electrical energy generated by all of the power production processes in a mix weighted by the amount of power obtained from each of those processes. Therefore, the CO_2 emissions from EVs and PHEVs can vary considerably depending on the CO_2 intensity of their grid-supplied electricity.

Hybrid electric vehicles come in many forms. They typically combine elements of both EVs and conventional vehicles, as they can be powered by energy stored onboard in a variety of forms such as chemically, electrically, and mechanically [12]. PHEVs are a specific type of HEV that use power obtained from the electric grid in conjunction with power obtained from an onboard alternative power unit (APU). The APU can take on many forms such as a fuel cell or an ICE combined with a generator. Since ICE technology and infrastructure are more developed, ICE-based alternative power units are more likely to find wider adoption than fuel cells in the near future, and in order to allow for a more direct comparison between conventional vehicles and PHEVs, the PHEVs in this study were simulated with an alternative power unit consisting of an ICE with a generator.

In series PHEVs (the type used in this study), an electric motor provides all of the tractive force, and they generally have two modes of operation: one when its ICE-based APU is on and another when it is off. When a PHEV's ICE is off, a PHEV operates in an electric-only mode, identical to an EV. In electric-only mode, the ESS is used exclusively to power the vehicle, and as the PHEV drives, its state of charge of its energy storage system declines. A common naming convention for PHEVs is based on how much distance they can cover in their electric-only mode. For instance, a PHEV-20 will be able to travel 20 km in its electric-only mode. Typically once the SOC of the ESS is drained to a certain level, the APU is called upon to provide power and the PHEV is now in charge sustaining mode. In charge sustaining mode, PHEVs operate more like a conventional hybrid electric vehicle, using a blend of power derived from both the APU and ESS. It is possible for the APU on a PHEV to be running and to still have the state of charge of the energy storage system decline, though this is more common of parallel HEV powertrains and is rarely seen in series PHEVs, such as those examined in this study. Since PHEVs obtain their power from two different pathways, their overall efficiency depends on the interplay between the ESS and APU and the vehicle's operating characteristics in electric-only and charge sustaining modes.

While battery technology is constantly improving, the batteries used in EV applications are generally the heaviest single component in the powertrain [12]. For example in the case of the Tesla Roadster, the battery pack accounts for over a third of the weight of the vehicle [170]. A PHEV can have a significantly lower battery mass than an EV since its battery only needs to provide energy for the electric-only mode which is usually only a fraction of the vehicle's total range. Once the vehicle has exceeded its electric-only range, charge sustaining mode takes over, and the alternative power unit handles the energy requirements of the vehicle. Since PHEVs can have a lower battery mass than EVs, the curb mass of PHEVs can also be lower, which can enable them to operate more efficiently in electric-only mode than a similar EV.

Once a PHEV's APU has switched on in charge sustaining mode, PHEVs can generally operate more efficiently than conventional vehicles especially during urban driving. This is made possible by the fact that PHEVs' electric motors are typically more efficient at providing tractive power and enable the vehicle to recapture energy through braking. Also, in a PHEV when the ICE functions as an APU, it generally does not have to be directly coupled to the road load [12]. Without having to respond to the transients of normal driving, the ICE in a PHEV can be run continuously in its most efficient operating range to achieve a lower fuel consumption than could be achieved in a conventional vehicle [12]. However, there may be circumstances when the fuel economy of conventional vehicles could approach or exceed that of PHEVs such as during highway driving when a vehicle's speed is relatively constant. Depending on a vehicle's topology and energy management strategy, the power generated by the ICE onboard a PHEV may experience additional losses as it moves through the other components providing the tractive force, such as the electric motor, power electronics, and ESS. Therefore, though PHEVs generally have a higher tank-to-wheel efficiency in charge sustaining mode than conventional vehicles – that may not be true in all cases.

PHEVs have at least a theoretical justification for why they should be able to achieve lower CO_2 emissions than both EVs and conventional vehicles. The actual CO_2 emissions performance of a PHEV depends on many factors: its range in electric-only mode, its efficiency in electric-only and charge sustaining modes, and the CO_2 intensity of the power generation mix used to power the PHEV from the grid. This study uses OVEM's Level 3 models to simulate EV and PHEV operation to better understand the CO_2 emissions from PHEVs in order to examine the conditions under which PHEVs may achieve lower CO_2

emissions than EVs and conventional vehicles. It should also be made clear that the aim of this study is only to make reasonably accurate predictions (to within approximately 2-5%) about the relationship between CO_2 emissions stemming from conventional vehicles, EVs, and PHEVs given different power generation mixes. There are inherently many uncertainties in such a study, and as such its results are not meant to be interpreted as precise predictions about the relationship between every conventional vehicle, EV, and PHEV. Rather, this study provides an illustration of how that relationship could reasonably be expected to unfold.

6.2 Methods

The goal of this study is to compare the CO_2 emissions from vehicles with three different types of powertrains (conventional vehicles, EVs, and PHEVs) as the CO_2 intensity of their power generation mix varies. In order to do this, a standard vehicle platform was needed to ensure an equitable comparison between the different powertrains. It was decided that the vehicle serving as the platform in this study should be representative of a widely used automobile. The 2010 Ford Focus was selected to be the platform for the three different powertrain types because it is a high-selling midsize car in many markets around the world [171]. The conventional, ICE-based version of the Focus comes with manufacturer published figures for its CO_2 emissions. Since EV and PHEV versions of the Focus do not currently exist, the shape and mass specifications for EV and PHEV versions of the Focus were either approximated or obtained from the conventional version. This process is explained further in Section 6.2.2. The emissions performance of the EV and PHEVs was estimated by OVEM as explained in Section 6.2.1.

6.2.1 Vehicle Modeling

In order to arrive at the energy consumption and CO_2 emissions estimates for the EV and PHEVs, OVEM's Level 3 models were used [35] [36] [37]. OVEM was first used on both the simulated EV and PHEVs to determine the size of the battery pack required for them to achieve the target range. In the case of the EV, the only other figure required from the simulation was an estimate of the energy consumption of the vehicle expressed as the amount of energy consumed per unit distance traveled. In order to obtain CO_2 emissions estimates for the PHEVs, OVEM needed to provide figures for the energy consumption of the PHEV in both electric-only and charge sustaining modes. For more information on OVEM's Level 3 simulations refer to Chapter 4.

6.2.1.1 EV and PHEV Model

Below is an account of the assumptions and parameters used in the study for the electric and plug-in hybrid electric vehicle models.

Vehicle Blocks: For more information on the vehicle blocks, refer to Section 4.1. Section 6.2.2 contains more information on the parameters used by the vehicle block in this specific study.

Wheel-Axle Blocks: The wheel-axle losses were assumed to be fixed at 1% for all the simulated EVs and PHEVs [52]. For more information on the wheel-axle block refer to Section 4.2.

Gearbox Blocks: For both the EV and PHEVs, the gear ratio was set to 2 because that was the lowest, and hence lightest, fixed gearing that allowed the powertrain to achieve the requested drive cycle. The dimensionless gearbox coefficients k_{seal}, k_{mesh}, and $k_{bearing}$ were set to 0.00103, 0.02, and 0.005, respectively [44]. For more information on the Level 3 gearbox block, refer to Section 4.3.

Motor-Power Electronics Blocks: The motor used in this study was based on a commercially-available permanent magnet topology [61]. For more information on the motor-power electronics block, refer to Section 4.4. Section 6.2.2 contains more information on the motor parameters that were specific to this study.

Battery Block: The battery model in this study is based on a commercially available lithium-based cell marketed for use in vehicles [110] [172]. Lithium-based batteries were used in this study because their specific energy and power ratings are the highest of all battery technologies [161] [173]. The cells in this study have a specific energy of 390 kJ/kg and a specific power of 3.3 kW/kg. The simulation accounted for the energy losses incurred when charging the battery from the grid. The simulations showed that recharging the battery pack of the EV and PHEVs at a constant rate of 6 kW (such that the EV's pack would fully charge in approximately 6 hours) yielded a median efficiency of 94%. This efficiency figure agreed with published estimates on the typical efficiency of lithium-based batteries at low charge rates [12], and it was factored into the energy use calculations for the EVs. For more information on the inner workings of OVEM's battery model refer to 4.6.2.

ICE Block: In this study, the APU consisted of an ICE combined with a generator. When the SOC of the battery went below its lower limit (20% SOC), the ICE was called upon to provide extra power to recharge the battery. Once the battery recharged to a certain point (80% SOC), the ICE switched off and was no longer called upon to produce extra power to recharge the battery until the battery once again went below its lower limit. The lower and upper limits of the battery's SOC were set to 20% and 80% respectively because that is the range over which many batteries in HEV and EV applications are operated to prolong their cycle life [174].

A spark ignition ICE running on gasoline was used in the APU in this study because the PHEVs that are slated to be mass produced within the next several years have been announced to be spark ignition [31]. The advantage of having an ICE serve as an APU, rather than being coupled to the road load as in a conventional vehicle, is that the ICE can be downsized and operated more efficiently. Since it does not have to track transient spikes in the road load, it can have a lower power rating and spend more time operating in its most efficient range. For more information on the APU in a PHEV refer to Section 4.9.3 and refer to Section 4.7.1 in particular for more information on the ICE-based APU model.

Below is an account of the assumptions and parameters implemented to the ICE-based APU model for this study. In the case when the APU was called upon to recharge the battery, it was requested to produce power at its most efficient operating point which occurred at about 60% of its maximum power. The APU model steps through the possible torque and speed combinations whose product would meet the power request in increments of 10 rad/s. The efficiency of the generator and ICE when operating at each of those torque and speed combinations was determined from the efficiency maps seen in Figure 6.1 and Figure 6.2, respectively. In this study, it was assumed that the APU responded instantaneously to a power request, which is of course not entirely physically accurate. However, as the validation in Section 6.3 shows it was a reasonable approximation, which in the absence of concrete data on the APU's response time, produced results that were sufficiently accurate for this study.

The power rating and mass of both the ICE and generator were linearly scaled down as far as possible while still enabling the vehicle to successfully complete the drive cycle, such that the velocity achieved was within 0.2% of the velocity requested. This was done to minimize the mass of the APU. Note too that the power rating of the APU for each PHEV was always high enough so that the APU could sustain the vehicle traveling indefinitely at the maximum speed of the NEDC with no assistance from power stored in the ESS. The power rating of the APU was adjusted by scaling the torque and speed axes on the ICE's and generator's efficiency maps along with the mass of the ICE and generator by a scalar percentage – chosen through an iterative approach such that the resized map allowed the vehicle to achieve the highest efficiency. The validation in Section 6.3 showed that this approach produced reasonably accurate results (within 5%) for the purposes of this study.

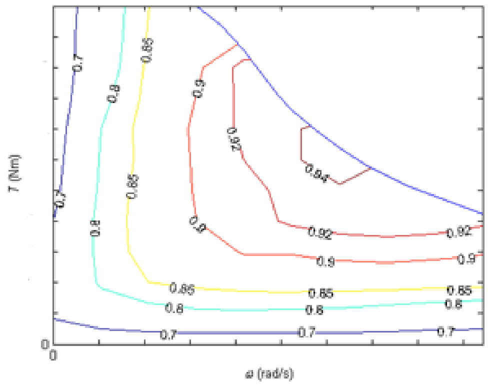

Figure 6.1: Efficiency map of the generator in the APU, note that the torque and speed axes are normalized by their maximum values so they can be rescaled to suit the specifications of the simulation

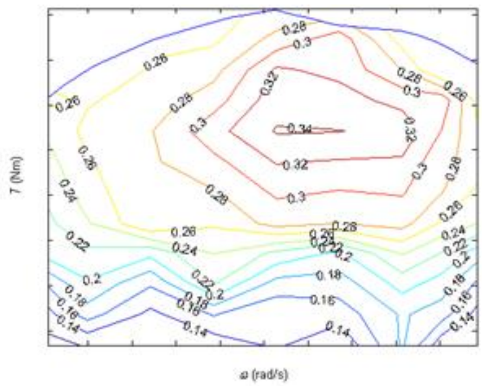

Figure 6.2: Efficiency map of the ICE in the APU, note that the torque and speed axes are normalized by their maximum values so they can be rescaled to suit the specifications of the simulation

6.2.2 Converting the Conventional Vehicle to an EV and PHEV

The 2010 Ford Focus is manufactured as a conventional, ICE-based vehicle. There are 13 different versions of the 2010 3-door Focus in the UK market each with their own engine, transmission, curb mass, and CO_2 emissions. Of all the versions of the Focus in its model line, the version with the lowest emissions was the 2010 Focus 3-door 1.6 TDCi ECOnetic, producing 114 gCO_2/km [31]. Though this vehicle uses diesel fuel, since this study wanted to look at the best performers for each powertrain, this was the emissions value used for the conventional vehicle. It should be noted that the CO_2 emissions figures published by the manufacturer are derived from running the vehicle over the New European Drive Cycle (NEDC).

In order to convert a conventional Focus to an EV or PHEV, it first had to be stripped down to its glider mass. The glider mass is the curb mass of the conventional vehicle minus the mass of any components that are not needed for the conventional vehicle to function as an EV or PHEV. The ICE was the first component removed from each of the 13 conventional vehicles in the Focus model line. The mass of the ICE was approximated by assuming its specific power was 400 W/kg which was based on the median value from a range reported in [26]. The mass of the multi-gear transmission of each ICE was estimated based on the empirical equation from Lechner and Naunheimer [175]

$$m_{transmission} = 0.49(i_G T_{rated})^{0.58} z^{0.29} \tag{6.1}$$

where $m_{transmission}$ is the mass of the transmission in kilograms, i_G is the gear ratio of the highest gear, T_{rated} is the rated torque of the ICE, and z is the number of speeds in the transmission. Note that Equation 6.1 is a best-fit regression based on empirical observations. It is not derived from first principles. Thus, the dimensionality of the equation is handled by the units embedded in the coefficient of 0.49. The term i_G is dimensionless as it is the gear ratio of the highest gear. The term z is dimensionless as it is the number of speeds in the transmission. The term T_{rated} has units of Nm; however that term is raised to a power of 0.58. The units of the term $m_{transmission}$ are kg. Thus the units of the coefficient, 0.49, are kg/Nm$^{0.58}$. Note that this relationship was needed because information on the mass of a commercially available vehicle's transmission is rarely readily available whereas the parameters on the right hand side of Equation 6.1 generally are readily available. Also note that an additional 20 kg was removed to account for the mass of any ancillary components in the conventional versions that were not required in the electric of plug-in hybrid electric vehicles.

Since this study compares the best performers across conventional, EV, and PHEV powertrains, the glider mass that was used as the basis for the EV and PHEVs came from the vehicle in the 2010 3-door Focus model line with the lightest glider mass, the 2.5 Duratec ST with a glider mass of 913 kg. For both the EV and PHEVs, the traction motor that was added had a mass of 102 kg (including the mass of its power electronics) [61]. A battery pack was added to the EV, and the pack was sized such that the EV would be able to achieve a range of 300 km on the NEDC. The fixed ratio gearbox added back to the EV and PHEV had a mass of 19 kg.

Four different PHEV powertrains were examined in this study, each with a different electric-only range. The battery packs of the four different PHEVs were sized so as to allow for different electric-only ranges of 20, 40, 60, and 80 km. The PHEVs also had the additional mass of their alternative power unit, consisting of a generator and an ICE. The ICE used in the APU was based on a 1 L 41 kW GM engine with a mass of 100 kg, and the generator was based on a permanent magnet topology [31] [61]. The mass and rated power of the APU was scaled down by the same constant factor, so that the power rating was as low as possible while still enabling the vehicle to successfully complete its drive cycles. The power rating was also always made high enough to enable the PHEVs to cruise indefinitely at a constant speed equal to the maximum speed of the NEDC (120 km/h). Table 6.1 shows the mass parameters for the conventional vehicle, EV, and PHEVs used in this study. Note that the mass of the battery pack in the PHEVs increases in order to extend the range achievable in electric-only mode. The mass of the APU also increases as the electric-only range increases though not as much as the mass of the battery pack. This illustrates that since the APU is not directly coupled to the road, it does not have to increase in size as much to power the heavier cars.

Table 6.1: Specifications for the vehicles used in this study

Powertrain Type	Battery Pack Mass (kg)	APU Mass (kg)	Curb Mass (kg)
CV	--	--	1340
EV	340	--	1380
PHEV-20	30	104	1168
PHEV-40	50	107	1191
PHEV-60	80	110	1224
PHEV-80	110	113	1257

It was assumed that the exterior body shape and tire characteristics would not change in converting the conventional Focus to an EV and PHEV. Therefore, the specifications from the conventional Focus that were used on the EV and PHEVs were the drag coefficient (0.32), frontal area (2.2 m^2), tire radius (33 cm), and rolling resistance coefficient (0.01). These specifications were taken either from the manufacturer [31] or from independent sources [12] [176]. The air density was set to 1.2 kg/m^3 for all of the vehicles simulated in this study [12].

6.2.3 EV and PHEV Modeling Techniques

In order to ensure an equitable comparison with the conventional vehicle, the EV and PHEVs were also simulated on the NEDC. The energy consumption of the EV and PHEVs in electric-only mode was taken from one iteration over the NEDC assuming that the SOC began at 100%. The energy consumption of the PHEVs in charge sustaining mode was taken from the average of multiple full charge-discharge cycles.

A charge-discharge cycle begins at the point when the ICE switches on to begin recharging the ESS, continues through to when the ICE has brought the energy storage system's state of charge back to its upper limit (80% in this study), carries on through the phase when the ICE has turned off and the state of charge is declining back towards its lower limit (20% in this study), and ends in the time step just prior to the ICE turning on once again to start a new charge-discharge cycle. The charge-discharge cycles are generally longer than the length of a single run through the NEDC, and that was true in this study as well. Their exact length depended primarily on the size of the ESS. As a result, charge-discharge cycles do not always begin and end at the same point on successive iterations of the NEDC. This leads each charge-discharge cycle to encompass a slightly different pool of driving conditions over the NEDC – each charge-discharge cycle will have presided over a different collection of acceleration, deceleration, high-speed, and low-speed events. To compensate for this, the simulated PHEVs were run over 30 iterations of the NEDC so that each simulation included multiple charge-discharge cycles. The energy consumption and thus CO_2 emissions over each of these charge-discharge cycles was calculated. The uncertainty in the energy consumption and CO_2 emissions across the different charge-discharge cycles for each PHEV never exceeded 2% of the mean, indicating that this approach was reasonably precise.

6.2.4 CO_2 Emissions Modeling

The tank-to-wheel CO_2 emissions for the conventional vehicle, EV, and PHEVs were all derived in different ways. The operating emissions from conventional vehicles can be measured by what comes out of their tailpipe. In Europe, automobile manufacturers publish the grams of CO_2 per kilometer (gCO_2/km) emitted by conventional, ICE-based automobiles. Therefore in this study, that manufacturer reported value was used as the constant CO_2 emissions from the conventional vehicle over its entire range.

The emissions from EVs depend on their own energy consumption and on the CO_2 intensity of the power generation mix from which the EV's energy was obtained. The energy consumption is the amount of energy used per unit distance traveled. The CO_2 intensity of a power generation mix is the average amount of CO_2 emitted per unit of electrical energy generated by all of the power production processes in a mix weighted by the amount of power obtained from each of those processes. By combining the energy consumption of the EV (E_{EV}) with the CO_2 intensity of its power generation mix (I_{CO2}), its emissions in gCO_2/km (e_{EV}) could be obtained

$$e_{EV} = I_{CO_2} E_{EV}. \qquad 6.2$$

It should also be noted that the CO_2 intensity figures used in this study only account for the CO_2 emissions involved in the actual process of power production.

The CO_2 emissions from PHEVs depend on the CO_2 intensity of the power generation mix, the efficiency of the vehicle in charge sustaining and electric-only modes, and the distance traveled in both modes. The equation used in this study to calculate the average gCO_2/km for a PHEV, e_{PHEV}, was

$$e_{PHEV} = \frac{e_{CS}d_{CS} + I_{CO_2}E_{EO}d_{EO}}{d_{CS} + d_{EO}} \qquad 6.3$$

where d_{EO} and d_{CS} are the distances traveled in electric-only and charge sustaining mode respectively, E_{EO} is the energy consumption in electric-only mode, and e_{CS} (expressed as the gCO_2/km) is the CO_2 emissions produced per unit distance by the PHEV in charge sustaining mode. Equation 6.3 calculates the cumulative CO_2 emissions for a PHEV from the time its journey began to its current point and then averages those CO_2 emissions over the distance traveled up to that point. Yet it should be noted that once a PHEV switches to charge sustaining mode, its instantaneous CO_2 emissions undergo a step up to the PHEV's charge sustaining mode CO_2 emissions rate.

6.3 Model Validation

In order to improve the confidence in the results from the model, the vehicle models were validated by successfully predicting the performance of a conventional vehicle, an EV, and a PHEV. No single vehicle currently exists with a conventional, EV, and PHEV platform which is why this study relies on computer models and why the models had to be validated against the three different vehicle types. The model's estimates were validated against lumped parameters for fuel, energy consumption, and CO_2 emissions as reported by the vehicle manufacturers or the EPA.

There is currently not an EV version of the Ford Focus available, so the EV model was validated against a Tesla Roadster. The Tesla Roadster has a curb mass of 1235 kg, a drag coefficient of 0.35, a frontal area of approximately 1.8 m^2, a rolling resistance coefficient of 0.01, a tire radius of 32 cm, and a battery pack with an energy capacity of 202 MJ [12] [11]. The manufacturer reports this vehicle to have an energy consumption of 459 kJ/km over the EPA combined drive cycle [11]. OVEM simulated this vehicle running over this drive cycle and arrived at an energy consumption figure of 450 kJ/km. This value was within 2% of the published data from the manufacturer.

The PHEV model was validated against the only PHEV currently in commercial production, the Chevrolet Volt. The Volt has a drag coefficient of 0.29, a frontal area of approximately 2.4 m^2, a tire radius of 33 cm, a curb mass of 1715 kg, a rolling resistance coefficient of 0.008, and a 16 kWh lithium-ion battery pack [17] [177]. The traction motor on the Volt has a rated torque of 369 Nm and a rated power of 112 kW [17]. The generator has a rated power of 55 kW, and the ICE it is attached to has a rated power of 63 kW [17]. The efficiency maps for the Volt's motor, generator, and ICE could not be attained, so their performance was simulated by rescaling the torque and speed axes of the generator and ICE efficiency maps described in Section 6.2 to match the specifications of the motors, generators, and ICE used in the Volt [31] [61]. The EPA reports that the Volt achieves an energy consumption of 770 kJ/km in electric-only mode and consumes 6.4 L/100 km of petrol in its petrol-only mode over the EPA's combined city/highway drive cycle (the EPA used the lower heating value of gasoline and assumed 1 US gallon of gasoline is equivalent to 33.7 kWh of energy) [17]. Over this same drive cycle, OVEM simulated the Volt consuming 800 kJ/km in electric-only mode and 6.7 L/100km in charge sustaining mode. In both modes, the OVEM Level 3 simulation was within 5% of the actual performance of the Volt. These validations showed that OVEM, along with its assumptions about the powertrain's components and their scaling and efficiency, had a level of accuracy that was sufficient for this study.

6.4 Results and Discussion

In order to characterize the CO_2 emissions from the conventional Focus, only the manufacturer's published figures were needed. The lowest emitting conventional Focus produced 114 gCO_2/km. The simulations showed that the modeled Focus EV had an energy consumption of 455 kJ/km. Table 6.2 shows the necessary information to characterize the emissions of the PHEVs in this study. It is interesting to note that the CO_2 emissions from the PHEVs in charge sustaining mode increased as the mass of the PHEV increased, yet only slightly, as the CO_2 emissions remained within 1% of each other. This illustrated that the energy consumption of the PHEVs' APU increased slightly as the mass of the PHEV increased; however, since the APU was decoupled from the road load and could operate in its most efficient range, it achieved similar performance even as the mass of the vehicle increased. Also note that all of the PHEVs in electric-only mode were more energy efficient than the EV. This is primarily because the PHEVs were lighter due to their smaller battery packs. With the relevant parameters for the vehicles determined, the only parameter that could be varied was the CO_2 intensity of the power generation mix, I_{CO2}, as seen in Equations 6.2 and 6.3.

Table 6.2: Energy use and CO_2 emissions specifications for the vehicle in this study

	PHEV-20	PHEV-40	PHEV-60	PHEV-80	EV	ICE-Based Vehicle
Range in electric-only mode (km)	20	40	60	80	300	--
Energy consumption in electric-only mode, E_{EO}, (kJ/km)	424	427	431	437	455	--
CO_2 Emissions in CS mode, e_{CS}, (gCO_2/km)	108	109	109	109	--	114

Note that Figure 6.3 through Figure 6.6 show the cumulative amount of CO_2 emitted by each of the vehicles averaged over the distance traveled (according to Equation 6.3), and they assume that the EV and PHEVs began with a fully charged battery. Figure 6.3 plots the tank-to-wheel CO_2 emissions averaged over the distance traveled for the PHEV-60 for power generation mixes of varying CO_2 intensities. This range of CO_2 intensities extends to about as high as currently exists in any country [178]. Figure 6.3 supplements Figure 6.4, Figure 6.5, and Figure 6.6 in showing how the emissions from a PHEV depend on the CO_2 intensity of the power generation mix from which it is charging. Note that the CO_2 emissions from the

PHEVs in electric-only mode depend directly on the CO_2 intensity of the power generation mix. Once the PHEV enters its charge sustaining mode, the CO_2 emissions averaged over the distance traveled pick up at the level they were at during electric-only mode before asymptotically approaching the APU's CO_2 emissions value.

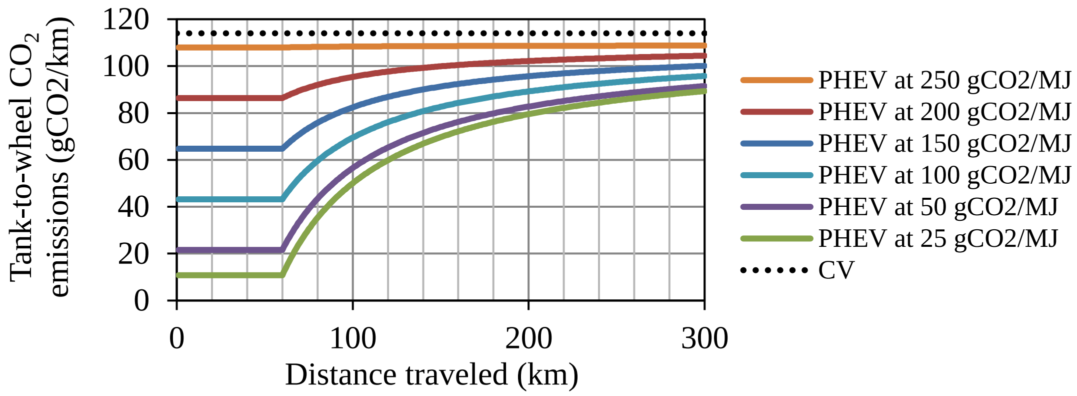

Figure 6.3: Cumulative CO_2 emissions averaged over the distance traveled for the PHEV-60 with power generation mixes of varying CO_2 intensity

Figure 6.4 shows how the average emissions profiles compare for the CV, EV, and PHEVs when the EV and PHEVs charge in France, a country with a power generation mix with a low CO_2 intensity (24 gCO_2/MJ) [178]. While, the PHEVs consumed less energy in their electric-only mode than the EV, which led to them having lower emissions than the EV in their electric-only range, the difference was almost negligible. Figure 6.4 shows that given France's low CO_2 intensity, there was less than a 1 gCO_2/km difference between the CO_2 emissions from the most efficient PHEV and EV. What was only a small difference in CO_2 emissions in electric-only mode became much larger once the PHEVs entered charge sustaining mode. As the average CO_2 emissions from the PHEVs asymptotically approached their ICE-based APU's emissions value over the course of their range, they moved farther away from the low, constant CO_2 emissions of the EV. Since the PHEVs operated more efficiently in charge sustaining mode than the conventional vehicle and since their CO_2 emissions in electric-only mode began at a point below those from the conventional vehicle, their average emissions were lower at all points in their range. From these results, the generalization could be made that if the CO_2 intensity of the power generation mix is low, then EVs provide a more consistent option than PHEVs or conventional vehicles for lowering CO_2 emissions in automobile transport.

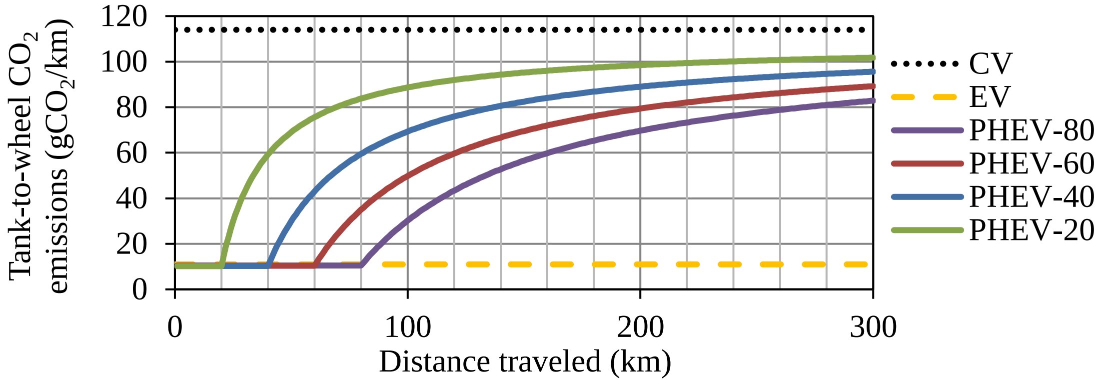

Figure 6.4: Cumulative CO_2 emissions averaged over the distance traveled for a conventional vehicle, EV, and PHEVs in France, a country with a power generation mix with a low CO_2 intensity

Figure 6.5 shows the average emissions for the conventional vehicle, EV, and PHEVs, over the course of their range as if they were charging in the USA which has a CO_2 intensity of 169 gCO_2/MJ [178]. A power generation mix with this level of CO_2 intensity is near the middle of the range for countries worldwide. Given this CO_2 intensity, the PHEVs emitted between 3 to 6 gCO_2/km less than the EV during their electric-only mode which was expected because of the lighter curb mass and higher efficiency of the PHEVs. The PHEVs even continued to emit less than the EV into their charge sustaining mode. For instance, the PHEV-80 continued to have lower emissions than the EV for several kilometers into its charge sustaining mode. There is clearly a range of distances over which the PHEVs emitted less than the EV. Thus, in a country with a mid-range CO_2 intensity, such as the USA, PHEVs offer the possibility of reducing CO_2 emissions relative to EVs when they begin with a full charge and are not driven too extensively in their charge sustaining mode. Yet, once the PHEVs extended further into their charge sustaining modes, they began to emit significantly more gCO_2/km than the EV. Both the EV and PHEVs emitted less CO_2 at all points in their range than the conventional vehicle. Thus, with power generation mixes of mid-range CO_2

intensity, PHEVs may provide for lower CO_2 emissions if the driving distances between charges are short relative to the maximum range of the vehicle. This is generally the case in the USA, as the national average commute distance is approximately 25 km [179] [180]. However, the CO_2 emissions reductions from PHEVs in electric-only mode compared to those from EVs were not too significant. The EV produced low CO_2 emissions over its entire range, and it achieved over 90% lower CO_2 emissions than the CV. EVs appear to be a better option than PHEVs for lowering CO_2 emissions in automotive transport given a power generation mix similar to the average one found in the USA.

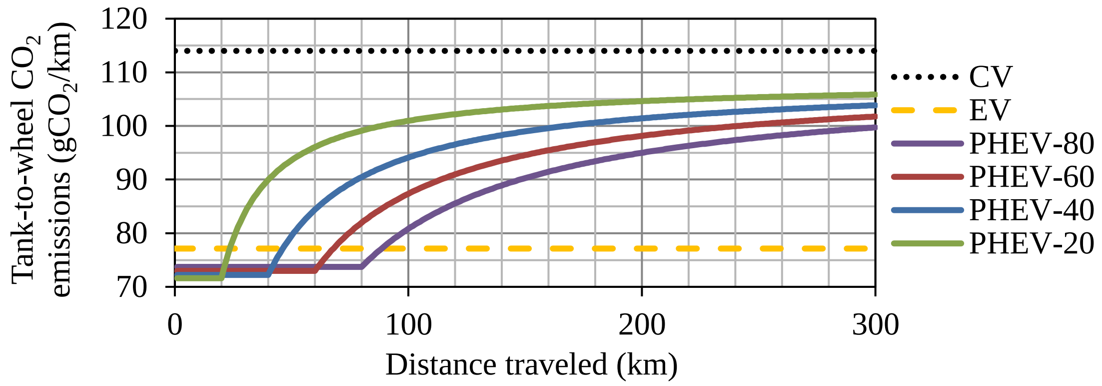

Figure 6.5: Cumulative CO_2 emissions averaged over the distance traveled for a conventional vehicle, EV, and PHEVs in the USA, a country with a power generation mix with a mid-range CO_2 intensity

When the CO_2 intensity of the power generation mix is high, a different picture began to emerge. It has been projected that by the year 2050, China alone will have nearly 600 million cars on its roads – more than existed worldwide in 2005 [4]. China has a power generation mix that is highly CO_2 intensive – 241 gCO_2/MJ [178]. This significantly impacts the emissions profiles for PHEVs and EVs. Figure 10 shows these profiles for China. Given China's power generation mix, the simulated PHEVs achieved lower emissions at all points over their range than the EV and conventional vehicle. This fact has not been reported on in the literature, and it demonstrates that PHEVs provide a stronger alternative than previously thought to lower the CO_2 emissions from transport in countries with a highly CO_2 intensive power generation mix. In a country like China, PHEVs have the potential to be more than a mere stopgap compensating for the current range deficiencies of EVs. Depending on how the CO_2 intensity of China's power generation mix evolves, PHEVs may be able to play a more prominent role in a long-term solution to lower CO_2 emissions in automobile transport. However, the reality of China's power generation mix also shows that even EVs and PHEVs will not be able to significantly lower China's CO_2 emissions from automobile transport in the short term. The EV and PHEV-20 in electric-only mode achieved less than a 5% and 11% CO_2 emissions reduction respectively compared to the conventional vehicle. This demonstrates that countries with highly CO_2 intensive power generation mixes clearly have an extra incentive to reduce their CO_2 intensity in order to maximize the potential of EVs and PHEVs to reduce CO_2 emissions in automotive transport.

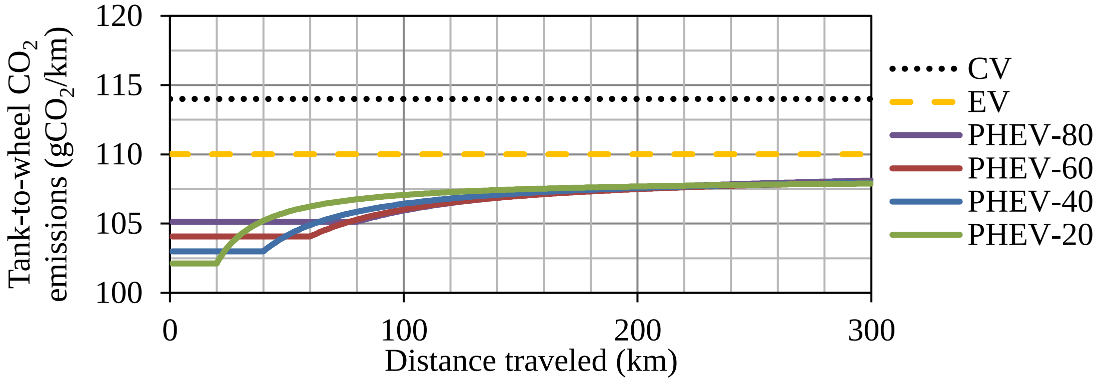

Figure 6.6: Cumulative CO_2 emissions averaged over the distance traveled for a conventional vehicle, EV, and PHEVs in China, a country with a power generation mix with a high CO_2 intensity

Granted, these results are derived from the assumptions and modeling techniques outlined earlier in this study. As such, these predictions should not necessarily be expected to be true for all possible EVs and PHEVs. Nevertheless, these results illustrate the central point that was hypothesized at the outset of this study: as the CO_2 intensity of the power generation mix increases, PHEVs can actually reach a point where they produce roughly as many or even fewer tank-to-wheel CO_2 emissions than EVs across their entire driving range.

6.5 Conclusion for Case Study 2

This study modeled the CO_2 emissions from EVs and PHEVs and compared the results to published values for the CO_2 emissions from a conventional vehicle based on an ICE. It was theorized that given certain power generation mixes with varying CO_2 intensities PHEVs may be able to emit less CO_2 than both conventional vehicles and EVs. Given a low CO_2 intensity, as is found in a country like France, EVs emerge as the best option for reducing CO_2 emissions from automobile transport. Given a mid-range CO_2 intensity, as is found in the USA, PHEVs were able to emit between 3 to 6 gCO_2/km less than the EV during their electric-only mode. However, the EVs still appeared to be the most reliable option for reducing automotive CO_2 emissions across their entire driving range. Yet, when a highly CO_2 intensive power generation mix was considered, such as in China, PHEVs were found to emit less over their entire range than both a similar EV and conventional vehicle. This shows that PHEVs are not only a stopgap making up for the current range shortcomings of EVs. This novel result could affect how countries with highly CO_2 intensive power generation think about lowering their automotive CO_2 emissions. Also, unless highly CO_2 intensive countries pursue a major decarbonization of their power generation, they will not be able to fully take advantage of the ability of EVs and PHEVs to reduce the CO_2 emissions of automotive transport.

This study also illustrates how OVEM's flexible structure and rapidity of implementation and simulation can be used to accurately compare a range of different powertrain topologies and technologies. OVEM's results can also be combined with outside data sets (in the case of the power generation mix CO_2 intensity data) to arrive at results that can provide a solid technical footing to discussions with policy implications on the impact of advanced powertrains.

7 Conclusions and Future Work

This dissertation addresses the problem of modeling the energy flows in new and rapidly evolving classes of automotive vehicles. It introduces a system of computer models, known collectively as the Oxford Vehicle Model (OVEM), which allows for the novel simulation of the powertrains of electric and hybrid electric vehicles.

The number of vehicles on the world's roads is expected to triple to 3 billion by 2050 [4]. Road transport is currently almost entirely dependent on fossil fuels, which leads to a host of environmental and economic problems [2]. Electric and hybrid electric vehicles have the potential to mitigate the negative impacts posed by the fossil fuel dependence of the current road transport fleet [8]. Electric and hybrid electric vehicles are complex systems that have the capacity to integrate many different technologies into a host of powertrain topologies. Building and testing each possible powertrain configuration would be prohibitively time, labor, and resource intensive. Yet, modeling these powertrains with computer simulations can provide accurate and useful information about their characteristics at a fraction of the cost, labor, and time.

In any modeling effort, it is imperative to determine what the model's objectives are in order to establish how to build the model in order to best meet those objectives. This study began by identifying a number of criteria for a novel vehicle modeling program that would make the program valuable to entities in industry, academia, and government. That list of criteria is repeated here for convenience:

1. The program should be able to rapidly simulate and incorporate existing and emerging technologies and capabilities.
2. The program should be able to facilitate scoping exercises across a spectrum of component technologies and sizes in order to understand the relationship between a range of technological options (including those that currently exist and have the potential to exist in the future) and key electric and hybrid electric vehicle characteristics, such as cost, emissions, energy consumption, and range.
3. The program should be concerned with timescales and conditions that align with widely used vehicle testing protocols for ascertaining values such as emissions, energy consumption, and range. The relevant timescales are approximately on the order of 1 to 10^4 s. The conditions are straight-line travel, typically over widely-used drive cycles representing urban, highway, or suburban driving (in order to enable comparison with other studies and reported vehicle characteristics). This excludes racing applications or other similarly extreme off-road or hill climb applications. The simulation should also have the ability to account for changes in elevation.
4. The program should be capable of obtaining a degree of accuracy that warrants reasonable justification to begin with experimental testing. This was concluded to be approximately between 2-5% of real world figures.

A survey of the current vehicle modeling landscape showed that while programs existed that could address some of these issues, they had significant deficiencies and no one program comprehensively addressed all of these criteria. It was thus concluded that there was room for a novel vehicle modeling program that could deliver across all of these criteria. This novel vehicle modeling program came to be OVEM.

In striving to meet the outlined criteria, OVEM was built around three levels that each incorporated a distinct modeling approach in order to facilitate vehicle modeling through varying stages of uncertainty, fidelity, and accuracy. Below is an overview of the three levels of modeling in OVEM, as well a description of how each level contributes towards OVEM meeting its design criteria.

Level 1 utilizes a backwards modeling approach where the component models are based on a fixed efficiency which is set by the user based on the user's particular component sizing and scoping ambitions. The fixed efficiency approach enables the component models to rapidly assess an array of technologies (Criteria #1) especially at a stage in the analysis process when uncertainty is likely to be high. The fixed efficiency approach enables the calculation of energy flows affecting values such as vehicle energy consumption, emissions, range, and component sizing and cost (Criteria #2). The fixed efficiency approach of the component models is in line with the timescales and conditions of interest (Criteria #3). The primary downside to the Level 1 model is that its accuracy can be low (Criteria #4) since it employs models with such low fidelity. But as was noted above, scoping a wide array of components is the focus of the Level 1 model, not obtaining highly accurate results via high-fidelity models. Thus, the accuracy criterion for Level 1 was not of critical importance.

Level 2 uses a backwards modeling approach where the component models use a varying efficiency which is based on an application of well-understood physical principles regarding broad technology types. The fact that the models are based on well-understood physical principles governing an array of technologies enables the rapid simulation of different technologies (Criteria #1). As a backwards model, it is suited towards performing component scoping to help determine parameters such as energy consumption, range, emissions, cost, and sizing (Criteria #2). The models are built so as to reflect the timescales and conditions of interest (Criteria #3). As a backwards simulation, accuracy is not a priority; therefore, the program is not concerned with meeting the Criteria #4 accuracy objective. However the models still seek to model the efficiency of the components in a physically meaningful yet product-independent way that should have a higher fidelity and accuracy and lower uncertainty than Level 1.

Level 3 is a backwards-forwards model, and as such it is the modeling approach in OVEM with the lowest uncertainty and highest accuracy. Level 3 enables the rapid simulation of existing and emerging technologies by basing its component models on readily available data from actual products (Criteria #1). In meeting this criterion, Level 3 seeks to reduce computational and experimental complexity to facilitate the rapid simulation of these powertrains. Level 3 is constructed in such a way that it allows for a library of components and capabilities so that scoping across many different dimensions can be performed to deliver figures for energy consumption, emissions, range, cost, and sizing (Criteria #2). The Level 3 component models are based around the timescales and conditions of interest (Criteria #3). Accuracy is an important criterion for Level 3, so it was developed in such a way as to meet the accuracy objective of Criteria #4.

Chapters 2, 3, and 4, contain detailed descriptions on the nature and inner workings of the Level 1, 2, and 3 programs. Refer to those chapters for further information on why and how each level was created. Each of these chapters also includes a case study and a sensitivity analysis for its particular level in order to help illustrate the functionality and important considerations of each level.

Following the account of why and how each level (along with each level's constituent models) was created. Chapters 5 and 6 present detailed case studies based articles published by the author in academic journals that demonstrate how OVEM can be used to address novel and pressing questions surrounding the development and impact of electric and hybrid electric vehicles.

The study in Chapter 5 exemplifies OVEM's ability to rapidly assess a range of existing and emerging components. In this study, the cutting-edge technologies of high-speed flywheels, advanced lithium-based batteries, and ultracapacitors functioning as the energy storage system onboard a series hybrid were compared on the bases of cost and fuel consumption. The study showed the novel result that series hybrid powertrains using high-speed flywheels can be competitive in price and fuel consumption to powertrains using batteries and ultracapacitors.

Chapter 6 further demonstrates OVEM's ability to compare emerging technologies and topologies on the bases of energy consumption, range and emissions. Currently, no single vehicle platform exists with electric, hybrid, and conventional variants. So for this study, OVEM created one. By using a conventional vehicle platform as the base, electric and hybrid electric versions were created so as to allow for an equitable comparison across the range of technologies and topologies used. The study ultimately used OVEM to model the tank-to-wheel CO_2 emissions from plug-in hybrid and electric vehicles recharging from power generation mixes of varying CO_2 intensities. The tank-to-wheel CO_2 emissions from the modeled plug-in hybrid and electric vehicles were compared to the reported emissions from a similar internal combustion engine-based vehicle. The results showed that in areas with a CO_2 intensive power generation mix, plug-in hybrids have the potential to emit less CO_2 across their entire range than both comparable electric and conventional vehicles. This study also demonstrates how OVEM can be used to inform high-level decisions regarding matters of transport policy.

7.1 Specific Contributions of this Dissertation

The novel contributions of this dissertation span the breadth of OVEM. This section provides a recount of these novel contributions, with reference to where a more detailed discussion of them can be found in the body of the text.

This section will first discuss the novel contributions made by the constituent component and capability models of OVEM and how these contributions were developed.

Then this section will discuss how these individual contributions combine into the broader contribution of OVEM – providing a view on the novel contribution of OVEM as a whole program. This section will then conclude with a discussion of the contributions made via the application of OVEM to real-world questions.

Level 1 makes four unique contributions with its capability and component modeling techniques. All four of these contributions appear in Levels 2 and 3 as well (with a degree of fidelity commensurate with the rest of that level's vehicle model). However, since the first incarnation of these techniques appear in the Level 1 program, they will be discussed as part of Level 1.

The first two novel capabilities of the Level 1 program are the ability to model multiple tractive electric motors (Sections 2.4, 3.4, and 4.4) and hybridized energy storage systems (Sections 2.6, 3.6, 4.6, and 4.9). Both of these capabilities are concepts that are emerging alongside the rise in electric and hybrid electric vehicles – as they were largely unexplored to a field dominated by the internal combustion engine. Though both of these capabilities have been discussed in the literature as concepts, no energy flow vehicle modeling programs have been built with these functionalities [40]. Thus, the novel work in this study came in turning these new concepts into a series of algorithms and modeling techniques that could be used in OVEM. For instance, the author did novel work to develop Equation 4.73, which was used to control the energy flow between hybridized energy storage systems in a speed-based energy management system.

The other two novel capabilities introduced in the Level 1 program came with the rolling resistance model and the ability to account for slope in the drive cycle (refer to Section 2.1 for a more detailed discussion on these topics). With both of these functionalities, an existing knowledge base was leveraged to turn the concepts into practical realities in OVEM. In the case of modeling rolling resistance, existing energy flow vehicle models had incorporated some means of accounting for rolling resistance; however, their approach was overly simplified and did not account for the effect that vehicle speed has on rolling resistance [40]. A survey of the literature was conducted, and empirical work on measuring rolling resistance was found. The results of this existing empirical work (Equation 2.11 and Figure 2.4) had never been adapted for use in an energy flow vehicle model [26] [40], so the author's novel contribution came in deriving this work into form capable of functioning within the structure of OVEM. This required novel programming to create the interpolation techniques and coding loops in the model to enable these empirical findings to actually work towards more accurately modeling rolling resistance.

Existing energy flow vehicle modeling programs did not include the ability to account for slope [26]. This is an important omission as electric and hybrid electric vehicles have the ability to benefit from modeling slope since they can recapture energy during descents. To incorporate slope into OVEM, standard Newtonian equations of motions were derived (Equations 2.5, 2.6, 2.8, 2.10, 2.12, and 2.13) and then adapted for use within OVEM. The novel work came in adapting these derivations for use within OVEM – programming the necessary loops and interpolation techniques with their unique dependence on distance traveled by the vehicle rather than time elapsed, which runs counter to the structure of the rest of OVEM and other existing energy flow vehicle modeling programs [40].

Level 2 has its own set of novel component modeling contributions. The first of these was the gearbox model. Existing energy flow vehicle modeling programs had gearbox models; however, they made the simplifying assumption that the efficiency of the gearbox was constant [26] [40]. Empirical evidence shows that this is not the case. So OVEM leveraged this empirical evidence to devise the backwards gearbox modeling technique explained in Section 3.3. The novel work in this regard came in creating Equation 3.2 based on the existing empirical work and in developing the programming algorithms required to enable Equation 3.2 to function with OVEM.

The rest of the novel component modeling techniques in the Level 2 program came from the motor, power electronics, and energy storage system models (Sections 3.4, 3.5, and 3.6, respectively). The existing body of knowledge on each of these components was leveraged to understand how their primary loss mechanisms could be modeled in a manner that was physically meaningful yet general enough to be product-independent (in accordance with the objectives of Level 2). However, understanding the primary loss mechanisms was only the first step in devising the models. Novel work was conducted by the author to create the equations to actually model these components' efficiency (Equations 3.6, 3.11, and 3.12). Novel work was also done to create the methodology, in its entirety, that enables the coefficients for Equations 3.6, 3.11, and 3.12 to be calculated which is essential to enable the models to function within OVEM (refer to Sections 3.4.1, 3.5.1, and 3.6.1 for more information).

The Level 3 model features eight novel contributions from its component and capability models. The first of these capabilities is the load transfer model (for more information refer to Section 4.1.1.3). Load transfer in vehicles is a well-understood phenomenon with an existing body of knowledge. However, it is a phenomenon that has been overlooked by energy flow vehicle models. Load transfer can significantly impact electric and hybrid electric vehicles – namely via the amount of energy capable of being captured through regenerative braking. For this reason, the Level 3 model in OVEM was designed with the capability to model load transfer. In building this capability into OVEM, the existing body of knowledge on load transfer was leveraged – the derivation of Equations 4.22 to 4.30 existed in the literature (though the author did perform the novel task of accounting for inertia in this derivation). The author also performed the novel task of combining the derivations from Equations 4.22-4.35 with Equations 4.36 and 4.37 to yield Equations 4.38 and 4.39 (which are novel in that they also account for inertia). Programming Equations 4.38 and 4.39 into an algorithm capable of functioning within OVEM was also a novel achievement as it had never been done before in an energy flow vehicle modeling program [26] [40].

The second novel contribution of the Level 3 program was concerned with improving the accuracy of calculating the final speed achieved by the vehicle at the end of each time step. Existing energy flow vehicle models made a simplifying assumption on this topic to avoid dealing with the complex quadratic that results from the Newtonian dynamics describing the final speed achieved by the vehicle [26] [40]. OVEM did not want to use this assumption in its attempt to achieve greater accuracy. To go beyond this simplifying assumption, the author performed a novel derivation, based on first principles from the standard Newtonian equations of motion (first described in Section 2.1), in order to improve the accuracy of the calculation to determine the final speed achieved by the vehicle at the end of each time step. This novel derivation required solving the complex quadratic referenced above and is reflected in Equations 4.8 through 4.20. To the best of the author's knowledge, this derivation has not been performed before, thus making it a novel contribution to the field of vehicle modeling. For more information on this novel derivation, refer to Section 4.1.1.2.

The third and fourth novel contributions of the Level 3 model have to do with the gearbox and epicyclic gear train models. Existing energy flow vehicle models included models for a gearbox and epicyclic gear train. However these models, made the simplifying assumption that the efficiency of these components was constant. Empirical evidence shows that the efficiency of these components is not constant and instead depends on their design (e.g. gear ratio and seal, bearing and meshing properties in the case of the gearbox) and the load they are transmitting [44] [57]. Thus, novel work was done to adapt this existing empirical work into equations and modeling principles that could be integrated into OVEM.

For the gearbox model, the efficiency equations (Equations 4.40 and 4.41) were novel contributions derived by the author based on the existing empirical findings (Section 4.3). For the epicyclic gear train (Section 4.8), the efficiency relationship shown in Figure 4.39 was a novel contribution derived by the author also based on empirical findings. Turning these equations in programmable algorithms also required novel work, since these relationships had not previously been reflected in energy flow vehicle models [26] [40].

The fifth novel contribution came from the Level 3 ultracapacitor model. Existing empirical and theoretical work on ultracapacitor modeling served as the foundation for the ultracapacitor model in OVEM. For example, the models in Figure 4.12 and Figure 4.14 were used to initially frame the structure of the ultracapacitor model. This required integrating a truncated version of these existing models into OVEM (refer to Figure 4.18), such that the model would meet OVEM's computational and experimental complexity criteria [47]. The novel work came in combining this truncated model with the relationship described in Figure 4.20 and Figure 4.21, which models how the capacitance of an ultracapacitor varies with its state of charge. This is a phenomenon which had heretofore not been included in existing ultracapacitor models in energy flow vehicle modeling, so developing the equations to merge the model in Figure 4.18 with the relationships in Figure 4.20 and Figure 4.21, and then translating those equations into a programmable code for an energy flow vehicle modeling program was novel. Refer to Section 4.6.1 for more information on the ultracapacitor model.

The sixth novel contribution of the Level 3 program comes from the battery model. With the battery model, an existing modeling technique (shown in the derivation of Equations 4.64 through 4.69) served as the foundation for the model integrated into OVEM. The novel work consisted firstly of converting these equations into programmable code capable of functioning within OVEM. The novel work also consisted of characterizing an array of battery technologies for use in this model (e.g. the characterized battery chemistries of Figure 4.28 and Figure 4.29). Refer to Section 4.6.2 for more information on the battery model.

The seventh novel contribution came with the high-speed flywheel model. Though non-high-speed flywheel models exist, high-speed flywheel models have not been seen before [31], likely due to the fact that high-speed flywheels are themselves a novel technology. Existing flywheel models were not suitable for describing the losses of high-speed flywheels because they make simplifying assumptions regarding the speed-dependent nature of high-speed flywheel efficiency. Since there were no existing templates on high-speed flywheel models which could be leveraged, OVEM built one from scratch. The author obtained empirical data on high-speed flywheel efficiency through collaborations with a high-speed flywheel manufacturer (Figure 4.30). All of the work to then translate the nature of high-speed flywheel efficiency (described in Figure 4.30) into an OVEM model was novel. This consisted firstly of deriving the algorithms that: input the power request to the high-speed flywheel, assess the operating efficiency of the high-speed flywheel based on its operating conditions, and then output the power the high-speed flywheel was capable of delivering. Then the novel work also consisted of deriving the algorithms to allow the high-speed flywheel to be either mechanically or electrically integrated into the powertrain. Refer to Section 4.6.3 for a more detailed explanation on the novel work required to create the high-speed flywheel model.

The eighth novel contribution of the Level 3 model came as a result of work done to support the fuel cell model (refer to Sections 4.7.2 and 5.2.2 for more information). The author conducted a survey of an array of commercially available fuel cells. From this survey, the author was able to derive two things. The first was a description of the relationship between fuel cell power rating and mass (Figure 5.4). The second was the observation that the power-current and efficiency-current curves describing fuel cell behavior had similar shapes and values across a range of fuel cell sizes when these curves were normalized by the maximum power and current ratings of the fuel cell (Figure 5.2 and Figure 5.3). Both of these observations were novel, and they enabled the fuel cell model in OVEM to be constructed in such a way as to allow for the continuous scaling of fuel cell size (within realistically defined bounds) rather than relying on the discrete sizes of a few products [40]. This capability made OVEM a more useful component sizing tool - the effects of which can be seen in the case study of Chapter 5.

The above enumeration of the novel constituent parts of OVEM should indicate the degree of novelty underpinning OVEM's development. But OVEM's novelty is more than just the sum of its parts. Each level in OVEM represents a novel modeling approach that was developed to address a current shortcoming of the vehicle modeling landscape. Levels 1 and 2 were the only backwards energy flow vehicle models available at the time of the development of OVEM. With no pre-existing template to follow, novel work was required to develop the modeling philosophies and overarching structures for both Levels 1 and 2. Novel work was also required to define the overall architecture for Level 3 given the extent of new components and capabilities that it introduced (e.g. high-speed flywheel and hybridized energy storage systems). OVEM as a whole also represents a novel achievement for vehicle modeling, as it is capable of addressing a broad array of questions by incorporating models of varying degrees of fidelity and accuracy capable of producing results given inputs of varying certainty into a single package.

Applications of OVEM's models also produced several new and important contributions. These contributions were presented in three journal-published articles, two of which were presented in this dissertation, as Chapters 5 and 6. The first of these journal-published studies (Chapter 5) made the first published comparison between high-speed flywheels, batteries, and ultracapacitors functioning as the energy storage system in a light-duty hybrid electric vehicle [35]. This study showed that high-speed flywheels could be competitive with batteries and ultracapacitors on the bases of cost and fuel economy.

The second study (the one not presented in this dissertation due to page limit constraints) made the novel contribution of quantitatively comparing the tank to wheel CO_2 emissions for a range of electric vehicles (with varying battery array sizes) to the CO_2 emissions from comparable ICE-based vehicles. This study demonstrated quantitatively that EVs have the potential to have higher tank to wheel emissions relative to similar ICE-based vehicles in regions where the CO_2 intensity of grid-generated electricity is high.

The third study (Chapter 6) used OVEM to predict the CO_2 intensity of electric and hybrid electric vehicles relative to conventional vehicles given the CO_2 intensity of the electric grid in four key countries around the world [37]. OVEM's novel contribution in this regard came in that it was able to make a comparison using a standard vehicle platform across conventional, electric, and hybrid electric vehicles by virtue of its simulation capabilities, even though no single vehicle platform that has conventional, electric, and hybrid variants exists. In this study, OVEM also demonstrated, in a quantitative way, the novel observation that in regions where the CO_2 intensity of grid electricity is high, plug-in hybrids can have lower CO_2 emissions across their entire range than electric and conventional ICE-based vehicles.

7.2 Future Work

The most direct next step for future work that could be done on OVEM involves continuing to develop its modeling capabilities. Overcoming the non-criteria outlined in Section 1.8 could be a significant achievement for OVEM. For instance, thermal modeling has been excluded from OVEM thus far because of a lack of readily available data on the thermal properties of many powertrain components. However, thermal issues can be significant, as evidenced by a recent publicized debate between electric vehicle manufacturers regarding questions of optimal battery thermal regulation methods and performance under different thermal conditions [181]. OVEM has also refrained from modeling sub-components of its individual components (such as individual battery cells within the battery module). This was done because of the lack of available data on the individual cell traits. In the case of batteries, this depends both on the manufacturer's ability to deliver a consistent product (something that can be difficult for manufacturers of advanced batteries) and for the vehicle's energy management strategy to properly monitor and load the individual cells in an array. Yet, this is also an important issue in electric and hybrid electric vehicle development. A tool like OVEM could serve as an independent means for evaluating issues such as these.

OVEM could also expand to include models for even more exotic technologies such as turbochargers for ICEs and on-board reformers for fuel cells. Part of this effort would also include expanding OVEM's scope of interest so that it encompassed a broader swath of vehicles, such as buses and heavy-duty trucks (lorries).

OVEM's modeling capabilities could further advance to a stage where OVEM begins to merge with the experimental world. Greater experimental resources would enable OVEM to thoroughly validate its own models which could then progress to be able to assess manufacturer's claims regarding their product data. OVEM would also be able to devise more advanced models based on parameters gleaned from experimental testing. OVEM could also incorporate hardware-in-the-loop simulations which would improve the accuracy of OVEM's results and enable it to test advanced technologies, topologies, energy management strategies, and other capabilities on real components.

OVEM could also use experimental means to gather data on how its components perform subject to conditions such as aging and adverse ambient environments. For instance, it would be a useful contribution if OVEM could accurately describe the degradation experienced by components due to an array of operating conditions and then predict how that would affect vehicle performance over time.

It could also be beneficial to advance its Level 2 modeling capabilities. A comprehensive modeling approach based on the first principles behind these powertrain technologies may be able to reveal further interesting insights into how these technologies may progress and where their upper performance limits may lay.

Another area of future work for OVEM involves publicizing and distributing OVEM to groups that are interested in its functionality in academia, industry, and government. There has been demand for OVEM from research groups in the UK and worldwide, and the author has collaborated with these research groups to aid in their vehicle simulation efforts. As OVEM becomes more widely-used, other research groups would likely enhance its functionality, perhaps in ways not envisioned by the author. If OVEM were to become more widely adopted, its opportunities for validation and improvement would increase, leading to a virtuous cycle where more groups seek to use OVEM because of its increasing validation and functionality.

References

[1] Plunkett Research, Ltd. (2011) Automobile Industry Introduction. [Online]. http://www.plunkettresearch.com/automobiles%20trucks%20market%20research/industry%20overview

[2] International Energy Agency, "CO2 emissions from fuel combustion," 2009.

[3] C.J. Campbell and J.H. Laherrere, "The End of Cheap Oil," *Scientific American*, pp. 78-83, March 1998.

[4] M. Chamon, P. Mauro, and Y. Okawa, "Mass car ownership in the emerging market giants," *Economic Policy*, vol. 23, no. 54, pp. 245-296, April 2008.

[5] The European Union and The Council of the European Union, "Setting Emissions Performance Standards for New Passenger Cars as Part of the Community's Integrated Approach to Reduce Carbon Dioxide Emissions from Light-Duty Vehicles," Regulation (EC) No. 443/2009, April 23, 2009.

[6] Environment News Service. (2011, August) U.S. Fuel Efficiency Standard to 54.5 mpg. [Online]. http://www.ens-newswire.com/ens/aug2011/2011-08-02-091.html

[7] J. O'Dell. (2009, May) Edmunds Auto Observer. [Online]. http://www.autoobserver.com/2009/05/china-sets-422-mpg-fuel-efficiency-standard-as-it-seeks-to-curb-oil-consumption.html

[8] A.A. Adly, A.F. Zobaa, and G.J. Nolan, "Trends, Features, and Recent Research Efforts in the Field of Hybrid Electic Vehicles," *International Journal of Alternative Propulsion*, vol. 1, no. 1, pp. 1-5, 2006.

[9] I. Husain, *Electric and Hybrid Vehicles: Design Fundamentals*. New York: CRC Press, 2003.

[10] T. Quiroga, "Driving the Future," *Car and Driver*, August 2009.

[11] Tesla Motors. (2010, July) Tesla Roadster Specifications. [Online]. www.teslamotors.com

[12] M. Ehsani, Y. Gao, S.E. Gay, and A. Emadi, *Modern Electric, Hybrid Electric, and Fuel Cell Vehicles: Fundamentals, Theory, and Design*. New York: CRC Press, 2005.

[13] J. Van Mierlo, P. Van den Bossche, and G. Maggetto, "Models of Energy Sources for EV and HEV: fuel cells, batteries, ultracapacitors, flywheels, and engine-generators," *Journal of Power Sources*, vol. 128, no. 1, pp. 76-89, 2004.

[14] C.C. Chan and K.T. Chau, *Modern Electric Vehicle Technology*. New York: Oxford University Press, 2001.

[15] S. Barsali, C. Miulli, and A. Possenti, "A Control Strategy to Minimize Fuel Consumption of Series Hybrid Electric Vehicles," *IEEE Transactions on Energy Conversion*, vol. 19, no. 1, pp. 187-195, March 2004.

[16] P. Thounthong, S. Raël, and B. Davat, "Energy management of fuel cell/battery/supercapacitors hybrid power source for vehicle applications," *Journal of Power Sources*, vol. 193, no. 1, pp. 376-385.

[17] D. Vanderwerp, "2011 Chevrolet Volt Full Test - Road Test," 2010.

[18] General Motors Communications. (2009, August) Chevrolet Volt Expects 230 MPG. [Online]. www.chevrolet.com

[19] Fotor Motor Company. (2009) Ford Escape Hybrid Specifications. [Online]. www.ford.com

[20] U.S. Department of Energy, Office of Energy Efficiency and Renewable Energy. (2009) Technology Snapshot of the Honda Civic Hybrid. [Online]. http://www.fueleconomy.gov/feg/tech/TechSnapCivic_Final.pdf

[21] J. Miller, *Propulsion Systems for Hybrid Vehicles*. London: The Institution of Engineering and Technology, 2004.

[22] Toyota Motor Company. (2009) Toyota Prius Specifications. [Online]. www.toyota.com/prius-hybrid

[23] J. Larminie and A. Dicks, *Fuel Cell Systems Explained*.: John Wiley & Sons, 2000.

[24] J. Larminie and J Lowry, *Electric Vehicle Technology Explained*. Chichester, England: John Wiley & Sons Ltd., 2003.

[25] Z. Rahman, K.L. Butler, and M. Ehsani, "Designing Parallel Hybrid Electric Vehicles Using V-ELPH 2.01," in *Proceedings of the American Control Conference*, San Diego, 1999, pp. 2693-2697.

[26] K.B. Wipke et al., "Advisor 2.0: A Second-Generation Advanced Vehicle Simulator for Systems Analysis," National Renewable Energy Laboratory, 1999.

[27] W.L. Oberkampf, S.M. DeLand, B.M. Rutherford, K.V. Diegert, and K.F. Alvin, "Error and Uncertainty in Modeling and Simulation," *Reliability Engineering and System Safety*, vol. 75, no. 3, pp. 333-357, 2002.

[28] A. Froberg and L. Nielsen, "Efficient Drive Cycle Simulation," *IEEE Transactions on Vehicular Technology*, vol. 57, no. 3, pp. 1442-1453, May 2008.

[29] Mechanical Simulation Corporation. (2009) CarSim Overview. [Online]. www.carsim.com

[30] A.T. Papagiannakis, "Calibration of Weigh-In-Motion Systems Through Dynamic Vehicle Simulation," *Journal of Testing and Evaluation*, vol. 25, no. 2, pp. 189-214, 1997.

[31] T. Markel et al., "ADVISOR: A Systems Analysis Tool for Advanced Vehicle Modeling," *Journal of Power Sources*, vol. 110, no. 2, pp. 255-266.

[32] J. Marco and E. Cacciatori, "The Use of Model Based Design Techniques in the Design of Hybrid Vehicles," *3rd Conference on Automotive Electronics, Institution of Engineering and Technology*, pp. 1-10, 2007.

[33] P. Potluri, V. Desai, D. Maillard, N. Shah, and B. Cho, "Which hybrid powertrain would be suitable for your vehicle to reduce CO2 emissions?," in *EVS24 International Battery, Hybrid, and Fuel Cell Electric Vehicle Symposium*, Stavanger, Norway, 2009, pp. 1-9.

[34] E. Cacciatori, N.D. Vaughan, and J. Marco, "Energy Management Strategies for a Parallel Hybrid Electric Powertrain: Fuel Economy Optimization with Driveability Requirements," *Proceedings of the PARD Hybrid Electric Vehicle Conference*, 2006.

[35] R.T. Doucette and M.D. McCulloch, "A comparison of high-speed flywheels, batteries, and ultracapacitors on the bases of cost and fuel economy as the energy storage system in a fuel cell based hybrid electric vehicle," *Journal of Power Sources*, vol. 196, no. 3, pp. 1163-1170, Feb. 2011.

[36] R.T. Doucette and M.D. McCulloch, "Modeling the CO2 emissions from battery electric vehicles given the power generation mixes of different countries," *Energy Policy*, vol. 39, no. 2, pp. 803-811, Feb. 2011.

[37] R.T. Doucette and M.D. McCulloch, "Modeling the prospects of plug-in hybrid electric vehicles to reduce CO2 emissions," *Applied Energy*, vol. 88, no. 7, pp. 2315-2323, July 2011.

[38] Argonne National Laboratory. (2010, October) Autonomie. [Online]. http://www.autonomie.net

[39] C.C. Lin et al., "Integrated, Feed-Forward Hybrid Electric Vehicle Simulation in SIMULINK and Its Use for Power Management Studies," , 2001.

[40] K.B. Wipke, M.R. Cuddy, and S.D. Burch, "ADVISOR 2.1: A User-Friendly Advanced Powertrain Simulation Using a Combined Backward/Forward Approach," *IEEE Transactions on Vehicular Technology*, vol. 48, no. 6, pp. 1751-1761, November 1999.

[41] A. Froberg, "Extending the Inverse Vehicle Propulsion Simulation Concept to Improve Simulation Performance," Linkoping Universitet, PhD Thesis 2005.

[42] A. Rousseau and M. Pasquier, "Validation of a Hybrid Modeling Software (PSAT) Using Its Extension for Prototyping (PSAT-PRO)," , 2001.

[43] AVL. (2011) AVL CRUISE - Vehicle and Driveline System Analysis for Conventional and Future Vehicle Concepts. [Online]. https://www.avl.com/cruise1

[44] T.J. Woolmer, "The YASA Machine: For High Performance Automotive Applications," University of Oxford, DPhil Thesis 2009.

[45] G. Mantriota and E. Pennestri, "Theoretical and Experimental Efficiency Analysis of Multi-Degrees-of-Freedom Epicyclic Gear Trains," *Multibody System Dynamics*, vol. 9, pp. 389-408, 2003.

[46] E.F. Thacher, *A Solar Car Primer*. Hauppauge, NY, USA: Nova Science Publishers Inc., 2003.

[47] T.D. Gillespie, *Fundamentals of Vehicle Dynamics*. Warrendale, PA, USA: Society of Automotive Engineers, Inc., 1992.

[48] J.Y. Wong, *Theory of Ground Vehicles*, 3rd ed. New York: Wiley, 2001.

[49] D.W. Gao, C. Mi, and A. Emadi, "Modeling and Simulation of Electric and Hybrid Vehicles," *Proceedings of the IEEE*, vol. 95, no. 4, 2007.

[50] A.J. Salkind, A.G. Cannone, and F.A. Trumbure, "Lead-Acid Batteries," in *Handbook of Batteries*, 3rd ed. New York: McGraw-Hill, 2002, ch. 23. [Online]. www.simrit.com

[51] E. Karden, S. Ploumen, B. Fricke, T. Miller, and K. Snyder, "Energy Storage Devices for Future Hybrid Electric Vehicles," *Journal of Power Sources*, vol. 168, no. 1, pp. 2-11, 2007.

[52] SKF Group. (2009) The New SKF Model for Calculation of the Frictional Moment. [Online]. www.skf.com

[53] E. Pennestri and P.P. Valentini, "A Review of Formulas for the Mechanical Efficiency Analysis of Two Degrees-of-Freedom Epicyclic Gear Trains," *Journal of Mechanical Design*, vol. 125, pp. 602-608, 2003.

[54] E. Pennestri and F. Freudenstein, "The Mechanical Efficiency of Epicyclic Gear Trains," *Journal of Mechanical Design*, vol. 115, pp. 645-651, 1991.

[55] R.H. Ewert, *Gears and gear manufacture*. New York: Chapman & Hall: International Thomson Pub., 1997.

[56] D.W. Dudley, *Handbook of practical gear design*. London: CRC Press, 1994.

[57] Hewland Engineering. (2008, February) Servicing Instructions and Illustrated Parts List from Hewland Family of Gearboxes. [Online]. www.hewland.com

[58] D. Hanselman, *Brushless Permanent Magnet Motor Design*, 2nd ed. Cranston, Rhode Island: The Writer's Collective, 2003.

[59] C.M. Ta and Y. Hori, "Convergence Improvement of Efficiency Optimization Control of Induction Motor Drives," *IEEE Transactions on Industry Applications*, vol. 37, no. 6, pp. 1746-1753, Nov/Dec 2001.

[60] N. Mohan, T.M. Undeland, and W.P. Robbins, *Power Electronics: Converters, Applications, and Design*, Third Edition ed. New York: John Wiley & Sons, Inc., 2003.

[61] UQM Technologies. (2009, June) PowerPhase Traction System Datasheet. [Online]. www.uqm.com

[62] S. Pay and Y. Baghzouz, "Effectiveness of Battery-Supercapacitor Combination in Electric Vehicles," in *PowerTech Conference Proceedings*, vol. 3, Bologna, 2003, pp. 23-26.

[63] H.B. Pacejka and E. Bakker, "The Magic Formula Tyre Model," *Vehicle Systems Dynamics*, vol. 21, no. 1, pp. 1-18, 1992.

[64] J. Wang and R.G. Longoria, "Combined Tire Slip and Slip Angle Tracking Control for Advanced Vehicle Dynamics Control Systems," in *Proceedings of the 45th IEEE Conference on Decision and Control*, San Diego, CA, USA, 2006, pp. 1733-1738.

[65] P.S. Fancher, H. Dugoff, K.C. Ludema, and L. Segel, "Experimental Studies of Tire Shear Force Mechanics," Highway Safety Research Institute, The University of Michigan, Ann Arbor, Michigan, 1970.

[66] J.E. Bernard, L. Segel, and R.E. Wild, "Tire Shear Force Generation During Combined Steering and Braking Maneuvers," Highway Safety Research Institute, The University of Michigan, Ann Arbor, Michigan, 1977.

[67] C. Canudas-de-Wit, P. Tsiotras, and E. Velenis, "Dynamic Friction Models for Road/Tire Longitudinal Interaction," *Vehicle System Dynamics*, vol. 39, no. 3, pp. 189-226, 2003.

[68] G. Dihua, S. Jin, and Yam L.H., "Establishment of Model for Tire Steady State Cornering Properties Using Experimental Modal Parameters," *Vehicle System Dynamics*, vol. 34, no. 1, pp. 45-56, 2000.

[69] H.B. Pacejka, *Tyre and Vehicle Dynamics*. 2006: Elsevier, Oxford.

[70] F. Braghin, F. Cheli, and E. Sabbioni, "Identification of Tire Model Parameters Through Full Vehicle Experimental Tests," *Journal of Dynamic Systems, Measurement, and Control*, vol. 133, May 2011.

[71] C.R. Carlson and J.C. Gerdes, "Nonlinear Estimation of Longitudinal Tire Slip Under Several Driving Conditions," in *Proceedings of the 2003 American Control Conference, 2003*, 2003, pp. 4975-4980.

[72] D.H., Hedrick, J.K., Shladover, S.E. McMahon, "Vehicle Modelling and Control for Automated Highway Systems," *American Control Conference*, pp. 297-303, May 1990.

[73] H. Xu, A. Kahraman, N.E. Anderson, and D.G. Maddock, "Prediction of Mechanical Efficiency of Parallel-Axis Gear Pairs," *Journal of Mechanical Design*, vol. 129, pp. 58-68, January 2007.

[74] W. Bartelmus, "Mathematical Modelling and Computer Simulations as an Aid to Gearbox Diagnostics," *Mechanical Systemns and Signal Processing*, vol. 15, no. 5, pp. 855-871, Sept. 2001.

[75] R.J. Drago, *Fundamentals of Gear Design*. London: Butterworth, 1988.

[76] Cobham CTS Ltd. (Kidlington, UK). (2011, April) Vector Fields. [Online]. http://www.cobham.com/about-cobham/aerospace-and-security/about-us/antenna-systems/kidlington.aspx

[77] W. Lajnef, J.M. Vinassa, O. Briat, S. Azzopardi, and E. Woirgard, "Characterization Methods and Modelling of Ultracapacitors for Use as Peak Power Sources," *Journal of Power Sources*, vol. 168, pp. 553-560, 2007.

[78] L. Gao, R.A. Dougal, and S. Liu, "Power Enhancement of An Actively Controlled Battery/Ultracapacitor Hybrid," *IEEE Transactions on Power Electronics*, vol. 20, no. 1, Jan. 2005.

[79] D. Rotenberg, A. Vahidi, and I. Kolmanovsky, "Ultracapacitor Assisted Powertrains: Modeling, Control, Sizing, and the Impact on Fuel Economy," *American Control Conference*, June 2008.

[80] G. Pede, A. Iacobazzi, S. Passerini, A. Bobbio, and G. Botto, "FC Vehicle Hybridization: An affordable solution for an energy-efficient FC powered drive train," *Journal of Power Sources*, vol. 125, no. 2, pp. 280-291, January 2004.

[81] R.M. Schupbach, J.C. Balda, M.D. Zolot, and B. Kramer, "Design methodology of a combined battery-ultracapacitor energy storage unit for vehicle power management," in *Power Electronics Specialist Conference, 2003. PESC '03. 2003 IEEE 34th Annual*, vol. 1, Acapulco, Mexico, June 2003, pp. 88-93.

[82] M. Uzunoglu and M.S. Alam, "Dynamic modeling, design and simulation of a PEM fuel cell/ultra-capacitor hybrid system for vehicular applications," *Energy Conversion & Management*, vol. 48, no. 5, pp. 1544-1553, May 2007.

[83] J. Chmiola et al., "Anomalous Increase in Carbon Capacitance at Pore Sizes Less Than 1 Nanometer," *Science*, vol. 313, no. 5794, pp. 1760-1763, 2006.

[84] B.E. Conway, *Electrical Supercapacitors: Scientific Fundamentals and Technological Applications*. New York: Kluwer Academic/Plenum Publishers, 1999.

[85] R. Kotz and M Carlen, "Principles and Applications of Electrochemical Capacitors," *Electrochimica Acta*, vol. 45, no. 15-16, pp. 2483-2498, 2000.

[86] H. El Brouji, J.M Vinassa, O. Briat, N. Bertrand, and E. Woirgard, "Ultracapacitors self-discharge modelling using a physical description of porous electrode impedance," in *Vehicle Power and Propulsion Conference 2008*, Harbin, China, 2008, pp. 1-6.

[87] N. Bertrand, O. Briat, J.M. Vinassa, J. Sabatier, and H. El Brouji, "Porous electrode theory for ultracapacitor modelling and experimental validation," in *Vehicle Power and Propulsion Conference* , Harbin, China, 2008, pp. 1-6.

[88] L. Gao, S. Liu, and R.A. Dougal, "Dynamic Lithium-Ion Battery Model for System Simulation," *IEEE Transactions on Components and Packaging Technologies*, vol. 25, no. 3, pp. 495-505, Sept. 2002.

[89] R.A. Dougal, L. Gao, and S. Liu, "Ultracapacitor Model with Automatic Order Selection and Capacity Scaling for Dynamic System Simulation," *Journal of Power Sources*, vol. 126, pp. 250-257, 2004.

[90] S. Buller, E. Karden, D. Kok, and R.W. De Doncker, "Modeling the Dynamic Behavior of Supercapacitors Using Impedance Spectroscopy," *IEEE Transaction on Industry Applications*, vol. 38, no. 6, pp. 1622-1626, 2002.

[91] J.R. Miller and A.F. Burke, "Electrochemical Capacitors: Challenges and Opportunities for Real-World Applications," *The Electrochemical Society Interface*, pp. 53-57, Spring 2008.

[92] E. Barsoukov and J.R. Macdonald, *Impedance Spectroscopy: Theory, Experiment, and Applications*, 2nd ed. Hoboken, New Jersey: Wiley-Interscience, 2005.

[93] W. Lajnef, J.M. Vinassa, O. Briat, S. Azzopardi, and C. Zardini, "Study of Ultracapacitors Dynamic Behavior Using Impedance Frequency Analysis on a Specific Test Bench," *2004 IEEE International Symposium on Industrial Electronics*, vol. 2, pp. 839-844, May 2004.

[94] Stanford Research Systems. (2009, January) Model SR830 DSP Lock-In Amplifier Manual. [Online]. www.thinksrs.com

[95] Maxwell Technologies. (2009, January) K2 Series Ultracapacitors Datasheet (2010).. [Online]. www.maxwell.com

[96] J.M. Miller, D. Debrigic, and M. Everett. (2010 , May) Ultracapacitor Distributed Model Equivalent Circuit for Power Electronic Circuit Simulation, Maxwell Technologies Inc. [Online]. www.ansoft.com

[97] Nissan Motor Company. (2010, November) Nissan Leaf Specifications. [Online]. http://www.nissan.co.uk/leaf

[98] M. Doyle, T.T. Fuller, and J. Newman, "Modeling of galvanostatic charge and discharge of the lithium/polymer/insertion cell," *Journal of the Electrochemical Society*, vol. 140, pp. 1526-1536, 1993.

[99] T.F. Fuller, M. Doyle, and J. Newman, "Simulation and optimization of the dual lithium ion insertion cell," *Journal of the Electrochemical Society*, vol. 141, pp. 1-10, 1994.

[100] M. Doyle and J. Newman, "Comparison of modeling predictions with experimental data from plastic lithium ion cells," *Journal of the Electrochemical Society*, vol. 143, pp. 1890-1903, 1996.

[101] P. Arora, M. Doyle, and R.E. White, "Mathematical modeling of the lithium deposition overcharge reaction in lithium-ion batteries using carbon-based negative electrodes," *Journal of the Electrochemical Society*, vol. 146, no. 10, pp. 3543-3553, 1999.

[102] L. Song and J.W. Evans, "Electrochemical-thermal model of lithium polymer batteries," *Journal of the Electrochemical Society*, vol. 147, no. 6, pp. 2086-2095, 2000.

[103] W.B. Gu and C.Y. Wang, "Thermal-electrochemical modeling of battery systems," *Journal of the Electrochemical Society*, vol. 147, no. 8, pp. 2910-2922, 2000.

[104] P.M. Gomadam, J.W. Weidner, R.A. Dougal, and R.E. White, "Mathematical modeling of lithium-ion and nickel battery systems," *Journal of Power Sources*, vol. 110, no. 2, pp. 267-284, Aug. 2002.

[105] P. Mauracher and E. Karden, "Dynamic Modeling of Lead/Acid Batteries Using Impedance Spectroscopy for Parameter Identification," *Journal of Power Sources*, vol. 6, pp. 69-84, 1997.

[106] S. Buller, M. Thele, R.W.A.A. De Doncker, and E. Karden, "Impedance-based simulation models of supercapacitors and Li-ion batteries for power electronics applications," *IEEE Transactions on Industry Applications*, vol. 41, no. 3, pp. 742-747, May-June 2005.

[107] O. Tremblay, L.A. Dessaint, and A.I. Dekkiche, "A Generic Battery Model for the Dynamic Simulation of Hybrid Vehicles," *IEEE Power and Propulsion Conference*, pp. 284-289, Sept. 2007.

[108] C.M. Shepherd, "Design of Primary and Secondary Cells - Part 2. An Equation describing Battery Discharge," *Journal of the Electrochemical Society*, vol. 112, pp. 657-664, July 1965.

[109] PowerGenix. (2009, July) Datasheet for PowerGenix PGX 1500 AA Battery. [Online]. www.powergenix.com

[110] A123 Systems. (2009) High Power Lithium Ion ANR26650 M1A Datasheet. [Online]. www.a123systems.com

[111] Saft Industrial Battery Group. (2009) Nickel-Metal Hydride Module Datasheet. [Online]. www.saftbatteries.com

[112] J. O'Dell. (2010, October) Green Car Advisor, Edmunds.com. [Online]. http://blogs.edmunds.com/greencaradvisor/2010/02/2010-geneva-auto-show-porsches-flywheel-hybrid-911-gt3-r.html

[113] O. Briat, J.M. Vinassa, W. Lajnef, S. Azzopardi, and E. Woirgard, "Principle, design and experimental validation of a flywheel-battery hybrid source for heavy-duty electric vehicles," *IET Electr. Power Appl.*, vol. 1, no. 5, pp. 665-674, September 2007.

[114] H. Liu and J. Jiang, "Flywheel energy storage-an upswing technology for energy sustainability," *Energy and Buildings*, vol. 39, no. 5, pp. 559-604, May 2007.

[115] P.P. Acarnley et al., "Design principles for a flywheel energy store for road vehicles," *IEEE Transactions on Industry Applications*, vol. 32, no. 6, pp. 1402-1408, Nov-Dec 1996.

[116] Flybrid Systems, "Datasheet for Flybrid Systems' Flywheel," May 2009, Obtained from personal correspondence with Flybrid.

[117] D. Cross and C. Brockbank, "Mechanical Hybrid System Comprising a Flywheel and CVT for Motorsport and Mainstream Automotive Applications," *SAE World Congress and Exhibition*, 2009.

[118] McKinsey Quarterly, "Tomorrow's Cars, Today's Engines," January, 2010.

[119] N.N. Mustafi and R.R. Raine, "Application of a Spark Ignition Engine Simulation Tool for Alternative Fuels," *Journal for Gas Turbines and Power*, vol. 130, pp. 1-6, January 2008.

[120] D. Buttsworth, "Multizone Internal Combustion Engine Modelling," in *Proceedings of ICEE 2009 3rd International Conference on Energy and Environment*, Malacca, Malaysia, December 2009, pp. 343-347.

[121] S.P. Marshall, R. Stone, C. Heghes, T.J. Davies, and R.F. Cracknell, "High pressure laminar burning velocity measurements and modelling of methane and n-butane," *Combustion Theory and Modelling*, vol. 14, no. 4, pp. 519-540, 2010.

[122] AVL. (2011) AVL Boost Product Description. [Online]. https://www.avl.com/boost1

[123] W. Volker, C.J. Brace, and N.D. Vaughan, "The potential for simulation of driveability of CVT vehicles," *Society of Automotive Engineers*, pp. 1-7, 1998.

[124] M. Brusstar and M. Bakenhus. (2010) Economical, High-Efficiency Engine Technologies for Alcohol Fuels. [Online]. www.methanol.org

[125] S. Ahmed and M. Krumpelt, "Hydrogen from Hydrocarbon Fuels for Fuel Cells," *International Journal of Hydrogen Energy*, vol. 26, no. 4, pp. 291-301, 2001.

[126] S.H. Chan, C.F. Low, and O.L. Ding, "Energy and Exergy Analysis of Simple Solid-Oxide Fuel-Cell Power Systems," *Journal of Power Sources*, vol. 103, no. 2, pp. 188-200.

[127] L.F. Brown, "A Comparative Study of Fuels for On-Board Hydrogen Production for Fuel-Cell-Powered Automobiles," *International Journal of Hydrogen Energy*, vol. 26, no. 4, pp. 381-397, April 2001.

[128] U. Bossel, "Well-to-wheel studies, heating values, and the energy conservation principle," European Fuel Cell Forum, Oberrohrdorf, Switzerland, 2003.

[129] K.S. Jeong and B.S. Oh, "Fuel Economy and Life-Cycle Cost Analysis of a Fuel Cell Hybrid Vehicle," *Journal of Power Sources*, vol. 105, no. 1, pp. 58-65, March 2002.

[130] B.C.H. Steele and A. Heinzel, "Materials for Fuel-Cell Technologies," *Nature*, vol. 414, pp. 345-352, November 2001.

[131] C.E. Thomas, B.D. James, F.D. Lomax, and I.F. Kuhn, "Fuel Options for the Fuel Cell Vehicle: Hydrogen, Methanol, or Gasoline," *International Journal of Hydrogen Energy*, vol. 25, pp. 551-567, 2000.

[132] T.E. Springer, T.A. Zawodzinski, and S. Gottesfeld, "Polymer Electrolyte Fuel Cell Model," *Journal of the Electrochemical Society*, vol. 138, no. 8, pp. 2334-2342, 1991.

[133] D.M. Bernardi and M.W. Verbrugge, "A mathematical model of the solid-polymer-electrolyte fuel cell," *Journal of the Electrochemical Society*, vol. 139, no. 9, pp. 2477-2491, 1992.

[134] M. Eikerling and A.A. Kornyshev, "Modeling the performance of the cathode catalyst layer of polymer electrolyte fuel cells," *Journal of Power Sources*, vol. 453, pp. 89-106, 1998.

[135] V. Gurau, S. Kakac, and H. Liu, "Mathematical model of proton exchange membrane fuel cells," in *Proceedings of the ASME Advanced Energy Systems Division*, vol. 38, 1998, pp. 205-214.

[136] R.P. O'Hayre, S.W. Cha, W. Colella, and F.B. Prinz, *Fuel Cell Fundamentals*. Hoboken, N.J.: John Wiley & Sons, 2006.

[137] J. Bauman and M. Kazerani, "A Comparative Study of Fuel-Cell-Battery, Fuel-Cell-Ultracapacitor, and Fuel-Cell-Battery-Ultracapacitor Vehicles," *IEEE Transactions on Vehicular Technology*, vol. 57, no. 2, pp. 760-769, March 2008.

[138] Hydrogenics, "Hydrogenics HyPM Fuel Cell Power Modules Datasheet," June 2009.

[139] S. Cho, K. Ahn, and J.M. Lee, "Efficiency of the planetary gear hybrid powertrain," *Proceedings of the Institution of Mechanical Engineers, Part D: Journal of Automobile Engineering*, vol. 220, no. 10, pp. 1445-1454, 2006.

[140] J.M. del Castillo, "The Analytical Expression of the efficiency of planetary gear trains," *Mechanism and Machine Theory*, vol. 37, pp. 197-214, 2002.

[141] J. Schiffer, O. Bohlen, R.W. De Doncker, D.U. Sauer, and K.Y. Ahn, "Optimized energy management for fuel cell-supercap hybrid electric vehicles," *Proceedings IEEE Vehicle Power Propulsion Conference*, pp. 341-348, January 2005.

[142] M.R. Cuddy and K.B. Wipke, "Analysis of the Fuel Economy Benefit of Drivetrain Hybridization," 1997.

[143] Exide Technologies, "Industrial Energy EPzB Series Datasheet," 2009.

[144] M. Ehsani, Y. Gao, and J.M. Miller, "Hybrid Electric Vehicles: Architecture and Motor Drives," *Proceedings of the IEEE*, vol. 95, no. 4, pp. 719-728, April 2007.

[145] S. Campanari, G. Manzolini, and F. Garcia de la Iglesia, "Energy analysis of electric vehicles using batteries or fuel cells through well-to-wheel driving cycle simulations," *Journal of Power Sources*, vol. 186, no. 2, pp. 464-477, January 2009.

[146] L. Carrette, K.A. Friedrich, and U. Stimming, "Fuel cells: principles, types, fuels, and applications," *ChemPhysChem*, vol. 1, no. 4, pp. 162-193, 2000.

[147] W. Gao, "Performance comparison of a fuel cell battery hybrid powertrain and fuel cell ultracapacitor hybrid powertrain," *Power Electronics in Transportation*, vol. 54, no. 3, pp. 846-855, October 2004.

[148] R. de Andrade Jr. et al., "A superconducting high-speed flywheel energy storage system," in *Proceedings of the International Conference on Materials and Mechanisms of*

Superconductivity, vol. 408-410, August 2004, pp. 930-931.

[149] P.J. Hall and E.J. Bain, "Energy-Storage Technologies and Electricity Generation," *Energy Policy*, vol. 36, no. 12, pp. 4352-4355, December 2008.

[150] F.V. Conte, "Battery and Battery Management for Hybrid Electric Vehicles: A Review," *Elektrotecknik und Informationstechnik*, vol. 123, no. 10, pp. 424-431, 2006.

[151] Y. Gao, S.E. Gay, M. Ehsani, R.F. Thelen, and R.E. Hebner, "Flywheel electric motor/generator characterization for hybrid vehicles," *Vehicular Technology Conference, 2003. VTC 2003-Fall. 2003 IEEE 58th*, vol. 5, pp. 3321-3325, October 2003.

[152] J.W. Kimball, B.T. Kuhn, and R.S. Balog, "A System Design Approach for Unattended Solar Energy Harvesting Supply," *IEEE Trans. on Power Electronics*, vol. 24, no. 4, April 2009.

[153] A. Burke, "Ultracapacitors: why, how, and where is the technology," *Journal of Power Sources*, vol. 91, no. 1, pp. 37-50, November 2000.

[154] C.S. Hearn et al., "Low Cost Flywheel Energy Storage for a Fuel Cell Powered Transit Bus," in *IEEE Vehicle Power And Propulsion Conference*, 2007, pp. 829-836.

[155] H. Tsuchiya and O. Kobayashi, "Mass Production Cost of PEM Fuel Cell by Learning Curve," *International Journal of Hydrogen Energy*, vol. 29, pp. 985-990, 2004.

[156] Horizon Fuel Cell Technologies, "H-Series PEM Fuel Cell Systems Datasheet," 2010.

[157] Nedstack, "Datasheet for Nedstack P5 Fuel Cells," availablie online: www.nedstack.com, 2007.

[158] K.S. Jeong and B.S. Oh, "Fuel economy and life-cycle cost analysis of a fuel cell hybrid vehicle," *Journal of Power Sources*, vol. 105, no. 1, pp. 58-65, March 2002.

[159] R. Rose, "Questions and answers about hydrogen and fuel cells," Washington D.C., 2005.

[160] A. Burke, "Comparisons of lithium-ion batteries and ultracapacitors in hybrid-electric vehicle applications," *EET-2007 European Ele-Drive Conference*, May-June 2007.

[161] A. Burke, "Batteries and ultracapacitors for electric, hybrid, and fuel cell vehicles," *Proceedings of the IEEE*, vol. 95, no. 4, April 2007.

[162] M. Andre, "Real-world driving cycles for measuring cars' pollutant emissions - part a: The artemis European driving cycles.," Laboratory Transport and Environment, Bron, France, nLTE 0411, 2004.

[163] J. Wu, A. Emadi, M.J. Duoba, and T.P. Bohn, "Plug-in Hybrid Electric Vehicles: Testing, Simulations, and Analysis," *IEEE Vehicle Power and Propulsion Conf.*, pp. 469-476, 2007.

[164] C. Samaras and K. Meisterling, "Life Cycle Assessment of Greenhouse Gas Emissions from Plug-in Hybrid vehicles: Implications for Policy," *Environmental Science and Technology*, vol. 42, no. 9, pp. 3170-3176, 2008.

[165] L. Yufang and L. Zhou, "Impact of driving cycles and all-electric range on plug-in hybrid vehicle component size and cost," *IEEE Vehicle Power and Propulsion Conference*, pp. 1708-1711, 2009.

[166] T.J. Wallington, E.W. Kaiser, and J.T. Farrell, "Automotive fuels and internal combustion engines: a chemical perspective," *Chemical Society Reviews*, vol. 35, pp. 335-347, 2005.

[167] V. Sreedhar, "Plug-In Hybrid Electric Vehicles with Full Performance," *IEEE Conference on Electric and Hybrid Vehicles*, pp. 1-2, 2006.

[168] C.C. Chan, "The State of the Art of Electric, Hybrid, and Fuel Cell Vehicles," *Proceedings of the IEEE*, vol. 95, no. 4, pp. 704-718, 2007.

[169] M.A. Kromer and J.B. Heywood, "Electric Powertrains: Opportunities and Challenges in the U.S. Light-Duty Vehicle Fleet," Sloan Automotive Laboratory, Laboratory for Energy and the Environment, Massachusetts Institute of Technology, 2007.

[170] G. Berdichevsky, K. Kelty, J.B. Straubel, and E. Toomre. (2006, August) Tesla Motors. [Online]. http://webarchive.teslamotors.com/display_data/TeslaRoadsterBatterySystem.pdf

[171] Ford Motor Company. (2010, March) 500,000th Focus Produced at Ford China's Chongqing Plant. [Online]. http://media.ford.com/article_display.cfm?article_id=32296

[172] S.B. Peterson, J. Apt, and J.F. Whitacre, "Lithium-ion battery cell degradation resulting from realistic vehicle and vehicle-to-grid utilization," *Journal of Power Sources*, vol. 195, no. 8, pp. 2385-2392, 2010.

[173] B. Scrosati and J. Garche, "Lithium batteries: Status, prospects and future," *Journal of Power Sources*, vol. 195, no. 9, pp. 2419-2430, 2010.

[174] M. Duvall, "Advanced Batteries for Electric-Drive Vehicles: A Technology and Cost-Effectiveness Assessment for Battery Electric, Power Assist Hybrid Electric, and Plug-in Hybrid Electric Vehicles," Electric Power Research Institute, 2003.

[175] G. Lechner and H. Naunheimer, *Automotive Transmissions: Fundamentals, Selection, Design, and Application*.: Springer, 1999.

[176] Data from Carfolio (www.carfolio.com).

[177] General Motors, "Chevrolet Volt Specifications 2011," 2010.

[178] Data from CARMA (www.carma.org).

[179] B. Lee, P. Gordon, H.W. Richardson, and J.E. Moore, "Commuting Trends in U.S. Cities in the 1990s," *Journal of Planning Education and Research*, vol. 29, no. 1, pp. 78-89, Sept. 2009.

[180] A.E. Pisarski, "Commuting in America III: the Third National Report on Commuting Patterns and Trends," Transportation Research Board, Washington D.C., 9780309098533, 2006.

[181] J. Garthwaite. (2010, August) Gigaom. [Online]. http://gigaom.com/cleantech/tesla-ceo-nissans-leaf-battery-is-primitive/